Reinforced Elastomer Composites and Metamaterials for Neo-aorta Applications

by

Dinara Zhalmuratova

A thesis submitted in partial fulfillment of the requirements for the degree of

Master of Science

in

CHEMICAL ENGINEERING

Department of Chemical and Materials Engineering
University of Alberta

Abstract

This thesis describes materials and strategies developed to replace rigid and noncompliant plastic tube, which causes injuries to the heart at the junction between the tissue and the tube in an ex-vivo heart perfusion device. The research is composed of two main parts. The first part addresses mimicking the rapidly strain-stiffening *J-shaped* and anisotropic stress-strain behavior of human and porcine aorta, necessary for producing the Windkessel effect to ensure continuous blood flow through the aorta. First, the mechanical properties of human and porcine aorta were measured to quantify the nonlinear and anisotropic behavior under uniaxial tensile stress. Secondly, fabric-reinforced elastomer composites were prepared by reinforcing silicone elastomers with embedded knitted fabrics in trilayer geometry. Finally, improved analytical constitutive models based on Gent's and Mooney-Rivlin's constitutive model (to describe the elastomer matrix) combined with Holzapfel–Gasser–Ogden's model (to represent the stiffer fabrics) were developed to verify aorta-like behavior of fabric-reinforced composites. The second part of this thesis included design of a material that limits the peak pressure in aorta by expanding to accommodate a large stroke volume. Recent advances in additive manufacturing techniques have enabled the development of novel materials with enhanced mechanical properties derived from carefully designed geometry known as metamaterials. To eliminate the consequences of aortic stiffening at high pressure, a metamaterial with unique strain-softening property at peak pressure coming after *J-shaped* strain-stiffening property is proposed. Thus, the second part of this thesis includes a thorough review covering design criteria and fabrication strategies of the bioinspired metamaterials, followed by a few of my original experimental trials.

Preface

(Mandatory due to collaborative work and research ethics approval)

Research presented in Chapters 3 and 4 was conducted as a part of research collaboration, led by Dr. Darren Freed in Department of Surgery, with Dr. David Nobes from Department of Mechanical Engineering and Dr. Hyun-Joong Chung from Department of Chemical and Materials Engineering. The work was supported by the Canadian Institutes of Health Research (CIHR) (CPG 151977) and Natural Sciences and Engineering Research Council of Canada (NSERC) (CHRP 508412-17) for funding through Collaborative Health Research Projects.

The mechanical property measurements of porcine and human aorta was done by Katherine Yu with the help of Dr. Thanh-Giang La, Alexander R. A. Szojka, Stephen H, J. Andrews and Dr. Adetola B. Adesida. The animal and human experiments were performed in compliance with the guidelines of the Canadian Council on Animal Care and the guide for the care and use of laboratory animals. The protocols were approved by the institutional animal care committee of the University of Alberta, protocol #AUP00000943. All literature review, synthetic material synthesis and characterization, and analytical modelling are my original work. Danae Chipoco Haro and Kaelyn Nicolson provided helps in 3D printing of metamaterials. Dr. Thanh-Giang La and Dr. Chun-il Kim provided advice on analytical modelling. Dr. Hyun-Joong Chung guided and revised all mentioned activities.

Chapter 3 of this thesis is currently in press in *ACS Applied Materials & Interfaces* as Dinara Zhalmuratova, Thanh-Giang La, Katherine Ting-Ting Yu, Alexander R. A. Szojka, Stephen H, J. Andrews, Adetola B. Adesida, Chun-il Kim, David S. Nobes, Darren H. Freed, and Hyun-Joong Chung, "Mimicking '*J-shaped*' and anisotropic stress-strain behavior of human and porcine aorta by fabric-reinforced elastomer composites" (doi:10.1021/acsami.9b10524). Selected contents in Chapter 2 and Chapter 4 will be used to constitute an Invited Review Paper to be submitted to *ACS Applied Polymer Materials* in October. Dr. Hyun-Joong Chung will plan and edit the contents.

Acknowledgments

First and foremost, I would like to express my appreciation and gratitude to my supervisor, Dr. Hyun-Joong Chung for providing me with continuous and unconditional support through the course of my studies. I am very grateful for his patience, inspiration and knowledge he shared with me.

I would like to thank our collaborators, Dr. Darren Freed and Dr. David Nobes for the opportunity to work on this project. Thanks to Dr. Chun-Il Kim for his advices for the modeling part of this thesis. Special thanks to Dr. Anastasia Elias for the use of tensile tester.

Thanks for co-supervised undergraduate students Minshan Meng, Danae Chipoco Haro and Kaelyn Nicolson for helping with experiments.

I would like to acknowledge the sponsors Canadian Institutes of Health Research (CIHR) and Natural Sciences and Engineering Research Council of Canada (NSERC) for funding through Collaborative Health Research Projects.

Thanks to my roommates, Lelin and Wendy, for being my family and thanks to my friends at Soft Material and Device Lab for making lab a better place. Thanks to Qazaqs in Edmonton for making Edmonton feel like home.

Thanks to all my family and friends for their encouragement and support throughout this period.

Finally, I would like to dedicate this thesis to my mom for her love and care. She has been a source of inspiration for everything.

Table of contents

List of Tables

List of Figures

1 Introduction

1.1 Heart Perfusion Device

Heart transplant is a live-saving operation because it is the only definitive therapeutic option for patients with end-stage heart disease [1]. Following the pioneering success of heart transplant surgery in 1967, more than 100 000 heart transplants have been completed globally [2]. Most of these procedures depended on cold bath preservation of the donor heart at 4 °C due to simplicity, inexpensiveness and reliability of this method [2]. However, this method is far from ideal for this application, prolonged ischemia time has been demonstrated to be one of the most important factors in early graft dysfunction, therefore the most frequent cause of death within the first month [3]. Within one year, less than two hours of ischemic time is associated with less than 15% of treated rejection, while 6 hours is associated with more than 20% of treated rejection, after this time the donor heart is discarded [4]. This cold ischemic time limits this operation because of the small donor organ supply [5] and the transportation is limited to short distances [3]. Furthermore, while amount of people in need of a heart transplant continues to increase, the donor pool remained stalled [1]. A promising alternative for heart preservation is transportation of the heart in a beating normothermic perfused state.

Studies have shown that normothermic ex-vivo heart perfusion contributes to a significant reduction in time spent in cold ischemia, as well as better outcomes after transplantation in terms of recipient survival, episodes of primary graft dysfunction, and acute rejection [3], [6], [7], [8]. It also allows for heart procurement at longer distances and biochemical and functional monitoring of the donor heart. Although the theoretical advantages of normothermic donor heart perfusion have been recognized for over a century, the technology to implement this method has only been developed within the last decade. The Organ Care System (OCS) shown in Figure 1.1a, which is designed and manufactured by TransMedics Inc. is currently the only commercially available device with this capability [2].

A current challenge facing our ex-vivo perfusion device includes a judicial material design for the blood outlet tubing from the heart, which replaces the role of the ascending aorta from the left ventricle. Commercially available plastic tubings, such as Tygon tube, are too rigid and non-compliant and can thereby cause injury of the soft and beating heart tissue at the heart-simulated aorta junction as shown in Figure 1.1b. The problem is aggravated with the lack of the Windkessel effect when the heart is ejecting in working mode, by which the human aorta acts as a shock-absorbing reservoir to prevent injury from the pulsed supply of blood from the beating heart and to produce "nearly continuous peripheral blood flow" [9]. Conversely, soft tubing materials, such as room-temperature vulcanizing (RTV) silicones, do not allow blood to circulate due to overexpansion at minimal pressure changes [10].

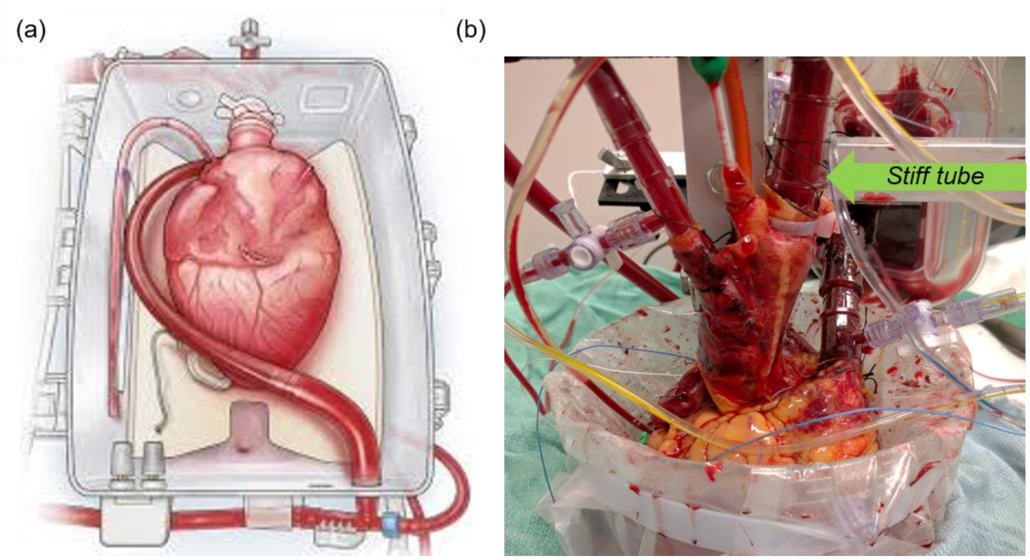

Figure 1.1. Ex-vivo heart perfusion. a) Schematic of The Organ Care System (OCS). Reproduced with permission from [1]. b) Stiff blood outlet tubing from the heart.

The goal of the first part of this thesis is (i) to measure stress-strain behavior of the human and porcine aortas, (ii) to design and fabricate the fabric-reinforced elastomers that mimic the mechanical properties of the aortas, and (iii) to develop analytical models to describe the mechanical properties of the aortas and the fabric-reinforced elastomers.

The second part of this thesis is to design a metamaterial that is able to achieve a steady-state blood flow in high blood pressure conditions and limit the peak pressure in aorta by expanding to accommodate a large stroke volume.The material must ensure that maximum blood pressure does not rise above physiological systolic pressure range. Strain hardening at low strains to allow Windkessel effect, followed by strain softening at high strains to eliminate peak pressure, is the key feature to enable the steady state. Such mechanical behavior does not exist in natural materials but is hypothesized to be achieved with synthetic material design. Recent advances in additive manufacturing techniques have enabled the development of novel materials with enhanced mechanical properties derived from carefully designed geometry known as metamaterials. While the project is unfinished during my MSc years, I comprised a thorough review covering design criteria and fabrication strategies of the strain-stiffening-softening metamaterial, followed by a few of my original experimental trials.

1.2 Mechanical properties of arterial walls

1.2.1 Windkessel effect

As mentioned above, natural aorta possesses a Windkessel function, which is crucial for normal heart operation. During systole the left ventricle ejects a stroke volume of about 60-100 ml into the aorta and arterial system. As shown in Figure 1.2, approximately 50% of the stroke volume is directly forwarded to the peripheral circulation. Peripheral resistance and elastic extension of the aortic wall are responsible for storage of the other 50% of the stroke volume, the storage volume. During diastole the aortic valve is closed and there is no further blood ejection. With a fall in aortic pressure, the aorta recoils slowly and the elastic forces of the aorta press the storage volume into the periphery of the circulation. Thus, during diastole as well, pressure and blood flow are maintained and a nearly continuous peripheral flow of blood results in spite of the noncontinuous, rhythmic actions of the heart.

One other mechanism important for maintenance of a relatively high diastolic pressure and blood flow should be mentioned here: In a healthy organism, the pulse wave velocity of the aorta and large vessels is relatively slow. When this wave is reflected in the peripheral circulation, it returns to the ascending aorta during early diastole, inducing the dicrotic wave [11]. This mechanism supports the elastic function of the aorta. It should also be noted that this second increase in pressure is dampened by the Windkessel function. The Windkessel function depends on the elasticity of the aorta. Physics defines deformable materials as elastic when after discontinuation of an external force they readopt their original shape. Any elastic body can store energy without loss of energy [9]. During one heart action, the kinetic energy of the ejected stroke volume is first transformed into potential energy within the distended aortic wall. This stored potential energy is then reconverted into kinetic energy during diastole, when the aorta slowly recoils. Thus, in spite of the diastolic pauses of the heart, the column of blood within the peripheral arteries does not come to a diastolic stop and blood pressure does not drop to zero, as would happen in a system of stiff tubes [9].

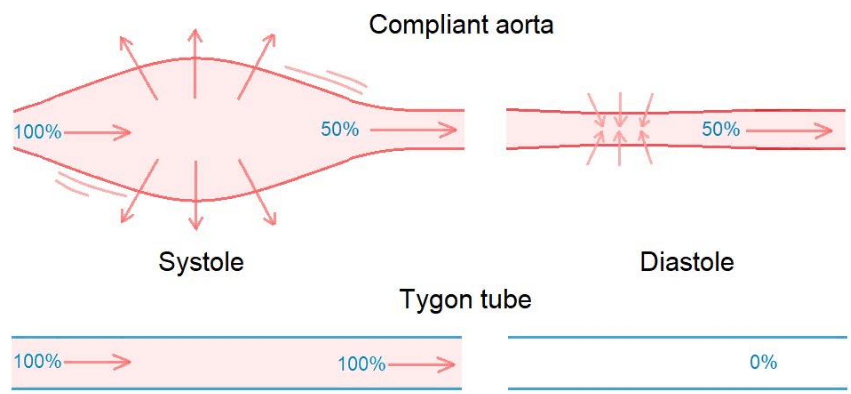

Figure 1.2. The effect of compliance in the Windkessel function of aorta. During systole, the compliant aorta expands to store 50% of the stroke volume and delivers it during diastole, thus ensuring continuous blood flow. Tygon tube is unable to expand to store blood and deliver continuous flow.

1.2.2 *J-shaped* stress-stress behavior (rapid stress-stiffening) of aorta

Windkessel effect relies on the interaction between the stroke volume and the compliance of the aorta. Arteries must be distensible to provide capacitance and pulse-smoothing in the circulation, but they must also be stable to inflation over a range of pressure. This is achieved by the most important mechanical property of the artery wall, which is non-linear elasticity. Over the last century, this has been well-documented in vessels in many animals, from humans to lobsters [16]. Strain-dependent increases in the elastic modulus of the vascular wall, manifest by a *J-shaped* stress–strain curve, as typically exhibited by other soft biological tissues. All vertebrates and invertebrates with closed circulatory systems have arteries with this non-linear behaviour, but specific tissue properties vary to give correct function for the physiological pressure range of each species. In all cases, the non-linear elasticity is a product of the parallel arrangement of rubbery and stiff connective tissue elements in the artery wall, and differences in composition and tissue architecture can account for the observed variations in mechanical properties. This phenomenon is most pronounced in large whales, in which very high compliance in the aortic arch and exceptionally low compliance in the descending aorta occur and is correlated with specific modifications in the arterial structure. It turns out that non-linear behaviour is the key to elastic stability in any highly distensible pressure vessel, protecting against aneurysms and 'blowout' [12].

1.2.3 Anisotropic stress-stress behavior of aorta

In addition to its *J-shaped* stress-strain behavior, human aorta is also known to have significant anisotropy [13], [14]. Here, higher stiffness in the longitudinal direction prevents excessive stimulation of the anastomotic regions, while compliance in the circumferential direction prevents flow disturbance [15]. Hence, anisotropy is another property of natural aorta that synthetic materials often lack and is important to mimic.

1.2.4 Anatomy of arterial wall

In order to mimic natural aorta with the *J-shaped* and anisotropic mechanical properties, it is critical to understand the underlying mechanism of these properties. The aorta has a composite structure and thus its nonlinear properties come from the combination of both elastic and stiff fibrous components. The main structural components of the arterial wall are elastin and collagen, elastin is a rubber-like protein with a modulus of 0.6–1 MPa [16], whereas collagen is stiff and relatively inextensible with a modulus of around 1 GPa [16]. Both elastin and collagen appear as wavy and crimped strands, thus the resulting structure is easy to accommodate a low level of strain [12], [17]. The initial low modulus response at low strain is attributed to elastic elastin fibers, while the stiffening at the higher strains is due to progressive straightening of elastin and collagen fibers [16]. Anisotropy mainly arises from the orientation of collagen fibers in the arterial wall [18]. As seen from Figure 1.3, healthy arterial wall constitutes of three main layers: intima (inner layer), media (middle layer), and adventitia (outer layer) [19]. The intima, the innermost layer, is thin and easily traumatized. This layer is in direct contact with the blood inside the vessel and mainly lined by endothelium [19]. The media is responsible for imparting strength to the artery and consists of laminated but intertwining sheets of elastic tissue. The arrangement of these sheets in a spiral provides the artery with its maximum allowable tensile strength. Media contains smooth muscle cells, a network of elastic and collagen fibrils and elastic laminae which separate media into a number of fiber-reinforced layers. The outermost layer is adventitia, which largely consists of collagen to prevent the artery from over inflation and stretch [20]. The collagen fibrils in media, for example, are arranged in helical structures and are mostly circumferentially oriented. This structured arrangement allows media to resist high loads in the circumferential direction [19]. Thus, differences in composition and orientation of stiff constituents give rise to anisotropy.

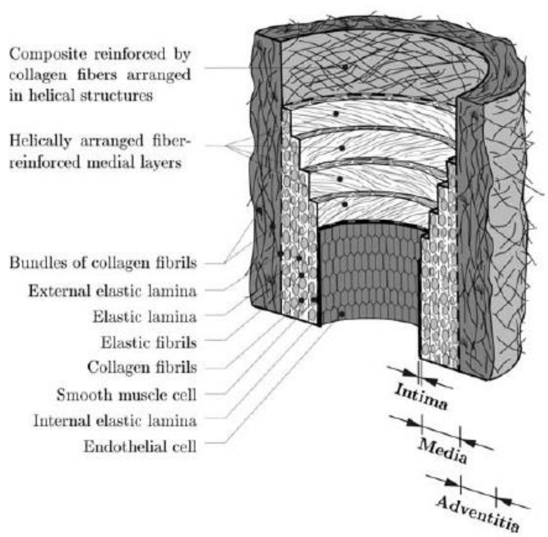

Figure 1.3. Schematic model of elastic artery composed of three layers: intima, media, and adventitia. Reproduced with permission from [21].

Therefore, as the aorta itself is a composite structure of rubber-like and fiber-like constituents, in the first part of this thesis, fabric-reinforced composites were developed to mimic mechanical properties of natural aorta. Commercially available fabrics and elastomers were tested to find the most suitable combination to mimic the *J-shaped* and anisotropic properties of aortas.

1.3 Beyond aorta – the *stress-stiffening-softening* property

Thee first part of this thesis focuses on achieving two material properties to mimic natural aorta: nonlinear *J-shaped* stress-strain behavior and anisotropy, which are known to underpin the Windkessel effect. Another challenge for the ex-vivo perfusion device is not only to mimic aorta behavior, but to achieve a steady-state condition in which regardless of the blood flow, the material is able to maintain the physiological pressure range. The basic hemodynamic effect of elevated blood stroke volume is increase in arterial pressure [22], which in turn increases aortic wall stress and causes aortic stiffening and descreased compliance [23]. Moreover, this condition gives rise to early pressure wave reflection to the aortic root, which causes greater vascular load on the heart, which can lead to myocardial hypertrophy and heart failure [24], [25]. The elevated pressure could also be the cause of endothelial dysfunction and hemolysis [24].

To eliminate the consequences of aortic stiffening at high pressure, we are aiming to introduce a metamaterial with unique strain-softening property coming after *J-shaped* strain-stiffening property. We anticipate that stress-softening at elevated pressure could decrease the stress on aortic wall and avoid counter flows that could damage heart. Hereafter, it is termed as the *strain-stiffening-softening* property.

For this study, an ideal strain-stiffening curve is built considering the physiological range of the aorta which is from 30 to 120 mmHg [6], [26], [27]. Regardless of stroke volume, the pressure in aorta should not rise above systolic pressure of 120 mmHg. It was established that pressure range of 80-120mmHg corresponds to average wall stress of 120kPa [28] to 200kPa [29] (Figure 1.4). For this thesis, 120kPa was set as maximum pressure on aortic wall and stress-softening will be introduced at the value.

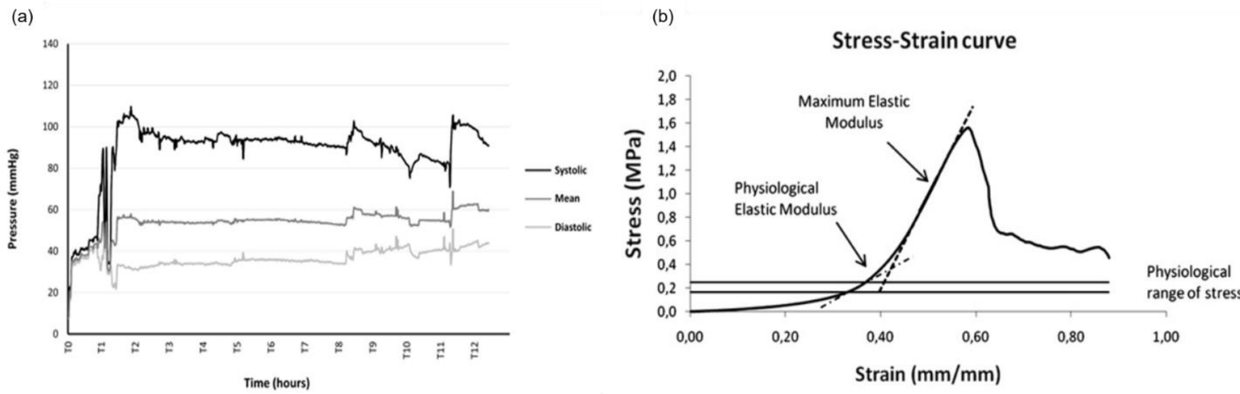

Figure 1.4. Physiological range of pressure. a) Trends in the aortic pressure during 12 h of ex-vivo heart perfusion. Reproduced with permission from [27]. b) Calculated wall stress (in MPa) corresponding to physiological pressure range of 80-120 mmHg. Reproduced with permission from [29].

Metamaterials are carefully structured materials that are composed of periodically arranged building blocks and display properties superior to their constituent materials. In the past two decades, metamaterials have been utilized to manipulate optical, acoustic and thermal fields to obtain unusual properties, such as a negative refraction index and resulted in new applications, such as perfect lenses [30]. Mechanical metamaterials represent a new branch of metamaterials research, where motion, deformations, stresses and mechanical energy are investigated. The meta-atoms, building blocks of mechanical metamaterials, deform, rotate, buckle, fold and snap in response to applied mechanical forces and are designed to act together to yield a desired collective behavior. We hypothesize that by careful design of mechanical metamaterial, the desired stress-hardening-softening behavior can be achieved.

The recent advances in computer-aided design (CAD) and additive manufacturing allow for a rapid and low-cost fabrication of complex structures with a fine resolution [31], [32]. In the proposed study, we aim to use two additive manufacturing techniques, SLA and PolyJet 3D printing to produce custom-developed sine-wave based models encapsulated in soft polymer matrices to achieve a metamaterial with unique strain-softening property coming after *J-shaped* strain-stiffening property, i.e., the *stress-stiffening-softening* property.

1.4 Research aims

Our research aims are to develop composite materials to be used in place of aorta in normothermic heart transportation device. In order to achieve the goal, we performed following activities.

(1) We thoroughly measured the mechanical properties of the human (n = 1) and porcine (n = 14) aorta as a function of location (distance from the heart), direction (longitudinal or circumferential), and the weight of the donor. (Chapter 3)

(2) We fabricated fabric-reinforced elastomeric composite to mimic the *J-shaped* strain-stiffening and anisotropic mechanical properties of the aortas. (Chapter 3)

(3) We developed an analytical model to create a library of parameters that can be used in the future to predict the behavior of similar composites. (Chapter 3)

(4) We suggested a design criterion for novel *strain-stiffening-softening* metamaterial with a critical review on the subjects of 3D printed metamaterials and their elastomeric composites. (Chapter 4)

(5) We introduced our preliminary results for the *strain-stiffening-softening* material development. (Chapter 4)

1.5 Outline of thesis

The basic theory and formulations of are summarized in Chapter 2. Chapters 3 and 4 are my original works with objectives described in Section 1.4. Finally, conclusions and outlooks for future works are given in Chapter 5.

2 Background: basic theory and formulations

2.1 Mechanical behavior of elastomers

Elastomers are suitable for biomedical applications due to their nearly instantaneous response to stresses and fully reversible deformation [33]. Particularly, silicone elastomers remain of interest in medical applications because of their recognized biocompatibility [34]. However, despite that the uniaxial tensile properties of elastomers are similar to soft tissues at low strains, they behave differently under larger deformation. As illustrated in Figure 2.1, soft tissues (human aorta) typically exhibit a strain-stiffening behavior at low strains (<100%). In contrast, the stress-strain curve of a rubber is usually concave from the beginning, indicating a strain-softening feature, while silicone and acrylic elastomers exhibit linear relationship at low strains, followed by strain stiffening at high strains (>300%). Thus, even though the initial modulus of a synthetic elastomer can be designed to match the modulus of the biological tissue, the mechanical behavior of the elastomer material is incapable of replicating strain-stiffening at low strains that is essential to biological tissue.

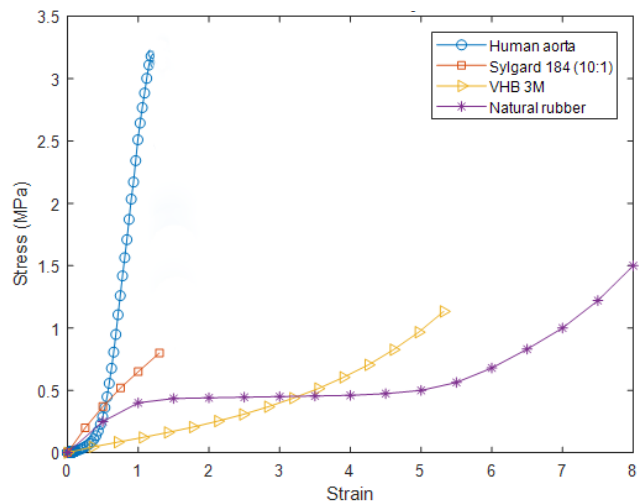

Figure 2.1. Measured stress-strain properties of Human aorta vs. Polymers.

Such mechanical behavior of silicone elastomers can be related to their structure. Traditional elastomers are lightly cross-linked networks with a quite large free volume, which allows for immediate response to external stresses resulting from rapid rearrangement of the polymer segments [35]. Main physics behind classical elasticity theory that describes polymer stress-strain relationship is entropic elasticity of polymer chains, which is driven from Gaussian statistics of freely jointed chains [36]. The simplest model that captures this idea of rubber elasticity is the affine network model originally proposed by Kuhn as shown in Figure 2.2a [36]. Affine network model assumes affine deformation: the relative deformation of each network strand is the same as the macroscopic relative deformation imposed on the whole network. Alternatively, in the phantom model, the strands are ideal chains with ends joined at crosslinks. The ends of strands at the surface of the network are attached to the elastic non-fluctuating boundary of the network. This attachment fixes the volume of the phantom network and prevents its collapse that would have been inevitable because such simple models ignore excluded volume interactions between monomers (Figure 2.2b).

Both the affine and phantom network models predict the same (classical) dependence of stress on deformation. The elastic stress of a rubber, *G*, under uniaxial extension is directly proportional to the number of network chains per unit volume (i.e. ρ/M) [36], here T is the temperature and λ is stretch, σ_{true} is the true stress.

$$G = \frac{\rho RT}{M}$$

$$\sigma_{true} = G\left(\lambda^2 - \frac{1}{\lambda}\right)$$

While this equation describes observed rubber-elastic behavior at low extensions quite well, it is unable to predict strain hardening at high deformations (Figure 2.2c), which can be explained by non-Gaussian statistics of highly deformed chains. Gaussian approximation for freely jointed chain model is valid for end-to-end distances much shorter that for fully stretched state.

$$R << R_{max} = bN$$

Finite chain extensibility and stress-induced crystallization are main reasons for such strain hardening [36].

The response of individual polymer chain to external stress depends on the rigidity of a polymer backbone. Normally, a flexible polymer chain can undergo very large deformations without resistance before reaching full elongation. In contrast, semi-flexible and rigid polymers, can exhibit non-linear behavior at small strains due to geometrical constraints. Most traditional synthetic polymers, however, lack the molecular complexity to experience hierarchical self-assembly to form stiffer structures [37].

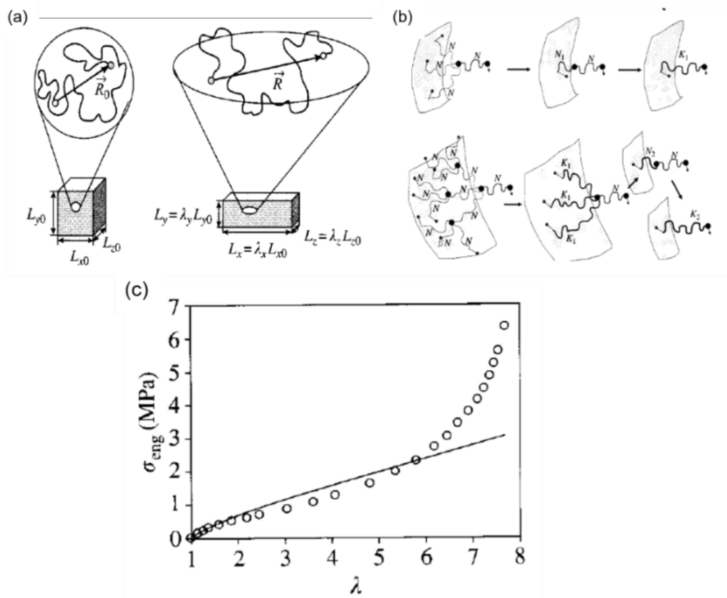

Figure 2.2. Classical elasticity theory: a) Affine network (Affine deformation requires each network strand to adopt the relative deformation of the macroscopic network), b) Phantom network (leftmost ends of effective chains are pinned to macroscopic boundary of the network), c) Engineering stress in tension for a crosslinked rubber (circles). The solid curve is prediction from affine classical elasticity theory. Reproduced with permission from [36].

2.2 Ways to achieve *J-shaped* behavior

Most natural biological tissues, such as skin, ligaments, blood vessels, display *J-shaped* nonlinear stress–strain behavior, which allows for combination of compliance and stretchability as well as strain-limiting and stiffening to prevent damage from excessive strain [17]. This type of stress–strain response is attributed to wavy and crimped collagen fibers in the tissue that progressively unfurl, uncoil, leading to an increase of the tangent modulus and eventually straighten, leading to linear response and a high tangent modulus at higher strains [17]. Design of synthetic materials with *J-shaped* behavior has a potential in many applications, such as tissue engineering, biomedical devices, soft robotics.

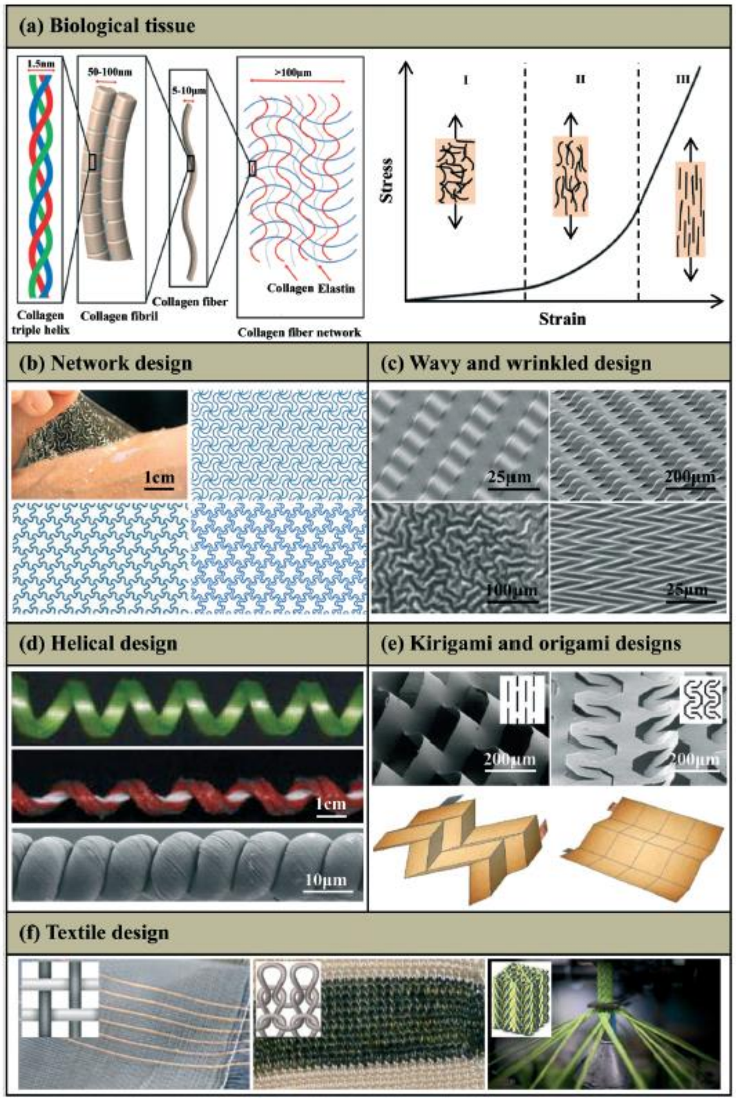

Figure 2.3. Strategies to achieve J-shaped stress-strain behavior: (a) biological tissue composed of collagen and elastin fibers, (b) 2D network design: triangular (right-top), honeycomb (left-bottom) and Kagome (right-bottom) embedded in an ultralow-modulus matrix, (c) wavy and wrinkled design, (d) helical design, (e) kirigami and origami designs, (f) Textile design: weaving (left), knitting (middle) and braiding (right). Reproduced with permission from [17].

The following section highlights different strategies to achieve *J-shaped* stress-strain property, including designing the network, wavy and wrinkled morphologies, helical designs, kirigami and origami constructs, polymer molecular design, and textile formats.

Network design. Curved and chained microstructures found in biological tissues are composed of cross-linked fiber networks with random distributions, which can be replicated in synthetic systems by various approaches, such as ionic liquid grinding, two-step shearing, plasma-induced modification and two-step polymerization [17], Jungebluth et al. [38] developed artificial scaffolds from electrospun synthetic fibers and used cells to fabricate a tissue engineered rat trachea with microstructures and mechanical properties similar to those of native tissues. Rogers and co-workers [17] developed bio-inspired design based on a two-dimensional wavy filamentary network embedded in an low-modulus matrix, where '*J-shaped*' stress–strain behavior can be carefully controlled by choices in geometry (Figure 2.3b). Using lithographic approaches, these microscale features can be produced in different materials, such as photopolymers, metals and semiconductors.

Wavy and wrinkled design. For a stiff thin film bonded to a compliant substrate, differences in strain (either by thermally induced mismatch or mechanical pre-strain) between the film and substrate can lead to wrinkling of the film into a sinusoidal form (Figure 2.3c). As the applied strain increases, the wrinkled film becomes flat and therefore contributes to the stiffness of the system, yielding a high tangent modulus. As a result, the wrinkled film/substrate structure has a bilinear stress–strain behavior with an extremely sharp transition point, and an exceptionally high ratio of tangent to elastic modulus, which is particularly valuable as a strategy for constructing strain-limiting materials.

Helical design. Helical microstructures also exhibit the '*J-shaped*' stress–strain behavior [39]. Three-dimensional printing (fused deposition modeling, UV-assisted 3D printing and solvent-cast 3D printing) represents one straightforward approach to helical microstructures.

Kirigami and origami design. Kirigami is an ancient art of paper cutting and folding to form 3D sculptures. For example, in a Kent paper, the plates deform mainly via in-plane buckling at small applied strain, whereas as the applied strain increases, out-of-plane buckling occurs, finally, straightening of the elementary plates in Kent induces an increase in the stiffness, thereby *J-shape* response is obtained [17].

Origami is an ancient art of paper folding that has similar mechanics as those of the wavy and wrinkled structures. At small strain, the parallelogram faces of origami experience negligible strains, so that the entire system has very low stiffness. As the applied strain increases, the folding creases straighten, and the parallelogram faces dominate the stretching such that the structure becomes stiff, which results in 'J-shaped' stress–strain behavior [17].

Molecular design. A recent study has demonstrated that modification of the intrinsic structure of polymers by implementing brush-like chains can deliver strain-stiffening effect at small strains [40]. In contrast to linear-chain networks, where the degree of polymerization of the network strand is the only parameter that determines stress-strain behavior, brush-like networks are defined by three independent structural parameters—the degrees of polymerization of the side chains, of the spacer between neighboring side chains, and of the strand backbone, which allows for precise tuning of mechanical properties.

Textile design. Textiles are flexible materials that consist of networks of natural or artificial yarns, as shown in Figure 2.3f. Weaving and knitting are the most widely used methods for manufacturing textiles. In the weaving process (Figure 2.3f, left), individual perpendicular yarns (warp and weft yarns) interlace together to form the fabric. In the knitting process (Figure 2.3f, middle), the yarns adopt wavy, looped configurations, with the potential to offer large stretchabilities.

2.3 Fiber-reinforced Composites

The definition of a composite material is that it must be made up of at least two distinguishable constituents demonstrating significantly different chemical or physical properties. The combination of these constituents into a composite creates a new material that displays a set of properties different from the individual properties of each of the constituent materials. There are many different composite types, however for the purpose of this thesis we will focus on fiber reinforced composites, due to its similarity to composite structure of natural aorta itself. There are two component materials: matrix and reinforcement. The matrix material surrounds and supports the reinforcement materials by maintaining their relative positions. Reinforcements impart their special mechanical and physical properties to enhance the matrix properties. A synergy produces material properties unavailable from the individual constituent materials [41]. In textile reinforced composites, the reinforcement is a textile material comprised of a network of natural or artificial fibers, typically arranged as tows or yarns [41].

The elastomer matrix. Selection of the constituent materials depends on the desired properties of the final product. The two most common matrix materials for fiber-reinforced composites are thermoplastics and thermosets. Thermoplastics are characterized by high application temperatures, high toughness and ease of repair, but require high processing temperatures and are difficult to handle due to high viscosity. Thermoset matrix materials are characterized by their low viscosity and low processing temperature with drawbacks in application temperature, and toughness. For biomedical applications, elastomers are commonly used due to their nearly instantaneous response to stresses and fully reversible deformation [33]. Particularly, silicone elastomers remain of interest in medical applications because of their recognized biocompatibility [34].

The choice of matrix material for composites mimicking biological systems depends on several criteria, namely tensile strength, maximum elongation (should be close to those of natural tissue) and most importantly, tear resistance. Table 2.1 presents main properties of common silicone rubbers. As seen from Table 2.1, Ecoflex and Shin-Etsu products have high elongation and low tensile strength, which is beneficial to mimic soft materials. In addition, they have higher tear strength compared to commonly used Sylgard 184. Ecoflex 0050 has a highest elongation, low tensile strength and high tear resistance, and thus is a promising candidate for this study.

Table 2.1.Common silicone rubbers and their properties.

Name	Durometer	Tensile Strength	Catalyst / Curing temp.	Elongation	Tear Strength
Nusil MED 4840[1]	43 Type A	8.14 MPa	Platinum / room temp.	590%	43.21 kN/m (ASTM D624)
Nusil MED 4244[2]	40 Type A	5.97 MPa	Platinum / room temp.	350%	26.46 kN/m (ASTM D624)
Dow Corning Sylgard 184[3]	50 A	6.7 MPa	Platinum / 4 hours at 65°C	120%	2.6 kN/m (ASTM D624)
Smooth-On Ecoflex 0030[4]	30	1.38 MPa	Platinum / room temp.	900%	6.7 kN/m (ASTM D624)
Smooth-On Ecoflex 0050[5]	50	2.17 MPa	Platinum / room temp.	980%	8.8 kN/m (ASTM D624)
Shin Etsu 45A & 45B[6]	45	2 Mpa	Platinum/ room temp.	670%	7kN/m (ASTM D624)
Shin Etsu 55A & 55B[7]	55	2.1 Mpa	Platinum/ room temp.	640%	9kN/m (ASTM D624)

FOOTNOTE OF TABLE 2.1

[1] Product information MED-4244 LOW CONSISTENCY SILICONE ELASTOMER
[2] Product information MED-4840 LIQUID SILICONE RUBBER
[3] Product information Dow Corning® 184 silicone
[4] Product information Smooth-On Ecoflex 0030
[5] Product information Smooth-On Ecoflex 0050
[6] Product information Shin Etsu 45A & 45B
[7] Product information Shin Etsu 55A & 55B

The fiber reinforcement. The fibers of the fiber-reinforced composite can be varied in size, shape, length, direction, architecture, and material in order to engineer a composite to the have specific properties. The length of the reinforcing fibers can be whiskers (short/staple) or continuous filament (Figure 2.4), and usually have an ovular or circular cross-sectional shape. Whisker reinforcement fibers are used to create non-woven, non-structural composites. When randomly oriented in the matrix material they create an isotropic composite, while orienting the fibers can give more strength in the orientation direction, generating an anisotropic composite [42]. Using filament fibers makes it possible to engineer the reinforcement architecture. Using more complex reinforcement architectures, such as woven, knit, braided, stitched, and z-pinned, provides more engineering opportunities. The main categories of textile architecture relevant to composite materials are woven, braided, weft-knit and non-crimp (Figure 2.4b) [41].

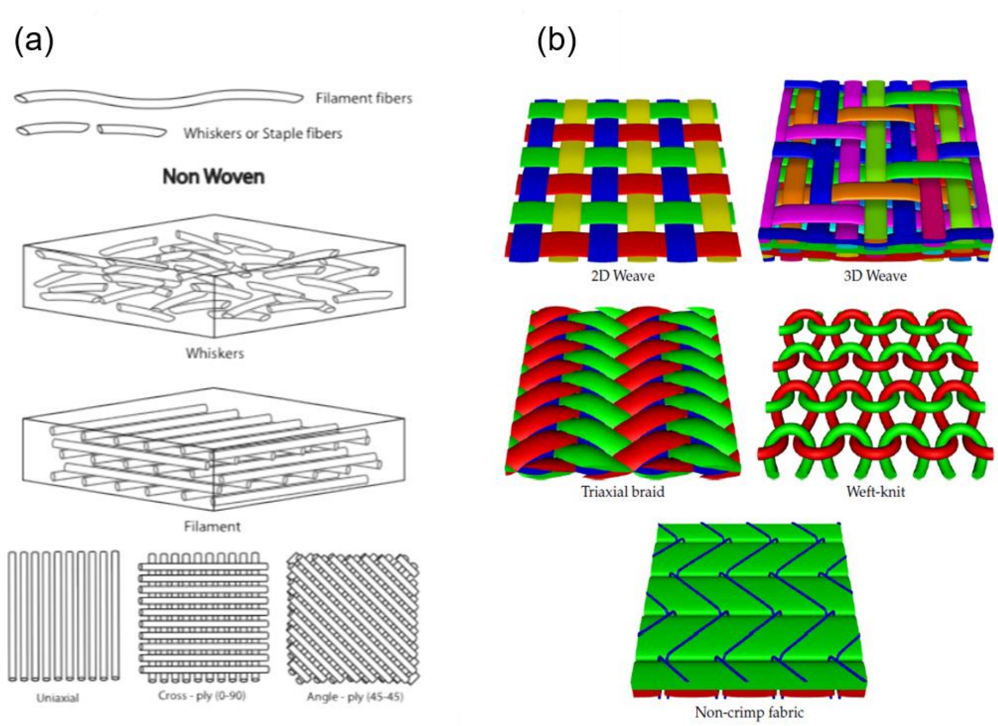

Figure 2.4. Fiber-reinforced composites. (a) Fiber types and non-woven composite. Adapted from [42]. (b) Types of textile architecture. Adapted from [41].

Woven fabrics consist of usually two orthogonal series of yarns, referred to as warp and weft yarns, interlaced to form a self-supporting textile structure. Multilayer woven fabrics, also known as 3D weaves, are composed of several layers of warp and weft yarns woven together [41]. *Braided fabrics* are created by interweaving three or more yarns in a diagonally overlapping pattern. Two types of braided fabrics are widely available, biaxial braids and triaxial braids. The former contains two sets of aligned yarns whereas the latter contains three sets of aligned yarns. Multilayered braided fabrics are also possible and are referred to as 3D braided fabrics. *Weft-knitted fabrics* consist of only one set of weft yarns. Here the yarns are interlaced with adjacent yarns to construct a self-supporting structure. The different interlacing patterns, such as jersey, rib, interlock, lacoste also exist. *Non-crimp fabrics (NCF)* consist of several layers of unidirectional straight yarns that are held together by stitching or knitting of a lightweight thread. Chemical agents may also be used to bond the yarns together [41].

The fiber material is also very important. For biomedical application, biocompatible materials are required, such as cotton, polypropylene, nylon, polyester and others (Figure 2.5). Figure 2.5 also presents a matrix to evaluate a medical textile developed by Atex Technologies [43], that produces implantable textile components for medical devices. It suggests that purpose of design (functional requirement), overall shape of design (dimensional configuration), type and size (material selection) and architecture (woven, knit, braid, non-woven, hybrid) should been taken into acctount when selecting a fiber reinforcement.

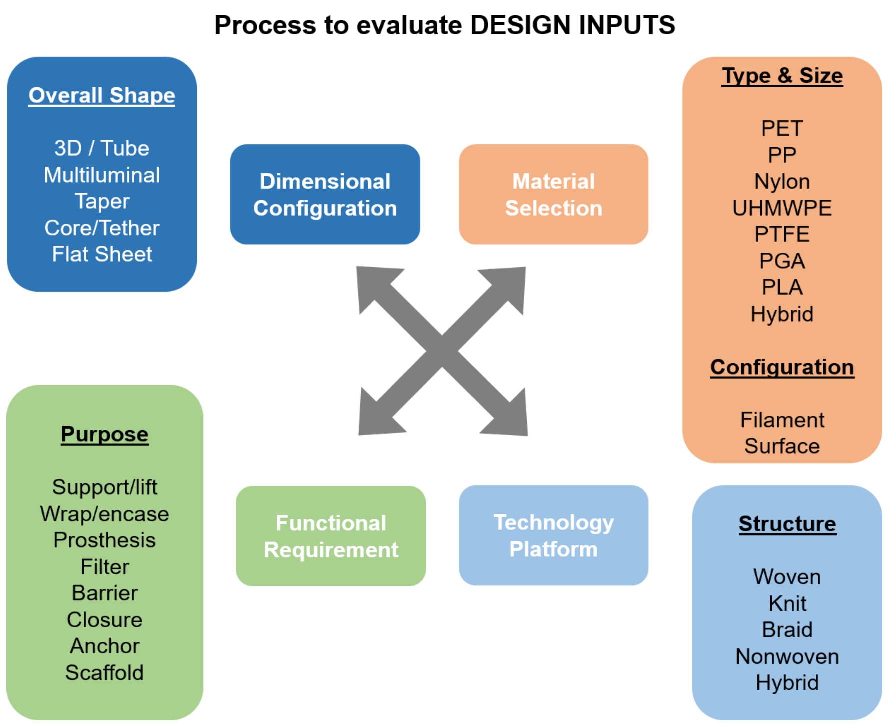

Figure 2.5. Process to evaluate fabric design for medical applications. Adapted from [43].

2.4 Continuum mechanics

2.4.1 Basic definitions

Linear elastic vs hyperelastic. Linear elastic constitutive relations model reversible behavior of a material that is subjected to small strains. Nearly all solid materials can be represented by linear elastic constitutive equations if they are subjected to sufficiently small stresses. Since the strains are small, all the governing equations for linear elastic materials can be linearized and are therefore relatively easy to solve. Linear elasticity theory is thus the best known and most widely used branch of solid mechanics. When loading and unloading a linear elastic material, the stress is driven along the same straight line in the stress-strain characteristic curve (Figure 2.6a).

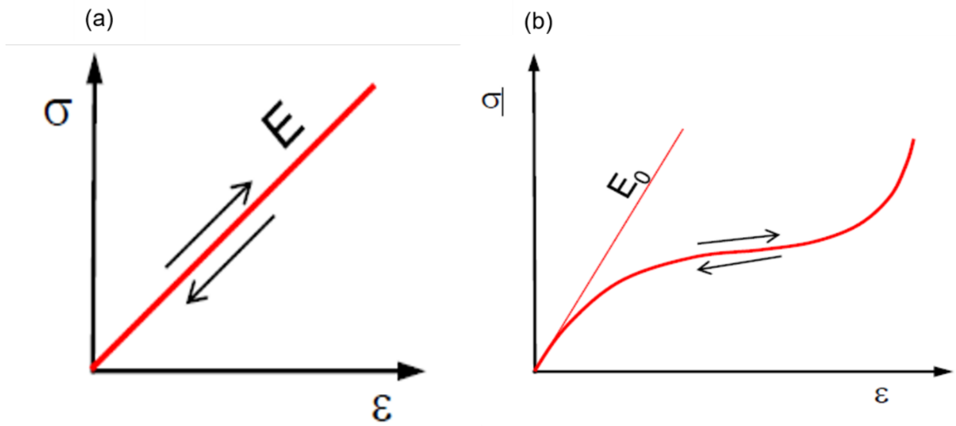

Figure 2.6. Stress-strain curve for a) linear elastic, b) hyperelastic material.

A hyperelastic material is still an elastic material, which means it returns to its original shape after the forces have been removed (Figure 2.6b). The difference to linear elastic material is that in hyperelastic material the stress-strain relationship derives from a strain energy density function, and not a constant factor. Hyperelastic constitutive laws are used to model materials that respond elastically when subjected to very large strains. They account both for nonlinear material behavior and large shape changes. The main applications of the theory are (i) to model the rubbery behavior of a polymeric material, and (ii) to model polymeric foams that can be subjected to large reversible shape changes (e.g. a sponge) [44].

The strain-energy density functions for hyperelastic materials are defined in terms of finite deformation quantities (i.e. Green's strain, invariants of the Cauchy-Green deformation tensor, or principal stretch ratios) [45]. Let's consider an arbitrary line element defined by points P & Q in the undeformed configuration. The same points are defined by P* and Q* in the deformed configuration. Let's denote f, g & h as functions that define the relationship between coordinates in the deformed and undeformed configurations.

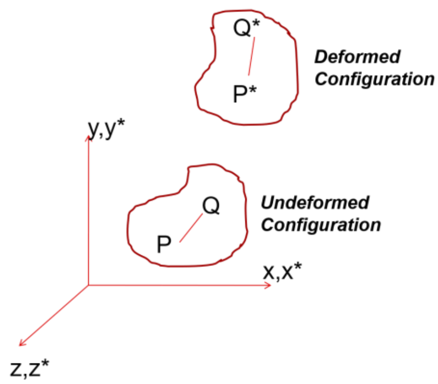

Figure 2.7. Schematic of arbitrary line element defined by points P & Q in the undeformed and deformed configuration.

$$x^* = f(x, y, z)$$

$$y^* = g(x, y, z)$$

$$z^* = h(x, y, z)$$

Finite Deformation Theory: Deformation Gradient. The differential changes in the coordinates of the deformed and undeformed configurations are:

$$dx^* = \frac{\partial f}{\partial x}dx + \frac{\partial f}{\partial y}dy + \frac{\partial f}{\partial z}dz$$

$$dy^* = \frac{\partial g}{\partial x}dx + \frac{\partial g}{\partial y}dy + \frac{\partial g}{\partial z}dz$$

$$dz^* = \frac{\partial h}{\partial x}dx + \frac{\partial h}{\partial y}dy + \frac{\partial h}{\partial z}dz$$

$$\begin{Bmatrix} dx^* \\ dy^* \\ dz^* \end{Bmatrix} = \begin{bmatrix} \frac{\partial f}{\partial x} & \frac{\partial f}{\partial y} & \frac{\partial f}{\partial z} \\ \frac{\partial g}{\partial x} & \frac{\partial g}{\partial y} & \frac{\partial g}{\partial z} \\ \frac{\partial h}{\partial x} & \frac{\partial h}{\partial y} & \frac{\partial h}{\partial z} \end{bmatrix} \begin{Bmatrix} dx \\ dy \\ dz \end{Bmatrix}$$

$$\{dx^*\} = [F]\{dx\}$$

The deformation gradient is defined as:

$$[F] = \begin{bmatrix} \frac{\partial f}{\partial x} & \frac{\partial f}{\partial y} & \frac{\partial f}{\partial z} \\ \frac{\partial g}{\partial x} & \frac{\partial g}{\partial y} & \frac{\partial g}{\partial z} \\ \frac{\partial h}{\partial x} & \frac{\partial h}{\partial y} & \frac{\partial h}{\partial z} \end{bmatrix}$$

Finite Deformation Theory: Stretch Tensor. The Deformation Gradient can be broken down into a product of two matrices.

The matrix *[R]* is an orthogonal rotation matrix, and *[U]* and *[V]* are symmetric matrices that are called the right and left stretch tensors.

$$[F] = [R][U] = [V][R]$$

[U] The Right Stretch Tensor because it appears on the right of the rotation matrix.

[V] The Left Stretch Tensor because it appears on the left of the rotation matrix.

Finite Deformation Theory: Right Cauchy-Green Deformation Tensor

The change in length squared of the line element PQ in the deformed configuration is

$$dS^2 = \{dx^*\}^T\{dx^*\} = \{dx\}^T[F]^T[F]\{dx\}dS^2 = \{dx\}^T[C]\{dx\}$$

Where *[C]* is the right Cauchy-Green deformation tensor given by

$$[C] = [F]^T[F]$$

$$[C] = [U]^T[R]^T[R][U]$$

$$[C] = [U]^T[U] = [U]^2$$

As shown below, the right Cauchy-Green deformation tensor is equal to the square of the right stretch tensor [45]. The square of the principal stretch ratios can be determined by extracting the eigenvalues of the Cauchy-Green deformation tensor.

The square of the principal stretch ratios can be found from the equation:

$$det\begin{bmatrix}(C_{11}-\lambda^2) & C_{12} & C_{13}\\ C_{12} & (C_{22}-\lambda^2) & C_{23}\\ C_{13} & C_{23} & (C_{33}-\lambda^2)\end{bmatrix}=0$$

which results in the characteristic equation [45]

$$(\lambda^2)^3 - I_1(\lambda^2)^2 + I_2(\lambda^2) - I_3 = 0$$

$$I_1 = \lambda_1^2 + \lambda_2^2 + \lambda_3^2$$

$$I_2 = \lambda_1^2\lambda_2^2 + \lambda_2^2\lambda_3^2 + \lambda_3^2\lambda_1^2$$

$$I_3 = \lambda_1^2\lambda_2^2\lambda_3^2$$

2.4.2 Hyperelastic models

A hyperelastic material model relies upon the definition of the strain-energy function, which assumes different forms according to the material or class of materials considered. This function is obtained from symmetry, thermodynamic and energetic considerations [46].

If the material is isotropic, the strain-energy functions (W) depend upon the strain invariants

$$W_{\ isotropic} = W(I_1, I_2, I_3)$$

$$I_1 = W(I_1, I_2, I_3)$$

In this thesis, silicone-rubber is assumed to be incompressible hyperelastic material. The general state of a finite deformation is defined by a second-order tensor, commonly known as gradient of deformation. The deformation tensor in the case of hyperelastic materials subjected to a uniaxial tension is:

$$[F] = \begin{bmatrix} \lambda & 0 & 0 \\ 0 & \dfrac{1}{\sqrt{\lambda}} & 0 \\ 0 & 0 & \dfrac{1}{\sqrt{\lambda}} \end{bmatrix}$$

$$J = \prod_{i=1}^{3} \lambda_i = det(F) = 1$$

The Right and Left Cauchy–Green tensors can be obtained from Equation (20):

$$[c] = [F]^T[F] = \begin{bmatrix} \lambda^2 & 0 & 0 \\ 0 & \lambda^{-1} & 0 \\ 0 & 0 & \lambda^{-1} \end{bmatrix}$$

Neo–Hookean model. Neo–Hookean model was established by the study of vulcanized rubber, using a statistical theory. In this approach, vulcanized rubber is seen as a three-dimensional network of long chain molecules that are connected at a few points:

$$W = c_1(I_1 - 3)$$

The constant c_1 allows us to know the shear modulus by the relation $\mu=2c_1$.

Mooney-Rivlin model. The importance of this model is well known, not only for historical reasons, as it was one of the first hyperelastic models, but also because of its high accuracy in predicting the nonlinear behaviour of isotropic rubber-like materials. For the incompressible material, it can be simplified as:

$$W = \sum_{i=1}^{2} c_i\,(I_i - 3)$$

Yeoh model. The Yeoh material model for incompressible (rubberlike) materials was presented for the first time in 1990. The strain-energy function that characterizes this model depends only on the first strain invariant (I_1):

$$W = \sum_{i=1}^{3} c_i \, (I_1 - 3)^i$$

The material constants c_1, c_2 and c_3 are the parameters to fit.

Ogden model. This model, due to Ogden's phenomenological theory of elasticity, [47] has the general form:

$$W = \sum_{i=1}^{N} \frac{\mu_i}{\alpha_i} ({\lambda_1}^{\alpha_i} + {\lambda_2}^{\alpha_i} + {\lambda_3}^{\alpha_i} - 3)$$

Sufficiently good convergence between theoretical and experimental results for rubber are achieved when $N=3$ [21].

Gent model. The strain energy per unit volume in the has the form:

$$W = -\frac{\mu J_{lim}}{2} ln\left(1 - \frac{I_1 - 3}{J_{lim}}\right)$$

where μ is the shear modulus, J_{lim} is the stretch limit of the elastomer, and I_1 is the 1st strain tensor invariant.

2.4.3 Composite theory: Holzapfel-Gasser-Ogden (HGO) model

Since arteries are composed of thick-walled layers, each of these layers is modeled with a separate strain-energy function. From the engineering point of view each layer may be considered as a composite reinforced by two families of (collagen) fibers which are arranged in symmetrical spirals. The model is based on the theory of the mechanics of fiber-reinforced composites [48] and embodies the symmetries of a cylindrically orthotropic material (Figure 2.8) [21]. It is assumed that each layer responds with similar mechanical characteristics and we therefore use the same form of strain-energy function (but a different set of material parameters) for each layer. It was suggested to split the isochoric strain-energy function W into a part W_{iso} associated with isotropic deformations and a part W_{aniso} associated with anisotropic deformations [29], [49]. Since the (wavy) collagen fibers of arterial walls are not active at low pressures (they do not store strain energy), W_{iso} is associated with the mechanical response of the non-collagenous matrix material, which is assumed to be isotropic. The resistance to stretch at high pressures is almost entirely due to collagenous fibers [49] and this mechanical response is therefore taken to be governed by the anisotropic function $W_{aniso.}$ Hence, the (two-term) potential is written as

$$W = W_{iso}(I_1) + W_{aniso}(I_4, I_6)$$

Note that the invariants I_4 and I_6 are stretch measures for the two families of (collagen) fibers and therefore have a clear physical interpretation. The anisotropy then arises only through the invariants I_4 and I_6, but this is sufficiently general to capture the typical features of arterial response.

Finally, the two contributions W_{iso} and W_{aniso} to the function W must be particularized so as to fit the material parameters to the experimentally observed response of the arterial layers. The (classical) neo-Hookean model is used to determine the isotropic response in each layer:

$$W_{iso}(I_1) = \frac{c}{2}(I_1 - 3)$$

where $c > 0$ is a stress-like material parameter. The strong stiffening effect of each layer observed at high pressures motivates the use of an exponential function for the description of the strain energy stored in the collagen fibers, and for this:

$$W_{aniso}(I_4, I_6) = \frac{k_1}{2k_2} \sum_{i=4,6} \{exp[k_2(I_i - 1)^2] - 1\}$$

where $k_1 > 0$ is a stress-like material parameter and $k_2 > 0$ is a dimensionless parameter. An appropriate choice of k_1 and k_2 enables the histologically based assumption that the collagen fibers do not influence the mechanical response of the artery in the low-pressure domain [49] to be modeled.

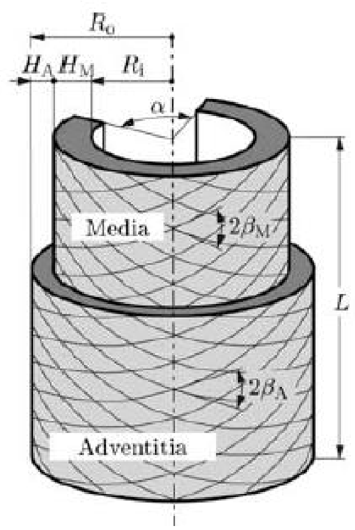

	Material	Geometry
Media	$c_M = 3.0000$ [kPa] $k_{1M} = 2.3632$ [kPa] $k_{2M} = 0.8393$ [–]	$H_M = 0.26$ [mm] $\beta_M = 29.0°$
Adventitia	$c_A = 0.3000$ [kPa] $k_{1A} = 0.5620$ [kPa] $k_{2A} = 0.7112$ [–]	$H_A = 0.13$ [mm] $\beta_A = 62.0°$

$R_i = 0.71$ [mm]	for	$\alpha =$	$0.0°$
$R_i = 1.43$ [mm]	for	$\alpha =$	$160.0°$

Figure 2.8. Demonstration of the two-layer arterial wall model and material and geometrical data for a carotid artery from rabbit. Reproduced with permission from [21].

2.5 Metamaterial definitions

Metamaterials are carefully structured materials that are composed of periodically arranged building blocks and display properties superior to their constituent materials. In the past two decades, metamaterials have been utilized to manipulate optical, acoustic and thermal fields to obtain unusual properties, such as a negative refraction index and resulted in new applications, such as perfect lenses [30].

Mechanical metamaterials represent a new branch of metamaterials research, where motion, deformations, stresses and mechanical energy are investigated. The meta-atoms, building blocks of mechanical metamaterials, deform, rotate, buckle, fold and snap in response to applied mechanical forces and are designed to act together to yield a desired collective behavior. The basic elements of meta-atoms and metamaterials are slender elements that enable very strong stiffness heterogeneities, shape morphing, topological protection, instabilities and nonlinear responses to obtain advanced functionalities. An example of mechanical metamaterials is auxetic materials, which either expand or contract in all directions when a force is applied and illustrate how structure controls the behavior of metamaterials [30].

2.5.1 Poisson ratio and auxetic materials

Poisson's ratio, denoted by the Greek letter ν and named after Siméon Poisson, is the negative of the ratio of (signed) transverse strain to (signed) axial strain [50]. For small values of these changes, ν is the amount of transversal expansion divided by the amount of axial compression [50].

$$\nu = -\frac{\varepsilon_{\mathrm{lateral}}}{\varepsilon_{\mathrm{axial}}}$$

The Poisson's ratio of a stable, isotropic, linear elastic material must be between −1.0 and +0.5 because of the requirement for Young's modulus, the shear modulus and bulk modulus to have positive values [51]. Most materials have Poisson's ratio values ranging between 0.0 and 0.5 (Table 2.2). A perfectly incompressible isotropic material deformed elastically at small strains would have a Poisson's ratio of exactly 0.5. Most steels and rigid polymers when used within their design limits (before yield) exhibit values of about 0.3, increasing to 0.5 for post-yield deformation which occurs largely at constant volume [52]. Rubber has a Poisson ratio of nearly 0.5. Cork's Poisson ratio is close to 0, showing very little lateral expansion when compressed. Some materials, e.g. some polymer foams, origami folds, and certain cells can exhibit negative Poisson's ratio, and are referred to as auxetic materials (Figure 2.9) [50]. The factors that give rise to auxetic behavior include co-operation between the material’s internal structure (geometry), the way the internal structure deforms when loaded (deformation mechanism) (Figure 2.9c).

Table 2.2. Common values of Poisson ratio for different materials. Adapted from [50].

Material	Poisson’s ratio
Rubbers	0.5
Lead	0.45
Aluminum	0.33
Common steels	0.27
Cellular solids, such as polymer foams	0.1-0.4
Cork	0.0

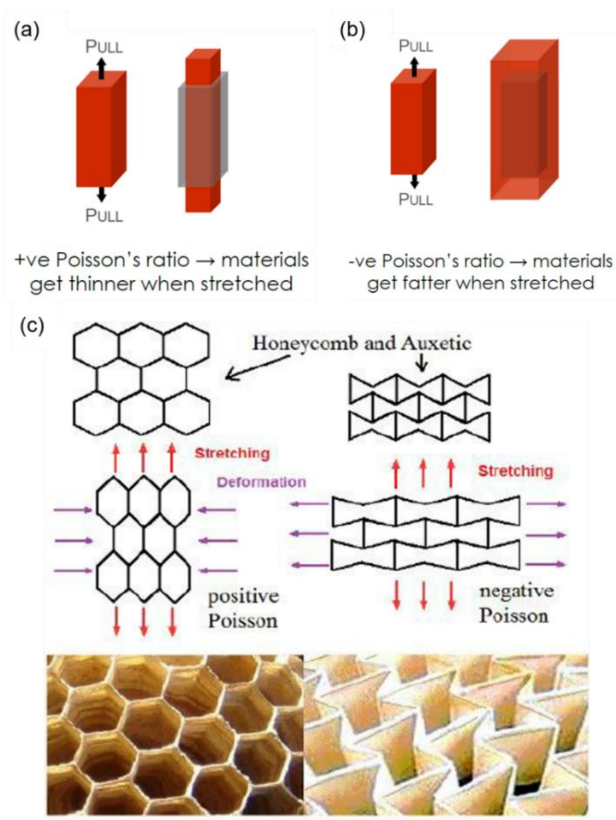

Figure 2.9. Poisson ratio of materials. a) Positive ν>0, b) negative ν<0. Adapted from [50]. c) Comparison of the honeycomb and auxetic structures when stretched. Adapted from [53].

2.5.2 Ways to design metamaterials

Linear mechanical metamaterials. While isotropic materials are identified by two elastic coefficients, such as the Poisson's ratio and Young's modulus, for anisotropic materials the elasticity tensor can contain up to 21 independent coefficients, offering a large room for mechanical metamaterials design. In 1995, Milton and Cherkaev showed that architectures consisting of ordinary elastic materials and vacuum can be used to develop metamaterials with any form of elasticity tensor allowed by thermodynamics [30]. By layering different extremal materials, metamaterials with any desired elasticity tensor can be created. Thus, bulk elastic properties of metamaterials are dependent on the geometry of network, which allows for architecting different networks with complex mechanical behavior [30].

Mechanism-based metamaterials. Mechanisms are defined as collections of rigid elements connected with flexible hinges that accept zero-energy, free motion geometrical design, such as levers, pulleys, linkages and gears. Mechanisms are also used to build mechanical metamaterials (Figure 2.10). For instance, a collection of squares connected at their tips form an auxetic structure, that uniformly contract or expand when they experience a free hinging motion (Figure 2.10a). Plates linked by flexible hinges form shape-shifting and programmable origami metamaterials (Figure 2.10b). An asymmetric mechanism comprised of linked bars that enables motions to propagate from the right edge to the left edge but not in the opposite direction is an example of a topological mechanical metamaterial (Figure 2.10c). The geometric design of mechanisms can also be used to create soft mechanism-based metamaterials with slender, flexible parts as hinges, linking stiffer elements that can easily rotate. These soft metamaterials can be stimulated by external forces and undergo programmable shape shifting, ranging from 2D and 3D auxetic materials to size-morphing spheres that can be used as reversible encapsulation systems [30].

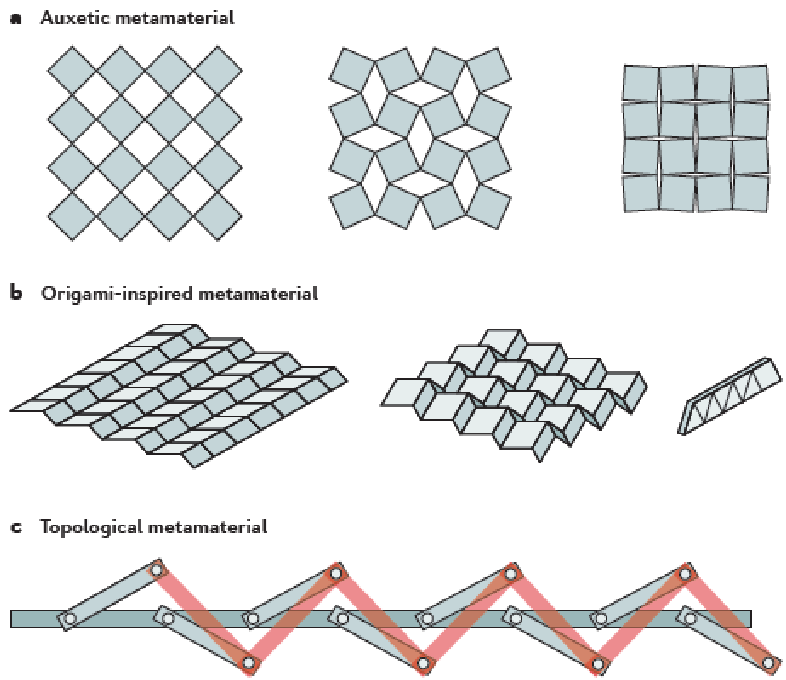

Figure 2.10. Mechanism-based metamaterials: a) a collection of squares linked at their tips can undergo a volume-changing shape transformation, b) rigid plates linked by flexible hinges are the basis of origami metamaterials, c) flexibly linked, rigid bars form a topologically polarized mechanism. Reproduced with permission from [30].

Instability-based metamaterials. Various mechanical metamaterials made of meta-atoms can give access to strongly nonlinear relations derived from elastic instabilities and large deformations.

Buckling-based instabilities. The mechanical properties of highly porous materials made of networks of beams rely on both the deformation mechanism of the ligaments that undergo buckling under compression at relatively low strains, and on their microscopic geometry. Buckling in metamaterials containing regular arrays of elastic beams, can cause striking homogeneous and reversible pattern transformations. For instance, in a metamaterial composed of square array of circular holes embedded in an elastomeric sheet, buckling of the beam-like ligaments induces a transformation of the holes into a periodic pattern of alternating and mutually orthogonal ellipses upon uniaxial compression (Figure 2.11a) [30].

Snapping-based instabilities. Elastic beams can snap between two different stable configurations and keep their deformed shape after unloading [54], [55] These bistable elastic beams have been recently used to develop fully elastic and reusable energy-trapping metamaterials that trap in energy provided to the system during loading (Figure 2.11b). A metamaterial composed of snapping units (two curved parallel beams that are centrally clamped) can also undergo a large extension under tension caused by sequential snap-through instabilities [56].

Frustrated and programmable instabilities. Multistable and programmable metamaterials can be obtained through controlled frustration. For instance, a programmable stiffness can be achieved by 'popping through' some of the origami folds (Figure 2.11c) [57]. For frustration-free operation in beam networks, all elastic elements should buckle into the most energy-favored configuration (a half sinusoid), while maintaining the angles with their neighbors to minimize the deformation energy. In 2D, this requirement can be easily met for a square lattice, but not for a triangular lattice, thus triangular system becomes frustrated and favors the formation of complex ordered patterns (Figure 2.11d) [58].

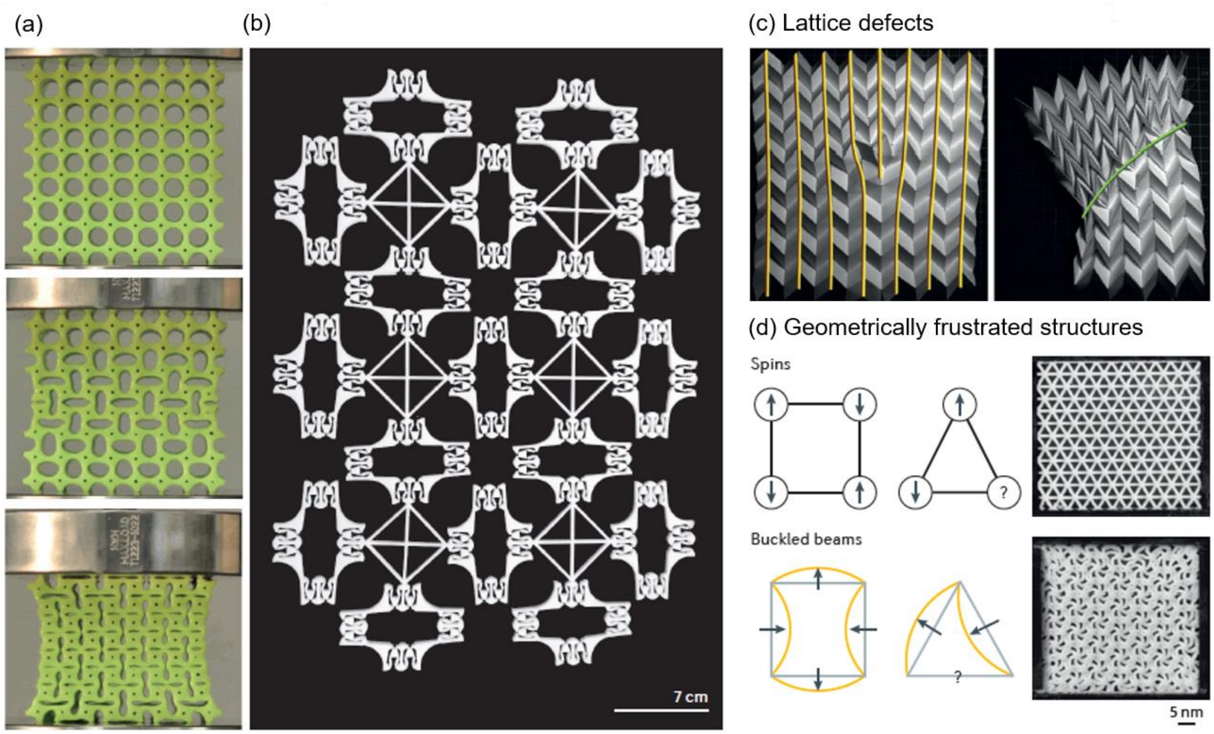

Figure 2.11. Instability-based metamaterials: a) a rubber slab patterned with circular holes undergoes a reversible pattern transformation when compressed as a result of a collective buckling-like instability, b) a metamaterial containing complex hinge units that provide multiple kinematic degrees of freedom and multistability. Frustration and tunable metamaterials: c) by locally 'popping through' the Miura-ori pattern, the compressive modulus of the overall structure can be rationally and reversibly tuned, d) in geometrically frustrated cellular structures, buckling triggered under equibiaxial compression results in the formation of complex ordered patterns. Reproduced with permission from [30].

Topological metamaterials. Topological mechanical metamaterials exhibit topologically protected properties that are not affected by deformations of the underlying geometry or by the presence of disorder [30]. Hence, topological metamaterials have a great potential in designing materials with robust functionalities. Examples of topological metamaterials are presented in Figure 2.12.

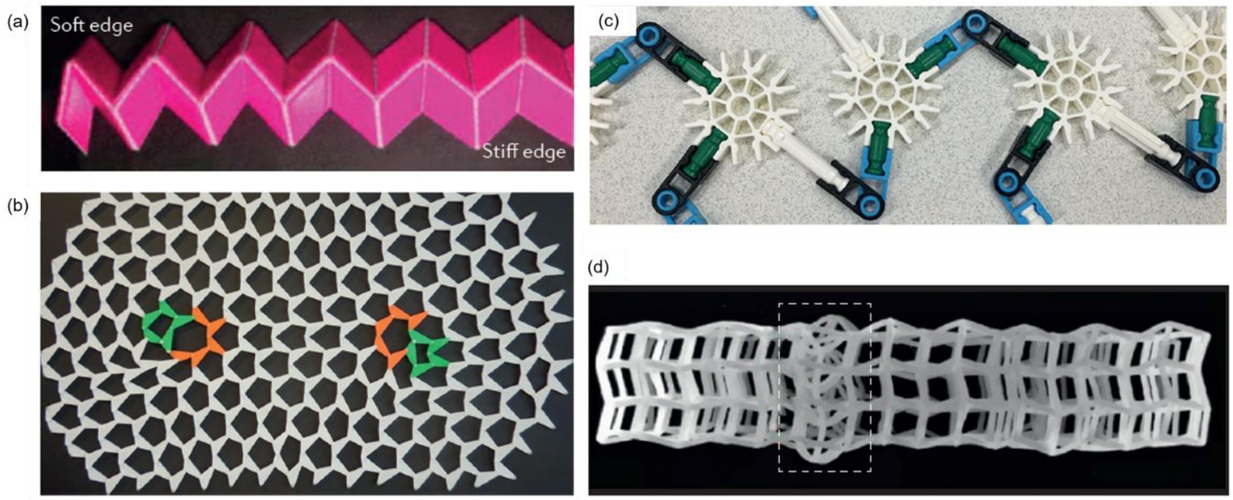

Figure 2.12. Topological mechanical metamaterials: a) Topological origami, b) zero mode localized at a dislocation on the left of the topological metamaterial and corresponding state of self-stress localized at a dislocation on the right, c) detail of a metamaterial that can switch its topological polarization51, d) Topological state of self-stress localized at a domain wall, under compression, stresses concentrate here, leading to selective buckling. Reproduced with permission from [30].

Challenges in metamaterial design. Although latest advancements in additive manufacturing and computational design have driven research in mechanical metamaterials, metamaterial design faces some challenges discussed further. One of the potential problems includes that large metamaterial structures are unexplored, and current research mostly focuses on small, pristine structures. Larger samples may include defects, gradients, domain walls or grain boundaries which will affect the material behavior [59]. Another challenge for metamaterial design is architecting aperiodic structures, which may create a wide variety of controllable spatial features, such as metamaterials that can morph into a distinct number of predefined shapes [30]. Moreover, metamaterial fabrication mostly relies on additive manufacturing techniques, such as 3D printing, laser cutting and two-photon lithography, which suffer from limitation of base material selection.

Expanding the material library and enabling mixing of multiple (contrasting) materials as well inclusion of materials with specific functionalities (opto-mechanical, thermo-mechanical or electro-mechanical) could lead to new classes of mechanical meta-behaviors [30]. Furthermore, translation of metamaterial concepts to smaller scales, for instance, by combining graphene origami, colloidal self-assembly and even chemistry to create designer materials sculpted over a wide range of scales should be further explored [30]. Metamaterial functionalities could be combined with motors and external fields to create robotic structures and smart metamaterials. Lastly, tailoring metamaterial structures so far has been intuitive and precise design of metamaterials with a target property remains a challenge to overcome.

2.5.3 Beam mechanics theories

Beam theories. Highly slender fiber-like or rod-like components represent essential constituents of mechanical systems in countless fields of application and scientific disciplines such as civil, mechanical and biomedical engineering, material science and bio- or molecular physics. Examples are high-tensile industrial webbings, fiber-reinforced composite materials, fibrous materials with tailored porosity, synthetic polymer materials or also cellulose fibers. Often, these slender components can be modeled as 1D Cosserat continuum based on a geometrically nonlinear beam theory. In all mentioned cases, mechanical contact interaction significantly affects the overall system behavior. Most geometrically exact beam element formulations available in the literature are based on the Simo–Reissner theory of thick rods. Alternatively, Kirchhoff–Love theory of thin rods can be used to describe beam mechanics [60]. Meier and co-workers made a detailed review and careful evaluation of Kirchhoff–love theory and Simo–Reissner theory for slender beams [60]. They classified geometrical beam theories with respect to deformation modes (axial tension, shear, torsion and bending), cross-section shapes (isotropic, identical moments of inertia of area $I_2 = I_3$

and anisotropic, different moments of inertia of area $I_2 \neq I_3$) and arbitrary initial curvatures ($\kappa_0 \neq 0$). An overview of these different beam models and theories is given in Table 2.3.

Table 2.3. Different (geometrically exact) beam models **κ** and theories. Adapted from [60].

Name	Theory	$\kappa \neq 0$	$I_2 \neq I_3$	Tension	Shear	Torsion	Bending
Simo-Reissner	Nonlinear	+	+	+	+	+	+
(Anisotropic) Kirchhoff - Love	Nonlinear	+	+	+	-	+	+
Straight Kirchhoff - Love	Nonlinear	-	+	+	-	+	+
Isotropic Kirchhoff - Love	Nonlinear	-	-	+	-	+	+
Torsion-free Simo-Reissner	Nonlinear	-	-	+	+	-	+
Torsion-free Kirchhoff - Love	Nonlinear	-	-	+	-	-	+
Timoshenko	Linear	-	+	+	+	+	+
Euler- Bernoulli	Linear	-	+	+	-	+	+

Qiu et al. [61] has developed a model for a single initially curved beam without any mode imperfection, was extended to allow the presence of a mode shape imperfection based on Euler–Bernoulli beam theory. The design of the curved-beam bistable mechanism is inspired from bistable buckled straight-beam mechanisms, where a straight beam is axially compressed to buckle to stable positions at either side. Modeling buckling modes of the latter mechanism is critical to modeling the curved-beam mechanism.

Che K et al. has developed a model to describe multistable mechanical metamaterials are materials that have multiple stable configurations. The geometrical changes caused by the transition of the metamaterial from one stable state to another, could be exploited to obtain multifunctional and programmable materials. As the stimulus amplitude is varied, a multistable metamaterial goes through a sequence of stable configurations [62].

Soft spring theory. Rafsanjani et al. [56] has developed a soft spring model to describe the behavior of snapping double curved beams under tension. The mechanism stores the elastic strain energy via three connected elastic springs with constants k_1 and k_2 (Figure 2.13). The springs are initially unstressed, and their free ends are connected to the walls by joints, which allow rotation and restrain translation. The inclined springs (k_1) stand for the stiffness of the snapping segments, whereas the vertical spring (k_2) represents the interaction of the snapping segments with the rest of the structure. The geometry of this mechanism is characterized by the parameters l and a, qualitatively equivalent to the parameters l and a of the metamaterial shown in Figure 1b. The soft spring mechanism suggests that the interaction of the snapping segments with the rest of the structure can lead to mechanical responses with specific characteristics including incremental positive, zero or negative stiffness.

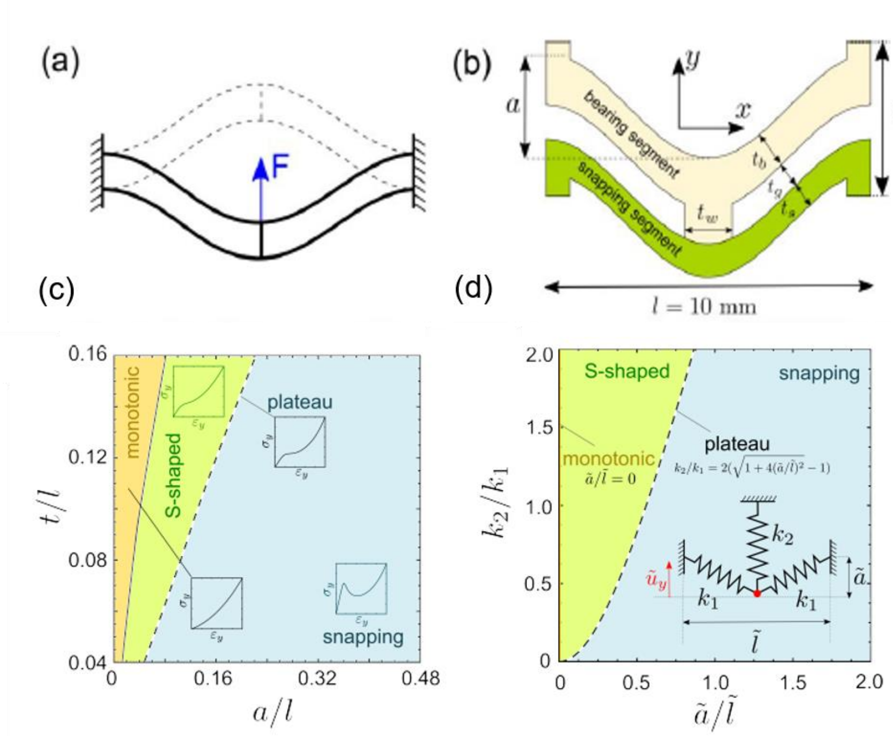

Figure 2.13. (a) Bistable mechanism of double curved beams which can snap between two stable configurations, under a vertical force applied in the middle, (b) Unit cell geometry of the designed metamaterial composed of load bearing and snapping segments, Phase diagrams for mechanical responses of (c) unit cells under uniaxial extension in the parameter space (a/l, t/l), (d) for a single degree of freedom soft spring mechanism in the parameter space (k_2/k_1, a/l) showing monotonic, S-shaped and snapping responses and the plateau region. Reproduced with permission from [56].

3 Fabric-reinforced elastomer composites: Mimicking '*J-shaped*' and anisotropic stress-strain behavior of human and porcine aorta

3.1 Introduction

The rapid strain stiffening of the human aorta, termed the *J-shaped* stress-strain behavior, [12] allows continuous blood flow by the generation of the Windkessel effect. The Windkessel effect of the aorta constitutes of the following processes. During systole, blood is pumped into the aorta, where half of the blood is distributed towards peripheral circulation while the other half remains stored in the aorta until diastole where it is released for peripheral circulation [9]. The aorta stores half of the blood because it experiences elastic extension (strain). As it becomes stiffer due to an increase in the strain as a result of systole (strain-stiffening), the internal stress of the strained aorta releases the stored half of the blood in a gradual manner during diastole [9]. In addition to storing blood temporarily and smoothing pulsatile flow, the aorta must withstand a wide range of pressures, as well as a large level of deformation [12]. The *J-shaped* strain-stiffening response is the key defensive strategy in highly expansive pressure vessels in biological systems against critical damage, such as aneurysm and disruption that lead to stroke [12], [63]. Consequently, the strain-stiffening phenomenon is an essential property of the simulated aorta to mimic the real aorta.

As *J-shaped* stress-strain behavior is a common property for many soft biological tissues, such as skeletal and cardiac muscles, ureter, taenia coli, arteries, veins, pericardium, mesentery, bile duct, skin, tendon, elastin, cartilage, and other tissues [64], [40]. There have been numerous attempts to reproduce the *J-shape* in synthetic materials. One strategy to achieve this property is to employ semiflexible biopolymers with stiff architectures, such as microtubules, actin, intermediate filaments, collagen, and synthetic proteins [63]. Synthetic hydrogels are often designed to have the

J-shape. Frank and co-workers [65] demonstrated the use of interpenetrating networks of hydrogels while Zeng and co-workers [63] have shown the use of a flexible self-healing network of hydrogels to achieve strain-stiffening. Synthetic elastomers have strain-stiffening behavior as an intrinsic property. But, such effects occur at only extreme strain levels, being stretched to a few times longer than the original dimension, whereas biologically relevant *J-shaped* stiffening happens at a few tens of percents [36]. A recent study has demonstrated that grafting thick comb-like side chains allows the strain-stiffening in a single elastomer material as its intrinsic property [40]. Introducing corrugations of higher dimension, such as wavy and wrinkled 2-D sheets and helically coiled 1-D wires, or judicially designed relief patterns, such as open networks, kirigami/origami geometries, and knitted/woven fabric structure, are also suggested to achieve the *J-shape* [17]. Despite the recent progress, developing a practical synthetic material that mimics natural aorta with operational stability has remained a challenge.

In addition to its *J-shaped* stress-strain behavior, human aorta is also known to have significant anisotropy [13], [14]. Here, higher stiffness in the longitudinal direction prevents excessive stimulation of the anastomotic regions, while compliance in the circumferential direction prevents flow disturbance [15]. Hence, anisotropy is another property of natural aorta that synthetic materials often lack and is important to mimic.

In order to design a vascular replacement with the *J-shaped* and anisotropic mechanical properties, it is critical to understand the underlying mechanism of these properties. The aorta has a composite structure and thus its nonlinear properties come from the combination of both elastic and stiff fibrous components. The main structural components of the arterial wall are elastin and collagen, elastin is a rubber-like protein with a modulus of 0.6–1 MPa, whereas collagen is stiff and relatively inextensible with a modulus of around 1 GPa [16]. Both elastin and collagen appear as wavy and crimped strands, thus the resulting structure is easy to accommodate a low level of strain [12], [17]. The initial low modulus response at low strain is attributed to elastic elastin fibers, while the stiffening at the higher strains is due to progressive straightening of elastin and collagen fibers [16]. Anisotropy mainly arises from the orientation of collagen fibers in the arterial wall [18].Healthy arterial wall constitutes of three main layers: intima (inner layer), media (middle layer), and adventitia (outer layer) [19]. The collagen fibrils in media, for example, are arranged in helical structures and are mostly circumferentially oriented. This structured arrangement allows media to resist high loads in the circumferential direction [19].

As the aorta itself is a composite structure of rubber-like and fiber-like constituents, it is intuitive to develop a fabric-reinforced composite to mimic its properties. Grande-Allen and co-workers [66] developed a composite scaffold from electrospun polyurethane fibers and PEG hydrogel to mimic the tensile strength, anisotropy, and extensibility of natural aortic valve. Haj-Ali and co-workers prepared collagen-fiber reinforced alginate hydrogel composites with hyperelastic behavior similar to soft tissue [67]. Bailly and co-workers performed a fundamental study about the mechanical effect of fabric-reinforcement by using a custom-designed jig to precisely control the density and angle of the fibers [68]. Employing knitted or woven textiles, wherein the density and the angle between yarns are precisely defined, can be a simpler and more practical approach to achieve the *J-shape* and anisotropy in the stress-strain behavior of the composite elastomer. In addition, textiles have been employed for medical uses since early ages in wound care applications, such as sutures and wound dressings. Textiles have been widely utilized in cardiovascular implants, which are used to replace/repair diseased arteries [18]. Their suitableness for medical purposes results from their structural and design flexibility, which can be modified to conform to the desired mechanical behavior (elasticity, strength, stiffness, fluid permeability) similar to that of biological tissue.

The first step for mechanical property mimicry is to measure precise properties from the actual human aorta. Porcine aorta has been examined as a model material because it is easier to access samples while their properties are expected to be similar to human. Karimi and co-workers determined the maximum stress and the linear elastic properties of the human umbilical vein and artery from uniaxial stress-strain curves [69]. Tseng and co-workers characterized the linear elastic properties of the porcine ascending aorta and aortic sinuses by subjecting them to equi-biaxial stretch testing [70]. In this study, the aortic specimens were subjected to uniaxial tensile testing to quantify nonlinear and anisotropic behavior.

The scope of this study is (i) to measure stress-strain behavior of the human and porcine aortas, (ii) to design and fabricate the fabric-reinforced elastomers that mimic the mechanical properties of the human and porcine aortas, and (iii) to develop analytical models to describe the mechanical properties of the aortas and the fabric-reinforced elastomers. Firstly, the *J-shaped* stress-strain behaviors were measured by the uniaxial tensile test for five different regions in the porcine aorta. Comparing the longitudinal direction as opposed to the circumferential direction showed an anisotropy in the mechanical property. Secondly, commercially available fabrics and elastomers were tested to find the most suitable combination to mimic the *J-shaped* and anisotropic mechanical properties of aortas. Thirdly, Gent's and Mooney-Rivlin hyperelasticity models were combined with Holzapfel–Gasser–Ogden model to take account of low modulus and its gradual stiffening at low strains and rapid stiffening at high strains.

3.2 Materials and methods

3.2.1 Materials

Phosphate buffered saline solution, Ethyl 2-cyanoacrylate, 1,6-Hexanediol diacrylate, Benzoyl peroxide (reagent grade), Poly(ethylene glycol) ($M_n=400$) were purchased from Sigma Aldrich, Canada. Ecoflex 0050 was purchased from Smooth-On, Inc. Sylgard 184 (Dow Corning) was purchased from Electron Microscopy Sciences (EMS). Shin-Etsu SES22330 10, 20 were purchased from Shin-Etsu Chemical Co. VHB 4910 was purchased Digi-Key Co. All fabrics (Telio, Montreal, CA) were purchased from local store Marshall's Fabrics.

3.2.2 Fabrication

Human and porcine aortic specimen preparation. The descending thoracic portion of the porcine aorta, which sits in the posterior mediastinum between the lungs and is anterior to the spine, was extracted from fourteen female pigs. The animal and human experiments were performed in compliance with the guidelines of the Canadian Council on Animal Care and the guide for the care and use of laboratory animals. The protocols were approved by the institutional animal care committee of the University of Alberta, protocol #AUP00000943. The lack of readily available human aortas resulted in the use of porcine aortas as a substitution in this study. However, there was one sample of the descending thoracic portion of the human aorta available. Upon extraction, the porcine (and human) aortic specimens were placed in 1× (standard) phosphate-buffered saline and stored at 4 °C for up to twelve hours before being subjected to uniaxial tensile testing. The aortic specimens were generally cut into five sections using a straight flat razor blade. The inferior, middle, and superior sections were obtained in the circumferential direction, whereas the low and high sections were obtained in the longitudinal direction. All aortic specimens were independent of one another, being harvested and tested on separate days by the same experimenters.

Elastomeric material preparation. Several elastomeric materials were fabricated with the use of the silicones Sylgard 184, Shin-Etsu SES22330 10, Ecoflex 0050 as well as the acrylic elastomer 3M VHB 4910. Sylgard 184 consists of a base and a curing agent. While 10:1 ratio is a standard from the manufacturer, softer Sylgard 184 can also be produced by decreasing the relative content of the curing agent. Shin-Etsu SES22330 10, Shin-Etsu SES22330 20 and Ecoflex 0050 are room temperature vulcanizing (RTV) silicones and have two components that are typically mixed in a 1:1 ratio. Blended silicone mixtures between the Sylgard 184 (8:1) and Shin-Etsu SES22330 20 (1:1) were also tested for various ratios between the two, 9:1, 8:2, 7:3, 6:4, 1:1, 4:6, 3:7, and 2:8.

The VHB 4910 acrylic elastomer was received as a solid tape form and was modified to become significantly stiffer. Here, a polymerizable and crosslinkable monomer, 1,6-hexanediol diacrylate was added to pre-strained VHB 4910 in varying weight percentages to increase its stiffness [71].Benzoyl peroxide was also prepared so that it could be used as a thermal initiator, and this was done by dissolving it in a 1:9 ratio of deionized water and polyethylene glycol 400. The additive, 1,6-hexanediol diacrylate was subsequently added to the dissolved benzoyl peroxide in a 1:1 ratio, and the entire mixture was applied to both sides of the VHB 4910 acrylic elastomer, which was stretched to 100% equibiaxial strain using a 3D printed rigid frame.

Fabric-elastomer composite preparation. Ecoflex 0050, which is RTV silicone, was selected as a matrix material for all composites in our study. Ecoflex 0050 has low stiffness, which meets the modulus of the aorta at very low strains, as well as large extensibility up to 1000% and high tear resistance. Four fabrics, including 93%-rayon/7%-spandex, 90%-polyester/35%-spandex blend, 85%-nylon/15%-spandex and 80%-nylon/20%-spandex were used to prepare fabric/elastomers composites. The fabrics (Telio, Montreal, CA) were purchased from local store Marshall's Fabrics (Figure 3.1d). The stress-strain properties of fabrics and their respective composites are shown in Figure 3.2.

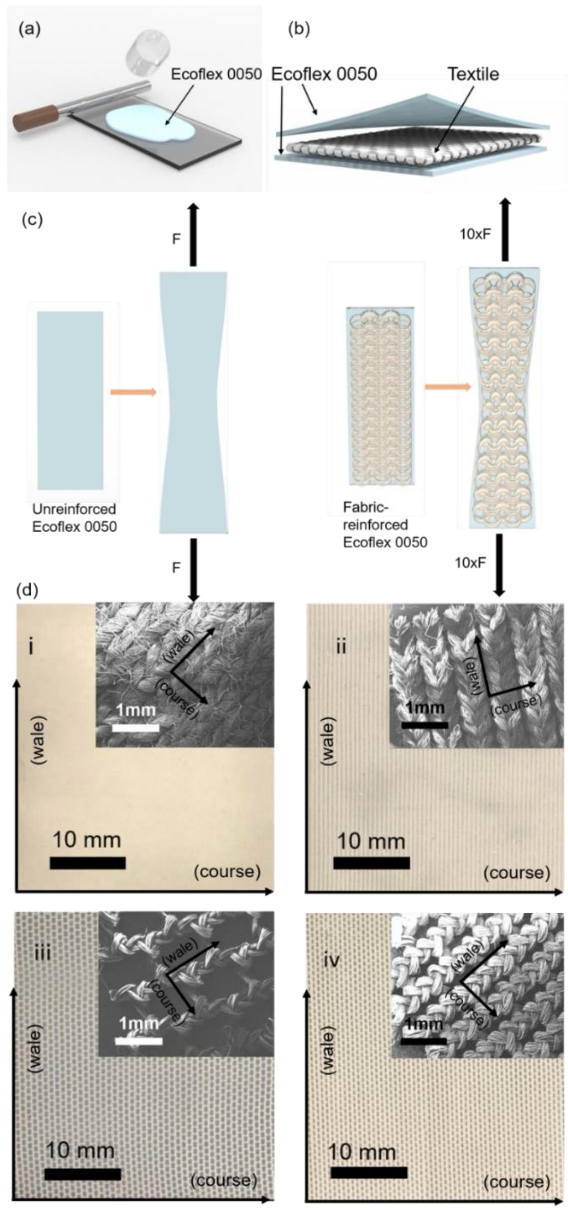

Figure 3.1. Sample preparation: a) schematic diagram of composite sample preparation and b) composite structure, c) schematic illustration about the general effect of fabric reinforcement on uniaxial strain of unreinforced and fabric-reinforced elastomer and d) optical microscopy images of fabricated composites: i) rayon/spandex, ii) polyester/spandex, iii) nylon/spandex 85/15, iv) nylon/spandex 80/20.

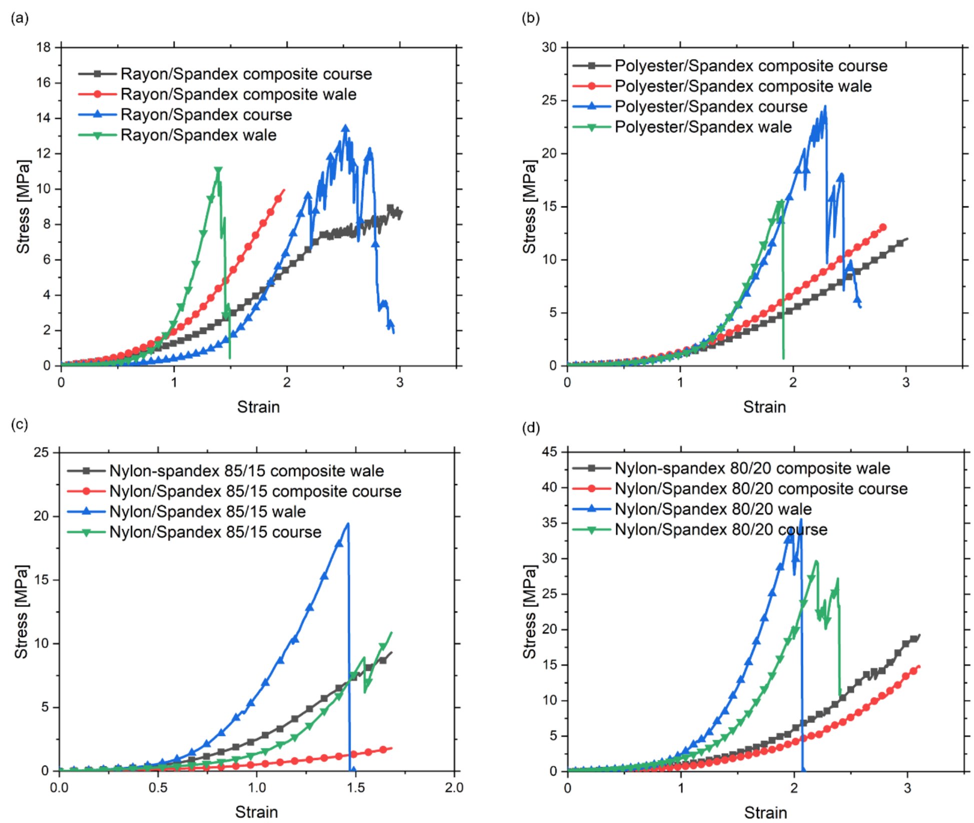

Figure 3.2. Uniaxial tensile behavior of the pure textiles and textile composites: a) rayon/spandex, b) polyester/spandex, c) nylon/spandex 85/15, d) nylon/spandex 80/20.

Fabric-reinforced elastomer composites were prepared in three-layer configuration (Figure 3.1) using layer by layer method. First, the Ecoflex 0050 elastomer was prepared by mixing two components (a base and curing agent) in 1:1 ratio and subsequent degassing in a vacuum to remove entrapped bubbles. The bottom elastomer layer was then prepared by pouring a sufficient amount of elastomer mixture on top of glass substrate and rolling the film applicator rod to make a uniform film. The second layer of fabric was then laid flat on elastomer and allowed to wet at the interface. The fabric was ironed beforehand to minimize any wrinkles. A small amount of elastomer was poured and rolled over the fabric to wet it again and to fill the gaps between pores and level the second layer. As a third layer, a sufficient amount of elastomer was poured over fabric and uniform film was made using film applicator rod.

It should be noted that, in all experiments, the thickness of the fabric layer is constant, specific to each fabric used, while the thickness of the elastomer layers below and above the textile layer can be varied. The thickness of the elastomer layers could be controlled by the amount of substance poured and the rolling area. In this experiment, samples with different thicknesses were prepared for rayon/spandex composite to study its effect on the composite's engineering modulus.

3.2.3 Uniaxial Mechanical Testing of Materials

Uniaxial tensile testing of human and porcine aortic specimens. The length, width and thickness of the aortic specimens (both circumferential and longitudinal directions) were measured using a caliper. The dimensions of porcine and human aortic specimen are listed in

Table *3.1* - Table 3.3. A Biodynamic 5200 (TA Instruments, USA) with a 22 N load cell was used for uniaxial testing of biological specimens in this study, all at room temperature. P150 grit sandpaper was folded so that only the grit side was exposed. It was affixed to the last 1 cm of either end of the aortic specimens using standard ethyl cyanoacrylate glue to minimize the risk of slipping. The upper knurled stainless steel grip of the test instrument was then loosely tightened to hold the sandpaper–aortic specimens so that they were hanging and could be straightened before tightening at both ends. Throughout the testing process, the aortic specimens were repeatedly wetted with phosphate-buffered saline. Each aortic specimen was subjected to a pre-load of 0.04 N and then the gauge length between grips was measured. Each specimen then underwent pre-conditioning, where 5% sinusoidal strain was applied for fifteen cycles at a frequency of 1 Hz. Aortic specimens were then subjected to a frequency sweep: 10% sinusoidal strain was applied for

20 cycles at each of 0.5 Hz, 1 Hz, and finally 2 Hz. The aortic specimens were then extended at 1 mm/s until failure. The test apparatus recorded the displacement and force as a function of the elapsed time.

Table 3.1. The dimensions of the porcine aortic samples in the circumferential direction.

Aorta Number	Gender	Weight (kg)	Section	Length (mm)	Width (mm)	Thickness (mm)
1	F	57.0	Inferior	11.3	4.85	1.70
			Superior	12.32	4.50	2.45
2	F	44.0	Inferior	13.1	5.60	2.40
			Middle	12.12	4.93	2.90
			Superior	12.5	4.66	3.12
3	F	37.0	Inferior	8.81	5.19	1.64
			Middle	9.07	5.37	2.12
			Superior	8.97	4.49	2.50
4	F	33.1	Inferior	6.73	4.98	1.89
			Middle	6.73	4.56	2.38
			Superior	11.69	4.18	2.36
5	F	41.2	Inferior	10.46	4.62	2.68
			Middle	10.8	5.08	2.60
			Superior	11.72	3.83	3.74
6	F	39.3	Inferior	13.55	4.82	2.07
			Middle	16.53	5.00	1.80
			Superior	12.32	4.77	2.04
7	F	47.0	Inferior	12.2	5.40	1.76
			Middle	15.68	4.11	2.18
			Superior	14.27	4.99	3.11
8	F	41.3	Inferior	10.16	5.02	1.66
			Middle	9.55	5.10	1.82
			Superior	9.65	4.69	2.81
9	F	35.9	Inferior	6.12	5.06	2.16
			Middle	5.84	4.80	2.53
			Superior	6.68	4.63	3.02
10	F	39.0	Inferior	9.97	5.18	1.86
			Middle	10.8	2.25	2.33
			Superior	7.33	5.34	2.59
11	F	41.9	Inferior	8.46	4.72	2.40
			Middle	5.75	5.33	2.61
			Superior	6.06	5.07	2.50
12	F	49.0	Inferior	11.9	5.04	2.38
			Middle	8.5	4.95	2.52
			Superior	6.64	5.03	2.55
13	F	40.0	Inferior	4.8	5.26	2.12
			Middle	5.82	5.29	2.30
			Superior	7.14	5.12	2.67
14	F	46.0	Inferior	7.04	5.09	1.51

		Middle	6.61	5.14	1.98
		Superior	7.82	5.05	2.56

Table 3.2. The dimensions of the porcine aortic samples in the longitudinal direction.

Aorta Number	Gender	Weight (kg)	Section	Length (mm)	Width (mm)	Thickness (mm)
9	F	35.9	High	8.36	5.22	2.83
			Low	8.24	5.32	2.63
10	F	39.0	High	7.15	5.27	2.21
			Low	7.01	5.54	1.90
11	F	41.9	High	5.71	5.32	2.22
			Low	8.2	5.79	2.60
12	F	49.0	High	7.4	5.57	2.40
			Low	6.06	5.47	2.33
13	F	40.0	High	9.26	5.01	2.69
			Low	5.5	5.33	2.28
14	F	46.0	High	6.79	5.19	2.17
			Low	7.92	5.45	2.02

Table 3.3. The dimensions of the human aortic samples in the longitudinal and circumferential direction.

Section	Length (mm)	Width (mm)	Thickness (mm)
Inferior	8.65	5.58	2.07
Middle	6.1	5.28	1.94
Superior	7	5.44	1.46
High	6.42	5.2	1.76
Low	6.24	4.7	1.81

Uniaxial tensile testing of the elastomeric materials and the fabric-elastomer composites. The length, width and thickness of the fabricated elastomeric materials and composites were measured using a caliper. The dimensions of elastomeric samples and composites are listed in Table 3.4 -

Table 3.6. Instron 5943 (Illinois Tool Works Inc., USA) was used to measure stress-strain behavior of synthetic elastomers and composites. The elastomeric material samples were subjected to testing conditions equivalent to that of the aortic specimens, with two differences. Firstly, sandpaper was not used because slippage from the grips of the test apparatus was not an issue. Secondly, silicone samples did not need to be sprayed with phosphate-buffered saline. Again, the test apparatus recorded the displacement and force as a function of time for each uniaxial tensile test that was conducted. The pure elastomeric materials were isotropic, while composites were anisotropic due to embedded fabric's structural differences between wale and course directions (Figure 3.6c).

Table 3.4. The dimensions of the elastomeric material samples fabricated using silicones.

Elastomeric Material	Ratios	Length (mm)	Width (mm)	Thickness (mm)
Sylgard 184 (10:1) and Shin-Etsu SES 22330 20 (1:1)	9:1	14.0	21.0	1.0
	8:2	14.0	14.0	1.0
	7:3	15.0	21.0	0.6
	6:4	14.0	22.0	0.9
	1:1	29.0	19.0	0.5
	4:6	19.0	18.0	1.0
	3:7	13.0	21.0	0.6
	2:8	20.0	17.0	1.0
Sylgard 184 (8:1) and Shin-Etsu SES 22330 20 (1:1)	2:1	26.0	23.0	1.0

Table 3.5. The dimensions of the elastomeric material samples fabricated using modified 3M VHB 4910.

Weight Percent of Additive	Length (mm)	Width (mm)	Thickness (mm)
29.1	26	20.0	1.2

36.1	27	17.0	1.0

Table 3.6. The dimensions of fabric-reinforced composite samples.

Composite	Direction	Length (mm)	Width (mm)	Thickness (mm)
Rayon/spandex	Course	25.16	9.65	1.32
Composite 1	Wale	26.3	11	1.32
Polyester/spandex	Course	22.06	10.99	1.8
Composite 2	Wale	20.35	10.99	1.6
Nylon/spandex 85/15	Course	23.35	9.63	0.92
Composite 3	Wale	22.37	11.28	0.91
Nylon/spandex 80/20	Course	22.52	10.88	1.05
Composite 4	Wale	24.02	9.1	1.2

3.2.4 Data Collection and Statistical Analysis

The uniaxial tensile test data was then used to determine the mechanical properties of the human and porcine aortas, as well as that of the fabricated elastomeric materials. The force and the cross-sectional area of the aortic specimens and elastomeric material samples were used to calculate stress, and the displacement and gauge length were used to obtain strain. To calculate principal strain, $\varepsilon = \frac{\Delta l}{l_0}$ and to calculate true tress $\sigma = \frac{F}{A} = \frac{F}{w_0 t_0}(\varepsilon + 1)$ were used, where Δl is extension, l_0 is original sample length, w_0 is initial width and t_0 is initial thickness. The human and porcine aorta and fabric-elastomer composite modulus E were determined as the tangent of stress-strain curve at ε =10%, 25%, 50%, 75% and 100% strain to evaluate local strain stiffening.

As for statistical analysis, Student's t-tests and analysis of variance (ANOVA) were both performed to determine whether there was a significant difference in the stiffness between the different sections of the porcine aorta at a given strain in both the circumferential and longitudinal directions, as well as to investigate dependence of aorta stiffness on the porcine weight.

3.2.5 Microscopic Characterization

The fabric structures and composite cross-sectional area were characterized using Zeiss EVO scanning electron microscope (SEM). All samples were coated with 10 nm of gold using Denton Gold Sputter Unit. The cross-section of the sample was viewed after breaking the sample by tensile testing. The samples were viewed in SE mode with an accelerating voltage of 10-20 kV EHT.

3.3 Results

3.3.1 Mechanical properties of porcine and human aorta

The aorta is the largest artery in the body [72]. The mechanical properties of the aorta vary with respect to location. There is considerable anisotropy between the circumferential and longitudinal directions. Here, we obtained uniaxial stress-strain curves from five different locations/directions from porcine aorta specimens as shown in Figure 3.3a. Figure 3.3b and c show the stress-strain curves from the porcine aorta specimens in the circumferential (superior, $n = 14$) and longitudinal (high, $n = 6$) directions, respectively. All of the aortic specimens, regardless of which section of the aorta that they were obtained from, exhibit the *J-shaped* behavior. The aortic samples became stiffer as the strain increases, which is an important feature to enable the Windkessel effect [73].Interestingly, the inferior section stiffened rapidly, whereas the middle and superior section stiffened rather gradually, which can be intuitively understood by considering the middle and superior sections as temporal blood reservoirs during systole (Figure 3.3b and Figure 3.4) [73] The same trend is observed in the longitudinal direction, as evidently shown from Figure 2c and Figure 3.4 that the low section is considerably stiffer than the high section samples at the same strain. Figure 3.3d shows a comparison of the uniaxial tensile behavior of the human (body mass of 58.0 kg) and porcine (49.0 kg) aortas. The stress-strain curves of the human and porcine aortas are compared at a maximum strain of 150%, although a previous study has shown that average physiological strain in the circumferential direction of healthy human aortas is approximately 32%, while the maximum is 57% [74]. When comparing these two samples, the human aorta was stiffer than the porcine aorta. The uniaxial tensile behaviors of the descending thoracic portion of the human aorta in all five sections are shown in Figure 3.4. As in the porcine samples, all sections of the human aorta demonstrated the *J-shaped* behavior [73]. Moreover, the circumferential samples showed lower modulus compared the longitudinal sample, thus anisotropy is evident.

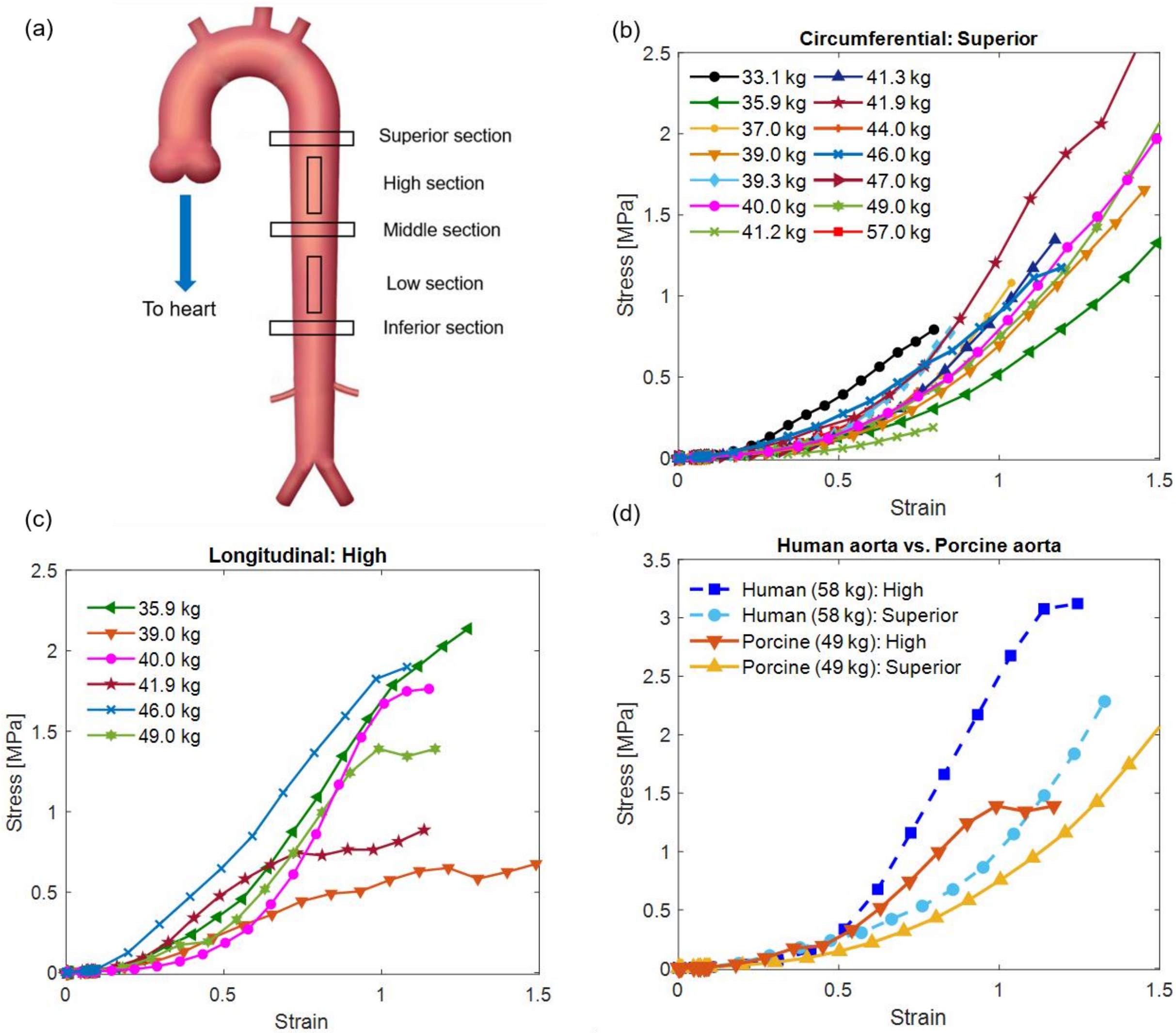

Figure 3.3. The uniaxial tensile behavior of the descending thoracic portion of aortas in the circumferential and longitudinal directions: a) the descending thoracic portion of aortas are cut into five sections for uniaxial tensile testing, uniaxial tensile behavior of b) circumferential (superior) and c) longitudinal (high) sections of porcine aorta, d) comparison between human and porcine aortas.

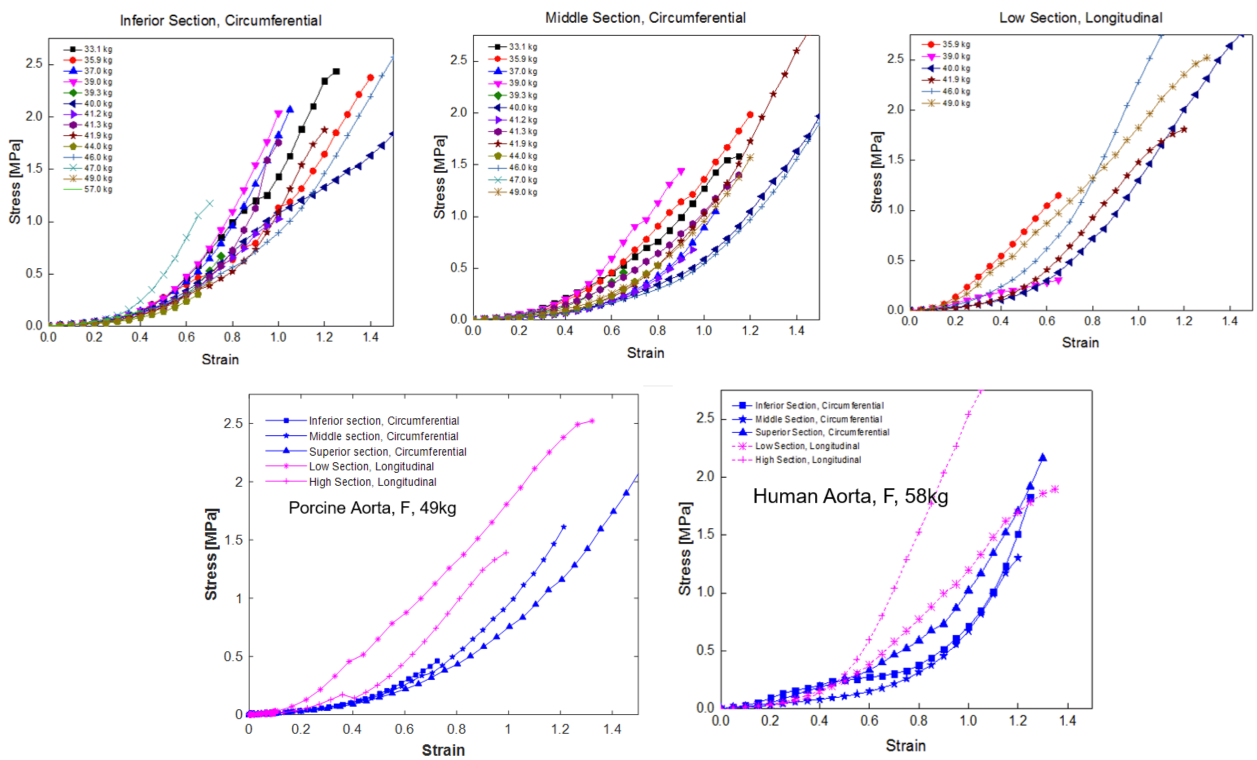

Figure 3.4. Uniaxial tensile properties for porcine and human aorta.

A previous study suggested that biomechanical properties of porcine tissue resemble human since the anatomy of the porcine heart and vasculature is similar to those of a human [75].The average modulus (stiffness) of the descending thoracic portion of the porcine aorta in the circumferential and longitudinal directions at 10%, 25%, and 50% strain are presented in Figure 3.5a and b. Here, the anisotropic trend is confirmed that the longitudinal direction is stiffer than the circumferential direction in a qualitative manner. In addition, the distal sections from the heart (low or inferior) appeared stiffer than the nearer sections (high/middle or superior) at lower strains (10% and 25%). However, at higher strains (50%), the moduli of the low and the high sections are almost the same.

Stiffness values are evaluated at strain levels of 10%, 25%, and 30% for the five sections of porcine aorta are plotted against each specimen's weight (n = 6) in Figure 3.5c. A series of comparisons were made using ANOVA to determine whether there was a significant difference in the stiffness between the different sections of the aorta at a given strain, that is in both the circumferential and longitudinal directions. A p-value less than 0.05 indicated that this difference was statistically significant.

The stiffness of each section from the porcine aorta did not show a significant difference against varying weights ($p>0.05$) at given strain. Thus, it can be concluded that the stiffness of porcine aorta varies significantly with orientation and position from the heart, but we could not find a correlation to the weight of the donor porcine.

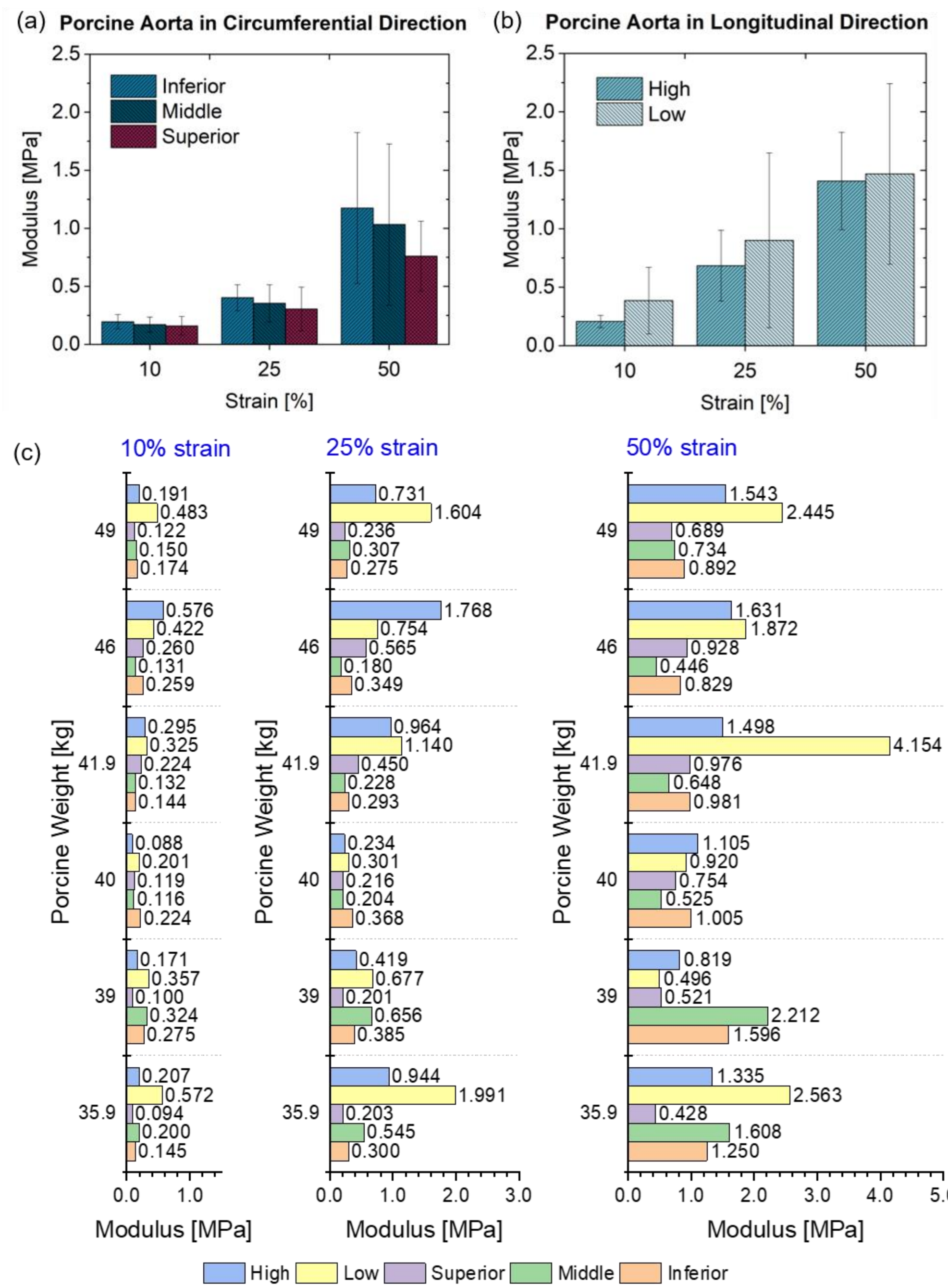

Figure 3.5. Stiffness of porcine aorta at 10%, 25% and 50% strain for a) circumferential (n = 14) and b) longitudinal directions (n = 6), c) for different pig weights (n = 6).

3.3.2 Mechanical properties of neat and blended commercial elastomers

As the first attempt to mimic the mechanical properties of a natural aorta, commercially available elastomers and their mixtures were tested. Figure 3.6a shows the stress-strain curves from uniaxial tensile tests of Sylgard 184 (10:1 and 20:1, matrix:crosslinker), Shin-Etsu SES22330 10 (1:1, Parts A:B), Ecoflex 0050 (1:1) and the unmodified VHB 4910 acrylic elastomer, while the human aortic specimen results are provided plotted for comparison. All silicone materials appeared too soft when compared to human aorta.

In addition, mixtures of Sylgard 184 (10:1) and Shin-Etsu SES 22330 20 (1:1) in the varying ratios of 9:1, 8:2, 7:3, 6:4, 1:1, 4:6, 3:7, and 2:8, as well as modified VHB acrylic elastomers were tested (Figure 3.7). All the abovementioned elastomeric materials were unable to mimic the *J-shaped* strain-stiffening behavior of the human aorta, vital for the Windkessel effect. In this study, only modified VHB 4910 with 29.1 wt% of the additive exhibited slightly rapid stiffening at moderate strain (Figure 3.7), albeit it was unable to mimic the useful range as an aorta substitute.

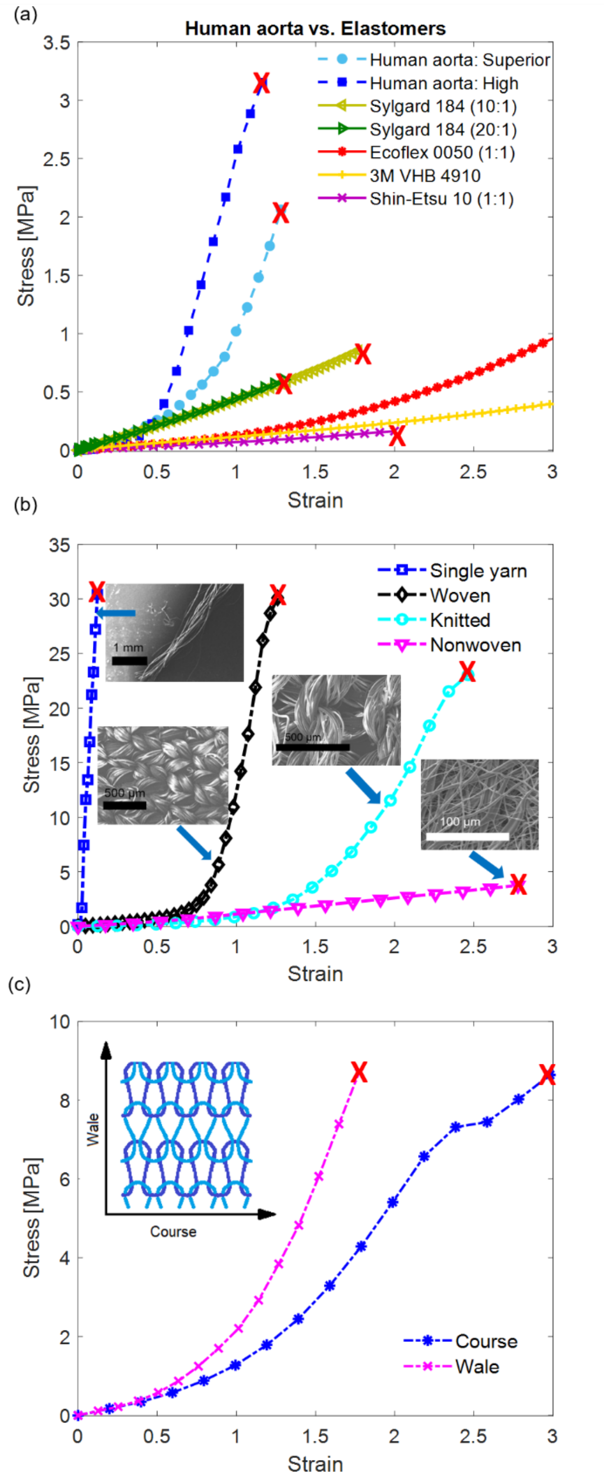

Figure 3.6. Stress-strain properties of constituting materials before compositing. a) elastomers (with human aorta values for comparing purpose), b) textiles with different fabric structures (single yarn of polyester/spandex, woven polyester/spandex, knitted polyester/spandex, and nonwoven

polyurethane), c) anisotropy of knitted rayon/spandex between wale and course directions (red "X" is the point of failure).

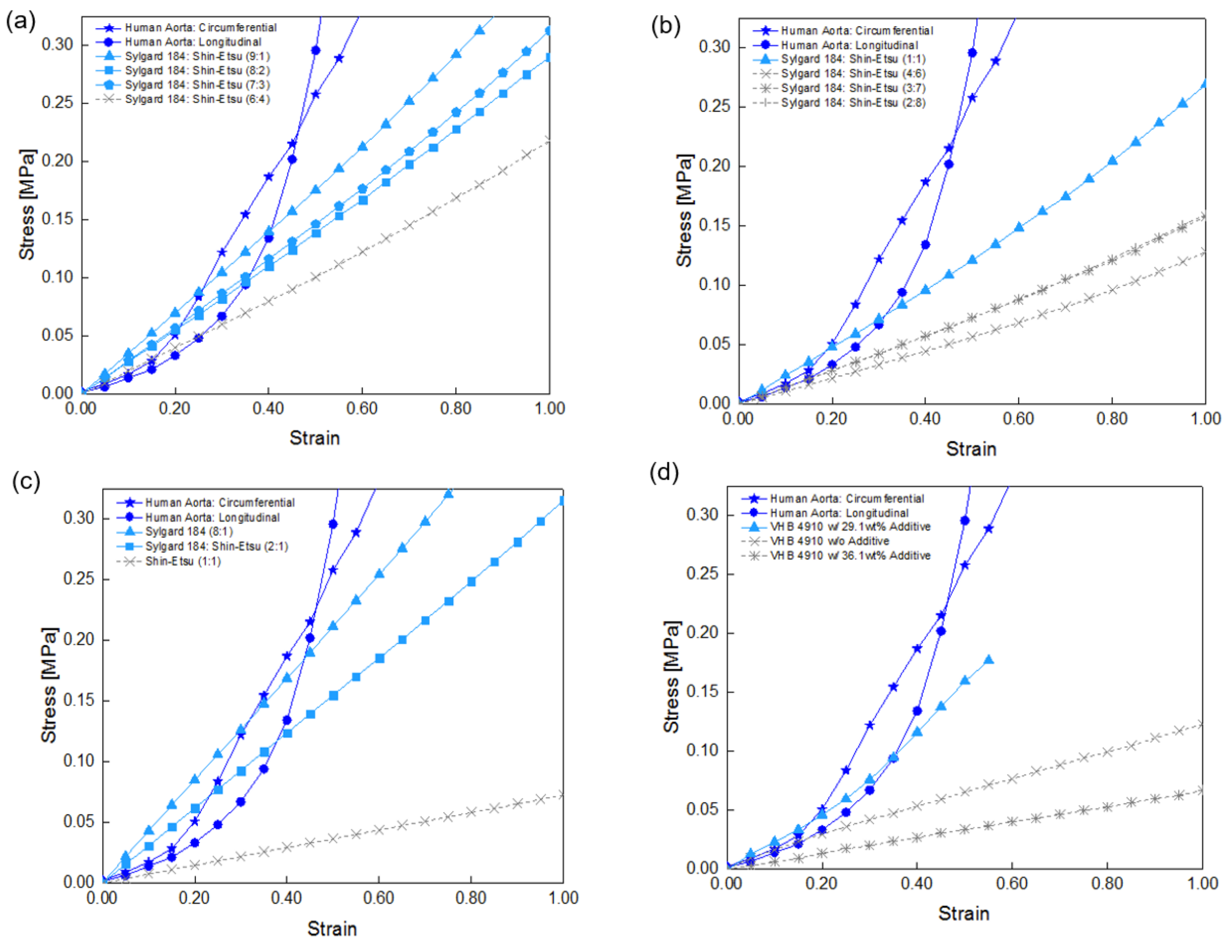

Figure 3.7. Uniaxial tensile properties of elastomeric blends compared to those of human aorta: a), b) mixing Sylgard 184 (10:1) and Shin-Etsu SES 22330 20 (1:1), c) mixing Sylgard 184 (8:1) and Shin-Etsu SES 22330 20 (1:1), d) VHB 4910 with different wt% of additive.

3.3.3 Mechanical properties of fabric-reinforced elastomer composites

Since commercial neat elastomers (without reinforcing substance) were unable to provide nonlinear response to strain, fiber reinforcement was implemented to achieve the desired strain-stiffening effect at low-strain range. First, we evaluated the stress-strain properties of various commercial textiles materials as candidates for reinforcements. The properties of fabrics largely depend on the constituting yarn's mechanical properties, as well as on the fabric structure between the yarns. All the fabrics used in this work were blends with spandex, as previous research suggested that the use of elastane amplifies the strain at break [76].

To select the type of textiles to be used in composites, different textile structures were evaluated. Figure 3.6d compares the stress-strain relationships of single yarn, knitted and woven textile made from polyester/spandex blend, and non-woven textile (polyurethane nanofiber). Here, a single yarn has a linear response to strain and the stiffest among the four. Woven textile exhibits a nonlinear response and is less stiff, followed by the knitted textile that is also nonlinear and is softer than the woven textile. This trend of decreasing stiffness is attributed to the structure of the textile. Yarns are interlacing in the woven fabric while knitwears are interloping [76].Knitwear textiles are designed to allow great mobility for the yarns at low strains by loop elongation. At higher strains, yarn straightening results in high stiffness. The woven textile does not have loops but yarns are interlocked, therefore this structure is stiffer than knitwear. The nonwoven textile is the softest and exhibits a linear response in Figure 3.6b. This is because the fibers in such a fabric are randomly oriented and not restricted by structure and hence allow for extension in different directions [77].

As shown in Figure 3.6c, the knitted structure has an anisotropy where wale orientation (vertical rows in a loop of knitted fabric) is stiffer than course (horizontal rows). The course direction allows the loops to be stretched more flexibly, whereas the mobility of the loops is limited in the wale direction. Therefore, the tensile strength of the wale direction is higher than that of the course [78]. Composites of four fabrics 93%-rayon/7%-spandex, 90%-polyester/35%-spandex blend, 85%-nylon/15%-spandex and 80%-nylon/20%-spandex were used to prepare fabric/elastomers composites. The results shown in Figure 3.8 of the fabricated composite materials show that knitted-fabric reinforced elastomer composites were able to mimic the *J-shaped* and anisotropic mechanical properties of the human aorta. Based on this discussion, it was concluded that knitted textile made from a spandex blend has the greatest potential to obtain both strain-stiffening and anisotropy of natural aorta.

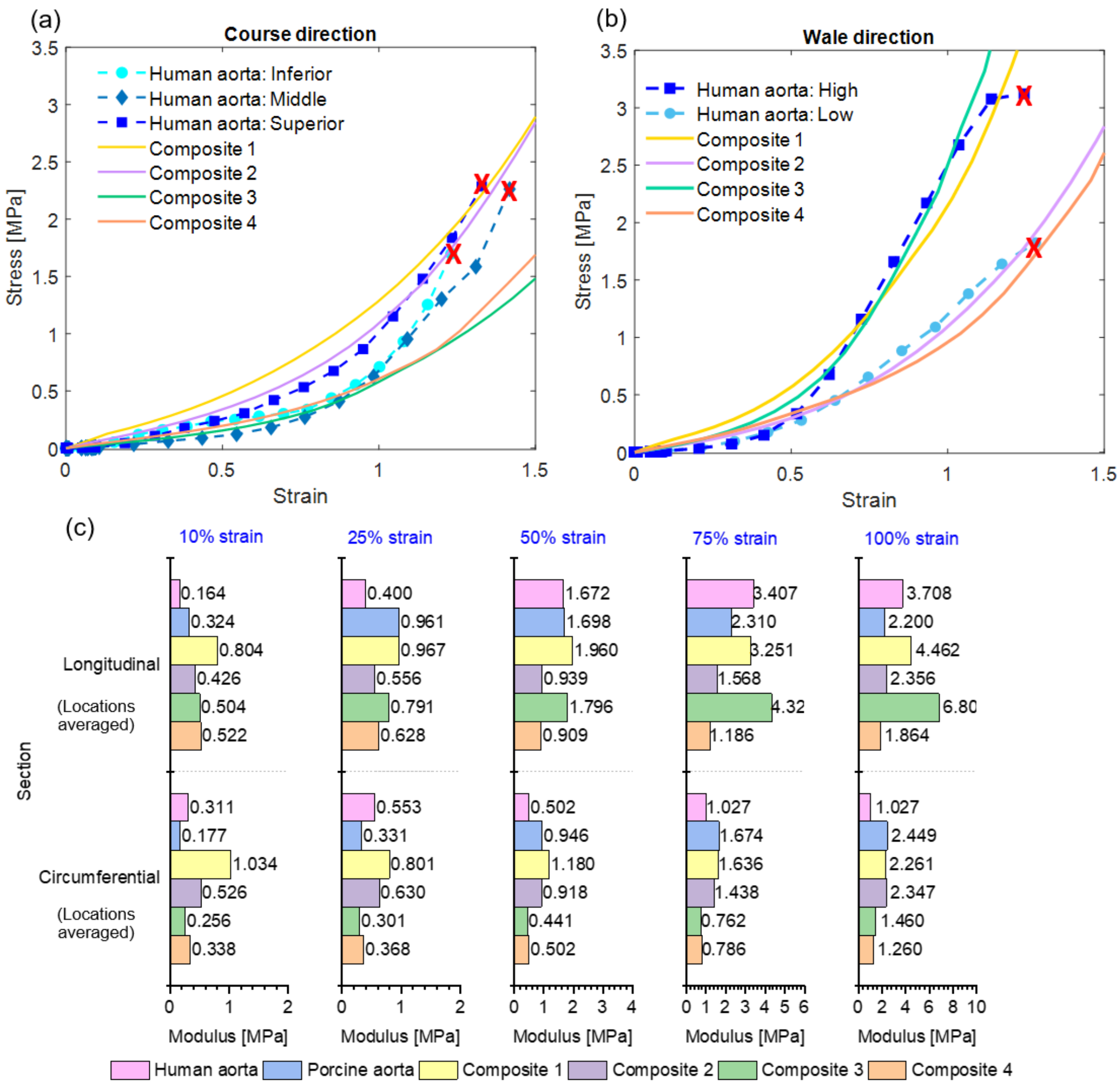

Figure 3.8. The mechanical properties of fabricated fabric-elastomer composites compared with the human and porcine aorta specimens: a) composites 1-4 in course direction compared to human aorta in circumferential direction, b) composites 1-4 in wale direction compared to human aorta in longitudinal direction, c) obtained stiffness values at 10%, 25%, 50%, 75%, and 100% strain. Composite 1: Ecoflex 0050 and rayon/spandex, Composite 2: Ecoflex 0050 and polyester/spandex, Composite 3: Ecoflex 0050 and nylon/spandex 85/15, Composite 4: Ecoflex 0050 and nylon/spandex 80/20.

All four fabric composites shown in Figure 3.8 are significantly stronger than the pure, unreinforced Ecoflex 0050 elastomer, which confirms fabric-reinforcement. Composite stiffness at 10%, 25%, 50%, 75%, and 100% strain were obtained by the slope of the stress-strain curve and are compared in Figure 3.8c. These moduli values show the composite's ability to resist tension. Here, the *J-shaped* strain-stiffening behaviors are clearly seen from all four composites. All composites also exhibited anisotropic behavior in two perpendicular directions: the softer direction was denoted as a course, while the stiffer direction as a wale. At all strains, except above 75% in the longitudinal direction, rayon composite is the stiffest in both directions. Moreover, it is highly anisotropic, significantly stiffer in the wale direction compared to course. Nylon/spandex 85/15 is the second stiffest material in the longitudinal (wale) direction, with a rapid stiffening even higher than for rayon/spandex above 75% strain. This material also shows anisotropy, where the modulus in course direction is significantly lower than for wale. Polyester/spandex and nylon/spandex 80/20 composites are softer than the two composites discussed earlier. Nylon/spandex 80/20 displays a less pronounced anisotropic behavior in two directions, whereas polyester/spandex composite shows a nearly isotropic trend.

As seen from Table 3.7, all composites have a higher or similar elongation at the point of breaking when compared to pure textiles and exhibit high stretchability against failure (150-300% ultimate elongation). Polyester/spandex and nylon/spandex 80/20 display the highest stretchability in both directions (>300%), followed by rayon/spandex (223% and 189% in course and wale respectively) and nylon/spandex 85/15. These differences in fabric-elastomer composite elongations can be attributed to the microscopic structure of embedded fabrics. As seen from Figure 3.1, the polyester/spandex and nylon/spandex 80/20 have a similar microscopic structure. Nylon/spandex

85/15 has the knitted structure, with limited loops, which only allows limited mobility and hence elongation of this fabric. The rayon/spandex fabric has the highest density among all textiles, which when pores are filled with elastomer can act as stress concentration, which restricts the composite stretchability.

Table 3.7. Measured anisotropic mechanical properties of fabrics and fabric/elastomer composites.

	Direction	Elongation at break (%)	Tensile strength (MPa)
Ecoflex 0050		801%	7.124
Rayon/spandex	Course	255%	13.481
	Wale	156%	11.144
Composite 1	Course	223%	6.880
	Wale	189%	9.945
Polyester/spandex	Course	248%	24.501
	Wale	220%	15.633
Composite 2	Course	301%	11.986
	Wale	305%	13.157
Nylon/spandex 85/15	Course	215%	10.395
	Wale	148%	13.644
Composite 3	Course	169%	2.009
	Wale	168%	9.312
Nylon/spandex 80/20	Course	270%	29.663
	Wale	263%	35.547
Composite 4	Course	311%	19.262
	Wale	334%	15.087

Figure 3.9a shows the stress-strain behavior of unreinforced Ecoflex 0050, rayon/spandex textile and their composite in course and wale directions. The modulus of the composite is higher than the neat elastomer or original fabric themselves in both directions. This can be explained by good adhesion of silicone elastomer and the fabrics, confirmed by cross-sectional SEM images of the composite (Figure 3.9c) , which results in the reduction of structural mobility due to textile pores filled with elastomer.

The effect of the composite thickness on the mechanical properties was studied for rayon/spandex composite and results are plotted in Figure 3.9b. It should be noted that the thickness of the embedded fabrics is constant, and the thickness of the composite was controlled by the thickness of elastomer on both sides. Strain limitation comes from the layer, where fabric is embedded due to the restricted stretchability, while the elastomer layers remain elastic [79]. The thinnest sample (1.22 mm) has the highest weight fraction of fabrics (17.7 %), and the thickest sample (1.78 mm) has the lowest weight fraction of fabrics (11.8%). As the thickness of the composite increases, the engineering modulus decreases, or the composite with lowest weight fraction of fabrics has the lowest engineering modulus. In this work, the tensile properties of the composites vary with both the test direction and fiber weight fraction, which is a marker of good interface obtained between the fabrics and elastomer and the absence of textile slipping without deforming the matrix [80].

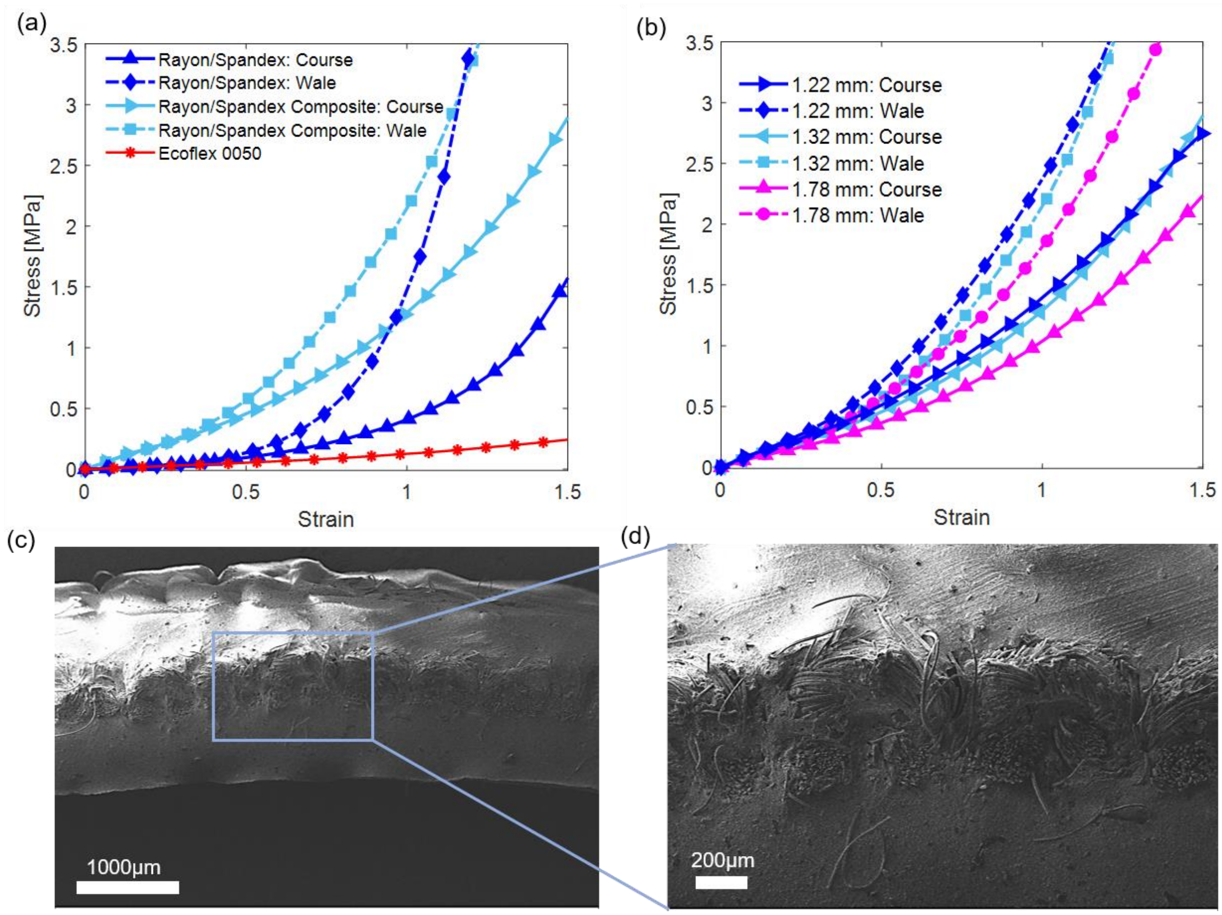

Figure 3.9. Uniaxial tensile behavior of a) unreinforced Ecoflex 0050 elastomer, knitted rayon/spandex, and the composite of them in wale and course directions, b) effect of composite thickness on engineering stress-strain behaviors of the composites, c), d) Cross-sectional SEM images of the composites.

3.4 Discussions

3.4.1 Stress-strain properties of neat elastomers

Elastomers are suitable medical materials due to their nearly instantaneous response to stresses and fully reversible deformation [81]. Silicone elastomers, in particular, remain of interest for medical applications because of their recognized biocompatibility [34]. However, despite that the uniaxial tensile properties of elastomers are similar to soft tissues at low strains, they are unable to capture strong strain-stiffening of soft tissue at low strains (<100%) Such mechanical behavior of silicone elastomers can be related to their macromolecular structure [35]. Traditional elastomers are lightly cross-linked networks with large chain mobility, which allows for immediate response to external stresses resulting from rapid rearrangement of the polymer segments. The response of an individual polymer chain to external stress depends on the rigidity of a polymer backbone [37]. Normally, a flexible polymer chain can undergo very large deformations without resistance before reaching full elongation. In contrast, semi-flexible and rigid polymers can exhibit nonlinear behavior at small strains due to geometrical constraints. Most commercial synthetic polymers, however, lack the molecular complexity to experience hierarchical self-assembly to form stiffer structures [37]. This study has evidenced this point, as none of the pure elastomers and elastomer blends were able to reproduce strain-stiffening at low strain range of interest (Figure 3.7).

Anisotropy is another essential biological property that is difficult to design. Anisotropy in biological tissues originates from the orientation of collagen fibers. Thus, the directional variation of the structure is required for mimicking anisotropy. In this work, the use of fabric-elastomer composites with embedded knitted textiles has shown both strain-stiffening and anisotropic response to uniaxial tensile testing.

3.4.2 Analytical model for the natural aorta and fabric-reinforced elastomers

To verify aorta-like stress-strain behavior of the fabric-reinforced composites, an analytical model was first developed to describe natural porcine and human aorta, which was used subsequently to examine composites. As mentioned earlier, aorta is composed of both elastic and stiff fibrous components. The main structural components of the arterial wall are elastin and collagen, with elastin being a rubber-like matrix with low modulus and collagen being a stiff reinforcing component [16].

Gundiah and co-workers demonstrated that the classical neo-Hookean model can be used to describe arterial elastin: [82]

$$W_{elastin} = \frac{c}{2}(I_1 - 3) \tag{2}$$

where $c > 0$ is a stress-like material parameter and I_1 is the 1st strain tensor invariant. However, classical elasticity theory assumes that the polymer stress-strain property depends on entropic elasticity of polymer chains, and thus is unable to capture the strain-stiffening and anisotropy in natural tissues. The strong stiffening effect and anisotropy of the tissue observed at high loadings is mainly due to collagen fibers, and hence using an exponential function is effective to describe strain energy stored in the collagen fibers as follows: [21]

$$W_{collagen} = \frac{k_1}{2k_2} \sum_{i=4,6} \{\exp[k_2(I_i - 1)^2] - 1\} \tag{3}$$

where $k_1 > 0$ is a stress-like material parameter and $k_2 > 0$ is a dimensionless parameter. It is assumed that I_4 and I_6 invariants contribute to both stiffening effect and anisotropy.

Thus, the following equation was proposed to capture the arterial response under tension: [71]

$$W_{artery} = \frac{c}{2}(I_1 - 3) + \frac{k_1}{2k_2} \sum_{i=4,6} \{\exp[k_2(I_i - 1)^2] - 1\} \tag{4}$$

In this study, the neo-Hookean law employed to describe elastin was substituted with more generalized Mooney-Rivlin and Gent models, which demonstrated a closer fitting to experimental data for the rubber-like materials.

Gent model. This analytical model makes use of the Gent's hyper-elastic material theory [83], [84], [85] coupled with the fiber–elastomer interaction effects [79] to describe the strain-stiffening, *J-shape* behavior in the highly strained fiber-elastomer composites. The strain energy of the fabric-reinforced elastomers was estimated as the sum of strain energies of the highly stretched elastomer, the strained fiber, and the fiber-elastomer interactions as: [79]

$$W_{composite} = W_{elastomer} + W_{fibers} + W_{interaction} \tag{5}$$

Firstly, the strain energy per unit volume in the elastomer $W_{elastomer}$ is given as: [83]' [84]' [85]

$$W_{elastomer} = -\frac{\mu J_{lim}}{2} ln\left(1 - \frac{I_1 - 3}{J_{lim}}\right) \tag{6}$$

where μ is the shear modulus, J_{lim} is the stretch limit of the elastomer, and I_1 is the 1st strain tensor invariant.

Next, the fabric fibers and the elastomer-fiber interactions have resulted in the sum of the strain energies (W_{fibers}+ $W_{interaction}$) when stretched. Holzapfel, Gasser, and Ogden [21] proposed to describe the fabric-reinforced behavior of a multi-walled structure of elastic artery as:

$$W_{fibers} + W_{interaction} = \frac{k_1}{2k_2} \sum_{i=4,6} \{exp[k_2(I_i - 1)^2] - 1\}$$

(7)

where k_1 and k_2 are the constants associated with continuum properties of `the fibers and the elastomer-fiber interactions, respectively, and I_i (i = 4,6) is the i-th invariant of the strain tensor of the elastomer-fiber composite [21].

The elastomer used in this study was assumed incompressible so that the volumetric product is a unit constant $\lambda_1\lambda_2\lambda_3 = 1$ [86]. Therefore, the state equations of the principal Cauchy stresses or true stresses t_i (i=1,2,3) are given as:

$$t_i = \lambda_i \frac{\partial W_{composite}}{\partial \lambda_i} - p \quad (4)$$

where p is the Lagrange multiplier which is determined by kinetic boundary conditions. For example, in uniaxial tensile state, the boundary conditions are examined as λ_2=λ_3=$1/\sqrt{\lambda_1}$ and t_2= t_3=0 [87]. Consequently, the true stress t_{1Gent} in the tensile direction is yielded as:

$$t_{1\,Gent} = 3\mu J_{lim} \frac{\left({\lambda_1}^2 - {}^{1}\!/_{\lambda_1}\right)}{\left[J_{lim} - \left({\lambda_1}^2 + {\lambda_2}^2 + {\lambda_3}^2 - 3\right)\right]} + 6k_1{\lambda_1}^2\left({\lambda_1}^2 - 1\right) exp[k_2(\lambda_1^2 - 1)^2]$$

(5)

Mooney-Rivlin model. The Mooney-Rivlin model was developed to compare with Gent's model to describe behavior of the fabric-reinforced elastomers. The strain energy per unit volume Welastomer in the stretched elastomer is given as: [88]

$$W_{elastomer} = C_{10}(I_1 - 3) + C_{01}(I_2 - 3) + \frac{1}{D_1}(J - 1)^2 \tag{6}$$

where C_{10} and C_{01} are material constants, I_i is the i-th strain tensor invariant, D_1 is a temperature-dependent material parameter that reflects material compressibility and J is the volume variation ratio. For nearly incompressible materials, such as the elastomers used in this study, J value is nearly 1, and thus the third term in Equation (6) is assumed to be zero.

Applying Equation 5 and the same boundary conditions as for Gent's model, the true stress t_{1MR} in the tensile direction for the fabric-reinforced composite is:

$$t_{1\,MR} = 6C_{10}\left(\lambda_1^2 - \frac{1}{\lambda_1}\right) + 6C_{01}\left(\lambda_1 - \frac{1}{\lambda_1^2}\right) + 6k_1{\lambda_1}^2\left({\lambda_1}^2 - 1\right) exp[k_2(\lambda_1^2 - 1)^2] \tag{7}$$

$$\lambda_1 = \varepsilon + 1 \tag{8}$$

Using Equations (5), (7) and (8), all porcine and human aorta uniaxial tensile data were fitted to the developed analytical models to determine main parameters. These parameters include shear modulus μ and limit of extensibility J_{lim}, k_1 and k_2 for Gent model, and stress-like parameters C_{10}, C_{01}, and k_1, and k_2, and for Mooney-Rivlin's model. For Gent's model, μ, J_{lim} values were determined by fitting the experimental curves, where the shear modulus was determined at the small-strain region. J_{lim} values were the maximum values of (λ_1^2+λ_2^2+λ_3^2-3) from the human and porcine aorta, or from the elastomer matrix for composites [89], [90], [91]. For Mooney-Rivlin model, the C_{10} and C_{01} coefficients were determined solely from the elastomeric matrix for composites. In other words, we defined the C_{10}, C_{01}, μ and J_{lim} coefficients from neat elastomers and applied these values to all composites using the respective elastomers, instead of applying different coefficients for different composites just to obtain the best fitting.

Figure 3.11 and Figure 3.10 show that both developed models are in good agreement with experimental data (R^2>0.9, Table 3.8 and Table 3.9). Generally, fabric-elastomer composites have shown better correlation compared to natural aortas. This is because biological materials are not as homogeneous as synthetic composites [46]. The only parameter that was significantly different for the aortas and the composites was the average J_{lim}, which was found to be 6.61 ± 5.40 and 5.63 ±0 .00 for porcine and human aorta, respectively, and 197.63±0.00 for the fabric-elastomer composites. This is because the biological tissue has limited extensibility (typically less than 200%), while the fabric composite contains the elastomer matrix which has a high elongation at break (1000%).

All other parameters were found to be very close. Shear moduli (μ) for the human and porcine aorta were 8.10 ± 0.00 kPa and 7.10±1.09 kPa, respectively. The value was slightly higher for composites, 18.10 ± 0.00 kPa. The k_1 for aortas and the composites were very similar at 11.84 ± 9.06 kPa, 11.99 ± 10.44 kPa and 13.68 ± 10.26 kPa for porcine, human aortas, and composites, respectively. Same was true for k_2, whose values were 0.08 ± 0.14, 0.03 ± 0.03 and 0.001 ± 0.005, respectively. As for the Mooney-Rivlin model, we restricted all the fitted data to be $C_{10} > 0$ and $C_{01} < 0$. Here, C_{10} stands for the elastic behavior of the material [92], [93] and was similar to shear modulus obtained in Gent's model. In this study, composites exhibited a similar C_{10} (15.00±0.00 kPa) to human and porcine aorta (15.00±0.00 kPa and 12.52±3.30 kPa respectively). The term C_{01} describes the nonlinearity of the stress-strain curve and was useful to capture the strain-stiffening of the pure Ecoflex elastomer at high strains [92]. For both the natural aorta and composites k_1 and k_2 for Mooney-Rivlin's were the same with those obtained for Gent's model.

Overall, it was established from analytical modeling that the elasticity of natural aorta at low strains is attributed to the elastin (described by Mooney-Rivlin and Gent models) and stiffening of the curve at higher strains originates from collagen contribution and k_1 and k_2 parameters (Holzapfel model). In the fabric-reinforced elastomers, the low elastic modulus at low strains comes from the elastomer matrix (described by Mooney-Rivlin and Gent models) and the stiffening at higher strains comes from embedded fabric (Holzapfel model). Moreover, the values of the main parameters, namely μ, k_1 and k_2 for Gent's model, and stress-like parameters C_{10}, C_{01}, and k_1, and k_2, and for Mooney-Rivlin's were very similar between the natural aorta and our fabric-reinforced composites. These support the aorta-like behavior of the developed fabric-reinforced composites.

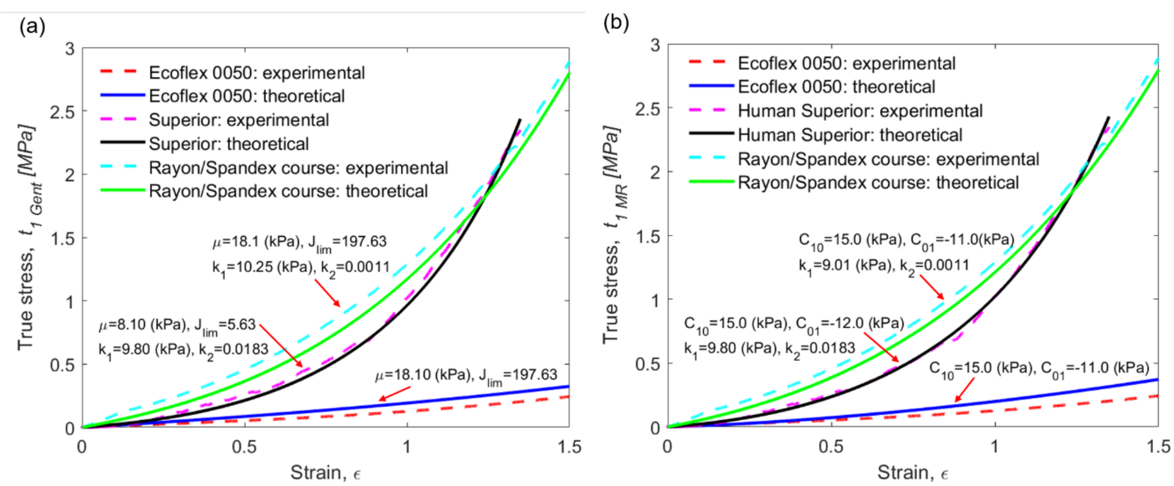

Figure 3.10. Analytical model predictions compared to the experimental values for the human aorta and the fabric-reinforced elastomers. Experimental and fitted data for unreinforced Ecoflex 0050, human aorta in circumferential superior sections and rayon/spandex fabric-reinforced composite in course direction for a) Gent-Holzapfel model and b) Mooney-Rivlin-Holzapfel model.

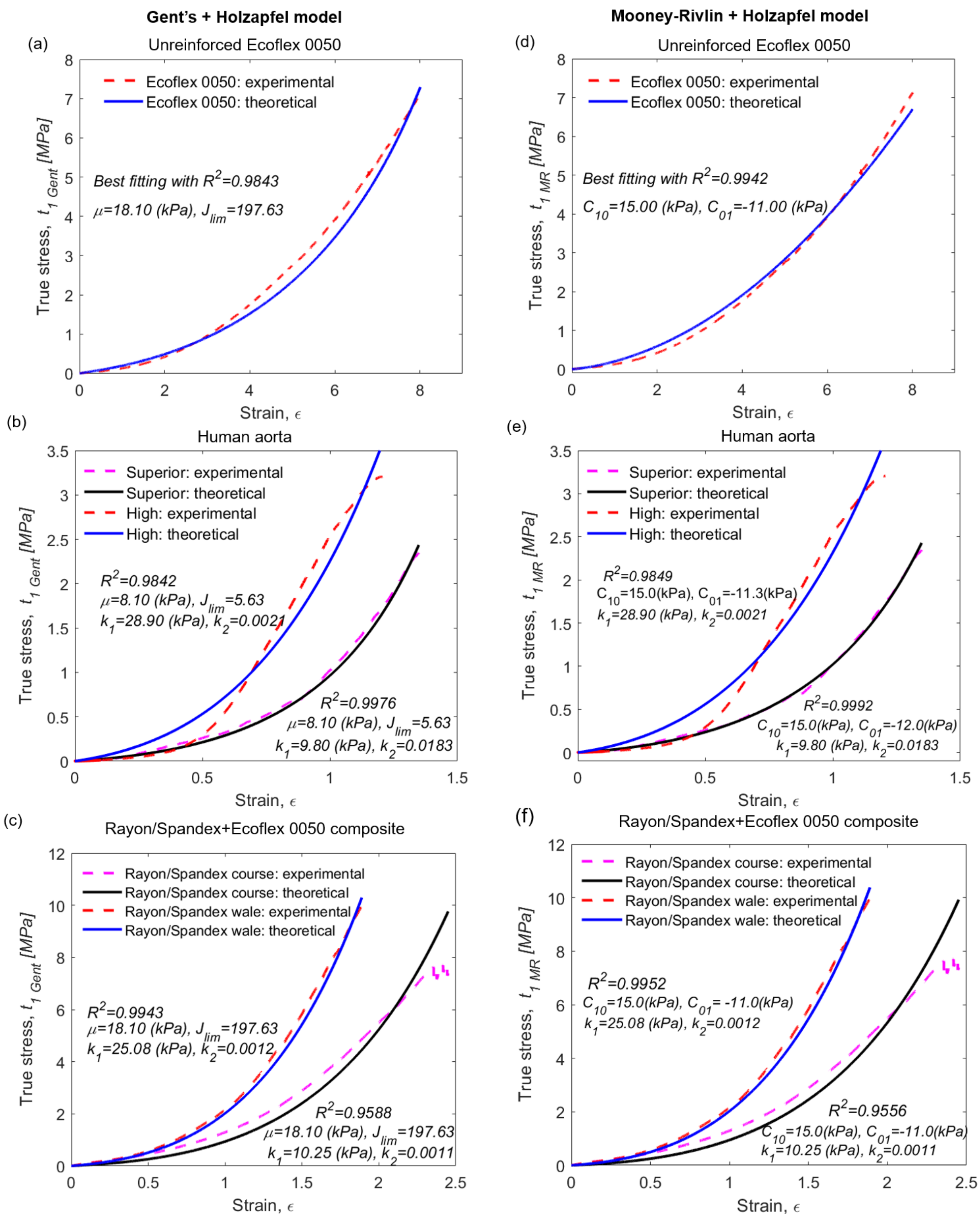

Figure 3.11. Analytical model predictions compared to the experimental values for the human aorta and the fabric-reinforced elastomers. Experimental and fitted data for Gent-Holzapfel model

for a) unreinforced Ecoflex 0050, b) human aorta circumferential superior and longitudinal high sections, and c) rayon/spandex fabric-reinforced composite, d), e), f) respectively for Mooney-Rivlin-Holzapfel model.

Table 3.8. Material parameters for Gent model obtained from our experimental data.

Aorta #	Weight [kg]	Section	μ [kPa]	J_{lim}	k_1 [kPa]	k_2	Rsq
Human	58	Inf	8.10	5.63	4.20	0.0647	0.9847
		Mid	8.10	5.63	3.03	0.0600	0.9660
		Sup	8.10	5.63	9.80	0.0183	0.9976
		High	8.10	5.63	2.89	0.0021	0.9829
		Low	8.10	5.63	14.00	0.0012	0.9851
			Porcine				
1	57	Inf	6.00	2.00	9.20	0.1931	0.9864
		Sup	6.20	2.00	6.30	0.1629	0.9982
2	44	Inf	8.20	2.00	2.10	0.3949	0.9896
		Mid	8.20	4.00	4.60	0.1624	0.9942
		Sup	8.20	3.50	3.10	0.2500	0.9977
3	37	Inf	8.10	5.50	14.60	0.0526	0.9961
		Mid	8.10	5.50	4.80	0.0882	0.9987
		Sup	8.10	5.50	10.90	0.0587	0.9956
4	33.1	Inf	8.30	5.00	17.90	0.0033	0.9957
		Mid	7.40	5.00	14.60	0.0095	0.9887
		Sup	7.40	4.00	18.50	0.0113	0.9821
5	41.2	Inf	7.40	3.50	10.90	0.0162	0.9939
		Mid	7.40	5.00	4.50	0.0898	0.9969
		Sup	4.40	5.00	1.72	0.1384	0.9928
6	39.3	Inf	6.40	2.00	6.10	0.1995	0.9972
		Mid	7.20	2.00	7.40	0.2091	0.9989
		Sup	7.20	2.40	6.02	0.1511	0.9959

7	47	Inf	5.30	2.00	16.90	0.2456	0.9913
		Mid	5.30	2.00	8.80	0.6581	0.9938
		Sup	5.32	5.00	2.50	0.5864	0.9954
8	41.3	Inf	8.30	4.00	9.80	0.0734	0.9948
		Mid	8.30	3.80	10.50	0.0111	0.9964
		Sup	8.30	5.00	7.50	0.0310	0.9954
9	35.9	Inf	6.50	5.00	12.82	0.0016	0.9971
		Mid	6.50	4.00	14.10	0.0164	0.9878
		Sup	8.20	10.00	5.20	0.0028	0.9981
		High	8.20	5.00	14.70	0.1196	0.9874
		Low	6.40	5.00	38.20	0.0300	0.9639
10	39	Inf	7.20	3.50	16.60	0.0513	0.9947
		Mid	7.20	3.50	20.20	0.0276	0.9932
		Sup	7.20	3.50	40.40	0.0375	0.9958
		High	7.20	5.00	5.40	0.0027	0.9266
		Low	7.20	35.00	2.40	0.0001	0.8859
11	41.9	Inf	8.20	5.00	8.50	0.0443	0.9976
		Mid	7.20	5.00	12.10	0.0035	0.9939
		Sup	7.20	7.00	13.50	0.0020	0.9763
		High	6.30	7.00	2.90	0.0010	0.8307
		Low	6.30	7.00	41.80	0.0110	0.9828
12	49	Inf	8.10	5.00	6.00	0.1674	0.9969
		Mid	8.10	5.00	9.00	0.0202	0.9979
		Sup	6.50	7.00	7.20	0.0081	0.9940
		High	6.20	5.00	17.00	0.0152	0.9892
		Low	6.20	7.00	15.90	0.0133	0.9324
13	40	Inf	8.20	15.00	4.51	0.0052	0.9151
		Mid	7.20	15.00	5.30	0.0110	0.9740
		Sup	6.20	15.00	8.10	0.0104	0.9916
		High	3.00	15.00	13.60	0.0591	0.9869
		Low	7.20	15.00	12.50	0.0057	0.9816

14	46	Inf	7.50	10.00	11.20	0.0029	0.9993
		Mid	7.50	10.00	6.39	0.0069	0.9931
		Sup	7.50	10.00	9.75	0.0053	0.9874
		High	7.50	10.00	25.54	0.0122	0.9511
		Low	7.50	10.00	27.30	0.0042	0.9940
			Composites				
Embedded fabric		Section	μ [kPa]	J_{lim}	k_1 [kPa]	k_2	Rsq
Polyester/Spandex		Course	18.10	197.63	8.50	0.0001	0.9682
		Wale	18.10	197.63	9.50	0.0001	0.9673
Rayon/Spandex		Course	18.10	197.63	10.25	0.0011	0.9588
		Wale	18.10	197.63	25.08	0.0012	0.9943
Nylon/Spandex 80/20		Course	18.10	197.63	6.78	0.0001	0.9987
		Wale	18.10	197.63	10.10	0.0011	0.9834
Nylon/Spandex 85/15		Course	18.10	197.63	5.11	0.0001	0.9898
		Wale	18.10	197.63	34.11	0.0007	0.9946

Table 3.9. Material parameters for Mooney-Rivlin model obtained from our experimental data.

Aorta #	Weight [kg]	Section	C_{10} [kPa]	C_{01} [kPa]	k_1 [kPa]	k_2	Rsq
Human	58	Inf	15.00	-11.00	4.20	0.0647	0.9917
		Mid	15.00	-11.00	3.03	0.0060	0.9736
		Sup	15.00	-12.00	9.80	0.0183	0.9992
		High	15.00	-11.26	28.90	0.0021	0.9849
		Low	15.00	-11.00	14.00	0.0012	0.9825
			Porcine				
1	57	Inf	15.00	-11.00	6.80	0.2654	0.9854
		Sup	15.00	-11.00	4.30	0.2495	0.9976
2	44	Inf	15.00	-11.00	2.10	0.3949	0.9971
		Mid	8.50	-5.00	4.40	0.1733	0.9943
		Sup	8.50	-5.50	3.10	0.2500	0.9985
3	37	Inf	15.00	-11.00	13.10	0.0602	0.9959
		Mid	15.00	-11.00	3.90	0.0966	0.9975
		Sup	10.00	-7.50	5.50	0.0847	0.9967
4	33.1	Inf	15.00	-11.00	16.30	0.0091	0.9957
		Mid	10.00	-7.50	14.60	0.0092	0.9914
		Sup	10.00	-7.50	18.50	0.0113	0.9822
5	41.2	Inf	15.00	-11.00	9.10	0.0339	0.9938
		Mid	10.00	-7.50	4.10	0.0996	0.9972
		Sup	5.00	-3.40	1.80	0.1150	0.9920
6	39.3	Inf	10.00	-7.50	5.70	0.2296	0.9973
		Mid	10.00	-7.50	7.20	0.2268	0.9991
		Sup	10.00	-7.50	6.20	0.1511	0.9973
7	47	Inf	10.00	-7.50	16.10	0.2592	0.9913
		Mid	15.00	-11.00	6.10	0.8681	0.9941
		Sup	10.00	-7.50	1.70	0.6996	0.9963

8	41.3	Inf	15.00	-11.00	8.60	0.0857	0.9941
		Mid	15.00	-11.00	10.50	0.0111	0.9989
		Sup	15.00	-11.00	6.10	0.0444	0.9947
9	35.9	Inf	10.00	-7.50	12.90	0.0016	0.9987
		Mid	10.00	-7.50	14.00	0.0164	0.9912
		Sup	10.00	-7.50	5.20	0.0028	0.9991
		High	10.00	-7.50	14.80	0.1196	0.9897
		Low	5.00	-3.40	38.20	0.0268	0.9659
10	39	Inf	10.00	-7.50	16.20	0.0566	0.9949
		Mid	15.00	-11.00	18.30	0.0376	0.9932
		Sup	10.00	-7.50	39.90	0.0397	0.9959
		High	10.00	-7.50	5.40	0.0271	0.9315
		Low	10.00	-7.50	3.00	0.0001	0.9205
11	41.9	Inf	15.00	-11.00	7.20	0.0553	0.9973
		Mid	15.00	-11.00	10.20	0.0123	0.9944
		Sup	15.00	-11.00	13.50	0.0002	0.9828
		High	15.00	-11.00	2.90	0.0009	0.8906
		Low	15.00	-11.00	39.30	0.0146	0.9829
12	49	Inf	15.00	-11.00	4.40	0.2127	0.9973
		Mid	15.00	-11.00	7.50	0.0312	0.9976
		Sup	15.00	-11.00	7.00	0.0081	0.9971
		High	15.00	-11.00	15.10	0.0227	0.9890
		Low	15.00	-11.50	15.90	0.0133	0.9494
13	40	Inf	15.00	-11.00	4.50	0.0052	0.9396
		Mid	15.00	-11.00	5.20	0.0100	0.9841
		Sup	15.00	-11.00	7.00	0.0104	0.9945
		High	1.50	-1.10	14.00	0.0572	0.9874
		Low	15.00	-11.00	11.50	0.0052	0.9831
14	46	Inf	15.00	-11.00	9.50	0.0065	0.9991
		Mid	15.00	-11.00	6.10	0.0069	0.9927
		Sup	15.00	-11.00	9.50	0.0007	0.9947

	High	15.00	-11.00	25.00	0.0125	0.9473
	Low	15.00	-11.00	25.40	0.0065	0.9939
		Composites				
Embedded fabric	Section	C_{10} [kPa]	C_{01} [kPa]	k_1 [kPa]	k_2	Rsq
Polyester/Spandex	Course	15.00	-11.00	8.50	0.0001	0.9656
	Wale	15.00	-11.00	9.50	0.0001	0.9659
Rayon/Spandex	Course	15.00	-11.00	10.25	0.0011	0.9539
	Wale	15.00	-11.00	25.08	0.0012	0.9951
Nylon/Spandex 80/20	Course	15.00	-11.00	6.78	0.0001	0.9993
	Wale	15.00	-11.00	10.10	0.0011	0.9874
Nylon/Spandex 85/15	Course	15.00	-11.00	5.11	0.0001	0.9916
	Wale	15.00	-11.00	34.11	0.0007	0.9950

3.5 Conclusion

The purpose of this study was to develop fabric-reinforced elastomers that mimic the mechanical properties of the natural aorta, and then to establish analytical models to extract material parameters. Here, the human and porcine aortas demonstrated the *J-shaped* strain-stiffening in uniaxial tensile testing and were stiffer in the longitudinal direction when compared to the circumferential direction. In terms of location dependence, we observed that the porcine aorta appears to be stiffer at the distal sections from the heart when compared proximal regions. In order to find the optimal combination between the elastomeric matrix and the fabric reinforcement, the uniaxial tensile properties of various commercial elastomers (VHB 4910 acrylic elastomers with/without additives, Sylgard 184 with various curing agent concentrations, Ecoflex 0050, Shin-Etsu SE S22330, and natural rubber) and commercial fabrics/textiles (woven and knitted polyester/spandex with various spandex content, rayon/spandex, nylon/spandex, and nonwoven polyurethane) were tested and the data were archived. Here, neat elastomer materials could not mimic the *J-shape*, nor the anisotropy. Among composite elastomers, knitted rayon/spandex fabric sandwiched by the two layers of Ecoflex 0050 was the best in mimicking both the strain-stiffening and anisotropy features of the aorta. Here, the knitted fabrics played a role of anisotropically crumped elastin and collagen, which enable low moduli at low strains and a rapid stiffening at high strains. Two analytical constitutive models were developed to represent the strain-stiffening behavior of natural aorta and confirm aorta-like behavior of fabric-reinforced composite. The two models were based on Holzapfel–Gasser–Ogden's model (to represent the stiff fibers) in conjunction with Gent's and Mooney-Rivlin's constitutive model (to describe elastic matrix), respectively. These models were used to extract parameters to describe the mechanical properties.

3.6 Analytical constitutive model details

Derivation details of analytical models for stress-strain behavior

(i) Holzapfel model combined with Gent model:

Free strain energy W:

$$W = W_{elastomer} + W_{fibers} + W_{interactions} \tag{1}$$

With

$$W_{elastomer} = -\frac{\mu J_{lim}}{2} ln\left(1 - \frac{I_1 - 3}{J_{lim}}\right) \tag{2}$$

$$W_{fibers} + W_{interactions} = \frac{k_1}{2k_2} \sum_{i=4,6} \{exp[-k_2(\overline{I_\iota} - 1)^2] - 1\} \tag{3}$$

$$W_{fibers} + W_{interactions} = \frac{k_1}{2k_2} (exp[k_2(I_4 - 1)^2] + exp[k_2(I_6 - 1)^2] - 2)$$

Known:

$$I_1 = \lambda_1^2 + \lambda_2^2 + \lambda_3^2 \tag{4}$$

$$I_2 = \lambda_1^2\lambda_2^2 + \lambda_2^2\lambda_3^2 + \lambda_3^2\lambda_1^2 \tag{5}$$

$$I_4 = \lambda_1^2 cos^2 \alpha + \lambda_2^2 sin^2 \alpha \tag{6}$$

$$I_6 = (\lambda_1^4 cos^2 \alpha + \lambda_2^4 sin^2 \alpha) cos \theta \tag{7}$$

$$W_{fibers} + W_{interactions} = \frac{k_1}{2k_2} (exp[k_2(\lambda_1^2 - 1)^2] + exp[k_2] - 2)$$

$$\frac{\partial W}{\partial \lambda_1} = 2k_1\lambda_1(\lambda_1^2 - 1)\, exp[k_2(\lambda_1^2 - 1)^2]$$

Where,

- α is the angle between the fiber-reinforced direction and stretching direction. So, α is always zero in this work.
- θ is the angle between the two fiber directions of the fiber matrix. Here, the fibers in matrix is orthogonal, hence θ is taken as $pi/2$.

Then:

$$I_4 = \lambda_1^2 \quad \text{and} \quad I_6 = 0 \tag{8}$$

The elastomer is considered as incompressible material due to larger shape deformation than change in volume [86], so

$$\lambda_1\lambda_2\lambda_3 = 1 \tag{9}$$

As stated in [87], we examined the state equations of the stresses in the membrane as

$$t_i = \lambda_i \frac{\partial W(\lambda_1, \lambda_2, \lambda_3)}{\partial \lambda_i} - p, \qquad i = 1,2,3 \tag{10}$$

where p is hydrostatic pressure which is determined by kinetic boundary conditions. For example, in uni-axially tensile state, the boundary condition is examined as $\lambda_2 = \lambda_3 = 1/\sqrt{\lambda_1}$ and $t_2 = t_3 = 0$.

$$\begin{cases} t_1 = \lambda_1 \dfrac{\partial W}{\partial \lambda_1} - p \\ t_2 = \lambda_2 \dfrac{\partial W}{\partial \lambda_2} - p = 0 \\ t_3 = \lambda_3 \dfrac{\partial W}{\partial \lambda_3} - p = 0 \end{cases}$$

$$\Leftrightarrow \begin{cases} t_1 = \lambda_1 \dfrac{\partial W}{\partial \lambda_1} - p \\ t_{2,3} = \lambda_{2,3} \dfrac{\partial W}{\partial \lambda_1} \dfrac{d\lambda_1}{d\lambda_{2,3}} - p = 0 \end{cases} \qquad (for\ uni-axial\ condition\colon \lambda_1 = f(\lambda_{2,3}) = \frac{1}{\lambda_{2,3}^2})$$

$$\Leftrightarrow \begin{cases} t_1 = 3\mu J_{lim} \dfrac{\left({\lambda_1}^2 - {}^1/_{\lambda_1}\right)}{\left[J_{lim} - \left({\lambda_1}^2 + {\lambda_2}^2 + {\lambda_3}^2 - 3\right)\right]} + 6k_1{\lambda_1}^2\left({\lambda_1}^2 - 1\right) exp[k_2(\lambda_1^2 - 1)^2] \\ p = -2\left\{\mu J_{lim} \dfrac{\left({\lambda_1}^2 - {}^1/_{\lambda_1}\right)}{\left[J_{lim} - \left({\lambda_1}^2 + {\lambda_2}^2 + {\lambda_3}^2 - 3\right)\right]} + 6k_1{\lambda_1}^2\left({\lambda_1}^2 - 1\right) exp[k_2(\lambda_1^2 - 1)^2]\right\} \\ t_{2,3} = 0 \end{cases}$$

<u>(ii) Holzapfel model combined with Mooney-Rivlin model:</u>

Free strain energy W:

$$W = W_{elastomer} + W_{fibers} + W_{interactions} \tag{11}$$

With

$$W_{elastomer} = C_{10}(I_1 - 3) + C_{01}(I_2 - 3) + \frac{1}{D_1}(J - 1)^2 \tag{12}$$

Ii is the i-th strain tensor invariant. D1 is a temperature-dependent material parameter that reflects material compressibility. J is the volume variation ratio. For nearly incompressible materials, such as rubber, the third term in Equation (6) is assumed to be zero with J=1.

$$W_{elastomer} = C_{10}\left(\lambda_1^2 + \frac{2}{\lambda_1} - 3\right) + C_{01}\left(2\lambda_1 + \frac{1}{\lambda_1^2} - 3\right)$$

$$\frac{\partial W}{\partial \lambda_1} = C_{10}\left(2\lambda_1 - \frac{2}{\lambda_1^2}\right) + C_{01}\left(2 - \frac{2}{\lambda_1^3}\right)$$

$$W_{fibers} + W_{interactions} = \frac{k_1}{2k_2}\sum_{i=4,6}\{exp[-k_2(\overline{I_i} - 1)^2] - 1\} \tag{13}$$

$$\Leftrightarrow \begin{cases} t_1 = \lambda_1 \dfrac{\partial W}{\partial \lambda_1} - p \\ t_{2,3} = \lambda_{2,3}\dfrac{\partial W}{\partial \lambda_1}\dfrac{d\lambda_1}{d\lambda_{2,3}} - p = 0 \end{cases} \quad (for\ uni-axial\ condition\colon \lambda_1 = f(\lambda_{2,3}) = \frac{1}{\lambda_{2,3}^2})$$

$$\Leftrightarrow \begin{cases} t_1 = 6C_{10}\left(\lambda_1^2 - \dfrac{1}{\lambda_1}\right) + 6C_{01}\left(\lambda_1 - \dfrac{1}{\lambda_1^2}\right) + 6k_1{\lambda_1}^2({\lambda_1}^2 - 1)\, exp[k_2(\lambda_1^2 - 1)^2] \\ p = -4\left\{C_{10}\left(\lambda_1^2 + \dfrac{2}{\lambda_1} - 3\right) + C_{01}\left(2\lambda_1 + \dfrac{1}{\lambda_1^2} - 3\right) + k_1{\lambda_1}^2({\lambda_1}^2 - 1)\, exp[k_2(\lambda_1^2 - 1)^2]\right\} \\ t_{2,3} = 0 \end{cases}$$

The selection criteria for Mooney-Rivlin coefficients C_{10} and C_{01} for Ecoflex 0050

Table 3.10. Coefficients C_{10} and C_{01} for Ecoflex 0050 found in literature.

Material	C_{10} (kPa)	C_{01} (kPa)	Ratio	Reference
Ecoflex 0050	2.68	0.10	27:1	[94]
Ecoflex 0050	21.3628	10.4018	2:1	[95]

$$t_{Elastomer\,(MR)} = 6C_{10}\left(\lambda_1^2 - \frac{1}{\lambda_1}\right) + 6C_{01}\left(\lambda_1 - \frac{1}{\lambda_1^2}\right)$$

$$\frac{\partial t}{\partial \lambda_1} = 6C_{10}\left(1 + \frac{2}{\lambda_1^3}\right) + 6C_{01}\left(2\lambda_1 + \frac{1}{\lambda_1^2}\right)$$

Constraints on the stress:

$\frac{\partial t}{\partial \lambda_1}(t = 0) = 0$, no energy is stored, if not loaded

$\frac{\partial t}{\partial \lambda_1} > 0$ must be satisfied for increasing function

$$\frac{\partial t}{\partial \lambda_1} = \gamma > 0 \; (\gamma = \text{constant})$$

The second derivative of the function must be positive too, otherwise the function is unstable.

$$\frac{\partial^2 t}{\partial {\lambda_1}^2} = 6C_{10}\left(2 - \frac{2}{\lambda_1^3}\right)\frac{-36C_{01}}{\lambda_1^4} > 0$$

For fitting the experimental curve for Ecoflex 0050, C_{10} and C_{01} were selected, such that the difference between derivative of the experimental curve at each point and the γ was minimized and $\gamma > 0$ was satisfied.

The coefficients C10=15 kPa and C_{01}=-11kPa were selected based on criteria described above. The results can be seen from Figure 3.12 below.

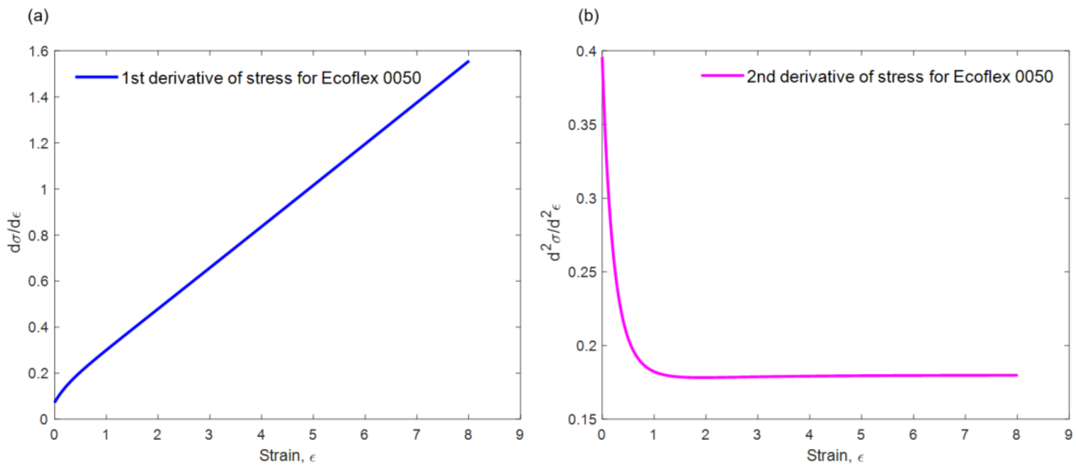

Figure 3.12. Choice of coefficients C10 and C01 for Ecoflex 0050: a) 1st derivative of stress and b) 2nd derivative of stress for Ecoflex 0050.

4 3D Printed Structure Reinforced Metamaterials: Beyond Natural Aorta's Capacity to Regulate Blood Flow

4.1 Introduction

One of the current challenges of ex-vivo perfusion devices is to find a suitable material for the blood outlet tubing from the allograft which can play the same role as the ascending aorta from the left ventricle. Nowadays, plastic tubes found in the market are too rigid for the allograft. As a consequence, it may cause injuries to the heart at the junction, which results in scars formation in the left ventricle. Furthermore, these rigid structures are unable to replicate the Windkessel effect which is extremely relevant for the cardiovascular function. During systole, the aorta stores half of the left ventricular stroke volume. Then, during diastole, the elastic forces of the aortic wall forward the storage volume to the peripheral circulation, as can be seen in Figure 4.1c and Figure 4.1d. As a result, there is a continuous blood pump through the body regardless of the pulses of the heart, so the coronary blood flow and the left ventricular relaxation is improved, and the afterload of the left ventricular is reduced [9]. As many biological tissues, the aorta presents a non-linear strain-stiffening behavior, also known as '*J-shaped*′ behavior to fulfill its function, as can be seen in Figure 4.1a. The fiber-reinforced elastomer tube in Chapter 3 can provide solution up to this point by addressing the requirement of *J-shaped* and anisotropic behavior.

Another challenge for the ex-vivo perfusion devices is to limits the peak pressure in aorta by expanding to accommodate a large stroke volume and thus achieve a steady-state condition regardless of the blood flow – including high blood pressure situations, which may happen more frequently in heart at unhealthy condition, such as ventricular tachycardia. The aorta substitute material is required to ensure that maximum aorta pressure does not rise above the maximum systolic pressure to avoid counter flows that could seriously damage the donor heart as can be seen in Figure 4.1e. Such self-regulation at high blood pressure does not exist in natural aorta, nor in any naturally existing materials. For this study, an ideal strain-stiffening curve is built considering a the physiological range of the aorta which is from 30 to 120 mmHg (maximum systolic pressure is 120 mmHg) [96], [97]. Researchers have estimated that it corresponds to average wall stress from 20 and 100 kPa [97], [29], [28]. This curve is shown in Figure 4.1b. Introducing compliance at 100kPa will allow aorta to expand to accommodate large stroke volume and will reduce wall stress, thus avoiding aortic stiffening and its negative consequences on the heart.

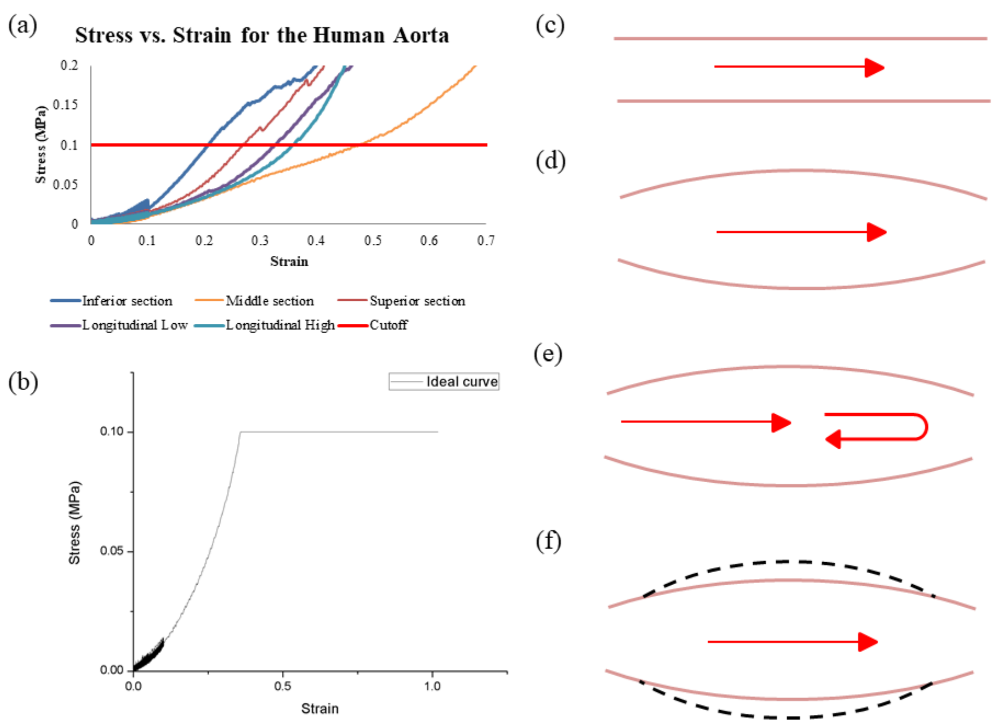

Figure 4.1. Behavior of the human aorta and the desired stress-stiffening-softening behavior. (a) Stress-strain behavior for different sections of the human aorta, the physiological maximum systolic pressure is marked in red. (b) Stress-strain curve aimed with the metamaterial design, which will limit pressure above 100 kPa. (c) and (d) show the Windkessel effect of the human

aorta. (e) shows a backflow that could happen if the aorta becomes stiffer. (f) shows in dot lines the aimed behavior of the metamaterial atpeak pressure.

Metamaterials are carefully structured materials that are composed of periodically arranged building blocks and display properties superior to their constituent materials. In the past two decades, metamaterials have been utilized to manipulate optical, acoustic and thermal fields to obtain unusual properties, such as a negative refraction index and resulted in new applications, such as perfect lenses [30]. Mechanical metamaterials represent a new branch of metamaterials research, where motion, deformations, stresses and mechanical energy are investigated. The meta-atoms, building blocks of mechanical metamaterials, deform, rotate, buckle, fold and snap in response to applied mechanical forces and are designed to act together to yield a desired collective behavior. We hypothesize that by careful design of mechanical metamaterial, the desired stress-hardening-softening behavior can be achieved. The recent advances in computer-aided design (CAD) and additive manufacturing allow for a rapid and low-cost fabrication of complex structures with a fine resolution [31], [32]. In the proposed study, we aim to use two additive manufacturing techniques, SLA and PolyJet 3D printing to produce custom-developed sine-wave based models encapsulated in soft polymer matrices to achieve a metamaterial with unique strain-stiffening-softening property.

The tuning of metamaterials for different applications have been achieved by changing the structures of the unit cells and, with them, their deformation mechanisms. Most research has been focused on microstructures configurations with straight ligament topologies and three main deformation mechanisms: re-entrant structures, chiral structures and rotating structures [32], [98]. Among them, honeycomb structures have been worldwide studied and some modifications to its structures have been made in order to gain stiffness. Ingrole et. al worked for the enhancement of the in-plane strength in this structure [99]. This group tested with honeycomb and re-entrant honeycomb structures. First, they split the strut at both ends and then they combine this configuration in two hybrid arrangement with normal honeycombs cells. They studied the behavior of this structures under compression until its final collapse [99]. Li et. al worked in the comparison of honeycomb and re-entrant honeycomb as well as chiral truss and truss structures for energy absorption [100]. Florijn et. al studied the influence of some parameters in holar samples to tailor different applications [101].

Recent numerical and experimental studies indicate that curved microstructures can have improved stretchability. Chen et. al proposed the use of sinusoidal-based metamaterials for tuning its vibrational control capability, in their studied they included a comparison with other straight-beam structures: hexagonal, kagome, square and triangular ones. They concluded that the sinusoidal-based metamaterials switch from bending-dominated behavior to stretching-dominated behavior under tension, while the straight beams structures do not. As a result, the tuning of the Poisson's ratio, even from negative to positive is possible [98]. Rafsanjani et. al exploit the mechanical instability of sine wave forms for metamaterial creation, here, they realized that when the snap occurs, the increment of the stiffness becomes negative and that different behaviors can be achieved by tuning the amplitude of the sine wave used [56]. Clausen et. al used direct ink writing (DIW) for the creation of nine topologies with different Poisson's ratio from -0.8 and 0.8 [102].

Metamaterials can be applied to different fields, among them, mimicking of soft tissues behavior is an active field that many research groups are currently competing. Wang et. al used dual-material 3D printed metamaterials with micro-structured reinforcement embedded in soft polymeric matrix mimicking the strain-stiffening behavior. They are investigating the complex influence of design parameters from sinusoidal waves and double helix structures in the strain-stiffening behavior, which has been reached for a range of 0% to 8% [31]. This group has previously worked on mimicking the aorta behavior showing that textiles encapsulated in polydimethylsiloxane (PDMS) can achieve the strain-stiffening curve.

In this study, tuning the wavelength of orthogonally arranged sine-wave based structures was proposed to tailor the mechanical properties of metamaterials. Two additive manufacturing techniques, SLA and PolyJet 3D printing, were used to print metamaterials that were further encapsulated in soft polymer matrices.

While the project is unfinished during my MSc years, I comprised a thorough review covering design criteria and fabrication strategies of the strain-stiffening-softening metamaterial, followed by a few of my original experimental trials.

(1) A design criterion for novel *strain-stiffening-softening* metamaterial is suggested with a critical review on the subjects of 3D printed metamaterials and their elastomeric composites.

(2) Our preliminary results for the *strain-stiffening-softening* material development are introduced.

4.2 Literature review of 3D printed metamaterials

4.2.1 Advantages of metamaterial composites

The distinct shared property of animal armors, such as fish scales, lobster claws, and abalone nacre, which are capable of stopping crack propagation, deflecting cracks, or bridging gaps made by cracks, is that they are composed of rigid plates connected to the body and to themselves by collagen fibers/mussels [103]. Nature inspires the design of reinforced mechanics for flexible body armor and recent advancement in 3D-printing technology allows for building complicated bioinspired structures [104], [105]. Consequently, the 3D-printed mechanics reinforced structures can be designed based on the mechanics of the natural biological systems [106].

Composite materials with carefully designed structures and compositions possess improved properties when compared with the individual constituent materials. In a two-phase composite, each component phase can contribute its own properties in an independent manner to the overall performance of the composites synergistically [100]. For example, composite materials with auxetic lattice structures used as the reinforcements and the nearly incompressible soft material as a matrix have great potential in achieving prominent mechanical properties. Previous studies have suggested that auxetic materials with a negative Poisson's ratio have better indentation resistance, impact shielding capability, and enhanced toughness [100]. In theory, by harnessing negative Poisson's ratio effect of the auxetic reinforcement, the soft matrix experiences biaxial or triaxial compression leading to a synergistic improvement in the mechanical response. This coupled geometry and material design concept can be enabled by the state-of-the-art additive manufacturing technique [100].

Li T et al. has compared auxetic lattice and auxetic lattice reinforced composites by fabricating composites from glassy polymer lattice and rubber-like polymer matrix [100]. They have concluded the mutual constraints between two phases of the auxetic lattice reinforced composites enable enhanced stress resistance by additional support of the matrix phase to the lattice phase, which was not observed for non-auxetic reinforced composites [100]. These results suggest the possibility to tailor the properties of reinforcing metamaterial and the soft matrix to achieve the desired stress-softening mechanical behavior.

4.2.2 Tuning properties of metamaterials

First step in developing metamaterial composite with desired mechanical behavior is to design the structure of reinforcing metamaterial. Milton and Cherkaev showed that metamaterials with any form of elastic tensor can be designed with architectures of ordinary elastic materials [107]. Thus, careful design of architecture can lead to any desired mechanical property. Architecting materials induces heterogeneity of stresses and deformations, which results in breakdown of the affine assumption, where deformations are supposed to be uniform, as in a homogeneous rubber sample [108]. For instance, in auxetic metamaterials the global response of the material is entirely different from the local behavior of its constituents due to localization of deformations at the hinges. Thus, tuning of the material geometry enables design of variety of specific bulk elastic properties. Minor changes in the geometry of networks cause qualitatively different deformations and elastic properties, which demonstrates rich and complex relations between the architecture and collective properties [30].

4.2.3 3D printing as a rapid manufacturing tool

Conventional fabrication techniques of composites such as molding, casting and machining create products with complex geometry through material removal processes [109], [110] While the manufacturing process and performance of composites in these methods are well-controlled and understood, the ability to control the complex internal structure is limited. 3D printing is able to fabricate complex composite structures without the typical waste. The size and geometry of composites can be precisely controlled with the help of computer aided design. Thus, 3D printing of composites attains an excellent combination of process flexibility and high-performance products [110]. Additive manufacturing (three-dimensional (3D) printing) has created new opportunities for manipulating and mimicking the intrinsically multiscale, multimaterial, and multifunctional structures in nature. Recent progress in additive manufacturing, especially the ability to print multiple materials at upper micrometer resolution, has given researchers an excellent instrument to design and reconstruct natural-inspired materials. The most advanced 3D-printer can now be used to manufacture samples to emulate their geometry and material composition with high fidelity [105]. Its capabilities, in combination with computational modeling, have provided us even more opportunities for designing, optimizing, and testing the function of composite materials, in order to achieve composites of high mechanical resilience and reliability.

According to the American Society for Testing and Materials, there are over 50 different AM technologies [106]. A number of mature AM technologies have been successfully commercialized such as fused deposition modeling (FDM), direct ink writing (DIW), selective laser sintering, stereolithography (SLA), powder bed inkjet 3D printing (inkjet 3D), two-photon polymerization, laminated object manufacturing, and their variants such as multijet printing (MJP) and selective laser melting (Figure 4.2) [106].

In the following review sections 4.2.4 – 4.2.6, information about existing 3D printing technologies used to mimic biological architectures and functions will be presented. First, single material printing will be discussed, followed by multimaterial printing. Furthermore, the limitations of 3D-printing will be pointed out, and possible future developments will be suggested. Finally, applications of 3D printed metamaterials will be presented.

Figure 4.2. Integration of 3D printing with biomimicry, and the inset shows the categories of 3D-printing technology. Reproduced with permission from [106].

4.2.4 Single material printing

The single material used in 3D-printed bioinspired structures includes polymer, metal, graphene and other materials. In addition to the printing material itself, the biomimetic structural design plays a crucial role in mechanical property of final product. Figure 4.3 presents bioinspired mechanics reinforced 3D-printing structures with single material found in literature. Using two-beam super resolution lithography, biomimetic nanostructures inspired from butterfly wings were fabricated by Gan et al. [111]. By using an aerosol jet 3D printer, micro-scaffolds with lattice shapes, such as trusses, donut-shaped pillars, spirals, and accordion-like electronic connections were built by Saleh et al. (Figure 4.3f) [112]. In the macroscale, 3D-printed armor inspired by fish scale was studied due to its flexibility and high impact resistance by Song et al. (Figure 4.3b) [113].

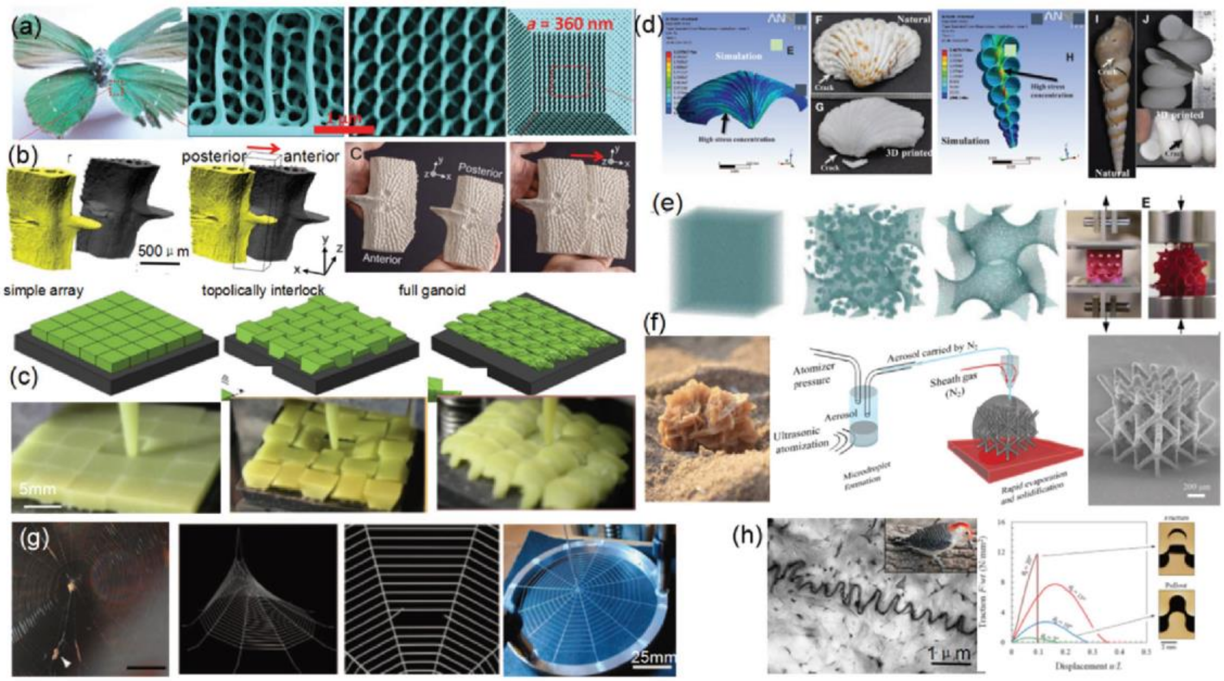

Figure 4.3. Bioinspired mechanics reinforced 3D-printing structures with single material [106]. a) Butterfly wings inspired strong gyroid nanostructures with high modulus [111]. b) 3D-printed prototypes of two lateral plates. Reproduced with permission [113]. c) Schematics of different scaled skin designs and their puncture performances. Reproduced with permission [104]. d) Digital images and stress distribution of natural and 3D-printed patelliform shell and Turritella shell. Reproduced with permission [114]. e) Different atomistic and 3D-printed models of gyroid geometry for mechanical tests [115]. f) Desert Rose and the 3D buildup of nanoparticles by pointwise printing to realize microarchitectures [112]. g) Spider web in nature and 3D-printed web. Reproduced with permission [116]. h) Examples of sutured interfaces in red-bellied woodpecker and experiments on the jigsaw interlocked tabs [117]. Reproduced with permission from [106].

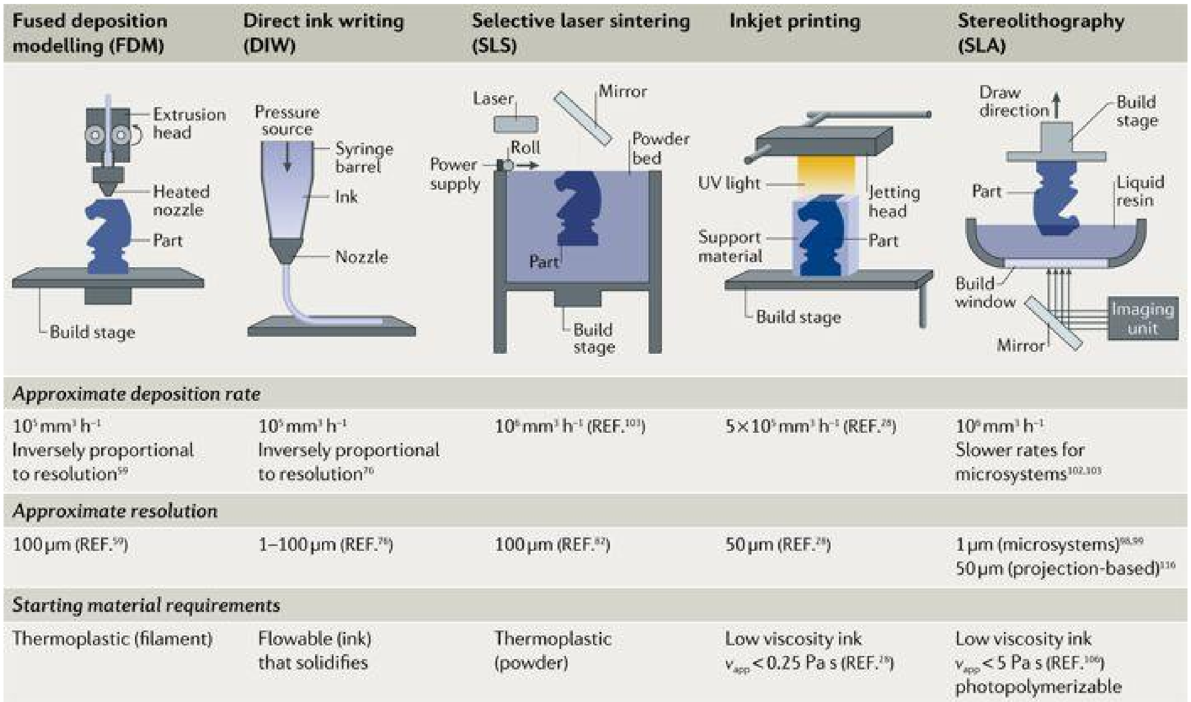

Figure 4.4. Differences between printing technologies. Reproduced with permission from [118].

Five common 3D printing technologies are typically used for single material printing, namely fused deposition modeling (FDM), direct ink writing (DIW), selective laser sintering, inkjet 3D printing (inkjet 3D), stereolithography (SLA). The working principles of this technologies are presented in Figure 4.4.

Fused Deposition Modelling (FDM). Fused deposition modeling (FDM) is a vastly used technique for 3D-printing that typically deposits semi-molten thermoplastic in consecutive layers to form 3D structure using heat [105]. Using this technique Tiwary et al. has printed the models of seashells with two natural shapes, one responsible for diametrically converging localization of stresses (Bivalves) and another one for helicoidally concentric localization of stresses (Terebridae) (Figure 4.3d) [114]. The results suggest that complex shapes are capable of sustaining loads twice as high as those based on simple shapes.

Direct ink writing (DIW). Similar to the fused deposition modeling method, direct ink writing is an extrusion-based technique that produces continuous filament material through a syringe nozzle, which is solidifies through chemical or physical mechanism after deposition in a printing tray (Figure 4.5a). DIW benefits from inexpensive hardware and opensource software already developed for fused deposition modeling together with affordable and disposable nozzles that help tolerate particle clogging. The main requirement for successful direct ink writing is formulation of inks with optimal rheological behavior that enables easy flow under applied shear stress during extrusion and simultaneously shows enough elasticity to prevent flow and deformation of the deposited material when shearing ends [119]. Compton and Lewis [120] have employed the ability of DIW to easily print particle loaded materials to fabricate cellular structures that mimic natural composite balsa (Figure 4.5). Two key features were replicated: the lightweight cellular architecture and the reinforcement of the walls of the cellular structure with stiff fibers. Figure 4.5c. displays various polymer-based cellular structures with different cell designs printed by DIW.

Inkjet printing. Inkjet printing that utilizes powder binding technique, was originally developed for 2D applications and has been later adapted to use in 3D printing. In 3D inkjet printing, a layer of powder is evenly placed on a stage and the desired surface of solidification is sprayed by droplets of binding agent [105]. The unbound powder is then released and the process is repeated for the following layer. The inkjet printing offers the advantage of using powders of diverse materials to construct a heterogeneous 3D model. However, the use of toxic glues in the process limit the medical applications [105].

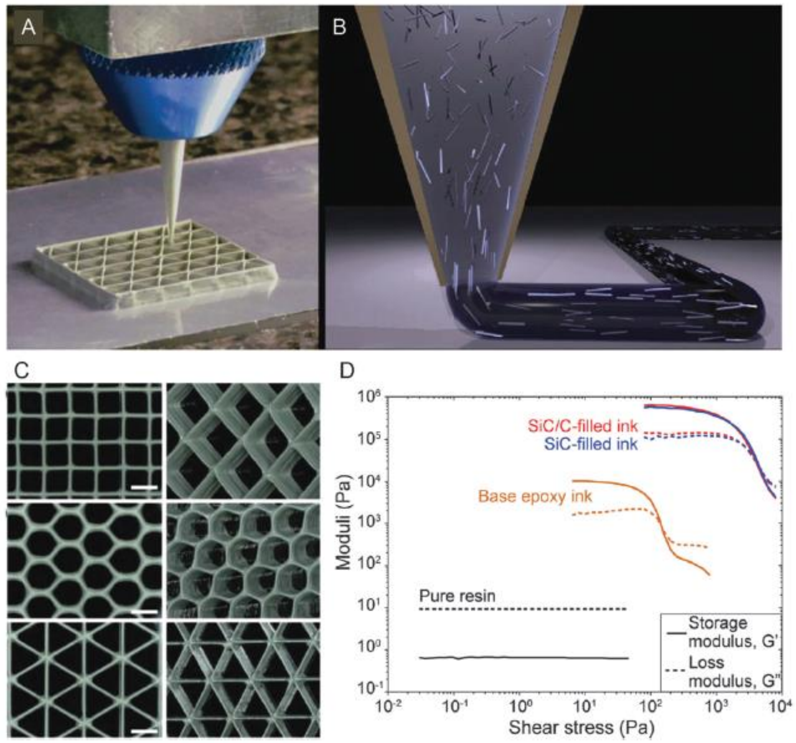

Figure 4.5. Direct ink writing (DIW) of cellular composites reinforced with stiff fibers and whiskers: (a) optical image showing the 3D printing of a triangular cellular structure, (b) schematics depicting the alignment of anisotropic particles due to shear at the dispensing nozzle, (c) examples of SiC-reinforced epoxy composites with cellular architectures of different geometries (scale bars, 2 mm), (d) rheological behavior of the epoxy-based inks used in (c). Reproduced with permission from [121].

Selective Laser Sintering (SLS). Alternatively, SLS utilizes high-power lasers to bound polymer powders together instead of toxic binding agents used inkjet printing. Due to constant heating and cooling effects from the laser, objects assembled using SLS often undergo deformation that reduces the precision of the printer and subsequently the applications of printed materials in areas that need high resolution, such as electronic chips and biomedical implants [105].

Stereolithography (SLA). In SLA, the shape of 3D object is traced by ultraviolet (UV) laser by focusing on a tank that is filled with liquid photopolymer. The curing of photoresin and solidification into desired 3D object is attained upon contact with UV radiation. The SLA possesses significant material limitation as only one resin can be used at a time and the photocurable resins used are either epoxy-based or acrylic. The resulting object is typically brittle and experiences shrinking upon polymerization [105].

The limitations that exist for various additive manufacturing techniques can be categorized by resolution, cost and material as summarized in Table 4.1.

Table 4.1. A summary of rapid prototyping techniques [110].

Technique	State of starting materials	Typical polymer materials	Working principle	Resolution (Z direction,μm)	Advantages	Disadvantages
FDM	Filament	Thermoplastics, such as PC, ABS, PLA, and nylon	Extrusion and deposition	50–200 (Rapide Lite 500)	Low cost, good strength, multi-material capability	Anisotropy, nozzle clogging
SLA	Liquid photo-polymer	Photocurable resin (epoxy or acrylate based resin)	Laser scanning and UV induced curing	10 (DWSLAB XFAB)	High printing resolution	Material limitation, cytotoxicity, high cost
SLS	Powder	PCL and polyamide powder	Laser scanning and heat induced sintering	80 (Spo230 HS)	Good strength, easy removal of support powder	High cost, powdery surface
3DP	Powder	Any materials can be supplied as powder, binder needed	Drop-on-demand binder printing	100–250 (Plan B, Ytec3D)	Low cost, multi-material capability, easy removal of support powder	Clogging of binder jet, binder contamination
3D plotting	Liquid or paste	PCL, PLA, hydrogel	Pressurized syringe extrusion, and heat or UV-assisted curing	5-200 (Fab@home)	High printing resolution, soft materials capability	Low mechanical strength, slow

4.2.5 Multimaterial printing

Most biological systems are typically composed of nonmineralized "soft" structures and mineralized "hard" structures, which are composites of minerals and fibrous organic polymers [106]. Single material is therefore not capable of fully mimicking the biological materials and multimaterial structures need to be investigated.

PolyJet 3D printing. Multimaterial 3D printer (by Stratasys) with its PolyJet technology offers numerous advantages, such as (1) printing complex geometries at micrometer resolution, (2) printing multiple materials with diverse mechanical properties, (3) inexpensive printing at a large-scale, and (4) good interfacial adhesion between constituent materials [105]. The method includes dispensing droplets of liquid monomers or oligomers that are polymerized upon UV radiation after deposition onto a build tray (Figure 4.6a). During the printing, the material of interest is supported by additional support material, which is removed upon washing and cleaning. Polyjet printing creates opportunity for local compositional control due to the possibility of adjustment of the relative fraction of printed droplets. Such flexibility allows for manufacturing of heterogeneous materials constituting individual voxels with controlled composition and properties [121].

The advanced capabilities of multi-material ink jet printing has been recently employed to produce stiff and flexible protective armors replicating exoskeleton of ancient fish, [122] self-shaping cellular structures similar to morphing natural seedpods [123], a combustion-powered soft robot, [124] flexible biomimetic shark skin with engineered surface roughness [125] and numerous structural materials mimicking the design of bone and biogenic calcite [126], [127] (Figure 4.6b-f). Using a multimaterial printer, Dimas et al. have studied typical bone-like biological composite, with a stiff and compliant phase and compared their computational model to experimental testing on 3D-printed samples [126]. They have found out that specific topological arrangements cause significant stress and strain delocalization in their 3D-printed system. In addition, they demonstrated that constituent materials in the printed composites possess strong interfacial adhesion that prevents failure at the interface, which proves outstanding potential of Polyjet 3D printing technology. Mirzaeifar et al. furthered the work to study defect tolerance of similar bio-inspired topologies with different classes of hierarchical structures [128] using multimaterial 3D-printing. The study established that composites with more hierarchical levels dramatically improve the defect tolerance of the material.

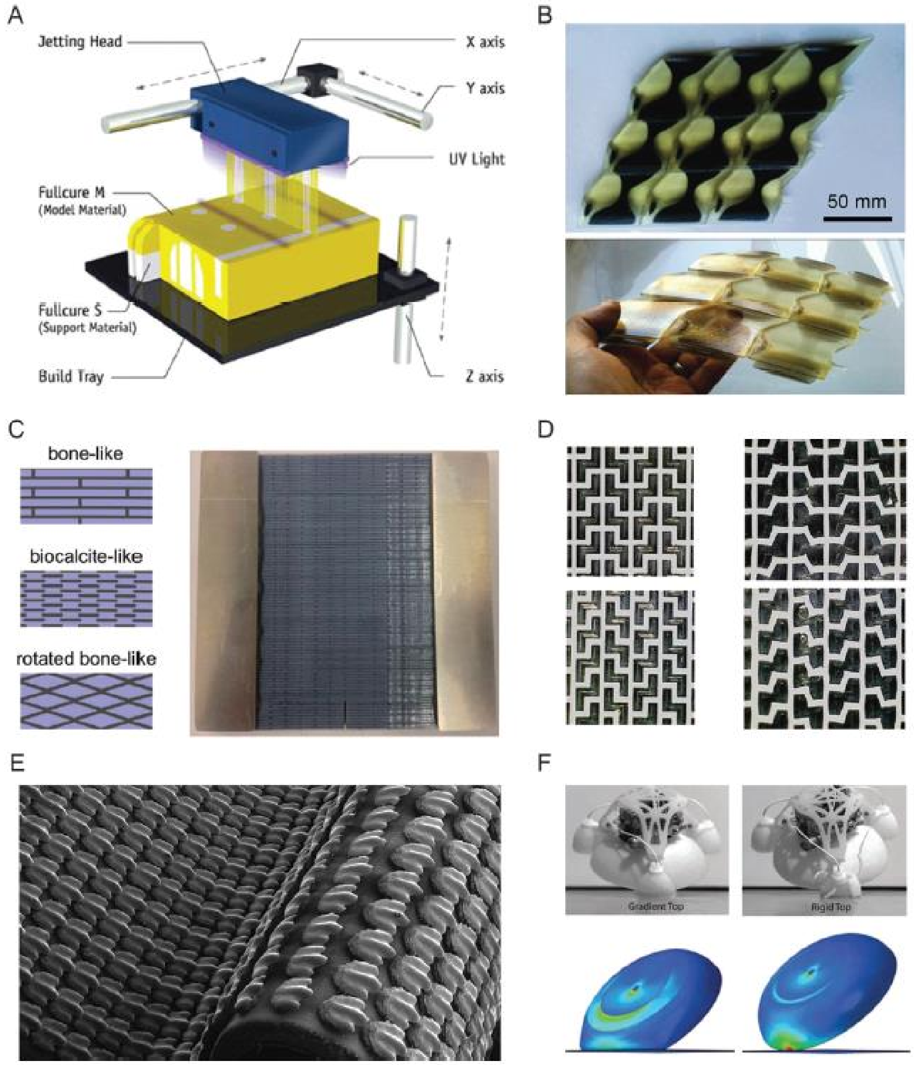

Figure 4.6. PolyJet 3D printing technology and bioinspired composites obtained using its multi-material capabilities [121]: (a) schematics of the hardware used in the PolyJet technology, (b) printed composite inspired by armored scale-jacket system of an ancient fish [122], (c) bioinspired structural motifs printed using a combination of soft and hard polymers (left) and a photograph of a bone-like 3D printed composite (right, typical width 6 cm) [126], [127], (d) periodic honeycomb structures inspired by the actuation mechanism of plants before (left) and after (right) swelling in a solvent [123], (e) 3D printed membrane comprising rigid denticles on a flexible substrate to mimic shark skin (each denticle 1.5 mm) [125], (f) combustion-propelled soft robots exhibiting intact, graded or broken, rigid top structures (left and right, respectively) [124]. Reproduced with permission from [121].

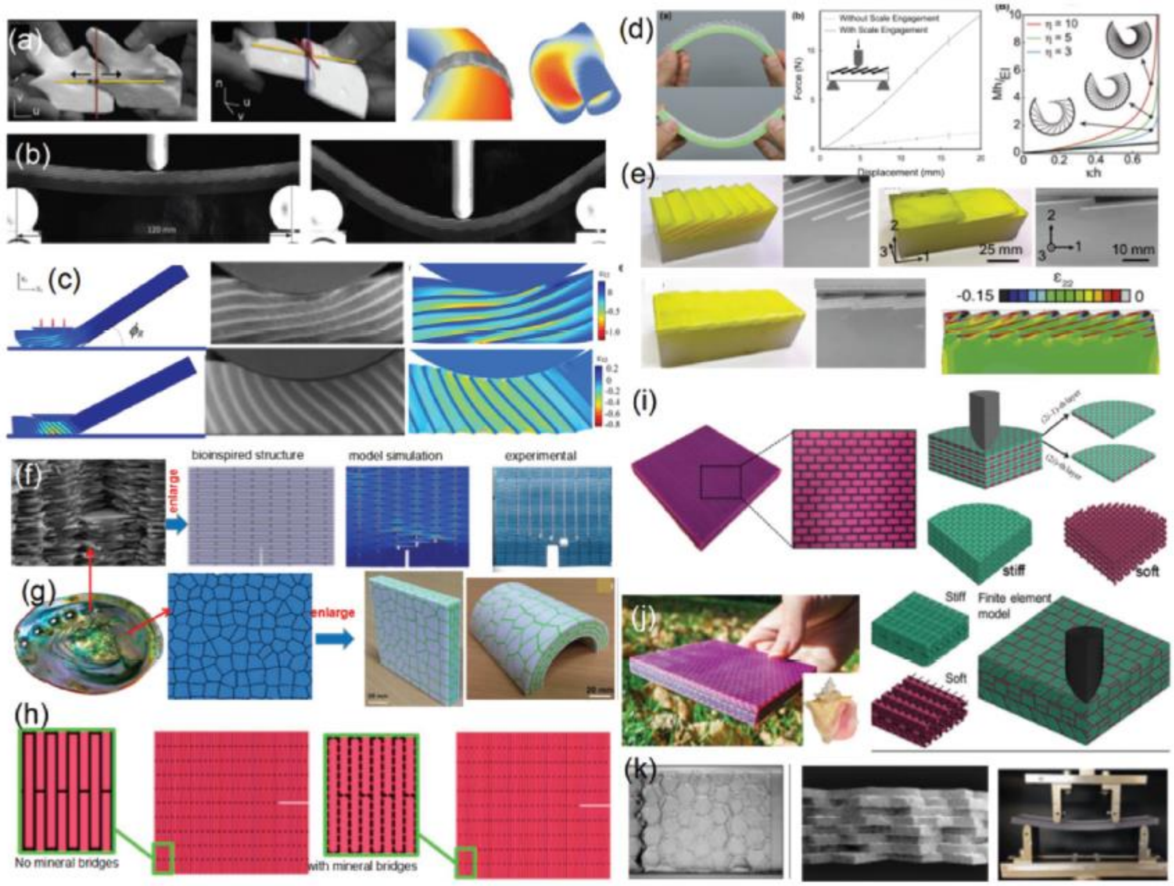

Figure 4.7. Bioinspired mechanics reinforced 3D-printing structures with multimaterials [106]. a) Allowable motions between 3D-printed adjacent scales and the printed armor on human body [129]. b) Fish scale inspired 3D-printed specimen at initial bending and finite bending [130]. c) 3D-printed actuated composites with different lamination angles and shear strain distributions with FE simulations [131]. d) An illustration of the 3D-printed biomimetic system deformation under bending in two opposite directions and curvature response with various overlap ratios [132]. e) Macroscale 3D-printed and molded synthetic fish scale [133]. f) Bioinspired composites with 3D printing and proceed to test the synthesized specimens [126]. g) 3D-printed nacre-like composite prototypes of different shapes.] [134] h) Comparison of Crack propagation of printed samples with and without mineral bridges [135]. i) 3D-printed nacre inspired sample and quarter geometry of the nacre-like design in simulation [136]. j) Conch-shell-inspired structure fabricated via multimaterial 3D printing [137]. k) Nacre-inspired sample fabricated by multimaterial 3D printing and under mechanical test [138]. Reproduced with permission from [106].

Figure 4.7 presents more bioinspired composites obtained using its multi-material capabilities of PolyJet 3D printing technology are presented. Despite that unique voxel-based feature of multimaterial printing enables fabrication of complex structures, this additive manufacturing method is unable to deposite inks loaded with high volume fractions of particles due to costly and delicate nature of the dispensing system, making particle clogging a major issue. This also limits the exploration of new material formulations. Because biological systems often contain anisotropic particles, multimaterial printing would benefit from possibility of using particle-loaded formulations.

Field-Assisted 3D Printing. Many biological systems are made of mineralized composites that are responsible for strong mechanical properties. These composites consist of a mineral reinforcement phase, such as hydroxyapatite, calcium carbonate, or silica, embedded in a biopolymer matrix, such as collagen or chitin. With evolution of 3D printing from single material to multimaterials, the addition of microfillers (ceramic platelets and microfibers) and nanofillers (carbon nanotubes, graphene) has been introduced to reinforce the 3D-printed structures [120], [139]. In addition, combination of shear force, electrical-field, and magnetic-field-assisted methods with 3D printing have been developed to achieve the anisotropic mechanical properties by controlled filler alignment to further mimic biological structures [106]. These "field-assisted 3D printing" methods are discussed in the following sections.

Multimaterial magnetically assisted 3D printing (MM-3D printing). Recently, Kokkinis et al. has applied magnetic manipulation of anisotropic particles in a direct ink writing (DIW) method to fabricate 3D composite architectures that incorporate particle orientation control and multi-material features [140]. In the novel technology referred as multimaterial magnetically assisted 3D printing (MM-3D printing), multiple materials can be printed by loading distinct syringes with different monomer composition and particle concentration inks (Figure 4.8a). By incorporating ultrahigh magnetic response (UHMR) particles into the DIW ink and fitting extrusion-based printer with a magnet or electromagnetic coils, magnetic control can be achieved [121]. Printing of 3D objects using MM-3D printing requires two sets of inks: a low viscosity "texturing ink" loaded with UHMR particles to achieve local orientation control, and "shaping ink" loaded with a rheological modifier to prevent the geometrical distortion of deposited filaments (Figure 4.8b) [140], [121].

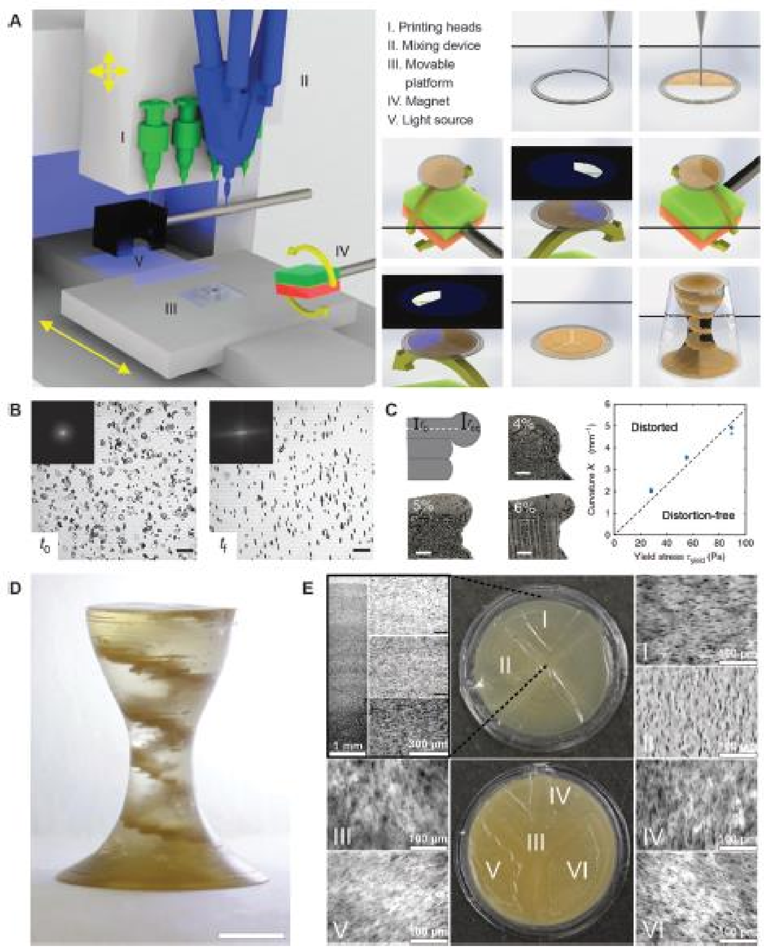

Figure 4.8. MM-3D printing technology and printed composite architecture [121]: (a) DIW setup equipped with a magnet and multiple cartridges (left), workflow of the magnetically-assisted printing process (right), (b) biaxial magnetic alignment of ultrahigh magnetic response (UHMR) platelets suspended in a texturing ink, (c) shape of overhangs obtained with a shaping ink

containing different concentrations of a rheology modifier (left), the rheological response required to generate distortion-free filaments (right), (d) MM-3D printed object with internal helicoidal staircase made by controlling the distribution and local orientation of stiff platelets. Scale bar, 5 mm, (e) Detailed features of the top (upper images) and the bottom (lower images) of the printed object [140]. Reproduced with permission from [121].

Although magnetically assisted direct ink writing and stereolithography approaches allow design of composite particle architecture at the individual voxel level, current technology is limited to low concentration of particles that can be loaded in the monomers (15 vol%) due to clogging issues inside the nozzle or resin bath. In extrusion-based processes, a low-shear viscosity ink (lower than 10^3 Pa s) is required [140], while stereolithographic processes necessitate even lower viscosity to ensure resin spreading. High particle concentrations inevitably raise the viscosity level above these upper limits.

4.2.6 Limitations of additive manufacturing techniques

Material. A universal limitation of 3D printing technologies is diversity of printing materials. Currently, only a limited number of polymers, such as thermoplastic polymers with low glass transition temperature and suitable melting viscosity, powder materials and several photopolymers, metals, and ceramics could be used in 3D printing [105], [110]. Moreover, most manufacturers require their proprietary materials only to be used in the printer. Thus, for printing materials with complex structures and superior properties, the diversity of materials must increase.

Precision. The precision of the printers, namely the ability to combine printing on nanoscale, microscale and macroscale is another limitation. For instance, printing methods, such as two-photon polymerization or inkjet printing can build materials with small features on the nanoscale but cannot be used to print large structures. Alternatively, printers that build that macro-objects are unable to print smaller ones. Development of versatile printer that combines printing of smaller and larger features with high resolution could further diversify applications of 3D printing [141], [142] [105].

Performance. Although 3D printing allows for design of complex objects, printed materials usually suffer from low mechanical strength and require additional post-treatment steps that further increase the cost and processing time. Print defects, imperfections and cracks typically act as catalyst for material failure due to stress concentrations around cracks and imperfections [127]. In multimaterial printing, low mechanical strength mainly arises from the presence of voids in printed parts due to poor interfacial bonding with matrix [110]. Furthermore, 3D printing lacks the repeatability and consistency of manufactured parts [110]. Therefore, further improvements of print quality, microstructure of individual layers, interfacial bonding between matrix and reinforcement are required.

Printing time. Many printers require long printing times, which hinders printing of large parts and limits large-scale applications of printing technology. Development of scalable and fast processing printing technologies is needed [110].

Support material. Many printers use support material to fill voids in complex designs, which are difficult to remove after printing and can damage to the printed structure upon removal. Design of more advanced support materials or improved methods for easy support removal will be beneficial, particularly in the microfluidics fields, where channels without support material are required [142], [105].

4.3 Materials and Methodology

Based on the literature review, two manufacturing methods, SLA and PolyJet 3D printing, were selected for this study to develop mechanical materials with the desired behavior. SLA printer has a Flexible Resin, which has favorable stiffness range and allows for wide choice of encapsulation matrix. The printed metamaterial can be further molded with any elastomer. The PolyJet printer on the other hand allows for multimaterial printing, which eliminates the need for molding and delamination problem, but limits the choice of matrix material. Both techniques have advantages and drawbacks and thus were selected in this study for comparison.

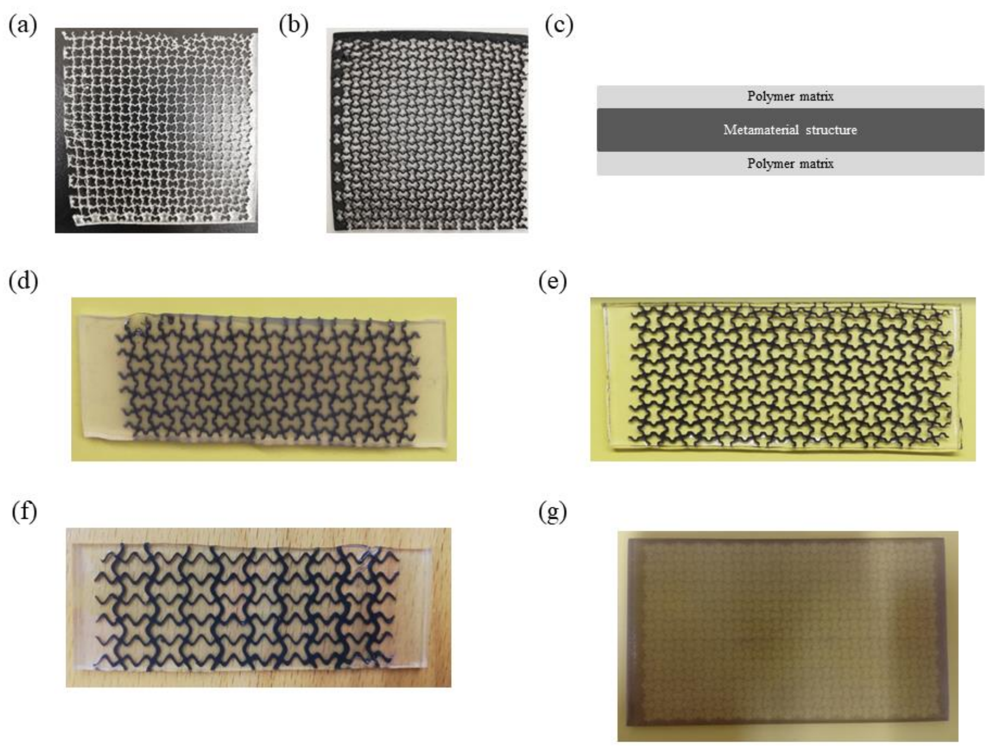

Figure 4.9. Materials and methods used for the study. Stretch ribbon model printed with SLA in (a) elastic resins and (b) flexible resin. (c) Schematic showing the encapsulation perform with polymer matrix. Stretch ribbon model encapsulated in (d) Ecoflex 00-50, (e) Sylgard 184 and (f) ShinEtsu SES-22330-20. (g) Stretch ribbon model printed with multi-material manufacturing technique.

4.3.1 CAD designs

Autodesk Inventor and Solidworks were used for the design of metamaterials. The samples were built by drawing the hollow part as unit cell designs and doing a cut through the base of 1 mm. The samples based on straight beams and circle models are shown in Figure 4.10. The circles with different sizes have radius of 4 mm and 2 mm, with a separation between center points of 5 mm. The other circled pattern, shown in Figure 4.10b, has circles of 5 mm of radius and a separation of 6 mm between center points. The re-entrant honeycombs, shown in Figure 4.10d, are based on a square of 7 mm x 4 mm and the distance between entrances is of 1 mm.

Figure 4.11 shows models of samples based on curved beams. Figure 4.11 a, b, d were based on rectangles from no more than 6 mm x 3 mm that were later shaped with lines created using fillet tool and arcs. Figure 4.11c and Figure ***4.11***e were created using sine waves. In the case of Figure 4.11c, four sine waves with the formula $y(x) = 1\, mm\; x\; sin\, \left(1\, rad\; x \frac{x}{1.2}\; mm\right)$, where $0\;\; mm < x < 3.768\, mm$, were connected to form a close loop. In the case of Figure 4.11e, a continuous wave with the formula $y(x) = 3\, mm\; x\; sin\, \left(1\, rad\; x \frac{x}{3}\; mm\right)$, where $-50\;\; mm < x < 50\, mm$. These sine waves are connected by a beam of 0.942 mm from thickness. For the simplicity of the design, every beam has the same thickness. The design principles from Figure 4.10 and Figure 4.11 are based on the literature [56], [99], [100], [101], [102].

Figure 4.12 shows the design created in this work. For these samples, the equation of the sine wave across the x-axis was maintained constant $y(x) = 1\, mm\; x\; sin\, \left(1\, rad\; x \frac{x}{1.2}\; mm\right)$, while the y-axis function presents sine wave equations with different wavelength. For this, two parameters, shown in the general parametric formula Equation (4.1), are established: l and t_{max}. l is used to change de wavelength and t_{max} establishes the length of the wave for a unit cell.

$$
\begin{gathered}
x(t) = 1\,mm\; x\; sin\left(1\,rad\; x\frac{t}{l}\; mm\right) \\
y(t) = t \text{ mm} \\
0\,mm < t < \; t_{max}\,mm
\end{gathered}
\tag{4.1}
$$

In the case of Figure 4.12a, the parametric function for drawing the y-axis function is $x(t) = 1\,mm\; x\; sin\left(1\,rad\; x\frac{t}{0.4}\; mm\right)$, $y(t) = t\,mm$, where $0\,mm < t < 6.283\,mm$. After that, this function is mirrored on an axis over the y-direction in the center of the unit cell. Figure 4.12b has a similar structure, but the parametric function is $x(t) = 1\,mm\; x\; sin\left(1\,rad\; x\frac{t}{0.6}\; mm\right)$, where $0\,mm < t < 5.655\,mm$, which gives a larger wavelength to the unit cell. In these two cases, the sine waves in the x-direction have a difference in phases of 1.2π. In the other hand, Figure 4.12c shows a structure in which the sine waves in the x-axis do not present any change in phases and the function in the y-axis, even though is the same as in Figure 4.12b, its range is $0\,mm < t < 3.768\,mm$. All these parameters are summarized in Table 4.2

Table 4.2. Parametric equations used for the designs of samples created by the author.

Model	Parametric equation	Range of t
Model 0.4	$1\,mm\; x\; sin\left(1\,rad\; x\frac{t}{0.4}\; mm\right)$ $y(t) = t\,mm$	$0\,mm < t < 6.283\,mm$
Model 0.6	$1\,mm\; x\; sin\left(1\,rad\; x\frac{t}{0.6}\; mm\right)$ $y(t) = t\,mm$	$0\,mm < t < 5.655\,mm$
Model E	$1\,mm\; x\; sin\left(1\,rad\; x\frac{t}{0.6}\; mm\right)$ $y(t) = t\,mm$	$0\,mm < t < 3.768\,mm$

In order to mimic the form of the aorta, tubular structures were also design with an outer diameter of 19.05 mm, a thickness of 1 mm and a length of 140 mm. The bone form was used as unit cell for this structure, as can be seen in Figure 4.14.

4.3.2 SLA manufacturing

The CAD designs were printed using Form2 from FormLabs in two different resins shown in Figure 4.9 (a) and (b): elastic resin and flexible resin. The first one has a white-transparent color while the second one is characterized by a gray color. All the printings were done with a horizontal orientation in theto PreForm, the Formlabs print preparation software. After printing, the print is washed in a sonicating bath with isopropanol (IPA) for 10 minutes and left to air dry. After drying, the print was UV cured (UV Cleaner Model N°342) for 15 minutes, flipping halfway through. When the material is stiff enough, the supports are trimmed with scissors and nail trimmers.

As was reported in literature [16], [24], an encapsulation in a soft matrix helped stiff structures to obtain an strain-stiffening behavior. In this work, the encapsulation was done using silicone elastomers Sylgard 184, ShinEtsu SES-22330-10 ShinEtsu SES-22330-20 and Ecoflex 00-30 and Ecoflex 00-50 in the configuration shown in Figure 4.1c. In the case of Sylgard 184, the base and the curing agent was mixed on a ratio of 10:1 and de-aerated after that. When the air bubbles were totally removed, one layer was applied by hand over a glass surface using acrylic molds, over it the structure was placed and then another layer of the elastomer was poured. The samples were left for drying overnight. The same procedure was used for the Ecoflex 00-30 and Ecoflex 00-50, the last one with a mixing ratio of 1:1.

4.3.3 Multi-material manufacturing

The CAD designs were used for creating assemblies, shown in Figure 4.9g, for printing using mixtures of two materials with Stratasys J750. With this configuration, the metamaterial structure was printed from a stiffer material than the matrix encapsulating it. The resins used were VeroCyan (stiff) and Agilus30Clear (flexible) and their combination on the samples are summarized on Table

4.3. To print with multiple materials on Stratasys J750, the CAD design needs to be an assembly with different parts for different materials. The metamaterial reinforcement (middle layer) is printed with a stiffer material, andthe surrounding matrix (inner and outer layers) is printed with more flexible material. The supports are dissolvable in a 2% solution of Sodium Hydroxide. The reinforcement has a thickness of 1mm, while the inner and outer matrices have a thickness of 0.5mm each.

Table 4.3. Concentrations of resins for different printed models using Stratasys printer.

Sample	Model	Metamaterial structure	Metamaterial structure resin	Matrix resin
1	Tubular	Bone form	70% VeryCyan with 30% Agilus30Clear	Pure Agilus30Clear
2	Planar	Stretch ribbon	70% VeryCyan with 30% Agilus30Clear	Pure Agilus30Clear
3	Planar	Stretch ribbon	70% VeroBlackPlus with 30% Agilus30Clear	40% VeroBlackPlus with 30% Agilus30Clear

The models were designed with three layers. The encapsulation was done with a thickness of 0.5 mm, while the metamaterial structure was designed with 1 mm of thickness.

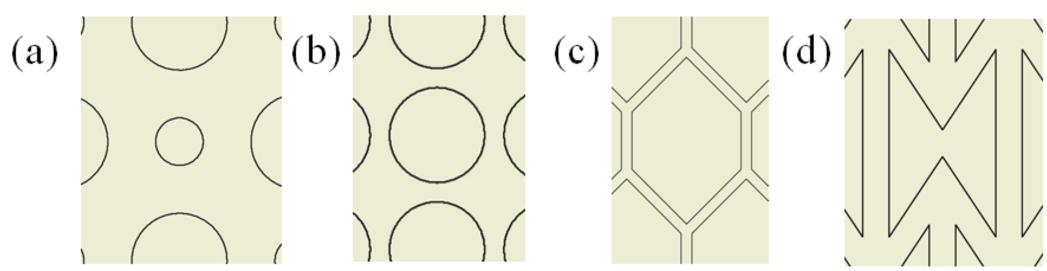

Figure 4.10. Designed unit cells for the samples based on straight beams and circles. (a) Circles of different sizes (radiuses 4mm and 2 mm, distance between center points 5 mm), (b), circles with radius of 5 mm and distance between center points of 6 mm [101] (c) honeycomb, (d) re-entrant honeycomb [100]. The re-entrant honeycombs are based on a square of 7 mm x 4 mm and the distance between entrances is of 1 mm. All samples have a thickness of 1mm.

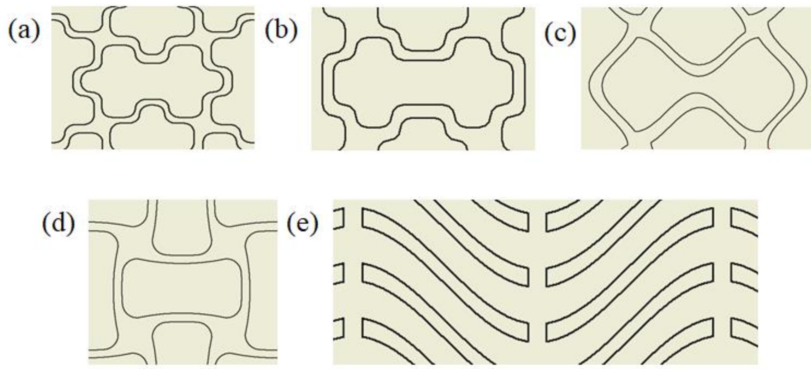

Figure 4.11. Designed unit cells for the samples based on curved beams. (a) Stretch ribbon form inspired in Clausen et. al model from -0.2 Poisson's ratio. (b) Ribbon form inspired in Clausen et. al model from -0.4 Poisson's ratio. (c) Eight-form inspired in Clausen et. al model from -0.6 Poisson's ratio. (d) Bone form inspired in Clausen et. al model from -0.8 Poisson's ratio [102]. (e) Sine wave form inspired in Rafsanjani et. al model [56]. All samples have a thickness of 1mm. (a), (b), (d) were based on rectangles from no more than 6 mm x 3 mm that were later shaped with lines created using fillet tool and arcs. (c) and (e) were created using sine waves. In (c), four sine waves with the formula $y(x) = 1\ mm\ x\ sin\ \left(1\ rad\ x\frac{x}{1.2}\ mm\right)$, where 0 mm<x<3.768 mm, were connected to form a close loop. In (e), a continuous wave with the formula $y(x) = 3\ mm\ x\ sin\ \left(1\ rad\ x\frac{x}{3}\ mm\right)$, where -50 mm<x<50 mm. These sine waves are connected by a beam of 0.942 mm from thickness.

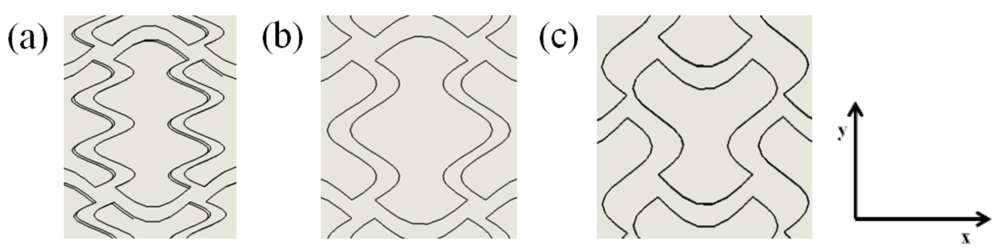

Figure 4.12. Designed unit cells for the samples based on curved beams created by the author: (a) model 0.4 (b) model 0.6 and (c) model E. Dimensions are shown in Table 4.2.

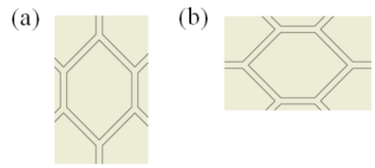

Figure 4.13. Different orientations of hexagonal structure used for tensile test: (a) direction 1 and (b) direction 2.

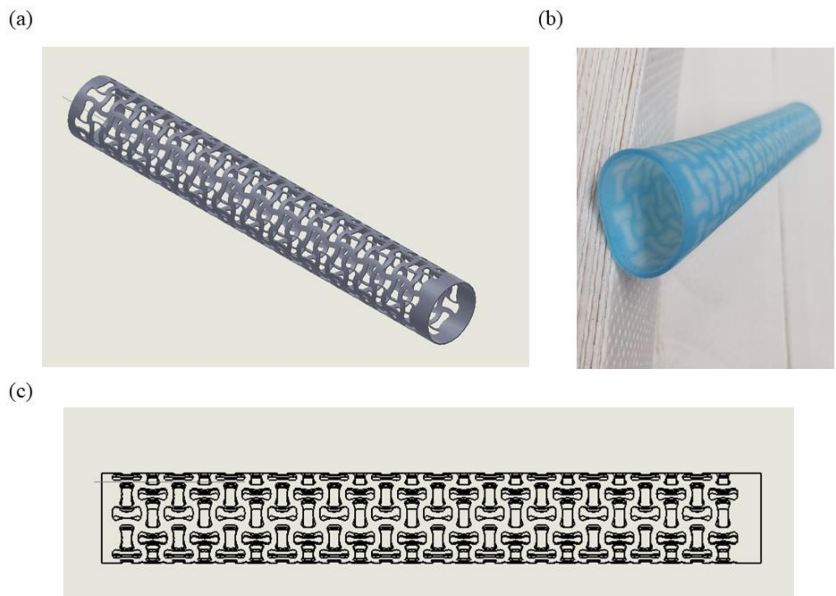

Figure 4.14. Bone form inspired in Clausen et. al model from -0.8 Poisson's ratio in a tubular structure [102] (a) CAD model, (b) printed sample with Stratasys, (c) top view of structure.

4.3.4 Tension test

In order to test the strain-stress behavior of the samples made, uniaxial test using 5943 Instron Tensile Test with a rate of extension of 10 mm/min. In the case of the hexagon samples shown in Figure 4.10c the tension test was done in two directions. As can be seen in Figure 4.13, the direction 1 has the corners with the smallest angle in the top and bottom of the structure, while direction 2 has these corners at the sides of the structures.

4.4 Results and discussion

In the SLA manufacturing, two resins were compared: elastic and flexible resins. The elastic one is softer than the flexible one, and as a result, it is easily bent and difficult to print. This material was not considered suitable for the application as it does not provide reinforcement due to very low modulus. Therefore, only flexible resin was used for SLA printing.

The results of the test done with the structures based on straight beams and circle hollow parts are shown in Figure 4.15. As seen from Figure 4.15, the structures without an encapsulation showed an approximately linear behavior. Circular structures break faster, followed by the hexagonal structure that was tested in the direction 1. The circular structures break easily because the structure was not able to deform upon tension. In order to avoid this, either less space between circles should be placed or the structure material must change. Due to the limitations in materials and focus of this study, these approaches were not explored. The re-entrant honeycomb structure and the hexagonal one tested in direction 2 could deform upon less stress and then broke. This type of behavior is different from the one this study aimed to achieved, however, this test revealed one problem. The encapsulation in Ecoflex 00-30 presented delamination due to the poor attachment of the structure to it. As a result, upon the break of the first beams of the structure, the out-of-plane broken beams started damaging the polymer matrix, as can be seen in Figure 4.15 (c). The Ecoflex could endure the strain four times more than the structure itself. However, as the metamaterial structure had the defects prior to testing, the properties may differ. The breaking of the beams can be seen from Figure 4.15 (b). Even though these samples were of interest in this study, they did not show a strain-stiffening behavior. Curved beams structure showed to be promising for to reduce stress concentrations and improve stretchability, therefore, this study focused on curved beam structures [56], [98], [102].

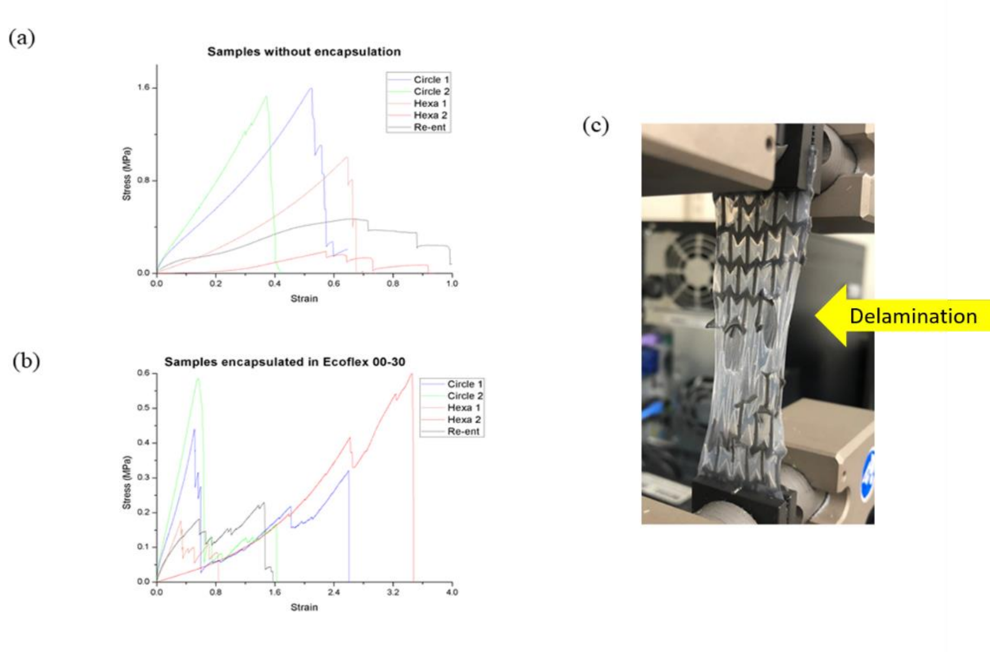

Figure 4.15. Tension test results of the samples with straight beams based on literature. (a) Stress vs. strain plot of structures without encapsulation. (b) Stress vs. strain plots of structures with Ecoflex 00-50 encapsulation. (c) Tension test for the re-entrant honeycomb structure encapsulated with Ecoflex 00-50. Delamination and early break of the beams of the metamaterial structure is seen.

The same procedure was used to evaluate the behavior of the curved beams samples. As can be seen in Figure 4.16, the behavior is strain-stiffening, however, the stress measured for a specific strain was lower than the one expected from an aorta, this was caused by a breakdown of the Instron machine in the time of the test. This is also the reason for high noise present in the resulting data. Moreover, the metamaterial structures give interesting mechanical properties due to unfolding of the beam structures (Figure 4.16d) during tension. In the case of the Ecoflex 00-50 encapsulation (Figure 4.16b), the strain-stiffening-softening behavior was absent due to the restriction of mobility of the metamaterial structure inside the polymer matrix. Thus, a more linear curve can be seen in Figure 4.16b. In the case of Sylgard 184 encapsulation, the matrix teared before the structure. Hence, the beams could unfold upon the strain and the strain-stiffening-softeningbehavior can be seen (Figure 4.16c).

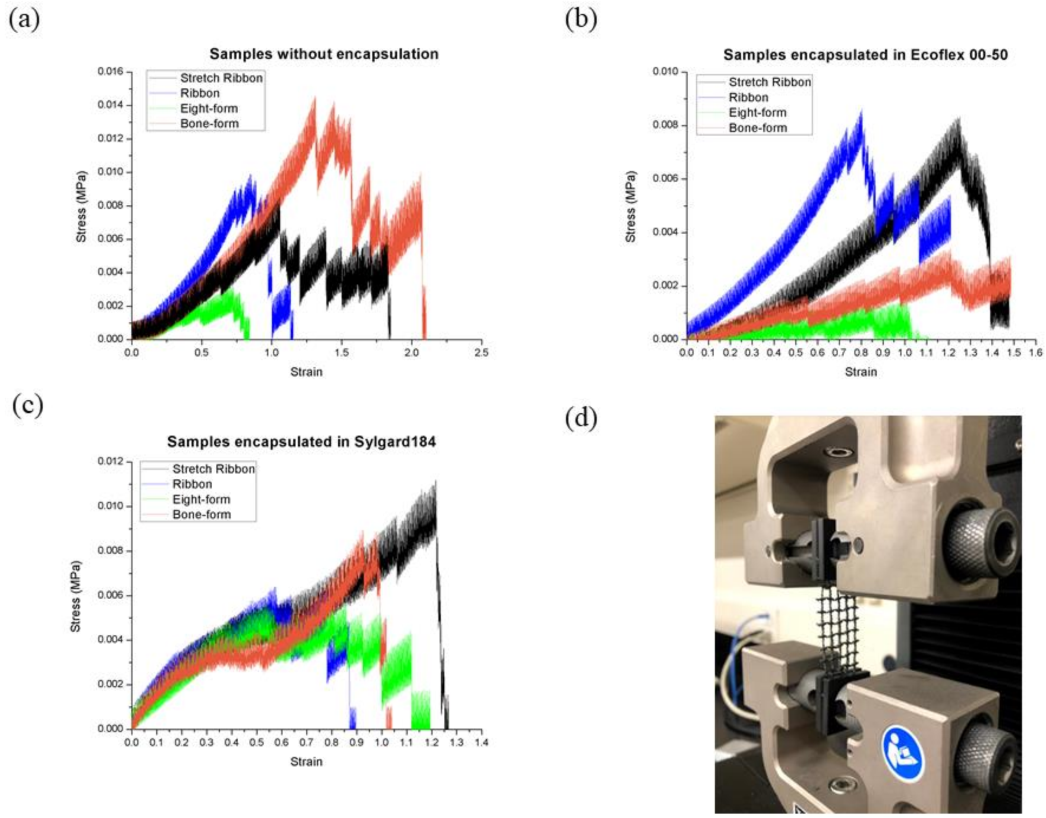

Figure 4.16. Tension test results of the samples with curved beams based on literature. (a) Stress vs. strain plot of structures without encapsulation. (b) Stress vs. strain plots of structures with Ecoflex 00-50 encapsulation. (c) Tension test for the re-entrant honeycomb structure encapsulated with Sylgard 184. (d) Unfolding of samples under high tensile stress. Note: due to equipment breakdown, the data has noise and the stress is very low. However, the data can be used to see the general trend in behavior of structures and composites.

Due to the strain-stiffening behavior of the curved lines structures, variations to the wavelength of the sine-wave based structure was chosen for a further study. The focus of this study is uniaxial tension, therefore, the wavelength of beams along the axis of tension was changed to study the effects on it over the stress-strain behavior of the metamaterial (Figure 4.17).

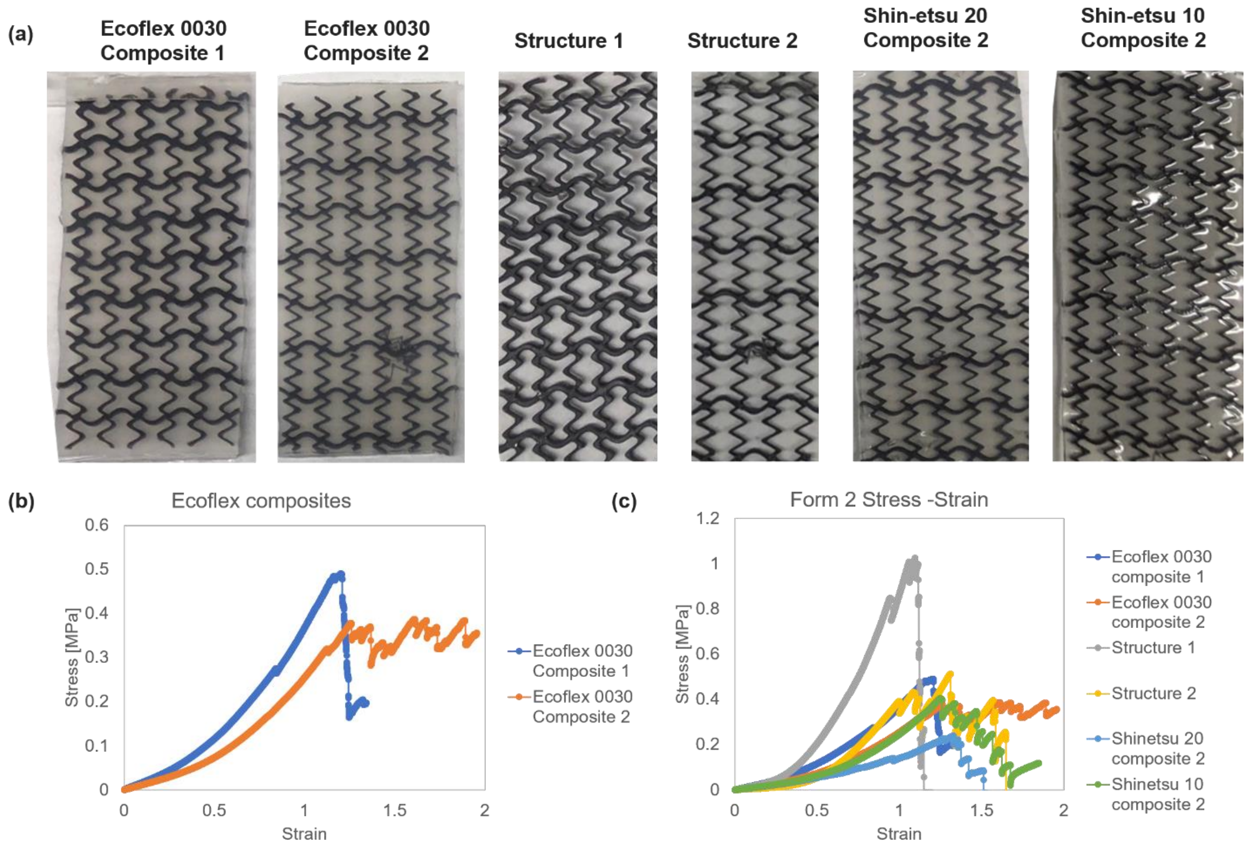

Figure 4.17. Tension test results of the samples fabricated using Form 2 SLA printer with Flexible Resin with two sine-wave designs (Structure 1 and Structure 2).

As seen from Figure 4.17 (b), the composite 2, which is based on Structure 2, which has an extra node of sine-wave is more elastic as well as has a snapping behavior after maximum stress. This was not observed from composite 1, which fails right after reaching maximum stress. The same behavior was observed for pure structures 1 and 2. The effect of soft elastomer matrix can be observed from Figure 4.17 (c). For composites with embedded structure 2, Ecoflex 0030 with durometer 30 is the stiffest, followed by Shin-Etsu 20 (durometer 20) and Shin-Etsu 10 (durometer 10) being softest.

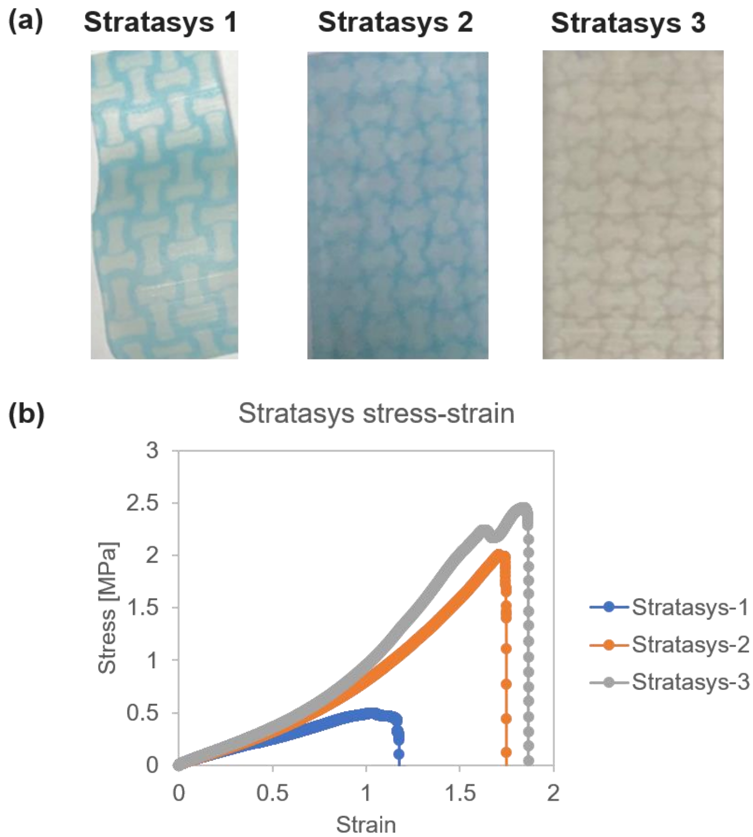

Figure 4.18. Tension test results of the samples fabricated using Stratasys PolyJet multimaterial printer according to Table 4.3. All tested samples have a thickness of 1 mm, width of 25 mm and length of 45 mm.

Figure 4.18 presents the results of tension test of Stratasys samples. It can be observed from Table 4.3 that Stratasys 3 sample has the highest concentration of stiff resin and therefore shows the stiffest response. Stratasys 1 sample fabricated in tubular form had the smallest thickness and a different structure and showed the softest response. Overall, it can be noticed that Stratasys samples did not show a snapping response to tension. Moreover, comparing the composites prepared using Form2 Flexible printer, the chosen concentration of Stratasys PolyJet resins show a much stiffer response (3MPa compared to approximately 0.5 MPa). Although, PolyJet printer produces samples that have a good attachment of the structure to the matrix, and delamination problems did not happen during tension test, we did not observe a strain-softening property or any unusual property in fabricated samples other that strain-stiffening. The developed sine-wave based structure should be tested further. Moreover, the choice of resin was limited. The samples were rather stiff, thus it can be suggested for further studies to use higher concentrations of flexible resin.

SLA printer samples with a Flexible Resin, on the other hand, had favorable stiffness range (much softer that Stratasys samples and similar to aorta) and allowed for wide choice of encapsulation matrix. The printed metamaterials were molded with different elastomers, which provided further adjustment of mechanical properties. The samples with sine-wave design demonstrated a snapping behavior, which is beneficial for desired application.

4.5 Conclusion

The results of this study reinforced previous observations on the use of curved beams and sine waves based structures encapsulated for mimicking soft tissues [143], [144] and the use of metamaterials for this particular application [56], [31], [145] First, an ideal curve for a material replacing the aorta tissue walls in ex-vivo perfusion devices was determined. A strain-stiffening behavior up to 100 kPa and a softening above that stress was proposed to avoid peak stresses in ex-vivo perfusion devices. Proper printing methods for SLA and multi-material printing were established was well as a methodology for building literature metamaterial structures and creating new ones based on sine waves. We presented metamaterials structures with different wavelength, along with a parameterization method. Interestingly, the sine-wave design allowed for snapping behavior, which can be further manipulated to achieve the desired stress-softening behavior. We identified that encapsulation of the metamaterial composite must be properly attached to the structure in order to avoid the out-of-plane movement of beams that destroys the matrix and it must allow the movement of the structure during the tension and achieve the desired behavior. Among the polymer matrix tested, the Sylgard 184 allows this freedom, but is not a suitable encapsulation because it breaks before the structure itself. The use of multi-material printing was promising for avoiding delamination, but variation of material concentrations should be studied further.

5 Conclusion and future work

5.1 Summary of my thesis works

The work described in this thesis is focused on synthetic materials to replace rigid and noncompliant plastic tubing used in an ex-vivo heart perfusion device. Two projects are included here: the first one is fabrication of fabric-reinforced elastomer composites to mimic the rapidly strain-stiffening *J-shaped* and anisotropic stress-strain behavior of human and porcine aorta, the second project is the design of the mechanical metamaterial composite with unique strain softening property that limits the peak pressure in aorta by expanding to accommodate a large stroke volume.

The main findings of the first project can be summarized as follows:

(1) uniaxial tensile stress tests were performed to find that the mechanical properties of human (n = 1) and porcine aorta (n = 14) are non-linear (*J-shaped* strain stiffening behaviour),

anisotropic (longitudinal direction stiffer than circumferential), and gradient (stiffer in regions where farer from the heart).

(2) fabric-reinforced silicone elastomer composites were fabricated to match the mechanical properties of human aorta, where the structural motif of the embedded fabric (knitted or woven) influences the mechanical properties of the composite in a deterministic manner.

(3) improved analytical constitutive models were suggested based on Gent's and Mooney-Rivlin's constitutive model (fitting parameters are widely available in previous literatures) combined with Holzapfel–Gasser–Ogden's model (rapid stiffening behaviour of fabric and aorta are effectively captured with the two fitting parameters) as a stepping stone towards judicial selection of the matrix and the fabric materials in future studies.

The second project can be summarized as follows:

(4) A thorough literature review of nature-inspired metamaterials was performed, and additive manufacturing technologies used to print them were evaluated.

(5) Promising metamaterial structures were identified.

(6) Using SLA and multi-material printing metamaterial structures based on sine waves were prepared. The wavelength was suggested as parameterization method.

The second project was not finished during my MSc but will be continued further after my graduation.

5.2 Broad context of contribution

Composites of elastomer or rubber-like material and fibers have a variety of applications in engineering, including geotechnical construction, transportation, aerospace, and health fields [146]. Automobile tires and belts are one example of synthetic rubber composites. Natural composite examples include biological tissues, such as blood vessels, tendons, ligaments [147]. Fiber-reinforced elastomers are great candidates for tissue engineering, soft robotics and microfluidic applications. This is because elastomer matrices can exhibit a wide range of deformations, much larger than stiffer matrices, such as metals, ceramics, or rigid polymers [148]. Soft elastomer matrix in combination with systematically arranged fiber families form dissipative materials that display direction-dependent properties and sustain finite strains, which can be widely used in biomechanics and medicine [147]. Fiber-reinforced composites appear as a great promise for long-term restorative materials in dentistry [149].

Soft robotics aims to produce robots made of flexible components that offer many useful capabilities, such as deformation of shape, manipulation of delicate objects, conformation to surroundings, and to movement in various environments [150]. Soft actuators' body is usually composed of elastomeric materials, due to their heat and chemical resistance, possibility to co-mold multiple materials, and ability to withstand large deformations while undergoing complex motion [79]. Fiber-reinforced composites are promising actuators tools, because after incorporating anisotropic fibers into the actuator body, elastomeric structures can produce numerous combinations of motion by expanding in less stiff regions [79], [151], [152]. Textiles are also capable of producing complex motions due to wide range of stretch and strain properties [79]. For example, warp-knitted mesh fabrics are promising structural products that can be used in composite reinforcement [153] and biomaterial patches [154], [155], due to their light weight, high porosity, strength, and easy design as well as complex geometric morphology and mechanical properties [146]. Baughman and co-workers developed artificial muscles by twisting inexpensive high strength fishing line and sewing thread polymer fibers to provide fast, scalable, nonhysteretic, long-life tensile and torsional muscles [156]. Wang and co-workers combined heterogeneous fabric material layers to create soft fabric-based actuators, such as airtight bladder as well as soft strain sensor [79].

Tissue engineering is another emerging area of research aiming to repair or regenerate the functions of damaged tissue by using synthetic scaffolds, where fiber-reinforced composites can play key role by providing a structural support to accommodate cells and spatially control their growth into a specific tissue, by tuning fiber orientation [157]. Specifically, in the field of vascular tissue engineering, fibrous composites can be widely designed as bioinspired scaffolds, because arterial walls have complex sandwich structure with varying distribution of collagen and elastin fibers, smooth muscle cells and other molecules of the extracellular matrix [19]. Bailly and co-workers performed a fundamental study about the mechanical effect of fabric-reinforcement by using a custom-designed jig to precisely control the density and angle of the fibers for mimicking human abdominal aortic tissue [68].

5.3 Future Works

5.3.1 Fabric-reinforced elastomer composites: Mimicking '*J-shaped*' and anisotropic stress-strain behavior of human and porcine aorta

This study focuses on the measurement of the mechanical properties of aortas and the establishment of the fabric-reinforced elastomers that mimic the aortic properties. The fabrication of actual tubes and the verification of the material's efficacy in generating the Windkessel effect is the scope of our future studies. In addition, fatigue and creep resistance should also be established for long-term use of the materials. The biocompatibility of these materials should also be established. Ultimately, a tube that can be used in our ex vivo heart perfusion device should be developed.

5.3.2 3D Printed Structure Reinforced Metamaterials: Beyond Natural Aorta's Capacity to Regulate Blood Flow

To eliminate the consequences of aortic stiffening at high pressure, a metamaterial with unique strain-softening property at peak pressure coming after *J-shaped* strain-stiffening property is proposed. A final structure that possesses the desired stress-strain property should be designed. A structure should be casted into silicone elastomer composite and any delamination problems need to be solved. Finally, the 3D printed structure reinforced metamaterial composite should be fabricated in tubular form to be used in the device to regulate blood flow. Designing and fabricating the junction between the perfusion device system (being developed in Dr. Nobes and Dr. Freed groups) and our reinforced metamaterial tube are also major tasks. Once integrated, the fabricated tube will be a subject of fundamental studies (for example, (i) studying time-variant local deformation profiles under simulated and actual blood flows, (ii) fluid dynamics of blood flow in the tube, and (iii) simulated aneurysm by introducing local defect in tube material), while the eventual goal is to design and fabricate ideally personalized neo-aorta tubes with tunable *strain-stiffening-softening* property that fits specific conditions that each donor heart may possess.

References

[1] Chan JL, Kobashigawa JA, Reich HJ, Ramzy D, Thottam MM, Yu Z, Aintablian TL, Liou F, Patel JK, Kittleson MM, Czer LS, "Intermediate outcomes with ex-vivo allograft perfusion for heart transplantation," *The Journal of Heart and Lung Transplantation. 2017 Mar 1,36(3):258-63.*

[2] Messer, S., Ardehali, A., Tsui, S, " Normothermic donor heart perfusion: current clinical experience and the future," *Transplant Int. 2015, 28, 634-642.*

[3] Vela, M.M.,, Sáez, D.G.,, Simon, A.R., "Current approaches in retrieval and heart preservation," *Ann. Cardiothorac. Surg. 2018, 7, 67.*

[4] Lund LH, Khush KK, Cherikh WS, Goldfarb S, Kucheryavaya AY, Levvey BJ, Meiser B, Rossano JW, Chambers DC, Yusen RD, Stehlik J, "The registry of the International Society for Heart and Lung Transplantation: thirty-fourth adult heart transplantation report—2017,, focus theme: allograft ischemic time," *The Journal of Heart and Lung Transplantation. 2017 Oct 1,,36(10):1037-46.*

[5] Schraufnagel DP, Steffen RJ, Vargo PR, Attia T, Elgharably H, Hasan SM, Bribriesco A, Wierup P, "Devices for ex vivo heart and lung perfusion," *Expert review of medical devices. 2018 Mar 4,15(3):183-91.*

[6] Koerner, M.M., Ghodsizad, A., Schulz, U., El Banayosy, A., Koerfer, R., Tenderich, G. , "Normothermic ex vivo allograft blood perfusion in clinical heart transplantation," *Heart Surg. Forum 2014, 17, 3, E141.*

[7] White, C.W., Ambrose, E., Müller, A., Li, Y., Le, H., Hiebert, B., Arora, R., Lee, T.W., Dixon, I., Tian, G., Nagendran, J, "Assessment of donor heart viability during ex vivo heart perfusion," *Can. J. Physiol. Pharmacol. 2015, 93, 893.*

[8] Messer, S.J., Axell, R.G., Colah, S., White, P.A., Ryan, M., Page, A.A., Parizkova, B., Valchanov, K., White, C.W., Freed, D.H., Ashley, E, "Functional assessment and transplantation of the donor heart after circulatory death," *J. Heart Lung Transplant. 2016, 35, 1443.*

[9] G. G. Belz, "Elastic properties and Windkessel function of the human aorta," *Cardiovasc. drugs Ther., vol. 9, no. 1, pp. 73–83, Feb. 1995.*

[10] Soldani, G., Murzi, M., Faita, F., Di Lascio, N., Al Kayal, T., Spanò, R., Canciani, B., Losi, P, "In vivo evaluation of an elastomeric small-diameter vascular graft reinforced with a highly flexible Nitinol mesh," *J. Biomed. Mater. Res., Part B 2019, 107, 951.*

[11] O'Rourke M, " Arterial stiffness, systolic blood pressure, and logical treatment of arterial hypertension," *Hypertension. 1990 Apr,15(4):339-47.*

[12] Shadwick, R.E, " Mechanical design in arteries," *J. Exp. Biol. 1999, 202, 3305.*

[13] Fung, Y.C., Mechanical properties and active remodeling of blood vessels, in Biomechanics, Springer, New York, NY 1993, pp. 321-391.

[14] Abé, H., Hayashi, K., in Data book on mechanical properties of living cells, tissues, and organs (Eds: M. Sato), Springer, Tokyo 1996, p. 106.

[15] Bonani, W., Maniglio, D., Motta, A., Tan, W., Migliaresi, C., "Biohybrid nanofiber constructs with anisotropic biomechanical properties," *J. Biomed. Mater. Res., Part B 2011, 96, 276.*

[16] Shadwick, R.E., "Elasticity in Arteries: A similar combination of rubbery and stiff materials creates common mechanical properties in blood vessels of vertebrates and some invertebrates," *Am. Sci. 1998, 86, 535.*

[17] Ma, Y., Feng, X., Rogers, J.A., Huang, Y., Zhang, Y., "Design and application of 'J-shaped'stress–strain behavior in stretchable electronics: a review," *Lab Chip 2017, 17, 1689.*

[18] Singh, C., Wong, C.S., Wang, X., "Medical textiles as vascular implants and their success to mimic natural arteries," *J. Funct. Biomater. 2015, 6, 500.*

[19] Holzapfel, G. A., Collagen in arterial walls: biomechanical aspects, in Collagen (Eds: P. Fratzl), Springer, Boston, MA 2008, pp. 285-324.

[20] Wang, L., 2016, "Modelling dissection of the arterial wall," *Doctoral dissertation, University of Glasgow.*

[21] Holzapfel GA, Gasser TC, Ogden RW., "A new constitutive framework for arterial wall mechanics and a comparative study of material models," *Journal of elasticity and the physical science of solids. 2000 Jul 1,61(1-3):1-48.*

[22] Guyton AC, "The relationship of cardiac output and arterial pressure control," *Circulation. 1981 Dec,64(6):1079-88.*

[23] Nemes A, Geleijnse ML, Forster T, Soliman OI, Ten Cate FJ, Csanády M., "Echocardiographic evaluation and clinical implications of aortic stiffness and coronary flow reserve and their relation," *Clinical Cardiology: An International Indexed and Peer-Reviewed Journal for Advances in the Treatment of Cardiovascular Disease. 2008 Jul,31(7):304-9.*

[24] Novelli EM, Hildesheim M, Rosano C, Vanderpool R, Simon M, Kato GJ, Gladwin MT, "Elevated pulse pressure is associated with hemolysis, proteinuria and chronic kidney disease in sickle cell disease," *PloS one. 2014 Dec 5,9(12):e114309.*

[25] Ou P, Celermajer DS, Raisky O, Jolivet O, Buyens F, Herment A, Sidi D, Bonnet D, Mousseaux E, "Angular (Gothic) aortic arch leads to enhanced systolic wave reflection, central aortic stiffness, and increased left ventricular mass late after aortic coarctation repair: evaluation with magnetic resonance flow mapping," *The Journal of thoracic and cardiovascular surgery. 2008 Jan 1,135(1):62-8.*

[26] J. T. Church et al, "Normothermic Ex Vivo Heart Perfusion: Effects of Live Animal Blood and Plasma Cross Circulation," *ASAIO J., vol. 63, no. 6, pp. 766–773, 2017.*

[27] Hatami S, White CW, Ondrus M, Qi X, Buchko M, Himmat S, Lin L, Cameron K, Nobes D, Chung HJ, Nagendran J , "Normothermic Ex Situ Heart Perfusion in Working Mode: Assessment of Cardiac Function and Metabolism," *JoVE (Journal of Visualized Experiments). 2019 Jan 12(143):e58430.*

[28] Sokolis DP, Kefaloyannis EM, Kouloukoussa M, Marinos E, Boudoulas H, Karayannacos PE, "A structural basis for the aortic stress–strain relation in uniaxial tension," *Journal of biomechanics. 2006 Jan 1,39(9):1651-62.*

[29] Duprey A, Khanafer K, Schlicht M, Avril S, Williams D, Berguer R, "In vitro characterisation of physiological and maximum elastic modulus of ascending thoracic aortic aneurysms using uniaxial tensile testing," *European Journal of Vascular and Endovascular Surgery. 2010 Jun 1,39(6):700-7.*

[30] Bertoldi K, Vitelli V, Christensen J, van Hecke M, "Flexible mechanical metamaterials," *Nature Reviews Materials. 2017 Nov,2(11):17066.*

[31] K. Wang, C. Wu, Z. Qian, C. Zhang, B. Wang, and M. A. Vannan, "Dual-material 3D printed metamaterials with tunable mechanical properties for patient-specific tissue-mimicking phantoms," *Addit. Manuf., vol. 12, pp. 31–37, 2016.*

[32] H. M. A. Kolken and A. A. Zadpoor, "Auxetic mechanical metamaterials," *RSC Adv., vol. 7, no. 9, pp. 5111–5129, 2017.*

[33] Anseth, K.S., Bowman, C.N., Brannon-Peppas, L, "Mechanical properties of hydrogels and their experimental determination," *Biomaterials 1996, 17, 1647.*

[34] Andriot, M., Chao, S.H., Colas, A.R., Cray, S.E., DeBuyl, F., DeGroot, J.V., Dupont, A., Easton, T., Garaud, J.L., Gerlach, E., Gubbels, F , "Silicones in industrial applications," *Inorg. Polym. 2007, 61.*

[35] Stricher, A.M., Rinaldi, R.G., Barrès, C., Ganachaud, F., Chazeau, L, "How I met your elastomers: from network topology to mechanical behaviours of conventional silicone materials," *RSC Adv. 2015, 5, 53713.*

[36] Rubinstein, M., Colby, R.H, " Polymer physics," *New York: Oxford University Press 2003.*

[37] Romera, M.F.C, "PhD thesis: Biomimetic Strain-stiffening Hydrogels," *Technische Universiteit Eindhoven, 2018.*

[38] Jungebluth P, Haag JC, Sjöqvist S, Gustafsson Y, Rodríguez AB, Del Gaudio C, Bianco A, Dehnisch I, Uhlén P, Baiguera S, Lemon G, "Tracheal tissue engineering in rats," *Nature protocols. 2014 Sep,9(9):2164.*

[39] Pham JT, Lawrence J, Lee DY, Grason GM, Emrick T, Crosby AJ, "Highly stretchable nanoparticle helices through geometric asymmetry and surface forces," *Advanced Materials. 2013 Dec,25(46):6703-8.*

[40] Vatankhah-Varnosfaderani, M., Daniel, W.F., Everhart, M.H., Pandya, A.A., Liang, H., Matyjaszewski, K., Dobrynin, A.V., Sheiko, S.S, "Mimicking biological stress–strain behaviour with synthetic elastomers," *Nature 2017, 549, 497.*

[41] Sherburn, M, "Geometric and Mechanical Modelling of Textiles," *PhD thesis, University of Nottingham..*

[42] Corinna A.Conway, "3D Reinforcement of composite Materials," *Master Thesis, Politecnico Di Milano.*

[43] A. T. Inc., ATEX Technologies Inc., [Online]. Available: https://www.atextechnologies.com. [Accessed 25 July 2019].

[44] Jakel IR, "Analysis of hyperelastic materials with Mechanica-theory and application examples," *PTC Presentation for the 2ndSAXSIM. Technische Universität Chemnitz 27. April 2010, Rev. 1.1.*

[45] Autodesk, "Nonlinear Analysis: Hyperelastic Material Analysis," 2011.

[46] Martins PA, Natal Jorge RM, Ferreira AJ, "A comparative study of several material models for prediction of hyperelastic properties: Application to silicone-rubber and soft tissues," *Strain. 2006 Aug,42(3):135-47.*

[47] Ogden RW, "Non-linear elastic deformations," *Courier Corporation, 1997.*

[48] Spencer AJ, "Constitutive theory for strongly anisotropic solids," *InContinuum theory of the mechanics of fibre-reinforced composites 1984 (pp. 1-32). Springer, Vienna.*

[49] Holzapfel GA, Weizsäcker HW, "Biomechanical behavior of the arterial wall and its numerical characterization," *Computers in biology and medicine. 1998 Jul 1,28(4):377-92.*

[50] Grima JN, "Auxetic metamaterials," 2010. [Online]. Available: http://esc.u-strasbg.fr/docs/2010/lectures/AUXETIC-METAMATERIALS_FIN.pdf. [Accessed 22 August 2019].

[51] Gercek, H, "Poisson's ratio values for rocks," *International Journal of Rock Mechanics and Mining Sciences. 44 (1): 1–13. doi:10.1016/j.ijrmms.2006.04.011.*

[52] Park RJ, "Seismic performance of steel-encased concrete piles," *Research Report. 1987.*

[53] Sparavigna AC., " Honeycomb and auxetic paper-based metamaterials".

[54] Fargette A, Neukirch S, Antkowiak A, "Elastocapillary snapping: Capillarity induces snap-through instabilities in small elastic beams," *Physical review letters. 2014 Apr 4,112(13):137802.*

[55] Pandey A, Moulton DE, Vella D, Holmes DP, "Dynamics of snapping beams and jumping poppers," *EPL (Europhysics Letters). 2014 Feb 10,105(2):24001.*

[56] Rafsanjani A, Akbarzadeh A, Pasini D, "Snapping mechanical metamaterials under tension," *Advanced Materials. 2015 Oct,27(39):5931-5.*

[57] Silverberg JL, Evans AA, McLeod L, Hayward RC, Hull T, Santangelo CD, Cohen I, "Using origami design principles to fold reprogrammable mechanical metamaterials," *Science. 2014 Aug 8,345(6197):647-50.*

[58] Kang SH, Shan S, Košmrlj A, Noorduin WL, Shian S, Weaver JC, Clarke DR, Bertoldi K, "Complex ordered patterns in mechanical instability induced geometrically frustrated triangular cellular structures," *Physical review letters. 2014 Mar 5,112(9):098701.*

[59] Coulais C, Kettenis C, van Hecke M, "A characteristic length scale causes anomalous size effects and boundary programmability in mechanical metamaterials," *Nature Physics. 2018 Jan,14(1):40.*

[60] Meier C, Popp A, Wall WA, "Geometrically exact finite element formulations for slender beams: Kirchhoff–love theory versus Simo–Reissner theory," *Archives of Computational Methods in Engineering. 2019 Jan 15,26(1):163-243.*

[61] Qiu J, Lang JH, Slocum AH, "A curved-beam bistable mechanism," *Journal of microelectromechanical systems. 2004 Apr 13,13(2):137-46.*

[62] Che K, Yuan C, Wu J, Qi HJ, Meaud J. , "Three-dimensional-printed multistable mechanical metamaterials with a deterministic deformation sequence," *Journal of Applied Mechanics. 2017 Jan 1,84(1):011004.*

[63] Yan, B., Huang, J., Han, L., Gong, L., Li, L., Israelachvili, J.N., Zeng, H., "Duplicating Dynamic Strain-Stiffening Behavior and Nanomechanics of Biological Tissues in a Synthetic Self-Healing Flexible Network Hydrogel," *ACS nano 2017, 11, 11074.*

[64] Fung, Y.C., "Structure and stress-strain relationship of soft tissues," *Am. Zool. 1984, 24, 13.*

[65] Myung, D., Koh, W., Ko, J., Hu, Y., Carrasco, M., Noolandi, J., Ta, C.N., Frank, C.W., "Biomimetic strain hardening in interpenetrating polymer network hydrogels," *Polymer 2007, 48, 5376.*

[66] Puperi, D.S., Kishan, A., Punske, Z.E., Wu, Y., Cosgriff-Hernandez, E., West, J.L., Grande-Allen, K.J., "Electrospun polyurethane and hydrogel composite scaffolds as biomechanical mimics for aortic valve tissue engineering," *ACS Biomater. Sci. Eng. 2016, 1546.*

[67] Sharabi, M., Benayahu, D., Benayahu, Y., Isaacs, J., Haj-Ali, R., "Laminated collagen-fiber bio-composites for soft-tissue bio-mimetics," *Compos. Sci. Technol. 2015, 117, 268.*

[68] Bailly, L., Toungara, M., Orgéas, L., Bertrand, E., Deplano, V., Geindreau, C., "In-plane mechanics of soft architectured fibre-reinforced silicone rubber membranes," *J. Mech. Behav. Biomed. Mater. 2014, 40, 339.*

[69] Karimi, A., Navidbakhsh, M., Alizadeh, M., Shojaei, A., "A comparative study on the mechanical properties of the umbilical vein and umbilical artery under uniaxial loading," *Artery Res. 2014, 8, 51.*

[70] Gundiah, N., Matthews, P.B., Karimi, R., Azadani, A., Guccione, J., Guy, T.S., Saloner, D., Tseng, E.E., "Significant material property differences between the porcine ascending aorta and aortic sinuses," *J. Heart Valve Dis. 2008, 17, 606.*

[71] Ha, S.M., Yuan, W., Pei, Q., Pelrine, R., Stanford, S., "Interpenetrating polymer networks for high-performance Electroelastomer artificial muscles," *Adv. Mater. 2006, 18, 887.*

[72] E.M. Isselbacher, in Essential Cardiology (Eds: C. Rosendorff), Humana Press 2005, pp. 681-690.

[73] Azadani, A.N., Chitsaz, S., Matthews, P.B., Jaussaud, N., Leung, J., Tsinman, T., Ge, L., Tseng, E.E., "Comparison of mechanical properties of human ascending aorta and aortic sinuses," *The Ann. Thorac. Surg. 2012, 93, 87.*

[74] Karatolios, K., Wittek, A., Nwe, T.H., Bihari, P., Shelke, A., Josef, D., Schmitz-Rixen, T., Geks, J., Maisch, B., Blase, C., Moosdorf, R., "Method for aortic wall strain measurement with three-dimensional ultrasound speckle tracking and fitted finite element analysis," *The Ann. Thorac Surg. 2013, 96, 1664.*

[75] Matthews, P.B., Azadani, A.N., Jhun, C.S., Ge, L., Guy, T.S., Guccione, J.M., Tseng, E.E., "Comparison of porcine pulmonary and aortic root material properties," *The Ann. Thorac. Surg. 2010, 89, 1981.*

[76] Maziz, A., Concas, A., Khaldi, A., Stålhand, J., Persson, N.K., Jager, E.W., "Knitting and weaving artificial muscles," *Sci. Adv. 2017, 3, 1600327.*

[77] She, Q., Wei, J., Ma, N., Sim, V., Fane, A.G., Wang, R., Tang, C.Y., "Fabrication and characterization of fabric-reinforced pressure retarded osmosis membranes for osmotic power harvesting," *J. Membr. Sci. 2016, 504, 75.*

[78] Choi, M.S., Ashdown, S.P., "Effect of changes in knit structure and density on the mechanical and hand properties of weft-knitted fabrics for outerwear," *Text. Res. J. 2000, 70, 1033.*

[79] Wang, Y., Gregory, C., Minor, M.A., "Improving Mechanical Properties of Molded Silicone Rubber for Soft Robotics Through Fabric Compositing," *Soft Robot. 2018, 5, 272.*

[80] De Carvalho, L.H., Cavalcante, J.M.F., d'Almeida, J.R.M., "Comparison of the mechanical behavior of plain weave and plain weft knit jute fabric-polyester-reinforced composites," *Polym.-Plast. Technol. Eng. 2006, 45, 791.*

[81] Anseth, K.S., Bowman, C.N., Brannon-Peppas, L., "Mechanical properties of hydrogels and their experimental determination," *Biomaterials 1996, 17, 1647.*

[82] Gundiah, N., Ratcliffe, M.B., Pruitt, L.A., "Determination of strain energy function for arterial elastin: experiments using histology and mechanical tests," *J. Biomech. 2007, 40, 586.*

[83] Gent A.N., "A new constitutive relation for rubber," *Rubber Chem. Technol. 1996, 69, 59.*

[84] Lu, T., Huang, J., Jordi, C., Kovacs, G., Huang, R., Clarke, D.R., Suo, Z., "Dielectric elastomer actuators under equal-biaxial forces, uniaxial forces, and uniaxial constraint of stiff fibers," *Soft Matter 2012, 8, 6167.*

[85] Zhao, X., Wang, Q., "Harnessing large deformation and instabilities of soft dielectrics: Theory, experiment, and application," *Appl. Phys. Rev. 2014, 1, 021304.*

[86] Zhao, X., Suo, Z., "Theory of dielectric elastomers capable of giant deformation of actuation," *Phys. Rev. Lett. 2010, 104, 178302.*

[87] Treloar, L.R.G., The physics of rubber elasticity, Oxford University Press, USA 1975.

[88] Rivlin, R.S., "Large elastic deformations of isotropic materials IV. Further developments of the general theory," *Philos. Trans. R. Soc., A 1948, 241, 379.*

[89] Zhao, X., Hong, W., Suo, Z., "Electromechanical hysteresis and coexistent states in dielectric elastomers," *Phys. Rev. B 2007, 76, 134113.*

[90] La, T.G., Lau, G.K., Shiau, L.L., Tan, A.W.Y., "Muscle-like high-stress dielectric elastomer actuators with oil capsules," *Smart Mater. Struct. 2014, 23, 105006.*

[91] Wissler, M., Mazza, E., "Modeling and simulation of dielectric elastomer actuators," *Smart Mater. Struct. 2005, 14, 1396.*

[92] Kumar, N., Rao, V.V., "Hyperelastic Mooney-Rivlin model: determination and physical interpretation of material constants," *Parameters 2016, 2, 01.*

[93] Putra, K.B., Plott, J., Shih, A.J., "Biaxial Mooney-Rivlin coefficient of silicone sheet by additive manufacturing," *Procedia CIRP 2017, 65, 189.*

[94] Jang, K.I., Li, K., Chung, H.U., Xu, S., Jung, H.N., Yang, Y., Kwak, J.W., Jung, H.H., Song, J., Yang, C., Wang, A., " Self-assembled three dimensional network designs for soft electronics," *Nat. Commun. 2017, 8, 15894.*

[95] Pineda, F., Bottausci, F., Icard, B., Malaquin, L., Fouillet, Y., " Using electrofluidic devices as hyper-elastic strain sensors: Experimental and theoretical analysis," *Microelectron. Eng. 2015, 144, 27.*

[96] N. M. Pahlevan and M. Gharib, "Aortic Wave Dynamics and Its Influence on Left Ventricular Workload," *PLoS One, vol. 6, no. 8, p. e23106, Aug. 2011.*

[97] Kassab GS, "Biomechanics of the cardiovascular system: the aorta as an illustratory example," *Journal of the Royal Society Interface. 2006 Jul 5,3(11):719-40.*

[98] Y. Chen, T. Li, F. Scarpa, and L. Wang, "Lattice Metamaterials with Mechanically Tunable Poisson's Ratio for Vibration Control," *Phys. Rev. Appl., vol. 7, no. 2, p. 024012, Feb. 2017.*

[99] A. Ingrole, A. Hao, and R. Liang, "Design and modeling of auxetic and hybrid honeycomb structures for in-plane property enhancement," *Mater. Des., vol. 117, pp. 72–83, Mar. 2017.*

[100] T. Li, Y. Chen, X. Hu, Y. Li, and L. Wang, "Exploiting negative Poisson's ratio to design 3D-printed composites with enhanced mechanical properties," *Mater. Des., vol. 142, pp. 247–258, 2018.*

[101] Florijn B, Coulais C, van Hecke M. , "Programmable mechanical metamaterials: the role of geometry," *Soft matter. 2016,12(42):8736-43.*

[102] Clausen A, Wang F, Jensen JS, Sigmund O, Lewis JA., "Topology Optimized Architectures with Programmable Poisson's Ratio over Large Deformations," *Adv. Mater., vol. 27, no. 37, pp. 5523–5527, Oct. 2015.*

[103] Yang W, Chen IH, Gludovatz B, Zimmermann EA, Ritchie RO, Meyers MA, "Natural flexible dermal armor," *Advanced Materials. 2013 Jan 4,25(1):31-48.*

[104] Martini R, Balit Y, Barthelat F, "A comparative study of bio-inspired protective scales using 3D printing and mechanical testing," *Acta biomaterialia. 2017 Jun 1,55:360-72.*

[105] Gu GX, Su I, Sharma S, Voros JL, Qin Z, Buehler MJ, "Three-dimensional-printing of bio-inspired composites," *Journal of biomechanical engineering. 2016 Feb 1,138(2):021006.*

[106] Yang Y, Song X, Li X, Chen Z, Zhou C, Zhou Q, Chen Y, "Recent progress in biomimetic additive manufacturing technology: from materials to functional structures," *Advanced Materials. 2018 Sep,30(36):1706539.*

[107] Cherkaev AV, "Which elasticity tensors are realizable," *ASME J. Eng. Mater. Technol. 1995,117(4):483-93.*

[108] van Hecke M, "Jamming of soft particles: geometry, mechanics, scaling and isostaticity," *Journal of Physics: Condensed Matter. 2009 Dec 16,22(3):033101.*

[109] Huang SH, Liu P, Mokasdar A, Hou L, "Additive manufacturing and its societal impact: a literature review," *The International Journal of Advanced Manufacturing Technology. 2013 Jul 1,67(5-8):1191-203.*

[110] Wang X, Jiang M, Zhou Z, Gou J, Hui D, "3D printing of polymer matrix composites: A review and prospective," *Composites Part B: Engineering. 2017 Feb 1,110:442-58.*

[111] Gan Z, Turner MD, Gu M, "Biomimetic gyroid nanostructures exceeding their natural origins," *Science advances. 2016 May 1,2(5):e1600084.*

[112] Saleh MS, Hu C, Panat R, "Three-dimensional microarchitected materials and devices using nanoparticle assembly by pointwise spatial printing," *Science advances. 2017 Mar 1,3(3):e1601986.*

[113] Song J, Reichert S, Kallai I, Gazit D, Wund M, Boyce MC, Ortiz C, "Quantitative microstructural studies of the armor of the marine threespine stickleback (Gasterosteus aculeatus)," *Journal of structural biology. 2010 Sep 1,171(3):318-31.*

[114] Tiwary CS, Kishore S, Sarkar S, Mahapatra DR, Ajayan PM, Chattopadhyay K, "Morphogenesis and mechanostabilization of complex natural and 3D printed shapes," *Science advances. 2015 May 1,1(4):e1400052.*

[115] Qin Z, Jung GS, Kang MJ, Buehler MJ, "The mechanics and design of a lightweight three-dimensional graphene assembly," *Science advances. 2017 Jan 1,3(1):e1601536.*

[116] Qin Z, Compton BG, Lewis JA, Buehler MJ, "Structural optimization of 3D-printed synthetic spider webs for high strength," *Nature communications. 2015 May 15,6:7038.*

[117] Malik IA, Mirkhalaf M, Barthelat F, "Bio-inspired “jigsaw”-like interlocking sutures: Modeling, optimization, 3D printing and testing," *Journal of the Mechanics and Physics of Solids. 2017 May 1,102:224-38.*

[118] Wallin TJ, Pikul J, Shepherd RF, "3D printing of soft robotic systems," *Nature Reviews Materials. 2018 Jun,3(6):84.*

[119] Smay JE, Cesarano J, Lewis JA, "Colloidal inks for directed assembly of 3-D periodic structures," *Langmuir. 2002 Jul 9,18(14):5429-37.*

[120] Compton BG, Lewis JA, "3D-printing of lightweight cellular composites," *Advanced materials. 2014 Sep,26(34):5930-5.*

[121] Studart AR, "Additive manufacturing of biologically-inspired materials," *Chemical Society Reviews. 2016,45(2):359-76.*

[122] Araya S, Zolotovsky K, Veliz F, Song JH, Reichert S, Boyce MC, Ortiz C. , *International Conference on Education and research in Computer Aided Architectural Design in Europe. Delft, The Netherlands. 2013 Sep 18.*

[123] Guiducci L, Weaver JC, Bréchet YJ, Fratzl P, Dunlop JW, "The geometric design and fabrication of actuating cellular structures," *Advanced Materials Interfaces. 2015 Jul,2(11):1500011.*

[124] Bartlett NW, Tolley MT, Overvelde JT, Weaver JC, Mosadegh B, Bertoldi K, Whitesides GM, Wood RJ, "A 3D-printed, functionally graded soft robot powered by combustion," *Science. 2015 Jul 10,349(6244):161-5.*

[125] Wen L, Weaver JC, Lauder GV, "Biomimetic shark skin: design, fabrication and hydrodynamic function," *Journal of Experimental Biology. 2014 May 15,217(10):1656-66.*

[126] Dimas LS, Bratzel GH, Eylon I, Buehler MJ, "Tough composites inspired by mineralized natural materials: computation, 3D printing, and testing," *Advanced Functional Materials. 2013 Sep 25,23(36):4629-38.*

[127] Dimas LS, Buehler MJ, "Modeling and additive manufacturing of bio-inspired composites with tunable fracture mechanical properties," *Soft Matter. 2014,10(25):4436-42.*

[128] Mirzaeifar R, Dimas LS, Qin Z, Buehler MJ, "Defect-tolerant bioinspired hierarchical composites: simulation and experiment," *ACS Biomaterials Science & Engineering. 2015 Apr 14,1(5):295-304.*

[129] Duro-Royo J, Zolotovsky K, Mogas-Soldevila L, Varshney S, Oxman N, Boyce MC, Ortiz C, "MetaMesh: A hierarchical computational model for design and fabrication of biomimetic armored surfaces," *Computer-Aided Design. 2015 Mar 1,60:14-27.*

[130] Rudykh S, Ortiz C, Boyce MC, "Flexibility and protection by design: imbricated hybrid microstructures of bio-inspired armor," *Soft Matter. 2015,11(13):2547-54.*

[131] Rudykh S, Boyce MC, "Transforming small localized loading into large rotational motion in soft anisotropically structured materials," *Advanced Engineering Materials. 2014 Nov,16(11):1311-7.*

[132] Ghosh R, Ebrahimi H, Vaziri A, "Frictional effects in biomimetic scales engagement," *EPL (Europhysics Letters). 2016 Feb 26,113(3):34003.*

[133] Browning A, Ortiz C, Boyce MC, " Mechanics of composite elasmoid fish scale assemblies and their bioinspired analogues," *Journal of the mechanical behavior of biomedical materials. 2013 Mar 1,19:75-86.*

[134] Tran P, Ngo TD, Ghazlan A, Hui D, "Bimaterial 3D printing and numerical analysis of bio-inspired composite structures under in-plane and transverse loadings," *Composites Part B: Engineering. 2017 Jan 1,108:210-23.*

[135] Gu GX, Libonati F, Wettermark SD, Buehler MJ, "Printing nature: Unraveling the role of nacre's mineral bridges," *Journal of the mechanical behavior of biomedical materials. 2017 Dec 1,76:135-44.*

[136] Gu GX, Takaffoli M, Hsieh AJ, Buehler MJ, "Biomimetic additive manufactured polymer composites for improved impact resistance," *Extreme Mechanics Letters. 2016 Dec 1,9:317-23.*

[137] Gu GX, Takaffoli M, Buehler MJ, "Hierarchically enhanced impact resistance of bioinspired composites," *Advanced Materials. 2017 Jul,29(28):1700060.*

[138] Frølich S, Weaver JC, Dean MN, Birkedal H, "Uncovering Nature's Design Strategies through Parametric Modeling, Multi-Material 3D Printing, and Mechanical Testing," *Advanced Engineering Materials. 2017 Jun,19(6):e201600848.*

[139] Taboas JM, Maddox RD, Krebsbach PH, Hollister SJ, " Indirect solid free form fabrication of local and global porous, biomimetic and composite 3D polymer-ceramic scaffolds," *Biomaterials. 2003 Jan 1,24(1):181-94.*

[140] Kokkinis D, Schaffner M, Studart AR, "Multimaterial magnetically assisted 3D printing of composite materials," *Nature communications. 2015 Oct 23,6:8643.*

[141] Gross BC, Erkal JL, Lockwood SY, Chen C, Spence DM, "Evaluation of 3D printing and its potential impact on biotechnology and the chemical sciences," *Anal. Chem. 2014, 86, 7, 3240-3253.*

[142] Campbell T, Williams C, Ivanova O, Garrett B, "Could 3D printing change the world," *Technologies, Potential, and Implications of Additive Manufacturing, Atlantic Council, Washington, DC. 2011 Oct,3.*

[143] J. Chen, K. Wang, C. Zhang, and B. Wang, "An efficient statistical approach to design 3D-printed metamaterials for mimicking mechanical properties of soft biological tissues," *Addit. Manuf., vol. 24, pp. 341–352, Dec. 2018.*

[144] Wang K, Chang YH, Chen Y, Zhang C, Wang B, "Designable dual-material auxetic metamaterials using three-dimensional printing," *Materials & Design. 2015 Feb 15,67:159-64.*

[145] Mirzaali MJ, Caracciolo A, Pahlavani H, Janbaz S, Vergani L, Zadpoor AA, "Multi-material 3D printed mechanical metamaterials: Rational design of elastic properties through spatial distribution of hard and soft phases," *Applied Physics Letters. 2018 Dec 10,113(24):241903.*

[146] Shao H, Li J, Chen N, Shao G, Jiang J, Yang Y, "Experimental Study on Bi-Axial Mechanical Properties of Warp-knitted Meshes with and without Initial Notches," *Materials. 2018 Oct,11(10):1999.*

[147] Holzapfel GA, Gasser TC, "A viscoelastic model for fiber-reinforced composites at finite strains: Continuum basis, computational aspects and applications," *Computer methods in applied mechanics and engineering. 2001 May 25,190(34):4379-403.*

[148] Huang ZM, Ramakrishna S, Tay AA, "Modeling the stress/strain behavior of a knitted fabric-reinforced elastomer composite," *Composites science and technology. 2000 Apr 1,60(5):671-91.*

[149] Bouillaguet S, Schütt A, Alander P, Schwaller P, Buerki G, Michler J, Cattani-Lorente M, Vallittu PK, Krejci I, "Hydrothermal and mechanical stresses degrade fiber–matrix interfacial bond strength in dental fiber-reinforced composites," *Journal of Biomedical Materials Research Part B: Applied Biomaterials: An Official Journal of The Society for Biomaterials, The Japanese Society for Biomaterials, and The Australian Society for Biomaterials and the Korean Society for Biomaterials.*

[150] Martinez RV, Branch JL, Fish CR, Jin L, Shepherd RF, Nunes RM, Suo Z, Whitesides GM, "Robotic tentacles with three-dimensional mobility based on flexible elastomers," *Advanced materials. 2013 Jan 11,25(2):205-12.*

[151] Cheng MY, Tsao CM, Yang YJ. , "An anthropomorphic robotic skin using highly twistable tactile sensing array," *In2010 5th IEEE Conference on Industrial Electronics and Applications 2010 Jun 15 (pp. 650-655). IEEE.*

[152] Pritts MB, Rahn CD. , "Design of an artificial muscle continuum robot," *InIEEE International Conference on Robotics and Automation, 2004. Proceedings. ICRA'04. 2004 2004 Apr 26 (Vol. 5, pp. 4742-4746). IEEE.*

[153] Jiang J, Chen N, Geng Y, Shao H, Lin F, "Advanced Grid Structure-Reinforced Composites," *InPorous lightweight composites reinforced with fibrous structures 2017 (pp. 129-155). Springer, Berlin, Heidelberg.*

[154] Leong KH, Ramakrishna S, Huang ZM, Bibo GA, "The potential of knitting for engineering composites—a review," *Composites Part A: applied science and manufacturing. 2000 Mar 1,31(3):197-220.*

[155] Maurer M, Röhrnbauer B, Feola A, Deprest J, Mazza E, " Prosthetic meshes for repair of hernia and pelvic organ prolapse: Comparison of biomechanical properties," *Materials. 2015,8(5):2794-808.*

[156] Haines CS, Lima MD, Li N, Spinks GM, Foroughi J, Madden JD, Kim SH, Fang S, de Andrade MJ, Göktepe F, Göktepe Ö , "Artificial muscles from fishing line and sewing thread," *Science. 2014 Feb 21,343(6173):868-72.*

[157] Murugan R, Ramakrishna S, "Design strategies of tissue engineering scaffolds with controlled fiber orientation," *Tissue engineering. 2007 Aug 1,13(8):1845-66.*

[158] Pattinson SW, Huber ME, Kim S, Lee J, Grunsfeld S, Roberts R, Dreifus G, Meier C, Liu L, Hogan N, Hart AJ, "Additive Manufacturing of Biomechanically Tailored Meshes for Compliant Wearable and Implantable Devices," *Advanced Functional Materials. 2019 Jun 19.*

[159] Goswami D, Liu S, Pal A, Silva LG, Martinez RV, "3D-Architected Soft Machines with Topologically Encoded Motion," *Advanced Functional Materials. 2019 Jun 1:1808713.*

[160] Y. Jiang and Q. Wang, "Highly-stretchable 3D-architected Mechanical Metamaterials," *Sci. Rep., vol. 6, no. 1, p. 34147, Dec. 2016.*

[161] M. Mohsenizadeh, F. Gasbarri, M. Munther, A. Beheshti, and K. Davami, "Additively-manufactured lightweight Metamaterials for energy absorption," *Mater. Des., vol. 139, pp. 521–530, 2018.*

[162] M. Hanifpour, C. F. Petersen, M. J. Alava, and S. Zapperi, "Mechanics of disordered auxetic metamaterials," *Eur. Phys. J. B, vol. 91, no. 11, p. 271, Nov. 2018.*

[163] M. Bodaghi, A. R. Damanpack, G. F. Hu, and W. H. Liao, "Large deformations of soft metamaterials fabricated by 3D printing," *Mater. Des., vol. 131, pp. 81–91, Oct. 2017.*

[164] X. Shang, L. Liu, A. Rafsanjani, and D. Pasini, "Durable bistable auxetics made of rigid solids," *J. Mater. Res., vol. 33, no. 3, pp. 300–308, Feb. 2018.*

[165] Mousanezhad D, Babaee S, Ebrahimi H, Ghosh R, Hamouda AS, Bertoldi K, Vaziri A., "Hierarchical honeycomb auxetic metamaterials," *Scientific reports. 2015 Dec 16,5:18306.*

[166] Chen Y, Wang L, "Harnessing structural hierarchy to design stiff and lightweight phononic crystals," *Extreme Mechanics Letters. 2016 Dec 1,9:91-6.*

[167] Oyewole OK, Yu D, Du J, Asare J, Oyewole DO, Anye VC, Fashina A, Zebaze Kana MG, Soboyejo WO, "Micro-wrinkling and delamination-induced buckling of stretchable electronic structures," *Journal of Applied Physics. 2015 Jun 21,117(23):235501.*

[168] Lyashenko-Miller T, Marom G, "Delamination fracture toughness of UHMWPE fibers/polyurethane laminates interleaved with carbon nanotube-reinforced polyurethane films," *Polymers for Advanced Technologies. 2017 May,28(5):606-12.*

[169] Palaganas NB, Mangadlao JD, de Leon AC, Palaganas JO, Pangilinan KD, Lee YJ, Advincula RC, "3D printing of photocurable cellulose nanocrystal composite for fabrication of complex architectures via stereolithography," *ACS applied materials & interfaces. 2017 Sep 25,9(39):34314-24.*

Appendices

Appendix A: Supporting Information for Chapter 3

Example of Raw Force-Displacement Data Generated during Tensile Test

0% of break (Extension) : Load at 0% of break (Extension)		N
Strain : Tensile strain (Extension) gauge length	15.46	mm
Specimen properties : Geometry	Rectangular	
Specimen properties : Length	15.46	mm
Specimen properties : Specimen label	meta	
Specimen properties : Thickness	0.65	mm
Specimen properties : Width	27.68	mm
Test : Rate 1	10	mm/min
0% of break (Extension) : Time at 0% of break (Extension)		s
0% of break (Extension) : 0% of break (Extension)		mm
0% of break (Extension) : Tensile extension at 0% of break (Extension)		mm
0% of break (Extension) : Tensile strain (Extension) at 0% of break (Extension)		mm/mm
0% of break (Extension) : Tensile stress at 0% of break (Extension)		MPa
0% of break (Extension) : Data point at 0% of break (Extension)		
0% of break (Extension) : Status number at 0% of break (Extension)	22	
Specimen properties : Area	17.992	mm^2
0% of break (Extension) : Energy at 0% of break (Extension)		J
0% of break (Extension) : Tenacity at 0% of break (Extension)		N/tex
General : End date	1/22/2019	
General : Excluded	FALSE	
General : Specimen number (included)	1	
General : Start date	1/22/2019	
General : Unique identifier	{9967DDA8-42B3-455C-B396-F05384CC6FC9}	
Modulus (Automatic) : Energy to X-intercept at Modulus (Automatic)		J
Modulus (Automatic) : Modulus (Automatic)	2.56021	MPa
Modulus (Automatic) : Status number at Modulus (Automatic)	1	
Modulus (Automatic) : X-intercept at Modulus (Automatic)	-0.02353	mm/mm
Modulus (Automatic) : Y-intercept at Modulus (Automatic)	0.06025	MPa
Specimen choice input : Specimen choice input 1	<None>	
Specimen choice input : Specimen choice input 2	<None>	
Specimen choice input : Specimen choice input 3	<None>	
Specimen choice input : Specimen choice input 4	<None>	
Specimen choice input : Specimen choice input 5	<None>	
Specimen choice input : Specimen choice input 6	<None>	

Specimen choice input : Specimen choice input 7	<None>	
Specimen choice input : Specimen choice input 8	<None>	
Specimen choice input : Specimen choice input 9	<None>	
Specimen choice input : Specimen choice input 10	<None>	
Specimen notes : Specimen note 1		
Specimen notes : Specimen note 2		
Specimen notes : Specimen note 3		
Specimen number inputs : Specimen number input 1	0	
Specimen properties : Final area	30	mm^2
Specimen properties : Final length	300	mm
Specimen properties : Final thickness	1	mm
Specimen properties : Final width	30	mm
Specimen text inputs : Specimen text input 1		
Strain : Time at removal		s

Time (s)	Extension (mm)	Load (N)
0	0	0.00126
0.1	0.01133	0.02498
0.2	0.02708	0.26348
0.3	0.04935	0.64669
0.4	0.0666	0.79652
0.5	0.08378	0.91461
0.6	0.09967	1.01553
0.7	0.11693	1.14132
0.8	0.13395	1.24545
0.9	0.15	1.3259
1	0.16725	1.43288
1.1	0.1839	1.49809
1.2	0.2004	1.5907
1.3	0.21713	1.67272
1.4	0.23347	1.74314
1.5	0.25043	1.81739
1.6	0.26685	1.8779
1.7	0.28372	1.96023
1.8	0.30075	2.04054
1.9	0.3165	2.07783
2	0.33375	2.16699
2.1	0.35055	2.22688
2.2	0.36682	2.28778
2.3	0.38355	2.35203
2.4	0.39998	2.39712
2.5	0.41708	2.46827
2.6	0.43372	2.52132

2.7	0.45008	2.57323
2.8	0.4674	2.64942
2.9	0.48345	2.6771
3	0.5004	2.74842
3.1	0.51728	2.80867
3.2	0.53325	2.843
3.3	0.55028	2.90317
3.4	0.56708	2.95074
3.5	0.58365	3.00224
3.6	0.60045	3.05729
3.7	0.61687	3.09891
3.8	0.63405	3.15855
3.9	0.65025	3.18668
4	0.66683	3.23879
4.1	0.6837	3.29372
4.2	0.6999	3.31921
4.3	0.71678	3.38093
4.4	0.73403	3.43605
4.5	0.74978	3.4578
4.6	0.76725	3.52375
4.7	0.78352	3.54289
4.8	0.80055	3.60077
----	------	--------
57.808	9.63518	2.05397
57.908	9.6516	2.0636
58.008	9.66825	2.0777
58.108	9.68513	2.09224
58.208	9.70125	2.10604
58.308	9.71813	2.1182
58.408	9.7356	2.13404
58.508	9.75098	2.13433
58.608	9.76875	2.15277
58.708	9.7851	2.16653
58.808	9.80175	2.17602
58.908	9.81833	2.18733
59.008	9.8349	2.19038
59.108	9.8517	2.20721
59.208	9.8685	2.21429
59.308	9.88493	2.2266
59.408	9.90218	2.23303
59.508	9.91778	2.24244
59.608	9.93525	2.24386
59.708	9.95168	2.26147
59.808	9.96825	2.2616

Matlab codes to determine hyperelastic model parameters

1) For unreinforced Ecoflex 0050 – Gent Model

```
 % input data
    d_eco = load('eco-thin.txt'), % load raw data
    f_eco = d_eco(:,3), % tensile force, unit: N
    ext_eco = (d_eco(:,2)-d_eco(1,2)).*1e-3, % tensile extension, unit: m
    time_eco = d_eco(:,1),
    % geometry
    to_eco = 0.93e-3,   % unit: m
    wo_eco = 14.92e-3, % unit: m
    lo_eco = 18.73e-3, % unit: m
% stress - strain calculation
    eps1_eco = ext_eco ./ lo_eco, % strain
    lambda1_eco = 1 + eps1_eco, % stretch
    nom_sigma1_eco = f_eco ./ (wo_eco*to_eco)/(10^6), % nominal stress, unit: Pa
    sigma1_eco = nom_sigma1_eco .* lambda1_eco, % true stress, unit Pa
    % mechanical failure point
    n=3,
    [max_sigma1_eco,ibrk_eco] = max(sigma1_eco)

mu_eco=0.0181,
Jm_eco=197.6262,
k1_eco=0,
k2_eco=0,
Y4_eco = sigma1_eco (1:9000),
X4_eco=eps1_eco (1:9000),
x1=eps1_eco(1:9000),
y1=sigma1_eco(1:9000),
p=polyfit(x1,y1,n),
p,
f=polyval(p,x1),
figure(1)
plot(x1,y1, x1,f,'-')
legend ('Exp data', 'PolyFit')

Yfcn_eco=@(b_eco,X4_eco)(3 .* b_eco(1)  .* b_eco(2).* ((X4_eco (:,1)+1).^2 - 1./ (X4_eco
(:,1)+1)) ./ (b_eco(2) - (X4_eco (:,1)+1).^2 - 2./ (X4_eco (:,1)+1) + 3))
SSECF_eco = @(b_eco) sum((Y4_eco - Yfcn_eco(b_eco,X4_eco)).^2),
B0_eco = rand(2,1)*100,                    % Initial Parameter Estimates
```

```
[B_eco,SSE_eco] = fminsearch(SSECF_eco, B0_eco)

Yfcn1_eco=(3 .* mu_eco .* Jm_eco.* ((X4_eco (:,1)+1).^2 - 1./ (X4_eco (:,1)+1)) ./ (Jm_eco -
(X4_eco (:,1)+1).^2 - 2./ (X4_eco (:,1)+1) + 3)),
Rsq1_eco = 1 - sum((Y4_eco-Yfcn1_eco).^2)/sum((Y4_eco - mean(Y4_eco)).^2)
ymin=min(Yfcn1_eco),
xmin=find(Yfcn1_eco==ymin),
X4_eco(326),

figure (5),
plot(lambda1_eco(1:9000),Yfcn1_eco)


figure, box on, hold on,
p_eco = plot(eps1_eco,sigma1_eco,'--r','linewidth',2,'displayname','Ecoflex 0050: experimental'),
p_eco_fit = plot(X4_eco,Yfcn1_eco,'-b','linewidth',2,'displayname','Ecoflex 0050: theoretical'),
leg_pe = legend([p_eco, p_eco_fit]),
legend boxoff,
   set(leg_pe,'location','best','fontsize',12),
   xlabel('Strain, \epsilon','fontsize',12),
   ylabel('True stress, \it t_{1 Gent} [MPa]','fontsize',12), %{\it T}_g
   text(0.25,5,sprintf('Best fitting with R^{2}=%1.4f',Rsq1_eco),'fontsize',12),
   text(0.25,4,sprintf('\\mu=%1.2f (kPa), J_{lim}=%1.2f',mu_eco*10^(3),Jm_eco),'fontsize',12),
   %text(0.25,8,sprintf('k_{1}=%1.2f (kPa), k_{2}=%1.2f',k1_eco*10^(3),k2_eco),'fontsize',12),
   set(gca,'xlim',[0 9],'ylim',[-1e-2 8],'fontsize',12),
```

2) For Ecoflex – Mooney-Rivlin

```
 % input data
   d_eco = load('eco-thin.txt'), % load raw data
   f_eco = d_eco(:,3), % tensile force, unit: N
   ext_eco = (d_eco(:,2)-d_eco(1,2)).*1e-3, % tensile extension, unit: m
   time_eco = d_eco(:,1),
   % geometry
   to_eco = 0.93e-3,   % unit: m
   wo_eco = 14.92e-3, % unit: m
   lo_eco = 18.73e-3, % unit: m
% stress - strain calculation
   eps1_eco = ext_eco ./ lo_eco, % strain
   lambda1_eco = 1 + eps1_eco, % stretch
```

```
   nom_sigma1_eco = f_eco ./ (wo_eco*to_eco)/(10^6), % nominal stress, unit: Pa
   sigma1_eco = nom_sigma1_eco .* lambda1_eco, % true stress, unit Pa
   % mechanical failure point
   n=3,
   [max_sigma1_eco,ibrk_eco] = max(sigma1_eco)


C10_eco=0.015,
C01_eco=-0.011,
Y4_eco = sigma1_eco (1:9000),
X4_eco=eps1_eco (1:9000),
x1=eps1_eco(1:9000),
y1=sigma1_eco(1:9000),
p=polyfit(x1,y1,n),
f=polyval(p,x1),
%figure(1)
plot(x1,y1, x1,f,'-')
legend ('Exp data', 'PolyFit')
dy=diff(f)./diff(x1),
%figure (2),
plot(x1(2:end),dy)
der_2=-36.*C01_eco./((X4_eco(:,1)+1).^4)+6.*C10_eco.*(2-2./((X4_eco (:,1)+1).^3)),
%figure (3),
plot(X4_eco,der_2,'-m','linewidth',2)
xlabel('Strain, \epsilon'), ylabel(' d^{2}\sigma/d^{2}\epsilon','fontsize',12)
legend('2nd derivative of stress for Ecoflex 0050')
der_1=6.*C10_eco.*(2.*(X4_eco(:,1)+1)+1./((X4_eco
(:,1)+1).^2))+6.*C01_eco.*(1+2./((X4_eco(:,1)+1).^3)),
%figure (4),
plot(X4_eco,der_1,'-b','linewidth',2)
xlabel('Strain, \epsilon'), ylabel(' d\sigma/d\epsilon','fontsize',12)
legend('1st derivative of stress for Ecoflex 0050')

Yfcn_eco=@(b_eco,X4_eco)(6.*b_eco(1).*(2.*(X4_eco(2:end)+1)+1./((X4_eco
(2:end)+1).^2))+6.*b_eco(2).*(1+2./((X4_eco(2:end)+1).^3))),
SSECF_eco = @(b_eco) sum((dy - Yfcn_eco(b_eco,X4_eco)).^2),
B0_eco = rand(2,1)*100,                    % Initial Parameter Estimates
[B_eco,SSE_eco] = fminsearch(SSECF_eco, B0_eco)
```

```
Yfcn1_eco=(6.*C10_eco.*((X4_eco (:,1)+1).^2-1./(X4_eco (:,1)+1))+6.*C01_eco.*((X4_eco
(:,1)+1)-1./((X4_eco (:,1)+1).^2))),
Rsq1_eco = 1 - sum((Y4_eco-Yfcn1_eco).^2)/sum((Y4_eco - mean(Y4_eco)).^2)

ymin=min(Yfcn1_eco)
xmin=find(Yfcn1_eco==ymin),
X4_eco(326),

figure (5),
plot(lambda1_eco(1:9000),Yfcn1_eco)

figure, box on, hold on,
p_eco = plot(eps1_eco,sigma1_eco,'--r','linewidth',2,'displayname','Ecoflex 0050: experimental'),
p_eco_fit = plot(X4_eco,Yfcn1_eco,'-b','linewidth',2,'displayname','Ecoflex 0050: theoretical'),
leg_pe = legend([p_eco, p_eco_fit]),
legend boxoff,
   set(leg_pe,'location','best','fontsize',12),
   xlabel('Strain, \epsilon','fontsize',12),
   ylabel('True stress, \it t_{1 MR} [MPa]','fontsize',12),
   text(0.25,5,sprintf('Best fitting with R^{2}=%1.4f',Rsq1_eco),'fontsize',12),
   text(0.25,4,sprintf('C_{10}=%1.2f (kPa), C_{01}=%1.2f
(kPa)',C10_eco*10^(3),C01_eco*10^(3)),'fontsize',12),
   set(gca,'xlim',[0 9],'ylim',[-1e-1 8],'fontsize',12),

   clear all
```

3) Sample code for composite

```
%wale direction --------------------------------
% input data
   d_rayon_y = load('Rayon_1y.txt'), % load raw data
   f_rayon_y = d_rayon_y(:,3), % tensile force, unit: N
   ext_rayon_y = (d_rayon_y(:,2)-d_rayon_y(1,2)).*1e-3, % tensile extension, unit: m
   time_rayon_y = d_rayon_y(:,1),
   % geometry
   to_rayon_y = 11e-3,   % unit: m
   wo_rayon_y = 1.32e-3, % unit: m
   lo_rayon_y = 26.3e-3, % unit: m
% stress - strain calculation
   eps1_rayon_y = ext_rayon_y ./ lo_rayon_y, % strain
   lambda1_rayon_y = 1 + eps1_rayon_y, % stretch
```

```
    nom_sigma1_rayon_y = f_rayon_y ./ (wo_rayon_y*to_rayon_y)/(10^6), % nominal stress,
unit: Pa
    sigma1_rayon_y = nom_sigma1_rayon_y .* lambda1_rayon_y, % true stress, unit Pa
    % mechanical failure point
    n=8,
    [max_sigma1_rayon_y,ibrk_rayon_y] = max(sigma1_rayon_y)

mu_rayon_y=0.01810,
Jm_rayon_y=197.63,
k1_rayon_y=0.02508,
k2_rayon_y=0.0012,
Y4_rayon_y = sigma1_rayon_y (1:2982),
X4_rayon_y=eps1_rayon_y (1:2982),

Yfcn_rayon_y=@(b_rayon_y,X4_rayon_y)(3 .* mu_rayon_y .* Jm_rayon_y.* ((X4_rayon_y
(:,1)+1).^2 - 1./ (X4_rayon_y (:,1)+1)) ./ (Jm_rayon_y - (X4_rayon_y (:,1)+1).^2 - 2./
(X4_rayon_y (:,1)+1) + 3) +6 .* b_rayon_y(1) .* (X4_rayon_y (:,1)+1).^2 .* ((X4_rayon_y
(:,1)+1).^2-1) .* (exp(b_rayon_y(2).*( (X4_rayon_y (:,1)+1).^2-1).^2))),
SSECF_rayon_y = @(b_rayon_y) sum((Y4_rayon_y -
Yfcn_rayon_y(b_rayon_y,X4_rayon_y)).^2),
B0_rayon_y = rand(2,1)*100,                    % Initial Parameter Estimates
[B_rayon_y,SSE_rayon_y] = fminsearch(SSECF_rayon_y, B0_rayon_y)

Yfcn1_rayon_y=(3 .* mu_rayon_y .* Jm_rayon_y.* ((X4_rayon_y (:,1)+1).^2 - 1./ (X4_rayon_y
(:,1)+1)) ./ (Jm_rayon_y - (X4_rayon_y (:,1)+1).^2 - 2./ (X4_rayon_y (:,1)+1) + 3) +6 .*
k1_rayon_y .* (X4_rayon_y (:,1)+1).^2 .* ((X4_rayon_y (:,1)+1).^2-1) .* (exp(k2_rayon_y.*(
(X4_rayon_y (:,1)+1).^2-1).^2))),
Rsq1_rayon_y = 1 - sum((Y4_rayon_y-Yfcn1_rayon_y).^2)/sum((Y4_rayon_y -
mean(Y4_rayon_y)).^2)

%course direction--------------------------------------------------------

% input data
    d_rayon_x = load('Rayon_1x.txt'), % load raw data
    f_rayon_x = d_rayon_x(:,3), % tensile force, unit: N
    ext_rayon_x = (d_rayon_x(:,2)-d_rayon_x(1,2)).*1e-3, % tensile extension, unit: m
    time_rayon_x = d_rayon_x(:,1),
    % geometry
    to_rayon_x = 9.65e-3,   % unit: m
    wo_rayon_x = 1.32e-3, % unit: m
```

```
   lo_rayon_x = 25.16e-3, % unit: m
% stress - strain calculation
   eps1_rayon_x = ext_rayon_x ./ lo_rayon_x, % strain
   lambda1_rayon_x = 1 + eps1_rayon_x, % stretch
   nom_sigma1_rayon_x = f_rayon_x ./ (wo_rayon_x*to_rayon_x)/(10^6), % nominal stress,
unit: Pa
   sigma1_rayon_x = nom_sigma1_rayon_x .* lambda1_rayon_x, % true stress, unit Pa
   % mechanical failure point
   n=8,
   [max_sigma1_rayon_x,ibrk_rayon_x] = max(sigma1_rayon_x)

mu_rayon_x=0.01810,
Jm_rayon_x=197.63,
k1_rayon_x=0.01025,
k2_rayon_x=0.0011,
Y4_rayon_x = sigma1_rayon_x (1:3700),
X4_rayon_x=eps1_rayon_x (1:3700),

Yfcn_rayon_x=@(b_rayon_x,X4_rayon_x)(3 .* mu_rayon_x .* Jm_rayon_x.* ((X4_rayon_x
(:,1)+1).^2 - 1./ (X4_rayon_x (:,1)+1)) ./ (Jm_rayon_x - (X4_rayon_x (:,1)+1).^2 - 2./
(X4_rayon_x (:,1)+1) + 3) +6 .* b_rayon_x(1) .* (X4_rayon_x (:,1)+1).^2 .* ((X4_rayon_x
(:,1)+1).^2-1) .* (exp(b_rayon_x(2).*( (X4_rayon_x (:,1)+1).^2-1).^2))),
SSECF_rayon_x = @(b_rayon_x) sum((Y4_rayon_x -
Yfcn_rayon_x(b_rayon_x,X4_rayon_x)).^2),
B0_rayon_x = rand(2,1)*100,                    % Initial Parameter Estimates
[B_rayon_x,SSE_rayon_x] = fminsearch(SSECF_rayon_x, B0_rayon_x)

Yfcn1_rayon_x=(3 .* mu_rayon_x .* Jm_rayon_x.* ((X4_rayon_x (:,1)+1).^2 - 1./ (X4_rayon_x
(:,1)+1)) ./ (Jm_rayon_x - (X4_rayon_x (:,1)+1).^2 - 2./ (X4_rayon_x (:,1)+1) + 3) +6 .*
k1_rayon_x .* (X4_rayon_x (:,1)+1).^2 .* ((X4_rayon_x (:,1)+1).^2-1) .* (exp(k2_rayon_x.*(
(X4_rayon_x (:,1)+1).^2-1).^2))),
Rsq1_rayon_x = 1 - sum((Y4_rayon_x-Yfcn1_rayon_x).^2)/sum((Y4_rayon_x -
mean(Y4_rayon_x)).^2)

%-------------------------------------------------------------------------------
%Plotting section

figure, box on, hold on,
p_rayon_x = plot(X4_rayon_x,Y4_rayon_x,'--m','linewidth',2,'displayname','Rayon/Spandex
course: experimental'),
```

```
p_rayon_x_fit = plot(X4_rayon_x,Yfcn1_rayon_x,'-
k','linewidth',2,'displayname','Rayon/Spandex course: theoretical'),
p_rayon_y = plot(X4_rayon_y,Y4_rayon_y,'--r','linewidth',2,'displayname','Rayon/Spandex
wale: experimental'),
p_rayon_y_fit = plot(X4_rayon_y,Yfcn1_rayon_y,'-
b','linewidth',2,'displayname','Rayon/Spandex wale: theoretical'),

leg_pe = legend([p_rayon_x, p_rayon_x_fit,p_rayon_y, p_rayon_y_fit]),
legend boxoff,
   set(leg_pe,'location','best','fontsize',12),
   xlabel('Strain, \epsilon','fontsize',12),
   ylabel('True stress,\it t_{1 Gent} [MPa]','fontsize',12),
   set(gca,'xlim',[0 2.5],'ylim',[0 12],'fontsize',12),

   text(1.6,2.0,sprintf('R^{2}=%1.4f',Rsq1_rayon_x),'fontsize',12),
   text(1.3,1.1,sprintf('\\mu=%1.2f (kPa),
J_{lim}=%1.2f',mu_rayon_x*10^(3),Jm_rayon_x),'fontsize',12),
   text(1.3,0.4,sprintf('k_{1}=%1.2f (kPa),
k_{2}=%1.4f',k1_rayon_x*10^(3),k2_rayon_x),'fontsize',12),


   text(0.1,6,sprintf('R^{2}=%1.4f',Rsq1_rayon_y),'fontsize',12),
   text(0.1,5.2,sprintf('\\mu=%1.2f (kPa),
J_{lim}=%1.2f',mu_rayon_y*10^(3),Jm_rayon_y),'fontsize',12),
   text(0.1,4.5,sprintf('k_{1}=%1.2f (kPa),
k_{2}=%1.4f',k1_rayon_y*10^(3),k2_rayon_y),'fontsize',12),
```

4) Alternative code for composite

```
%% Start: clearing
   close all,
   clear,
%% Polyester_Spandex
   % input data
   d_pe = load('PE_Spandex.txt'), % load raw data
   f_pe = d_pe(:,3), % tensile force, unit: N
   ext_pe = (d_pe(:,2)-d_pe(1,2)).*1e-3, % tensile extension, unit: m
   time_pe = d_pe(:,1),
   % geometry
   to_pe = 1.8e-3,   % unit: m
```

```
    wo_pe = 10.99e-3, % unit: m
    lo_pe = 22.06e-3, % unit: m
    % stress - strain calculation
    eps1_pe = ext_pe ./ lo_pe, % strain
    lambda1_pe = 1 + eps1_pe, % stretch
    nom_sigma1_pe = f_pe ./ (wo_pe*lo_pe), % nominal stress, unit: Pa
    sigma1_pe = nom_sigma1_pe .* lambda1_pe, % true stress, unit Pa
    % mechanical failure point
    [max_sigma1_pe,ibrk_pe] = max(sigma1_pe),
%% Model: Gent's hyper-elasticity - Bio-tissues
    % input parameters
    n = 8, % number of points
    mu_pe = linspace(10,12,n)*1e3, % shear modulus, unit: Pa
    Jm_pe = linspace(25,35,n),  % limit of stretch invariant
    k1_pe = linspace(1e3,2e3,n),
    k2_pe = linspace(0.025,0.075,n),
    syms sym_lambda1_pe
    % substitution
    m_lambda1_pe = linspace(1,lambda1_pe(ibrk_pe),ibrk_pe), % generate an equi-interval array
of stretch
    m_sigma1_pe = zeros(ibrk_pe,n),
    Rsqr = zeros(1,n),
    for i=1:n
        t1_pe = 3 * mu_pe(i) * Jm_pe(i) * (sym_lambda1_pe.^2 - 2./sym_lambda1_pe) / (Jm_pe(i)
- sym_lambda1_pe.^2 - 2./sym_lambda1_pe + 3) - 2 * k1_pe(i) * sym_lambda1_pe.^2 *
(sym_lambda1_pe.^2-1) * (exp(-k2_pe(i)*(sym_lambda1_pe.^2-1)^2) - 0.25)+0.015e6,
        m_sigma1_pe(:,i) = subs(t1_pe,m_lambda1_pe), % substitute for the stretch
        Rsqr(i) = 1 - sum((sigma1_pe(1:ibrk_pe)-
m_sigma1_pe(:,i)).^2)/sum((sigma1_pe(1:ibrk_pe) - mean(sigma1_pe(1:ibrk_pe))).^2),
    end
    [Rbest,ibest] = max(Rsqr),
    % plot fitting
    m_eps1_pe = m_lambda1_pe - 1,
    figure, box on, hold on,
    p_pe = plot(eps1_pe*1e2,sigma1_pe*1e-6,'--r','linewidth',2,'displayname','Polyester-Spandex:
experimental'),
    p_m_pe = plot(m_eps1_pe*1e2,m_sigma1_pe(:,ibest)*1e-6,'-
b','linewidth',2,'displayname','Polyester-Spandex: theoretical'),
    leg_pe = legend([p_pe, p_m_pe]),
    legend box off,
```

```
set(leg_pe,'location','best','fontsize',12),
xlabel('Strain, \epsilon (%)','fontsize',12),
ylabel('True stress, \sigma (MPa)','fontsize',12),
text(50,1,sprintf('Best fitting with R^{2}=%1.4f',Rbest),'fontsize',12),
text(65,0.9,sprintf('mu=%1.2f (kPa), J_{lim}=%1.2f',mu_pe(ibest)*1e-
3,Jm_pe(ibest)),'fontsize',12),
text(65,0.8,sprintf('k_{1}=%1.2f, k_{2}=%1.2f',k1_pe(ibest),k2_pe(ibest)),'fontsize',12),
set(gca,'xlim',[0 450],'ylim',[-1e-2 1.25],'fontsize',12),
```

Appendix B: Supporting Information for Chapter 4

Table B.1. Summary of different structures, manufacturing methods and strain-stress behavior in literature.

<table>
<tr><th rowspan="2">Ref.</th><th rowspan="2">Key concepts</th><th colspan="4">Key results</th></tr>
<tr><th>Structure</th><th>Manufacturing</th><th>Materials</th><th>Figures</th></tr>
<tr><td>[158]</td><td>Additive manufacturing (AM), tissue-support devices, such as ankle or knee braces, and hernia repair mesh, programming of the toolpath in an extrusion AM process, flexible mesh, digitally tailored mechanical properties and geometry, extrusion of thermoplastics, with continuous fiber reinforcement</td><td>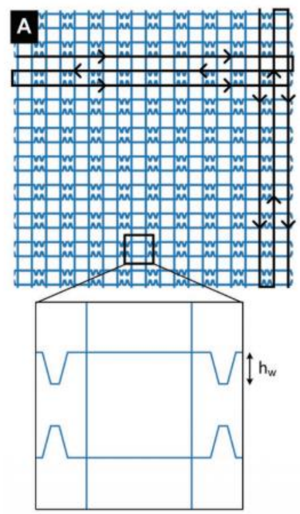
</td><td>Printing: Extrusion is done using a commercial 3D printer Printrbot</td><td>Simple Metal. Thermoplastic Polyurethane (Ninjaflex) is the primary matrix material used, while stainless steel thread (0.4 mm thick 3 ply thread, 316 L alloy, Adafruit Industries) is the premade continuous fiber.</td><td>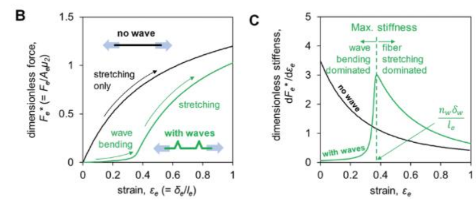
</td></tr>
</table>

[159]	Low-density, 3D-architected soft machines (ASMs) by combining Voronoi tessellation and additive manufacturing, topologically encoded buckling (contraction, twisting, bending, and cyclic motion), stereolithographi	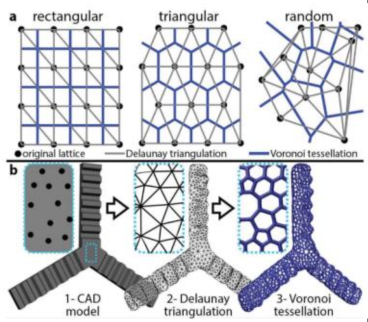	3D Printing ASMs: A high-resolution stereolithography (SLA) 3D printer (Form 2, Formlabs Inc.) was used to build	Flexible photocurable polymers (FLGR01 and FLGR02, bulk density = 1.15 g cm−3, Formlabs Inc.). Elastomeric ASMs by Injection Molding: dissolvable hollow polymeric molds (were 3D printed by fused deposition modeling using ABS) (FDM, F170, Stratasys Ltd.)	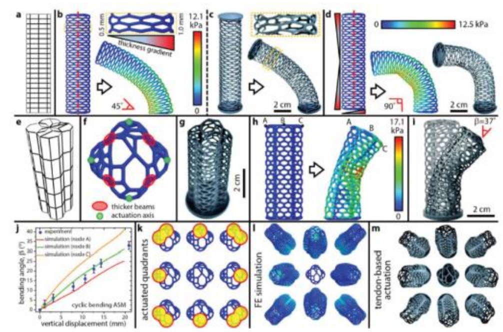

	c 3D printing of flexible photopolymers or the injection molding of elastomers, programming motion of ASMs by tuning beam thickness				
[136]	Biological materials, 3D-printing, Droptower testing, Nacre, Finite element modeling, Extreme mechanics	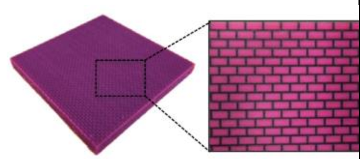	Additive manufacturing of the Nacre-like composites using a Stratasys Connex 3 multi-material printer	The two base materials are Stratasys photopolymers, Veromagenta and Tangoblackplus. The Veromagenta grade is the comparatively stiffer material, whereas the Tangoblackplus grade is more flexible and rubber-like.	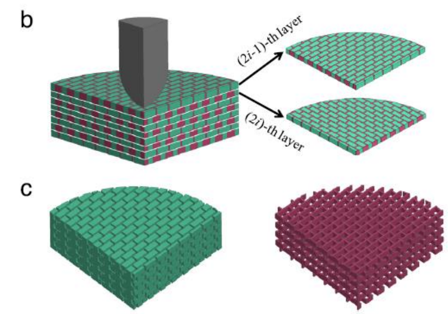

					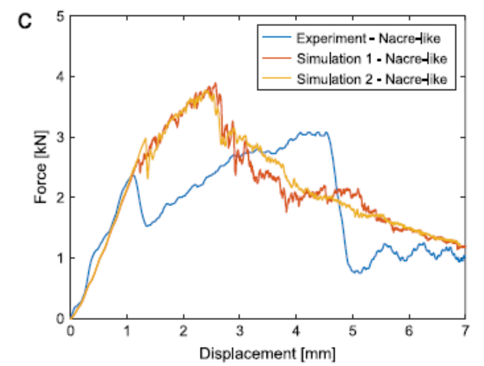
[56]	Mechanical metamaterials, negative stiffness, snap-through instabilities, uniaxial tension testing, finite element simulation, soft spring model, curved beams structures, bending-dominant, stretching dominant	Curved beams: sine waves connected 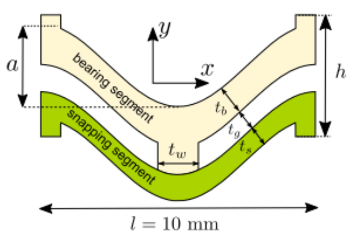	3D printing: selective laser sintering (EOS e-Manufacturing Solutions)	Nylon-based rubber-like material E = 78 MPa ν = 0.4	Uniaxial tension 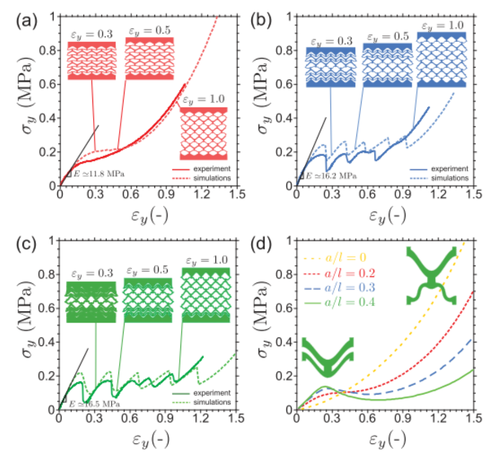

[100]	Auxetic, stiffness, energy absorption, composites, lattice materials, straight beams structures	Straight beams: re-entrant honeycomb, chiral truss, honeycomb and truss. 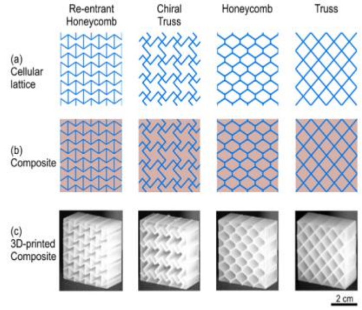 	3D printing: multi-material printing (Object Connex260, Stratasys Ltd.)	VeroWhite (a) resin for the reinforcement and TangoPlus (b) resin for the matrix 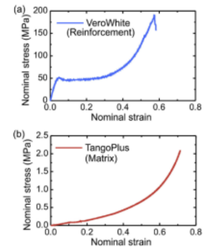 	Uniaxial compresion 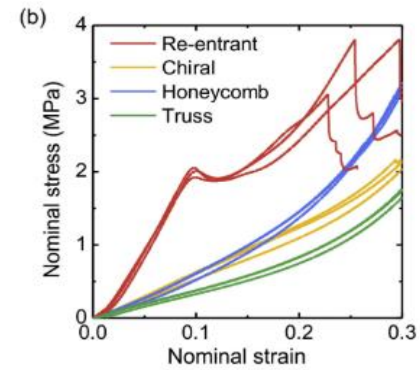
[160]	Mechanical properties, polymers, 3D structures bending-dominant, stretching dominant, reversible stretchability, low density, energy absorption efficiency, projection microstereolitography	3D straight beams: octet-truss, kelvin, kagome, octahedron and dodecahedron lattices. 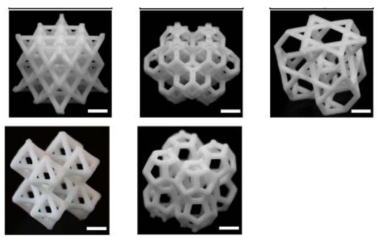	3D printing: projection microstereolitography, cure elastomers within the hollow channels, and finally chemically dissolve the hollow scaffold	Mold max NV14, tin-catalyzed silicone elastomers and urethane elastomers 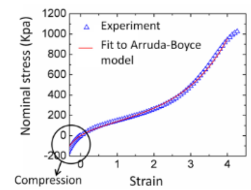 	Uniaxial tension 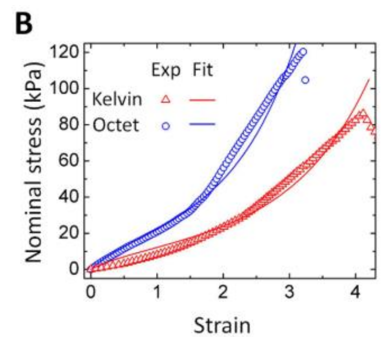 Uniaxial compression (Kelvin)

					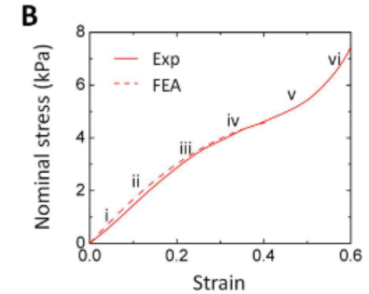
[31]	Multi-material 3D printing, tissue-mimicking phantom, metamaterials, nonlinear mechanical properties, finite element analysis	Curved fibers: sinusoidal wave, double helix and interblocking chain 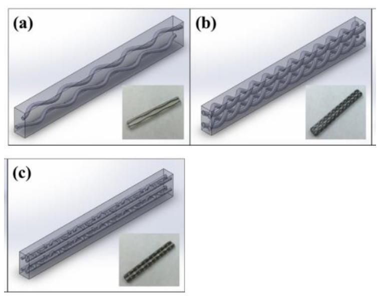	3D printing: multi-material printing (Connex350 Stratasys Ltd.)	VeroBlackPlus (RGD875) for stiff fiber and TangloPlus (FullCare 930) for elastic matrix 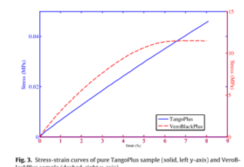	Uniaxial tension 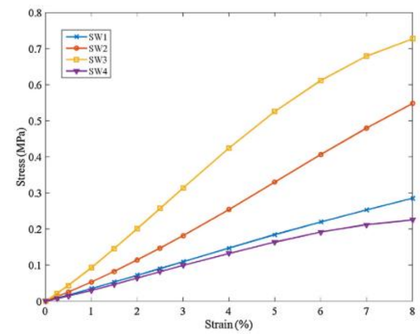

[143]	Multi-material 3D printing, tissue-mimicking phantom, metamaterials, nonlinear mechanical properties, finite element analysis, statistical approach, surrogate model, strain-softening and strain stiffening, systematic design	Curved fibers: sinusoidal wave 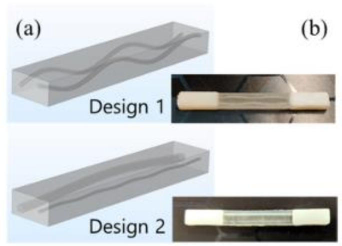	3D printing: multi-material printing (Connex350 Stratasys Ltd.)	VeroBlackPlus (RGD875) for stiff fiber and TangloPlus (FullCare 930) for elastic matrix	Uniaxial tension 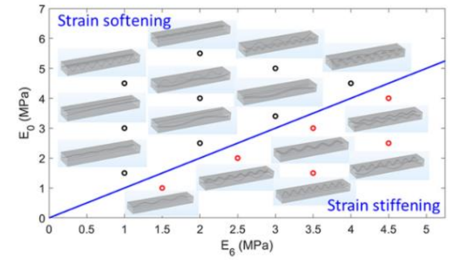
[99]	3D printing, 3D samples, hybrid structures, honeycomb, finite element simulation, fused deposition modeling, deformation mechanisms, energy absorption	Straight beams: honeycomb, re-entrant honeycomb, strut re-entrant honeycomb and hybrid structures 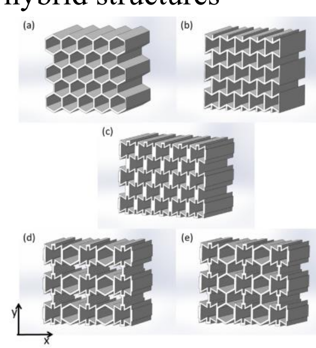	3D printing: fused deposition modeling	Acrylonitrile butadiene styrene (ABS) polymer E = 2.2 GPa ν = 0.35	Uniaxial compresion 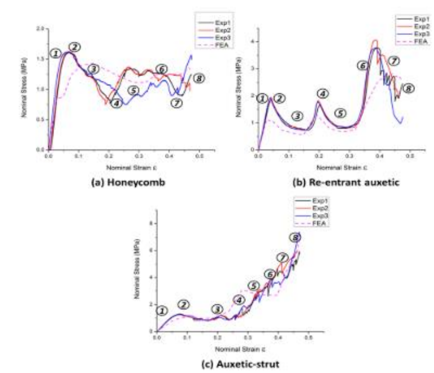

[161]	3D printing, shape-recovering, energy absorption, stretch-dominant, inverted stereolithography, deformation mechanisms, failure analysis, low density	Straight beams: octet-truss 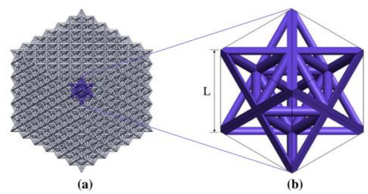 	3D printing: inverted stereolithography (Form 2, Formlabs Inc.)	Green resin with similar properties to ABS and gray similar properties to PMMA	Uniaxial compresion 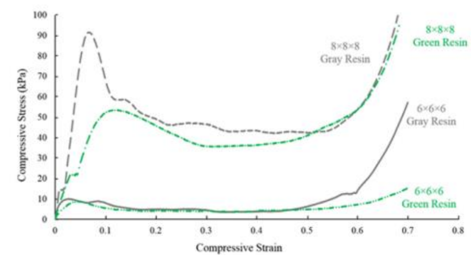

[98]	Acoustic metamaterials, mechanical deformation, vibrational control, strain-stiffening behavior, tuning of Poisson's ratio, amplitude and wavelength control, simulations, band gaps	Curved beams: sinusoidal waves, hexagonal, kagome, square, triangular 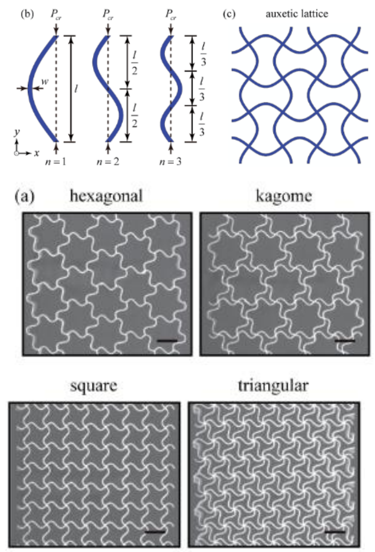	3D printing: (Objet Connex260, Stratasys Ltd.)	FLX9795-DM, rubber like material	Uniaxial tension 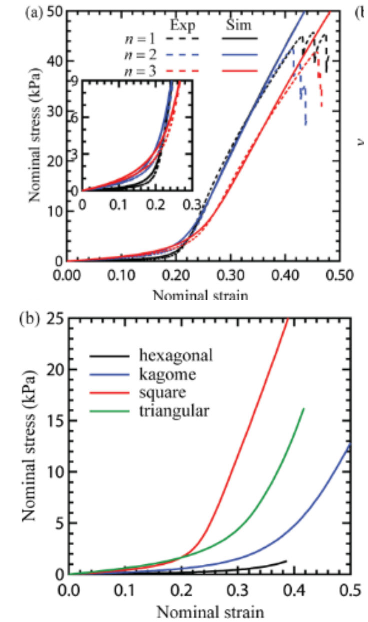
[102]	Tuning of Poisson's ratio, topology optimization, large deformations, direct ink writing, multi-nozzle	Curved beams: parametrized super ellipses 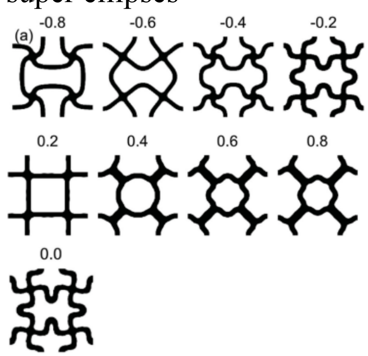	3D printing: Direct ink writing with an Aerotech 3-axis positioning stage (Aerotech, Inc.)	Poly(dimethylsiloxane) (PDMS) ink	Uniaxial tension (no strain-stress behavior analysis) 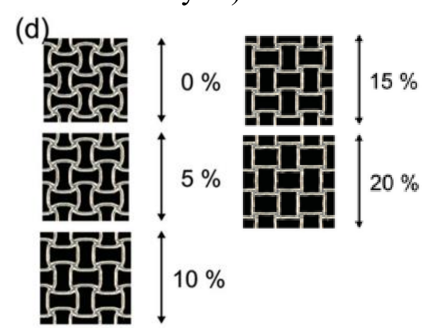

<table>
<tr>
<td>[162]</td>
<td>Disordered materials, simulation of molecular dynamics, Poisson’s ratio, Young’s modulus, out-of-plane buckling, topology modifications, fused deposition modeling technique, failure mechanisms</td>
<td>Straight beams: ordered or disordered re-entrant honeycombs
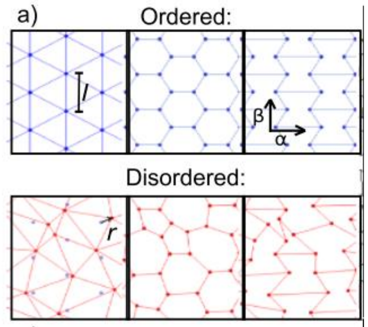
</td>
<td>3D printing: fused deposition modeling technique</td>
<td>NinjaFlex (thermoplastic polyurethane material), Flex PLA and Hard PLA
<table>
<tr><th>Material</th><th>Load</th><th>Young's modulus [GPa]</th><th>Poisson's ratio</th></tr>
<tr><td>NinjaFlex</td><td>Tensile</td><td>0.1124</td><td>0.344</td></tr>
<tr><td></td><td>Compressive</td><td>0.15</td><td>0.340</td></tr>
<tr><td>FlexPLA</td><td>Tensile</td><td>1.743</td><td>0.342</td></tr>
<tr><td></td><td>Compressive</td><td>1.4879</td><td>–</td></tr>
<tr><td>Hard PLA</td><td>Tensile</td><td>7.23</td><td>0.0855</td></tr>
<tr><td></td><td>Compressive</td><td>3.1613</td><td>–</td></tr>
</table></td>
<td>Uniaxial tension and compression (no strain-stress behavior analysis)
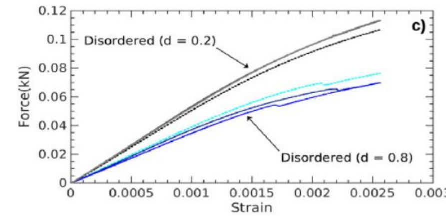
</td>
</tr>
<tr>
<td>[163]</td>
<td>Soft poly-lactic acid, large deformation, finite element analysis, fused deposition modeling</td>
<td>Straight beams: parallelogram and hexaonal
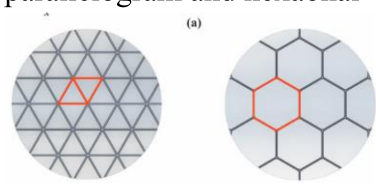</td>
<td>3D printing: fused deposition modeling</td>
<td>Soft poly-lactic acid (PLA)</td>
<td>Tension (hexagonal)
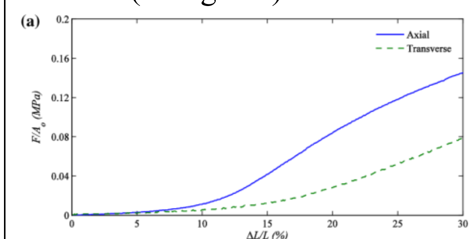

Compresion (hexagonal)
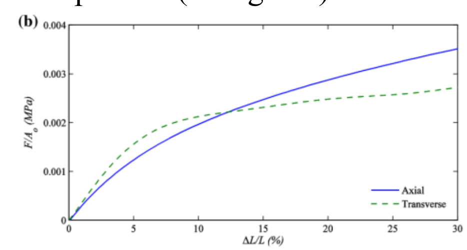
</td>
</tr>
</table>

[164]	Bistable auxetic materials, rigid structures, rotationary elements, slender ligaments, kirigami architecture, fatigue, polymer	Straight rotationary beams: triangles 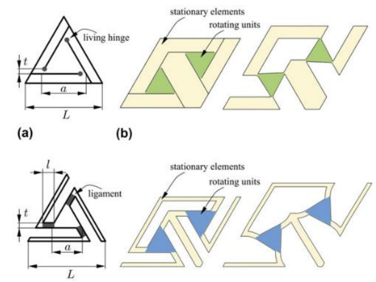	Incision	Derlin Acetal Resin and natural latex rubber	Uniaxial stress in cycles 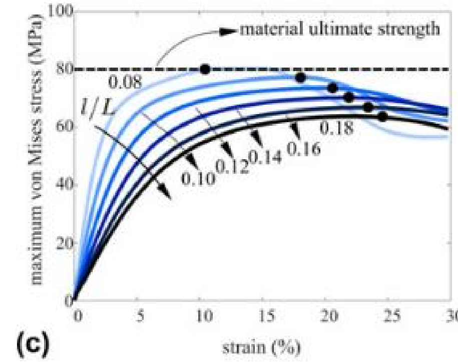
[165]	Mechanical properties, soft material, hierarchical straight beams, honeycomb, buckling, structural organization, finite element analysis	Straight beams: herarchical honeycomb 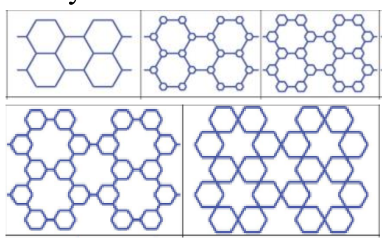	3D printing: PolyJet (Objet Eden260V, Stratasys, Ltd.)	TangoGrey E = 1.7 MPa ν = 0.3	Uniaxial compression on y and x axis 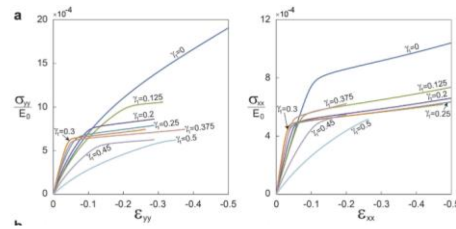

[166]	Phononic crystals, hierarchical wave propagation, honeycombs, band gaps, load-carrying capabilities, eigenfrequency analysis, in-plane propagation	Straight beams: herarchical honeycombs 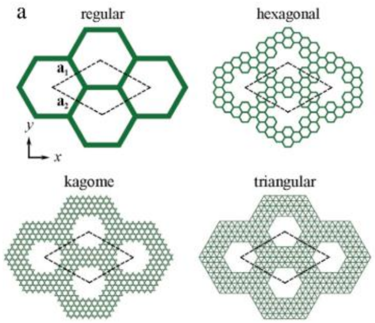	Only numerical analysis	Only numerical analysis	Uniaxial compresion 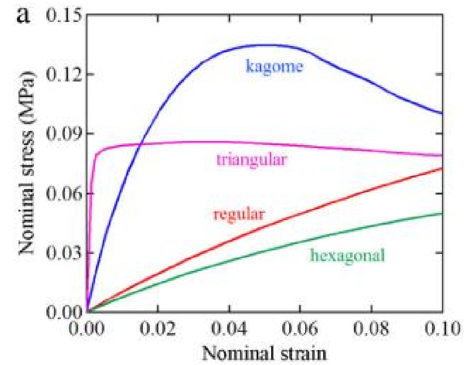

Table B.2. Summary of different solution for delamination problems with PDMS in literature.

<table>
<tr><th>Ref.</th><th>Key concepts</th><th>Alternative presented</th><th>Results</th></tr>
<tr><td>[167]</td><td>Atomic force microscopy, buckling, cracks, wrinkling and delamination, electronic structure, evaporation, finite element analysis, scanning electron microscopy, dipoles, Derjaguin-Muller-Toporov model</td><td>Adhesive layer of chromium
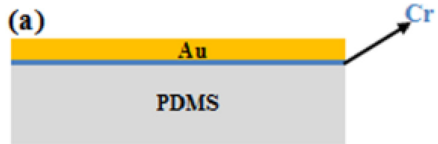
</td><td>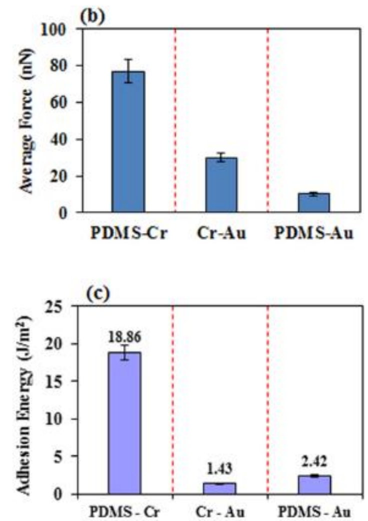
</td></tr>
<tr><td>[168]</td><td>Carbon nanotubes, fracture toughness, laminates, nanocomposites, polyurethane, functionalize, pristine carbon nanotubes</td><td>Add functionalize and pristine carbon nanotubes in polyurethane matrix
Table 1. The composite films and their nomenclature<table><tr><th>Film label</th><th>Nano filler</th><th>wt%</th><th>wt%</th><th>wt%</th><th>wt%</th></tr><tr><td>PU pure</td><td>—</td><td>—</td><td>—</td><td>—</td><td>—</td></tr><tr><td>PU TT</td><td>—</td><td>—</td><td>—</td><td>—</td><td>—</td></tr><tr><td>CNT Pr</td><td>CNT pristine</td><td>1</td><td>0.7</td><td>0.5</td><td>0.2</td></tr><tr><td>CNT–COOH</td><td>CNT–COOH</td><td>1</td><td>0.7</td><td>0.5</td><td>0.2</td></tr><tr><td>CNT–PPG</td><td>CNT–PPG</td><td>1</td><td>0.7</td><td>0.5</td><td>0.2</td></tr></table></td><td>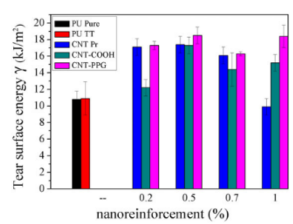

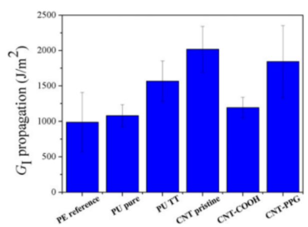
</td></tr>
</table>

Table B.3. Summary of novel resins in literature.

Ref.	Key concepts	Manufacturing	Materials	Results
[169]	Cellulose nanocrystal, stereolithography apparatus, nanocomposite hydrogel, photocurable, abaca pup fibers	3D printing: stereolithography 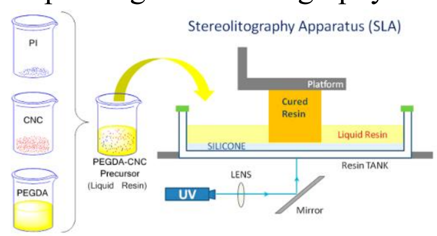	Poly(ethylene glycol) diacrylate matrix with cellulose nanocrystal nanofillers and photoinitiating	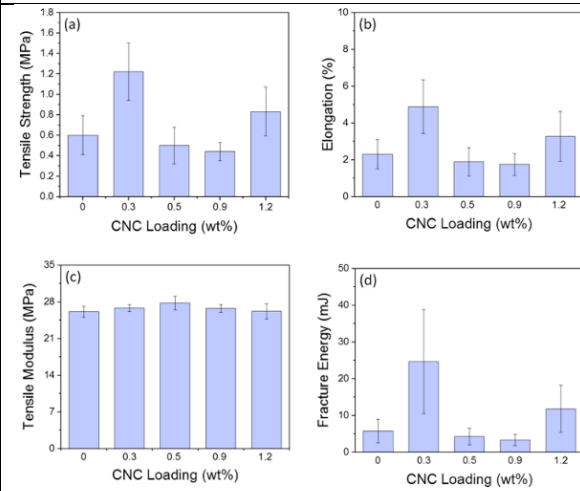

Permission for Figure 1.1a

ELSEVIER LICENSE
TERMS AND CONDITIONS

Appendix C: Permissions from Publishers to use Figures in Thesis

Sep 19, 2019

This Agreement between University of Alberta -- Dinara Zhalmuratova ("You") and Elsevier ("Elsevier") consists of your license details and the terms and conditions provided by Elsevier and Copyright Clearance Center.

License Number	4672280639466
License date	Sep 18, 2019
Licensed Content Publisher	Elsevier
Licensed Content Publication	The Journal of Heart and Lung Transplantation
Licensed Content Title	Intermediate outcomes with ex-vivo allograft perfusion for heart transplantation
Licensed Content Author	Joshua L. Chan,Jon A. Kobashigawa,Heidi J. Reich,Danny Ramzy,Maria M. Thottam,Zhe Yu,Tamar L. Aintablian,Frank Liou,Jignesh K. Patel,Michelle M. Kittleson,Lawrence S. Czer,Alfredo Trento,Fardad Esmailian
Licensed Content Date	Mar 1, 2017
Licensed Content Volume	36
Licensed Content Issue	3
Licensed Content Pages	6
Start Page	258
End Page	263
Type of Use	reuse in a thesis/dissertation
Portion	figures/tables/illustrations
Number of figures/tables/illustrations	1
Format	both print and electronic
Are you the author of this Elsevier article?	No
Will you be translating?	No
Original figure numbers	Figure 1
Title of your thesis/dissertation	Reinforced Elastomer Composites and Metamaterials for Neo-aorta Applications
Publisher of new work	University of Alberta
Expected completion date	Sep 2019
Estimated size (number of pages)	1
Requestor Location	University of Alberta 10907 65 Ave Edmonton, AB T6H 1W1 Canada Attn: University of Alberta

Publisher Tax ID	GB 494 6272 12
Total	0.00 CAD

Terms and Conditions

INTRODUCTION

1. The publisher for this copyrighted material is Elsevier. By clicking "accept" in connection with completing this licensing transaction, you agree that the following terms and conditions apply to this transaction (along with the Billing and Payment terms and conditions established by Copyright Clearance Center, Inc. ("CCC"), at the time that you opened your Rightslink account and that are available at any time at http://myaccount.copyright.com).

GENERAL TERMS

2. Elsevier hereby grants you permission to reproduce the aforementioned material subject to the terms and conditions indicated.
3. Acknowledgement: If any part of the material to be used (for example, figures) has appeared in our publication with credit or acknowledgement to another source, permission must also be sought from that source. If such permission is not obtained then that material may not be included in your publication/copies. Suitable acknowledgement to the source must be made, either as a footnote or in a reference list at the end of your publication, as follows:
"Reprinted from Publication title, Vol /edition number, Author(s), Title of article / title of chapter, Pages No., Copyright (Year), with permission from Elsevier [OR APPLICABLE SOCIETY COPYRIGHT OWNER]." Also Lancet special credit - "Reprinted from The Lancet, Vol. number, Author(s), Title of article, Pages No., Copyright (Year), with permission from Elsevier."
4. Reproduction of this material is confined to the purpose and/or media for which permission is hereby given.
5. Altering/Modifying Material: Not Permitted. However figures and illustrations may be altered/adapted minimally to serve your work. Any other abbreviations, additions, deletions and/or any other alterations shall be made only with prior written authorization of Elsevier Ltd. (Please contact Elsevier at permissions@elsevier.com). No modifications can be made to any Lancet figures/tables and they must be reproduced in full.
6. If the permission fee for the requested use of our material is waived in this instance, please be advised that your future requests for Elsevier materials may attract a fee.
7. Reservation of Rights: Publisher reserves all rights not specifically granted in the combination of (i) the license details provided by you and accepted in the course of this licensing transaction, (ii) these terms and conditions and (iii) CCC's Billing and Payment terms and conditions.
8. License Contingent Upon Payment: While you may exercise the rights licensed immediately upon issuance of the license at the end of the licensing process for the transaction, provided that you have disclosed complete and accurate details of your proposed use, no license is finally effective unless and until full payment is received from you (either by publisher or by CCC) as provided in CCC's Billing and Payment terms and conditions. If full payment is not received on a timely basis, then any license preliminarily granted shall be deemed automatically revoked and shall be void as if never granted. Further, in the event that you breach any of these terms and conditions or any of CCC's Billing and Payment terms and conditions, the license is automatically revoked and shall be void as if never granted. Use of materials as described in a revoked license, as well as any use of the materials beyond the scope of an unrevoked license, may constitute copyright infringement and publisher reserves the right to take any and all action to protect its copyright in the materials.
9. Warranties: Publisher makes no representations or warranties with respect to the licensed material.
10. Indemnity: You hereby indemnify and agree to hold harmless publisher and CCC, and their respective officers, directors, employees and agents, from and against any and all

claims arising out of your use of the licensed material other than as specifically authorized pursuant to this license.
11. No Transfer of License: This license is personal to you and may not be sublicensed, assigned, or transferred by you to any other person without publisher's written permission.
12. No Amendment Except in Writing: This license may not be amended except in a writing signed by both parties (or, in the case of publisher, by CCC on publisher's behalf).
13. Objection to Contrary Terms: Publisher hereby objects to any terms contained in any purchase order, acknowledgment, check endorsement or other writing prepared by you, which terms are inconsistent with these terms and conditions or CCC's Billing and Payment terms and conditions. These terms and conditions, together with CCC's Billing and Payment terms and conditions (which are incorporated herein), comprise the entire agreement between you and publisher (and CCC) concerning this licensing transaction. In the event of any conflict between your obligations established by these terms and conditions and those established by CCC's Billing and Payment terms and conditions, these terms and conditions shall control.
14. Revocation: Elsevier or Copyright Clearance Center may deny the permissions described in this License at their sole discretion, for any reason or no reason, with a full refund payable to you. Notice of such denial will be made using the contact information provided by you. Failure to receive such notice will not alter or invalidate the denial. In no event will Elsevier or Copyright Clearance Center be responsible or liable for any costs, expenses or damage incurred by you as a result of a denial of your permission request, other than a refund of the amount(s) paid by you to Elsevier and/or Copyright Clearance Center for denied permissions.

LIMITED LICENSE

The following terms and conditions apply only to specific license types:
15. **Translation**: This permission is granted for non-exclusive world **English** rights only unless your license was granted for translation rights. If you licensed translation rights you may only translate this content into the languages you requested. A professional translator must perform all translations and reproduce the content word for word preserving the integrity of the article.
16. **Posting licensed content on any Website**: The following terms and conditions apply as follows: Licensing material from an Elsevier journal: All content posted to the web site must maintain the copyright information line on the bottom of each image; A hyper-text must be included to the Homepage of the journal from which you are licensing at http://www.sciencedirect.com/science/journal/xxxxx or the Elsevier homepage for books at http://www.elsevier.com; Central Storage: This license does not include permission for a scanned version of the material to be stored in a central repository such as that provided by Heron/XanEdu.
Licensing material from an Elsevier book: A hyper-text link must be included to the Elsevier homepage at http://www.elsevier.com . All content posted to the web site must maintain the copyright information line on the bottom of each image.

Posting licensed content on Electronic reserve: In addition to the above the following clauses are applicable: The web site must be password-protected and made available only to bona fide students registered on a relevant course. This permission is granted for 1 year only. You may obtain a new license for future website posting.
17. **For journal authors:** the following clauses are applicable in addition to the above:
Preprints:
A preprint is an author's own write-up of research results and analysis, it has not been peer-reviewed, nor has it had any other value added to it by a publisher (such as formatting, copyright, technical enhancement etc.).
Authors can share their preprints anywhere at any time. Preprints should not be added to or enhanced in any way in order to appear more like, or to substitute for, the final versions of

articles however authors can update their preprints on arXiv or RePEc with their Accepted Author Manuscript (see below).
If accepted for publication, we encourage authors to link from the preprint to their formal publication via its DOI. Millions of researchers have access to the formal publications on ScienceDirect, and so links will help users to find, access, cite and use the best available version. Please note that Cell Press, The Lancet and some society-owned have different preprint policies. Information on these policies is available on the journal homepage.
Accepted Author Manuscripts: An accepted author manuscript is the manuscript of an article that has been accepted for publication and which typically includes author-incorporated changes suggested during submission, peer review and editor-author communications.
Authors can share their accepted author manuscript:

- immediately
  - via their non-commercial person homepage or blog
  - by updating a preprint in arXiv or RePEc with the accepted manuscript
  - via their research institute or institutional repository for internal institutional uses or as part of an invitation-only research collaboration work-group
  - directly by providing copies to their students or to research collaborators for their personal use
  - for private scholarly sharing as part of an invitation-only work group on commercial sites with which Elsevier has an agreement
- After the embargo period
  - via non-commercial hosting platforms such as their institutional repository
  - via commercial sites with which Elsevier has an agreement

In all cases accepted manuscripts should:

- link to the formal publication via its DOI
- bear a CC-BY-NC-ND license - this is easy to do
- if aggregated with other manuscripts, for example in a repository or other site, be shared in alignment with our hosting policy not be added to or enhanced in any way to appear more like, or to substitute for, the published journal article.

Published journal article (JPA): A published journal article (PJA) is the definitive final record of published research that appears or will appear in the journal and embodies all value-adding publishing activities including peer review co-ordination, copy-editing, formatting, (if relevant) pagination and online enrichment.
Policies for sharing publishing journal articles differ for subscription and gold open access articles:
Subscription Articles: If you are an author, please share a link to your article rather than the full-text. Millions of researchers have access to the formal publications on ScienceDirect, and so links will help your users to find, access, cite, and use the best available version. Theses and dissertations which contain embedded PJAs as part of the formal submission can be posted publicly by the awarding institution with DOI links back to the formal publications on ScienceDirect.
If you are affiliated with a library that subscribes to ScienceDirect you have additional private sharing rights for others' research accessed under that agreement. This includes use for classroom teaching and internal training at the institution (including use in course packs and courseware programs), and inclusion of the article for grant funding purposes.
Gold Open Access Articles: May be shared according to the author-selected end-user license and should contain a CrossMark logo, the end user license, and a DOI link to the formal publication on ScienceDirect.
Please refer to Elsevier's posting policy for further information.

18. **For book authors** the following clauses are applicable in addition to the above: Authors are permitted to place a brief summary of their work online only. You are not allowed to download and post the published electronic version of your chapter, nor may you scan the printed edition to create an electronic version. **Posting to a repository:** Authors are permitted to post a summary of their chapter only in their institution's repository.
19. **Thesis/Dissertation**: If your license is for use in a thesis/dissertation your thesis may be submitted to your institution in either print or electronic form. Should your thesis be published commercially, please reapply for permission. These requirements include permission for the Library and Archives of Canada to supply single copies, on demand, of the complete thesis and include permission for Proquest/UMI to supply single copies, on demand, of the complete thesis. Should your thesis be published commercially, please reapply for permission. Theses and dissertations which contain embedded PJAs as part of the formal submission can be posted publicly by the awarding institution with DOI links back to the formal publications on ScienceDirect.

Elsevier Open Access Terms and Conditions

You can publish open access with Elsevier in hundreds of open access journals or in nearly 2000 established subscription journals that support open access publishing. Permitted third party re-use of these open access articles is defined by the author's choice of Creative Commons user license. See our open access license policy for more information.

Terms & Conditions applicable to all Open Access articles published with Elsevier:

Any reuse of the article must not represent the author as endorsing the adaptation of the article nor should the article be modified in such a way as to damage the author's honour or reputation. If any changes have been made, such changes must be clearly indicated.

The author(s) must be appropriately credited and we ask that you include the end user license and a DOI link to the formal publication on ScienceDirect.

If any part of the material to be used (for example, figures) has appeared in our publication with credit or acknowledgement to another source it is the responsibility of the user to ensure their reuse complies with the terms and conditions determined by the rights holder.

Additional Terms & Conditions applicable to each Creative Commons user license:

CC BY: The CC-BY license allows users to copy, to create extracts, abstracts and new works from the Article, to alter and revise the Article and to make commercial use of the Article (including reuse and/or resale of the Article by commercial entities), provided the user gives appropriate credit (with a link to the formal publication through the relevant DOI), provides a link to the license, indicates if changes were made and the licensor is not represented as endorsing the use made of the work. The full details of the license are available at http://creativecommons.org/licenses/by/4.0.

CC BY NC SA: The CC BY-NC-SA license allows users to copy, to create extracts, abstracts and new works from the Article, to alter and revise the Article, provided this is not done for commercial purposes, and that the user gives appropriate credit (with a link to the formal publication through the relevant DOI), provides a link to the license, indicates if changes were made and the licensor is not represented as endorsing the use made of the work. Further, any new works must be made available on the same conditions. The full details of the license are available at http://creativecommons.org/licenses/by-nc-sa/4.0.

CC BY NC ND: The CC BY-NC-ND license allows users to copy and distribute the Article, provided this is not done for commercial purposes and further does not permit distribution of the Article if it is changed or edited in any way, and provided the user gives appropriate credit (with a link to the formal publication through the relevant DOI), provides a link to the license, and that the licensor is not represented as endorsing the use made of the work. The full details of the license are available at http://creativecommons.org/licenses/by-nc-nd/4.0.

Any commercial reuse of Open Access articles published with a CC BY NC SA or CC BY NC ND license requires permission from Elsevier and will be subject to a fee.

Commercial reuse includes:

- Associating advertising with the full text of the Article
- Charging fees for document delivery or access
- Article aggregation
- Systematic distribution via e-mail lists or share buttons

Posting or linking by commercial companies for use by customers of those companies.

20. **Other Conditions**:

v1.9

Questions? customercare@copyright.com or +1-855-239-3415 (toll free in the US) or +1-978-646-2777.

Copyright Clearance Center RightsLink®

Home | Account Info | Help | LIVE CHAT

SPRINGER NATURE

Title:	A New Constitutive Framework for Arterial Wall Mechanics and a Comparative Study of Material Models
Author:	Gerhard A. Holzapfel, Thomas C. Gasser, Ray W. Ogden
Publication:	Journal of Elasticity
Publisher:	Springer Nature
Date:	Jan 1, 2000

Logged in as:
Dinara Zhalmuratova
University of Alberta
Account #:
3001505643
LOGOUT

Permission for Figure 1.3

Order Completed

Thank you for your order.

This Agreement between University of Alberta -- Dinara Zhalmuratova ("You") and Springer Nature ("Springer Nature") consists of your license details and the terms and conditions provided by Springer Nature and Copyright Clearance Center.

Your confirmation email will contain your order number for future reference.

printable details

License Number	4672290346825
License date	Sep 19, 2019
Licensed Content Publisher	Springer Nature
Licensed Content Publication	Journal of Elasticity
Licensed Content Title	A New Constitutive Framework for Arterial Wall Mechanics and a Comparative Study of Material Models
Licensed Content Author	Gerhard A. Holzapfel, Thomas C. Gasser, Ray W. Ogden
Licensed Content Date	Jan 1, 2000
Licensed Content Volume	61
Licensed Content Issue	1
Type of Use	Thesis/Dissertation
Requestor type	academic/university or research institute
Format	print and electronic
Portion	figures/tables/illustrations
Number of figures/tables/illustrations	1
Will you be translating?	no
Circulation/distribution	1 - 29
Author of this Springer Nature content	no
Title	Reinforced Elastomer Composites and Metamaterials for Neo-aorta Applications
Institution name	University of Alberta
Expected presentation date	Sep 2019
Portions	Figure 1
Requestor Location	University of Alberta 10907 65 Ave Edmonton, AB T6H 1W1

Canada
Attn: University of Alberta

Total 0.00 CAD

ORDER MORE CLOSE WINDOW

Permission for Figure 1.4b

ELSEVIER LICENSE
TERMS AND CONDITIONS

Sep 19, 2019

This Agreement between University of Alberta -- Dinara Zhalmuratova ("You") and Elsevier ("Elsevier") consists of your license details and the terms and conditions provided by Elsevier and Copyright Clearance Center.

License Number	4672290784975
License date	Sep 19, 2019
Licensed Content Publisher	Elsevier
Licensed Content Publication	European Journal of Vascular and Endovascular Surgery
Licensed Content Title	In Vitro Characterisation of Physiological and Maximum Elastic Modulus of Ascending Thoracic Aortic Aneurysms Using Uniaxial Tensile Testing
Licensed Content Author	A. Duprey,K. Khanafer,M. Schlicht,S. Avril,D. Williams,R. Berguer
Licensed Content Date	Jun 1, 2010
Licensed Content Volume	39
Licensed Content Issue	6
Licensed Content Pages	8
Start Page	700
End Page	707
Type of Use	reuse in a thesis/dissertation
Intended publisher of new work	other
Portion	figures/tables/illustrations
Number of figures/tables/illustrations	1
Format	both print and electronic
Are you the author of this Elsevier article?	No
Will you be translating?	No
Original figure numbers	Figure 2
Title of your thesis/dissertation	Reinforced Elastomer Composites and Metamaterials for Neo-aorta Applications
Publisher of new work	University of Alberta
Expected completion date	Sep 2019
Estimated size (number of pages)	1
Requestor Location	University of Alberta 10907 65 Ave Edmonton, AB T6H 1W1 Canada Attn: University of Alberta

Publisher Tax ID	GB 494 6272 12
Total	0.00 CAD

Terms and Conditions

INTRODUCTION

1. The publisher for this copyrighted material is Elsevier. By clicking "accept" in connection with completing this licensing transaction, you agree that the following terms and conditions apply to this transaction (along with the Billing and Payment terms and conditions established by Copyright Clearance Center, Inc. ("CCC"), at the time that you opened your Rightslink account and that are available at any time at http://myaccount.copyright.com).

GENERAL TERMS

2. Elsevier hereby grants you permission to reproduce the aforementioned material subject to the terms and conditions indicated.
3. Acknowledgement: If any part of the material to be used (for example, figures) has appeared in our publication with credit or acknowledgement to another source, permission must also be sought from that source. If such permission is not obtained then that material may not be included in your publication/copies. Suitable acknowledgement to the source must be made, either as a footnote or in a reference list at the end of your publication, as follows:
"Reprinted from Publication title, Vol /edition number, Author(s), Title of article / title of chapter, Pages No., Copyright (Year), with permission from Elsevier [OR APPLICABLE SOCIETY COPYRIGHT OWNER]." Also Lancet special credit - "Reprinted from The Lancet, Vol. number, Author(s), Title of article, Pages No., Copyright (Year), with permission from Elsevier."
4. Reproduction of this material is confined to the purpose and/or media for which permission is hereby given.
5. Altering/Modifying Material: Not Permitted. However figures and illustrations may be altered/adapted minimally to serve your work. Any other abbreviations, additions, deletions and/or any other alterations shall be made only with prior written authorization of Elsevier Ltd. (Please contact Elsevier at permissions@elsevier.com). No modifications can be made to any Lancet figures/tables and they must be reproduced in full.
6. If the permission fee for the requested use of our material is waived in this instance, please be advised that your future requests for Elsevier materials may attract a fee.
7. Reservation of Rights: Publisher reserves all rights not specifically granted in the combination of (i) the license details provided by you and accepted in the course of this licensing transaction, (ii) these terms and conditions and (iii) CCC's Billing and Payment terms and conditions.
8. License Contingent Upon Payment: While you may exercise the rights licensed immediately upon issuance of the license at the end of the licensing process for the transaction, provided that you have disclosed complete and accurate details of your proposed use, no license is finally effective unless and until full payment is received from you (either by publisher or by CCC) as provided in CCC's Billing and Payment terms and conditions. If full payment is not received on a timely basis, then any license preliminarily granted shall be deemed automatically revoked and shall be void as if never granted. Further, in the event that you breach any of these terms and conditions or any of CCC's Billing and Payment terms and conditions, the license is automatically revoked and shall be void as if never granted. Use of materials as described in a revoked license, as well as any use of the materials beyond the scope of an unrevoked license, may constitute copyright infringement and publisher reserves the right to take any and all action to protect its copyright in the materials.
9. Warranties: Publisher makes no representations or warranties with respect to the licensed material.
10. Indemnity: You hereby indemnify and agree to hold harmless publisher and CCC, and their respective officers, directors, employees and agents, from and against any and all

claims arising out of your use of the licensed material other than as specifically authorized pursuant to this license.
11. No Transfer of License: This license is personal to you and may not be sublicensed, assigned, or transferred by you to any other person without publisher's written permission.
12. No Amendment Except in Writing: This license may not be amended except in a writing signed by both parties (or, in the case of publisher, by CCC on publisher's behalf).
13. Objection to Contrary Terms: Publisher hereby objects to any terms contained in any purchase order, acknowledgment, check endorsement or other writing prepared by you, which terms are inconsistent with these terms and conditions or CCC's Billing and Payment terms and conditions. These terms and conditions, together with CCC's Billing and Payment terms and conditions (which are incorporated herein), comprise the entire agreement between you and publisher (and CCC) concerning this licensing transaction. In the event of any conflict between your obligations established by these terms and conditions and those established by CCC's Billing and Payment terms and conditions, these terms and conditions shall control.
14. Revocation: Elsevier or Copyright Clearance Center may deny the permissions described in this License at their sole discretion, for any reason or no reason, with a full refund payable to you. Notice of such denial will be made using the contact information provided by you. Failure to receive such notice will not alter or invalidate the denial. In no event will Elsevier or Copyright Clearance Center be responsible or liable for any costs, expenses or damage incurred by you as a result of a denial of your permission request, other than a refund of the amount(s) paid by you to Elsevier and/or Copyright Clearance Center for denied permissions.

LIMITED LICENSE

The following terms and conditions apply only to specific license types:
15. **Translation**: This permission is granted for non-exclusive world **English** rights only unless your license was granted for translation rights. If you licensed translation rights you may only translate this content into the languages you requested. A professional translator must perform all translations and reproduce the content word for word preserving the integrity of the article.
16. **Posting licensed content on any Website**: The following terms and conditions apply as follows: Licensing material from an Elsevier journal: All content posted to the web site must maintain the copyright information line on the bottom of each image; A hyper-text must be included to the Homepage of the journal from which you are licensing at http://www.sciencedirect.com/science/journal/xxxxx or the Elsevier homepage for books at http://www.elsevier.com; Central Storage: This license does not include permission for a scanned version of the material to be stored in a central repository such as that provided by Heron/XanEdu.
Licensing material from an Elsevier book: A hyper-text link must be included to the Elsevier homepage at http://www.elsevier.com . All content posted to the web site must maintain the copyright information line on the bottom of each image.

Posting licensed content on Electronic reserve: In addition to the above the following clauses are applicable: The web site must be password-protected and made available only to bona fide students registered on a relevant course. This permission is granted for 1 year only. You may obtain a new license for future website posting.
17. **For journal authors:** the following clauses are applicable in addition to the above:
Preprints:
A preprint is an author's own write-up of research results and analysis, it has not been peer-reviewed, nor has it had any other value added to it by a publisher (such as formatting, copyright, technical enhancement etc.).
Authors can share their preprints anywhere at any time. Preprints should not be added to or enhanced in any way in order to appear more like, or to substitute for, the final versions of

articles however authors can update their preprints on arXiv or RePEc with their Accepted Author Manuscript (see below).
If accepted for publication, we encourage authors to link from the preprint to their formal publication via its DOI. Millions of researchers have access to the formal publications on ScienceDirect, and so links will help users to find, access, cite and use the best available version. Please note that Cell Press, The Lancet and some society-owned have different preprint policies. Information on these policies is available on the journal homepage.
Accepted Author Manuscripts: An accepted author manuscript is the manuscript of an article that has been accepted for publication and which typically includes author-incorporated changes suggested during submission, peer review and editor-author communications.
Authors can share their accepted author manuscript:

- immediately
  - via their non-commercial person homepage or blog
  - by updating a preprint in arXiv or RePEc with the accepted manuscript
  - via their research institute or institutional repository for internal institutional uses or as part of an invitation-only research collaboration work-group
  - directly by providing copies to their students or to research collaborators for their personal use
  - for private scholarly sharing as part of an invitation-only work group on commercial sites with which Elsevier has an agreement
- After the embargo period
  - via non-commercial hosting platforms such as their institutional repository
  - via commercial sites with which Elsevier has an agreement

In all cases accepted manuscripts should:

- link to the formal publication via its DOI
- bear a CC-BY-NC-ND license - this is easy to do
- if aggregated with other manuscripts, for example in a repository or other site, be shared in alignment with our hosting policy not be added to or enhanced in any way to appear more like, or to substitute for, the published journal article.

Published journal article (JPA): A published journal article (PJA) is the definitive final record of published research that appears or will appear in the journal and embodies all value-adding publishing activities including peer review co-ordination, copy-editing, formatting, (if relevant) pagination and online enrichment.
Policies for sharing publishing journal articles differ for subscription and gold open access articles:
Subscription Articles: If you are an author, please share a link to your article rather than the full-text. Millions of researchers have access to the formal publications on ScienceDirect, and so links will help your users to find, access, cite, and use the best available version.
Theses and dissertations which contain embedded PJAs as part of the formal submission can be posted publicly by the awarding institution with DOI links back to the formal publications on ScienceDirect.
If you are affiliated with a library that subscribes to ScienceDirect you have additional private sharing rights for others' research accessed under that agreement. This includes use for classroom teaching and internal training at the institution (including use in course packs and courseware programs), and inclusion of the article for grant funding purposes.
Gold Open Access Articles: May be shared according to the author-selected end-user license and should contain a CrossMark logo, the end user license, and a DOI link to the formal publication on ScienceDirect.
Please refer to Elsevier's posting policy for further information.

- Associating advertising with the full text of the Article
- Charging fees for document delivery or access
- Article aggregation
- Systematic distribution via e-mail lists or share buttons

Posting or linking by commercial companies for use by customers of those companies.

20. **Other Conditions**:

v1.9

Questions? customercare@copyright.com or +1-855-239-3415 (toll free in the US) or +1-978-646-2777.

Copyright Clearance Center RightsLink®

Home | Account Info | Help

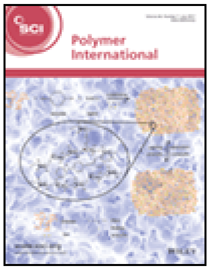

Title: Polymer physics. Edited by Michael Rubinstein and Ralph H Colby Oxford University Press, Oxford, 2003. ISBN 019852059X. pp 440

Author: RA Pethrick

Publication: Polymer International

Publisher: John Wiley and Sons

Date: Jul 26, 2004

Logged in as:
Dinara Zhalmuratova
University of Alberta
Account #:
3001505643

LOGOUT

Permission for Figure 2.2

Order Completed

Thank you for your order.

This Agreement between University of Alberta -- Dinara Zhalmuratova ("You") and John Wiley and Sons ("John Wiley and Sons") consists of your license details and the terms and conditions provided by John Wiley and Sons and Copyright Clearance Center.

Your confirmation email will contain your order number for future reference.

printable details

License Number	4672291305475
License date	Sep 19, 2019
Licensed Content Publisher	John Wiley and Sons
Licensed Content Publication	Polymer International
Licensed Content Title	Polymer physics. Edited by Michael Rubinstein and Ralph H Colby Oxford University Press, Oxford, 2003. ISBN 019852059X. pp 440
Licensed Content Author	RA Pethrick
Licensed Content Date	Jul 26, 2004
Licensed Content Volume	53
Licensed Content Issue	9
Licensed Content Pages	2
Type of use	Dissertation/Thesis
Requestor type	University/Academic
Format	Print and electronic
Portion	Figure/table
Number of figures/tables	1
Original Wiley figure/table number(s)	figure 7.2, 7.5, 7.8
Will you be translating?	No
Title of your thesis / dissertation	Reinforced Elastomer Composites and Metamaterials for Neo-aorta Applications
Expected completion date	Sep 2019
Expected size (number of pages)	1
Requestor Location	University of Alberta 10907 65 Ave

	Edmonton, AB T6H 1W1 Canada Attn: University of Alberta
Publisher Tax ID	EU826007151
Total	0.00 CAD

Would you like to purchase the full text of this article? If so, please continue on to the content ordering system located here: Purchase PDF

If you click on the buttons below or close this window, you will not be able to return to the content ordering system.

ORDER MORE CLOSE WINDOW

Copyright Clearance Center

Permission for Figure 2.3

Note: Copyright.com supplies permissions but not the copyrighted content itself.

1 PAYMENT 2 REVIEW 3 CONFIRMATION

Step 3: Order Confirmation

Thank you for your order! A confirmation for your order will be sent to your account email address. If you have questions about your order, you can call us 24 hrs/day, M-F at +1.855.239.3415 Toll Free, or write to us at info@copyright.com. This is not an invoice.

Confirmation Number: 11852402
Order Date: 09/19/2019

If you paid by credit card, your order will be finalized and your card will be charged within 24 hours. If you choose to be invoiced, you can change or cancel your order until the invoice is generated.

Payment Information

Dinara Zhalmuratova
University of Alberta
zhalmura@ualberta.ca
+1 (587) 937-5657
Payment Method: n/a

Order Details

Lab on a chip

Order detail ID: 72013326
Order License Id: 4672301252944
ISSN: 1473-0189
Publication Type: e-Journal
Volume:
Issue:
Start page:
Publisher: ROYAL SOCIETY OF CHEMISTRY
Author/Editor: Royal Society of Chemistry (Great Britain)

Permission Status: **Granted**

Permission type: Republish or display content
Type of use: Thesis/Dissertation

Requestor type	Academic institution
Format	Print, Electronic
Portion	chart/graph/table/figure
Number of charts/graphs/tables/figures	1
The requesting person/organization	Dinara Zhalmuratova
Title or numeric reference of the portion(s)	Figure 1
Title of the article or chapter the portion is from	Design and application of “J-shaped” stress–strain behavior in stretchable electronics: a review.

Editor of portion(s)	N/A
Author of portion(s)	Ma, Y., Feng, X., Rogers, J. A., Huang, Y., & Zhang, Y. (2017)
Volume of serial or monograph	Lab on a Chip, 17(10), 1689–1704. doi:10.1039/c7lc00289k
Page range of portion	page 3
Publication date of portion	September 2019
Rights for	Main product
Duration of use	Current edition and up to 5 years
Creation of copies for the disabled	no
With minor editing privileges	no
For distribution to	Canada
In the following language(s)	Original language of publication
With incidental promotional use	no
Lifetime unit quantity of new product	Up to 499
Title	Reinforced Elastomer Composites and Metamaterials for Neo-aorta Applications
Institution name	University of Alberta
Expected presentation date	Sep 2019

Note: This item will be invoiced or charged separately through CCC's **RightsLink** service. More info **$ 0.00**

Total order items: 1

This is not an invoice.

Order Total: 0.00 USD

Confirmation Number: 11852402

Special Rightsholder Terms & Conditions

The following terms & conditions apply to the specific publication under which they are listed

Lab on a chip
Permission type: Republish or display content
Type of use: Thesis/Dissertation

TERMS AND CONDITIONS

The following terms are individual to this publisher:

None

Other Terms and Conditions:

STANDARD TERMS AND CONDITIONS

1. Description of Service; Defined Terms. This Republication License enables the User to obtain licenses for republication of one or more copyrighted works as described in detail on the relevant Order Confirmation (the "Work(s)"). Copyright Clearance Center, Inc. ("CCC") grants licenses through the Service on behalf of the rightsholder identified on the Order Confirmation (the "Rightsholder"). "Republication", as used herein, generally means the inclusion of a Work, in whole or in part, in a new work or works, also as described on the Order Confirmation. "User", as used herein, means the person or entity making such republication.

2. The terms set forth in the relevant Order Confirmation, and any terms set by the Rightsholder with respect to a particular Work, govern the terms of use of Works in connection with the Service. By using the Service, the person transacting for a republication license on behalf of the User represents and warrants that he/she/it (a) has been duly authorized by the User to accept, and hereby does accept, all such terms and conditions on behalf of User, and (b) shall inform User of all such terms and conditions. In the event such person is a "freelancer" or other third party independent of User and CCC, such party shall be deemed jointly a "User" for purposes of these terms and conditions. In any event, User shall be deemed to have accepted and agreed to all such terms and conditions if User republishes the Work in any fashion.

3. Scope of License; Limitations and Obligations.

3.1 All Works and all rights therein, including copyright rights, remain the sole and exclusive property of the Rightsholder. The license created by the exchange of an Order Confirmation (and/or any invoice) and payment by User of the full amount set forth on that document includes only those rights expressly set forth in the Order Confirmation and in these terms and conditions, and conveys no other rights in the Work(s) to User. All rights not expressly granted are hereby reserved.

3.2 General Payment Terms: You may pay by credit card or through an account with us payable at the end of the month. If you and we agree that you may establish a standing account with CCC, then the following terms apply: Remit Payment to: Copyright Clearance Center, 29118 Network Place, Chicago, IL 60673-1291. Payments Due: Invoices are payable upon their delivery to you (or upon our notice to you that they are available to you for downloading). After 30 days, outstanding amounts will be subject to a service charge of 1-1/2% per month or, if less, the maximum rate allowed by applicable law. Unless otherwise specifically set forth in the Order Confirmation or in a separate written agreement signed by CCC, invoices are due and payable on "net 30" terms. While User may exercise the rights licensed immediately upon issuance of the Order Confirmation, the license is automatically revoked and is null and void, as if it had never been issued, if complete payment for the license is not received on a timely basis either from User directly or through a payment agent, such as a credit card company.

3.3 Unless otherwise provided in the Order Confirmation, any grant of rights to User (i) is "one-time" (including the editions and product family specified in the license), (ii) is non-exclusive and non-transferable and (iii) is subject to any and all limitations and restrictions (such as, but not limited to, limitations on duration of use or circulation) included in the Order Confirmation or invoice and/or in these terms and conditions. Upon completion of the licensed use, User shall either secure a new permission for further use of the Work(s) or immediately cease any new use of the Work(s) and shall render inaccessible (such as by deleting or by removing or severing links or other locators) any further copies of the Work (except for copies printed on paper in accordance with this license and still in User's stock at the end of such period).

3.4 In the event that the material for which a republication license is sought includes third party materials (such as photographs, illustrations, graphs, inserts and similar materials) which are identified in such material as having been used by permission, User is responsible for identifying, and seeking separate licenses (under this Service or otherwise) for, any of such third party materials; without a separate license, such third party materials may not be used.

3.5 Use of proper copyright notice for a Work is required as a condition of any license granted under the Service. Unless otherwise provided in the Order Confirmation, a proper copyright notice will read substantially as follows: "Republished with permission of [Rightsholder's name], from [Work's title, author, volume, edition number and year of copyright]; permission conveyed through Copyright Clearance Center, Inc. " Such notice must be provided in a reasonably legible font size and must be placed either immediately adjacent to the Work as used (for example, as part of a by-line or footnote but not as a separate electronic link) or in the place where substantially all other credits or notices for the new work containing the republished Work are located. Failure to include the required notice results in loss to the Rightsholder and CCC, and the User shall be liable to pay liquidated damages for each such failure equal to twice the use fee specified in the Order Confirmation, in addition to the use fee itself and any other fees and charges specified.

3.6 User may only make alterations to the Work if and as expressly set forth in the Order Confirmation. No Work may be used in any way that is defamatory, violates the rights of third parties (including such third parties' rights of copyright, privacy, publicity, or other tangible or intangible property), or is otherwise illegal, sexually explicit or obscene. In addition, User may not conjoin a Work with any other material that may result in damage to the reputation of the Rightsholder. User agrees to inform CCC if it becomes aware of any infringement of any rights in a Work and to cooperate with any reasonable request of CCC or the Rightsholder in connection therewith.

4. Indemnity. User hereby indemnifies and agrees to defend the Rightsholder and CCC, and their respective employees and directors, against all claims, liability, damages, costs and expenses, including legal fees and expenses, arising out of any use of a Work beyond the scope of the rights granted herein, or any use of a Work which has been altered in any unauthorized way by User, including claims of defamation or infringement of rights of copyright, publicity, privacy or other tangible or intangible property.

5. Limitation of Liability. UNDER NO CIRCUMSTANCES WILL CCC OR THE RIGHTSHOLDER BE LIABLE FOR ANY DIRECT, INDIRECT, CONSEQUENTIAL OR INCIDENTAL DAMAGES (INCLUDING WITHOUT LIMITATION DAMAGES FOR LOSS OF BUSINESS PROFITS OR INFORMATION, OR FOR BUSINESS INTERRUPTION) ARISING OUT OF THE USE OR INABILITY TO USE A WORK, EVEN IF ONE OF THEM HAS BEEN ADVISED OF THE POSSIBILITY OF SUCH DAMAGES. In any event, the total liability of the Rightsholder and CCC (including their respective employees and directors) shall not exceed the total amount actually paid by User for this license. User assumes full liability for the actions and omissions of its principals, employees, agents, affiliates, successors and assigns.

6. Limited Warranties. THE WORK(S) AND RIGHT(S) ARE PROVIDED “AS IS”. CCC HAS THE RIGHT TO GRANT TO USER THE RIGHTS GRANTED IN THE ORDER CONFIRMATION DOCUMENT. CCC AND THE RIGHTSHOLDER DISCLAIM ALL OTHER WARRANTIES RELATING TO THE WORK(S) AND RIGHT(S), EITHER EXPRESS OR IMPLIED, INCLUDING WITHOUT LIMITATION IMPLIED WARRANTIES OF MERCHANTABILITY OR FITNESS FOR A PARTICULAR PURPOSE. ADDITIONAL RIGHTS MAY BE REQUIRED TO USE ILLUSTRATIONS, GRAPHS, PHOTOGRAPHS, ABSTRACTS, INSERTS OR OTHER PORTIONS OF THE WORK (AS OPPOSED TO THE ENTIRE WORK) IN A MANNER CONTEMPLATED BY USER; USER UNDERSTANDS AND AGREES THAT NEITHER CCC NOR THE RIGHTSHOLDER MAY HAVE SUCH ADDITIONAL RIGHTS TO GRANT.

7. Effect of Breach. Any failure by User to pay any amount when due, or any use by User of a Work beyond the scope of the license set forth in the Order Confirmation and/or these terms and conditions, shall be a material breach of the license created by the Order Confirmation and these terms and conditions. Any breach not cured within 30 days of written notice thereof shall result in immediate termination of such license without further notice. Any unauthorized (but licensable) use of a Work that is terminated immediately upon notice thereof may be liquidated by payment of the Rightsholder's ordinary license price therefor; any unauthorized (and unlicensable) use that is not terminated immediately for any reason (including, for example, because materials containing the Work cannot reasonably be recalled) will be subject to all remedies available at law or in equity, but in no event to a payment of less than three times the Rightsholder's ordinary license price for the most closely analogous licensable use plus Rightsholder's and/or CCC's costs and expenses incurred in collecting such payment.

8. **Miscellaneous.**

8.1 User acknowledges that CCC may, from time to time, make changes or additions to the Service or to these terms and conditions, and CCC reserves the right to send notice to the User by electronic mail or otherwise for the purposes of notifying User of such changes or additions; provided that any such changes or additions shall not apply to permissions already secured and paid for.

8.2 Use of User-related information collected through the Service is governed by CCC’s privacy policy, available online here: http://www.copyright.com/content/cc3/en/tools/footer/privacypolicy.html.

8.3 The licensing transaction described in the Order Confirmation is personal to User. Therefore, User may not assign or transfer to any other person (whether a natural person or an organization of any kind) the license created by the Order Confirmation and these terms and conditions or any rights granted hereunder; provided, however, that User may assign such license in its entirety on written notice to CCC in the event of a transfer of all or substantially all of User’s rights in the new material which includes the Work(s) licensed under this Service.

8.4 No amendment or waiver of any terms is binding unless set forth in writing and signed by the parties. The Rightsholder and CCC hereby object to any terms contained in any writing prepared by the User or its principals, employees, agents or affiliates and purporting to govern or otherwise relate to the licensing transaction described in the Order Confirmation, which terms are in any way inconsistent with any terms set forth in the Order Confirmation and/or in these terms and conditions or CCC's standard operating procedures, whether such writing is prepared prior to, simultaneously with or subsequent to the Order Confirmation, and whether such writing appears on a copy of the Order Confirmation or in a separate instrument.

8.5 The licensing transaction described in the Order Confirmation document shall be governed by and construed under the law of the State of New York, USA, without regard to the principles thereof of conflicts of law. Any case, controversy, suit, action, or proceeding arising out of, in connection with, or related to such licensing transaction shall be brought, at CCC's sole discretion, in any federal or state court located in the County of New York, State of New York, USA, or in any federal or state court whose geographical jurisdiction covers the location of the Rightsholder set forth in the Order Confirmation. The parties expressly submit to the personal jurisdiction and venue of each such federal or state court.If you have any comments or questions about the Service or Copyright Clearance Center, please contact us at 978-750-8400 or send an e-mail to info@copyright.com.

v 1.1

Close

Confirmation Number: 11852402

Citation Information

Order Detail ID: 72013326

Lab on a chip by Royal Society of Chemistry (Great Britain) Reproduced with permission of ROYAL SOCIETY OF CHEMISTRY in the format Thesis/Dissertation via Copyright Clearance Center.

Close

SPRINGER NATURE LICENSE TERMS AND CONDITIONS

Sep 19, 2019

This Agreement between University of Alberta -- Dinara Zhalmuratova ("You") and Springer Nature ("Springer Nature") consists of your license details and the terms and conditions provided by Springer Nature and Copyright Clearance Center.

License Number	4672310979611
License date	Sep 19, 2019
Licensed Content Publisher	Springer Nature
Licensed Content Publication	Journal of Elasticity
Licensed Content Title	A New Constitutive Framework for Arterial Wall Mechanics and a Comparative Study of Material Models
Licensed Content Author	Gerhard A. Holzapfel, Thomas C. Gasser, Ray W. Ogden
Licensed Content Date	Jan 1, 2000
Licensed Content Volume	61
Licensed Content Issue	1
Type of Use	Thesis/Dissertation
Requestor type	academic/university or research institute
Format	print and electronic
Portion	figures/tables/illustrations
Number of figures/tables/illustrations	1
Will you be translating?	no
Circulation/distribution	1 - 29
Author of this Springer Nature content	no
Title	Reinforced Elastomer Composites and Metamaterials for Neo-aorta Applications
Institution name	University of Alberta
Expected presentation date	Sep 2019
Portions	Figure 14
Requestor Location	University of Alberta 10907 65 Ave Edmonton, AB T6H 1W1 Canada Attn: University of Alberta
Total	0.00 CAD
Terms and Conditions	

Springer Nature Customer Service Centre GmbH Terms and Conditions

This agreement sets out the terms and conditions of the licence (the **Licence**) between you and **Springer Nature Customer Service Centre GmbH** (the **Licensor**). By clicking 'accept' and completing the transaction for the material (**Licensed Material**), you also confirm your acceptance of these terms and conditions.

1. Grant of License

1. 1. The Licensor grants you a personal, non-exclusive, non-transferable, world-wide licence to reproduce the Licensed Material for the purpose specified in your order only. Licences are granted for the specific use requested in the order and for no other use, subject to the conditions below.

1. 2. The Licensor warrants that it has, to the best of its knowledge, the rights to license reuse of the Licensed Material. However, you should ensure that the material you are requesting is original to the Licensor and does not carry the copyright of another entity (as credited in the published version).

1. 3. If the credit line on any part of the material you have requested indicates that it was reprinted or adapted with permission from another source, then you should also seek permission from that source to reuse the material.

2. Scope of Licence

2. 1. You may only use the Licensed Content in the manner and to the extent permitted by these Ts&Cs and any applicable laws.

2. 2. A separate licence may be required for any additional use of the Licensed Material, e.g. where a licence has been purchased for print only use, separate permission must be obtained for electronic re-use. Similarly, a licence is only valid in the language selected and does not apply for editions in other languages unless additional translation rights have been granted separately in the licence. Any content owned by third parties are expressly excluded from the licence.

2. 3. Similarly, rights for additional components such as custom editions and derivatives require additional permission and may be subject to an additional fee. Please apply to Journalpermissions@springernature.com/bookpermissions@springernature.com for these rights.

2. 4. Where permission has been granted **free of charge** for material in print, permission may also be granted for any electronic version of that work, provided that the material is incidental to your work as a whole and that the electronic version is essentially equivalent to, or substitutes for, the print version.

2. 5. An alternative scope of licence may apply to signatories of the STM Permissions Guidelines, as amended from time to time.

3. Duration of Licence

3. 1. A licence for is valid from the date of purchase ('Licence Date') at the end of the relevant period in the below table:

Scope of Licence	Duration of Licence
Post on a website	12 months
Presentations	12 months
Books and journals	Lifetime of the edition in the language purchased

4. Acknowledgement

4. 1. The Licensor's permission must be acknowledged next to the Licenced Material in print. In electronic form, this acknowledgement must be visible at the same time as the figures/tables/illustrations or abstract, and must be hyperlinked to the journal/book's homepage. Our required acknowledgement format is in the Appendix below.

5. Restrictions on use

5. 1. Use of the Licensed Material may be permitted for incidental promotional use and minor editing privileges e.g. minor adaptations of single figures, changes of format, colour and/or style where the adaptation is credited as set out in Appendix 1 below. Any other changes including but not limited to, cropping, adapting, omitting material that affect the meaning, intention or moral rights of the author are strictly prohibited.

5. 2. You must not use any Licensed Material as part of any design or trademark.

5. 3. Licensed Material may be used in Open Access Publications (OAP) before publication by Springer Nature, but any Licensed Material must be removed from OAP sites prior to final publication.

6. Ownership of Rights

6. 1. Licensed Material remains the property of either Licensor or the relevant third party and any rights not explicitly granted herein are expressly reserved.

7. Warranty

IN NO EVENT SHALL LICENSOR BE LIABLE TO YOU OR ANY OTHER PARTY OR ANY OTHER PERSON OR FOR ANY SPECIAL, CONSEQUENTIAL, INCIDENTAL OR INDIRECT DAMAGES, HOWEVER CAUSED, ARISING OUT OF OR IN CONNECTION WITH THE DOWNLOADING, VIEWING OR USE OF THE MATERIALS REGARDLESS OF THE FORM OF ACTION, WHETHER FOR BREACH OF CONTRACT, BREACH OF WARRANTY, TORT, NEGLIGENCE, INFRINGEMENT OR OTHERWISE (INCLUDING, WITHOUT LIMITATION, DAMAGES BASED ON LOSS OF PROFITS, DATA, FILES, USE, BUSINESS OPPORTUNITY OR CLAIMS OF THIRD PARTIES), AND
WHETHER OR NOT THE PARTY HAS BEEN ADVISED OF THE POSSIBILITY OF SUCH DAMAGES. THIS LIMITATION SHALL APPLY NOTWITHSTANDING ANY FAILURE OF ESSENTIAL PURPOSE OF ANY LIMITED REMEDY PROVIDED HEREIN.

8. Limitations

8. 1. ***BOOKS ONLY:***Where **'reuse in a dissertation/thesis'** has been selected the following terms apply: Print rights of the final author's accepted manuscript (for clarity, NOT the published version) for up to 100 copies, electronic rights for use only on a personal website or institutional repository as defined by the Sherpa guideline (www.sherpa.ac.uk/romeo/).

9. Termination and Cancellation

9. 1. Licences will expire after the period shown in Clause 3 (above).

9. 2. Licensee reserves the right to terminate the Licence in the event that payment is not received in full or if there has been a breach of this agreement by you.

Appendix 1 — Acknowledgements:

For Journal Content:
Reprinted by permission from [**the Licensor**]: [**Journal Publisher** (e.g. Nature/Springer/Palgrave)] [**JOURNAL NAME**] [**REFERENCE CITATION** (Article name, Author(s) Name), [**COPYRIGHT**] (year of publication)

For **Advance Online Publication papers:**
Reprinted by permission from [**the Licensor**]: [**Journal Publisher** (e.g. Nature/Springer/Palgrave)] [**JOURNAL NAME**] [**REFERENCE CITATION** (Article name, Author(s) Name), [**COPYRIGHT**] (year of publication), advance online publication, day month year (doi: 10.1038/sj.[JOURNAL ACRONYM].)

For Adaptations/Translations:
Adapted/Translated by permission from [**the Licensor**]: [**Journal Publisher** (e.g. Nature/Springer/Palgrave)] [**JOURNAL NAME**] [**REFERENCE CITATION** (Article name, Author(s) Name), [**COPYRIGHT**] (year of publication)

Note: For any republication from the British Journal of Cancer, the following credit line style applies:

Reprinted/adapted/translated by permission from [**the Licensor**]: on behalf of Cancer Research UK: : [**Journal Publisher** (e.g. Nature/Springer/Palgrave)] [**JOURNAL NAME**] [**REFERENCE CITATION** (Article name, Author(s) Name), [**COPYRIGHT]** (year of publication)

For **Advance Online Publication** papers:
Reprinted by permission from The [**the Licensor**]: on behalf of Cancer Research UK: [**Journal Publisher** (e.g. Nature/Springer/Palgrave)] [**JOURNAL NAME**] [**REFERENCE CITATION** (Article name, Author(s) Name), [**COPYRIGHT**] (year of publication), advance online publication, day month year (doi: 10.1038/sj. [JOURNAL ACRONYM])

For Book content:
Reprinted/adapted by permission from [**the Licensor**]: [**Book Publisher** (e.g. Palgrave Macmillan, Springer etc) [**Book Title**] by [**Book author**(s)] [**COPYRIGHT**] (year of publication)

Other Conditions:

Version 1.2

Questions? customercare@copyright.com or +1-855-239-3415 (toll free in the US) or +1-978-646-2777.

SPRINGER NATURE LICENSE
TERMS AND CONDITIONS

Permission for Figure 2.10, 2.11, 2,12

Sep 18, 2019

This Agreement between University of Alberta -- Dinara Zhalmuratova ("You") and Springer Nature ("Springer Nature") consists of your license details and the terms and conditions provided by Springer Nature and Copyright Clearance Center.

License Number	4654580728330
License date	Aug 23, 2019
Licensed Content Publisher	Springer Nature
Licensed Content Publication	Nature Reviews Materials
Licensed Content Title	Flexible mechanical metamaterials
Licensed Content Author	Katia Bertoldi, Vincenzo Vitelli, Johan Christensen, Martin van Hecke
Licensed Content Date	Oct 17, 2017
Licensed Content Volume	2
Licensed Content Issue	11
Type of Use	Thesis/Dissertation
Requestor type	academic/university or research institute
Format	print and electronic
Portion	figures/tables/illustrations
Number of figures/tables/illustrations	3
High-res required	no
Will you be translating?	no
Circulation/distribution	<501
Author of this Springer Nature content	no
Title	Reinforced Elastomer Composites and Metamaterials for Neo-aorta Applications
Institution name	University of Alberta
Expected presentation date	Sep 2019
Portions	Figure 2, 5, 6, 7
Requestor Location	University of Alberta 10907 65 Ave Edmonton, AB T6H 1W1 Canada Attn: University of Alberta
Total	0.00 CAD

Terms and Conditions

Springer Nature Customer Service Centre GmbH
Terms and Conditions

This agreement sets out the terms and conditions of the licence (the **Licence**) between you and **Springer Nature Customer Service Centre GmbH** (the **Licensor**). By clicking 'accept' and completing the transaction for the material (**Licensed Material**), you also confirm your acceptance of these terms and conditions.

1. Grant of License

1. 1. The Licensor grants you a personal, non-exclusive, non-transferable, world-wide licence to reproduce the Licensed Material for the purpose specified in your order only. Licences are granted for the specific use requested in the order and for no other use, subject to the conditions below.

1. 2. The Licensor warrants that it has, to the best of its knowledge, the rights to license reuse of the Licensed Material. However, you should ensure that the material you are requesting is original to the Licensor and does not carry the copyright of another entity (as credited in the published version).

1. 3. If the credit line on any part of the material you have requested indicates that it was reprinted or adapted with permission from another source, then you should also seek permission from that source to reuse the material.

2. Scope of Licence

2. 1. You may only use the Licensed Content in the manner and to the extent permitted by these Ts&Cs and any applicable laws.

2. 2. A separate licence may be required for any additional use of the Licensed Material, e.g. where a licence has been purchased for print only use, separate permission must be obtained for electronic re-use. Similarly, a licence is only valid in the language selected and does not apply for editions in other languages unless additional translation rights have been granted separately in the licence. Any content owned by third parties are expressly excluded from the licence.

2. 3. Similarly, rights for additional components such as custom editions and derivatives require additional permission and may be subject to an additional fee. Please apply to Journalpermissions@springernature.com/bookpermissions@springernature.com for these rights.

2. 4. Where permission has been granted **free of charge** for material in print, permission may also be granted for any electronic version of that work, provided that the material is incidental to your work as a whole and that the electronic version is essentially equivalent to, or substitutes for, the print version.

2. 5. An alternative scope of licence may apply to signatories of the STM Permissions Guidelines, as amended from time to time.

3. Duration of Licence

3. 1. A licence for is valid from the date of purchase ('Licence Date') at the end of the relevant period in the below table:

Scope of Licence	Duration of Licence
Post on a website	12 months
Presentations	12 months
Books and journals	Lifetime of the edition in the language purchased

4. Acknowledgement

4. 1. The Licensor's permission must be acknowledged next to the Licenced Material in print. In electronic form, this acknowledgement must be visible at the same time as the figures/tables/illustrations or abstract, and must be hyperlinked to the journal/book's homepage. Our required acknowledgement format is in the Appendix below.

5. Restrictions on use

5. 1. Use of the Licensed Material may be permitted for incidental promotional use and minor editing privileges e.g. minor adaptations of single figures, changes of format, colour and/or style where the adaptation is credited as set out in Appendix 1 below. Any other changes including but not limited to, cropping, adapting, omitting material that affect the meaning, intention or moral rights of the author are strictly prohibited.

5. 2. You must not use any Licensed Material as part of any design or trademark.

5. 3. Licensed Material may be used in Open Access Publications (OAP) before publication by Springer Nature, but any Licensed Material must be removed from OAP sites prior to final publication.

6. Ownership of Rights

6. 1. Licensed Material remains the property of either Licensor or the relevant third party and any rights not explicitly granted herein are expressly reserved.

7. Warranty

IN NO EVENT SHALL LICENSOR BE LIABLE TO YOU OR ANY OTHER PARTY OR ANY OTHER PERSON OR FOR ANY SPECIAL, CONSEQUENTIAL, INCIDENTAL OR INDIRECT DAMAGES, HOWEVER CAUSED, ARISING OUT OF OR IN CONNECTION WITH THE DOWNLOADING, VIEWING OR USE OF THE MATERIALS REGARDLESS OF THE FORM OF ACTION, WHETHER FOR BREACH OF CONTRACT, BREACH OF WARRANTY, TORT, NEGLIGENCE, INFRINGEMENT OR OTHERWISE (INCLUDING, WITHOUT LIMITATION, DAMAGES BASED ON LOSS OF PROFITS, DATA, FILES, USE, BUSINESS OPPORTUNITY OR CLAIMS OF THIRD PARTIES), AND
WHETHER OR NOT THE PARTY HAS BEEN ADVISED OF THE POSSIBILITY OF SUCH DAMAGES. THIS LIMITATION SHALL APPLY NOTWITHSTANDING ANY FAILURE OF ESSENTIAL PURPOSE OF ANY LIMITED REMEDY PROVIDED HEREIN.

8. Limitations

8. 1. ***BOOKS ONLY:***Where **'reuse in a dissertation/thesis'** has been selected the following terms apply: Print rights of the final author's accepted manuscript (for clarity, NOT the published version) for up to 100 copies, electronic rights for use only on a personal website or institutional repository as defined by the Sherpa guideline (www.sherpa.ac.uk/romeo/).

9. Termination and Cancellation

9. 1. Licences will expire after the period shown in Clause 3 (above).

9. 2. Licensee reserves the right to terminate the Licence in the event that payment is not received in full or if there has been a breach of this agreement by you.

Appendix 1 — Acknowledgements:

For Journal Content:
Reprinted by permission from [**the Licensor**]: [**Journal Publisher** (e.g. Nature/Springer/Palgrave)] [**JOURNAL NAME**] [**REFERENCE CITATION** (Article name, Author(s) Name), [**COPYRIGHT**] (year of publication)

For **Advance Online Publication papers:**
Reprinted by permission from [**the Licensor**]: [**Journal Publisher** (e.g. Nature/Springer/Palgrave)] [**JOURNAL NAME**] [**REFERENCE CITATION** (Article name, Author(s) Name), [**COPYRIGHT**] (year of publication), advance online publication, day month year (doi: 10.1038/sj.[JOURNAL ACRONYM].)

For Adaptations/Translations:
Adapted/Translated by permission from [**the Licensor**]: [**Journal Publisher** (e.g. Nature/Springer/Palgrave)] [**JOURNAL NAME**] [**REFERENCE CITATION** (Article name, Author(s) Name), [**COPYRIGHT**] (year of publication)

Note: For any republication from the British Journal of Cancer, the following credit line style applies:

Reprinted/adapted/translated by permission from [**the Licensor**]: on behalf of Cancer Research UK: : [**Journal Publisher** (e.g. Nature/Springer/Palgrave)] [**JOURNAL NAME**] [**REFERENCE CITATION** (Article name, Author(s) Name), [**COPYRIGHT]** (year of publication)

For **Advance Online Publication** papers:
Reprinted by permission from The [**the Licensor**]: on behalf of Cancer Research UK: [**Journal Publisher** (e.g. Nature/Springer/Palgrave)] [**JOURNAL NAME**] [**REFERENCE CITATION** (Article name, Author(s) Name), [**COPYRIGHT**] (year of publication), advance online publication, day month year (doi: 10.1038/sj. [JOURNAL ACRONYM])

For Book content:
Reprinted/adapted by permission from [**the Licensor**]: [**Book Publisher** (e.g. Palgrave Macmillan, Springer etc) [**Book Title**] by [**Book author**(s)] [**COPYRIGHT**] (year of publication)

Other Conditions:

Version 1.2

Questions? customercare@copyright.com or +1-855-239-3415 (toll free in the US) or +1-978-646-2777.

Permission for Figure 2.13

JOHN WILEY AND SONS LICENSE
TERMS AND CONDITIONS

Sep 18, 2019

This Agreement between University of Alberta -- Dinara Zhalmuratova ("You") and John Wiley and Sons ("John Wiley and Sons") consists of your license details and the terms and conditions provided by John Wiley and Sons and Copyright Clearance Center.

License Number	4654580979643
License date	Aug 23, 2019
Licensed Content Publisher	John Wiley and Sons
Licensed Content Publication	Advanced Materials
Licensed Content Title	Snapping Mechanical Metamaterials under Tension
Licensed Content Author	Damiano Pasini, Abdolhamid Akbarzadeh, Ahmad Rafsanjani
Licensed Content Date	Aug 28, 2015
Licensed Content Volume	27
Licensed Content Issue	39
Licensed Content Pages	5
Type of use	Dissertation/Thesis
Requestor type	University/Academic
Format	Print and electronic
Portion	Figure/table
Number of figures/tables	1
Original Wiley figure/table number(s)	Figure 4
Will you be translating?	No
Title of your thesis / dissertation	Reinforced Elastomer Composites and Metamaterials for Neo-aorta Applications
Expected completion date	Sep 2019
Expected size (number of pages)	1
Requestor Location	University of Alberta 10907 65 Ave Edmonton, AB T6H 1W1 Canada Attn: University of Alberta
Publisher Tax ID	EU826007151
Total	0.00 CAD
Terms and Conditions	

TERMS AND CONDITIONS

This copyrighted material is owned by or exclusively licensed to John Wiley & Sons, Inc. or one of its group companies (each a"Wiley Company") or handled on behalf of a society with which a Wiley Company has exclusive publishing rights in relation to a particular work (collectively "WILEY"). By clicking "accept" in connection with completing this licensing transaction, you agree that the following terms and conditions apply to this transaction (along with the billing and payment terms and conditions established by the Copyright Clearance Center Inc., ("CCC's Billing and Payment terms and conditions"), at the time that you opened your RightsLink account (these are available at any time at http://myaccount.copyright.com).

Terms and Conditions

- The materials you have requested permission to reproduce or reuse (the "Wiley Materials") are protected by copyright.

- You are hereby granted a personal, non-exclusive, non-sub licensable (on a stand-alone basis), non-transferable, worldwide, limited license to reproduce the Wiley Materials for the purpose specified in the licensing process. This license, **and any CONTENT (PDF or image file) purchased as part of your order,** is for a one-time use only and limited to any maximum distribution number specified in the license. The first instance of republication or reuse granted by this license must be completed within two years of the date of the grant of this license (although copies prepared before the end date may be distributed thereafter). The Wiley Materials shall not be used in any other manner or for any other purpose, beyond what is granted in the license. Permission is granted subject to an appropriate acknowledgement given to the author, title of the material/book/journal and the publisher. You shall also duplicate the copyright notice that appears in the Wiley publication in your use of the Wiley Material. Permission is also granted on the understanding that nowhere in the text is a previously published source acknowledged for all or part of this Wiley Material. Any third party content is expressly excluded from this permission.

- With respect to the Wiley Materials, all rights are reserved. Except as expressly granted by the terms of the license, no part of the Wiley Materials may be copied, modified, adapted (except for minor reformatting required by the new Publication), translated, reproduced, transferred or distributed, in any form or by any means, and no derivative works may be made based on the Wiley Materials without the prior permission of the respective copyright owner.**For STM Signatory Publishers clearing permission under the terms of the STM Permissions Guidelines only, the terms of the license are extended to include subsequent editions and for editions in other languages, provided such editions are for the work as a whole in situ and does not involve the separate exploitation of the permitted figures or extracts,** You may not alter, remove or suppress in any manner any copyright, trademark or other notices displayed by the Wiley Materials. You may not license, rent, sell, loan, lease, pledge, offer as security, transfer or assign the Wiley Materials on a stand-alone basis, or any of the rights granted to you hereunder to any other person.

- The Wiley Materials and all of the intellectual property rights therein shall at all times remain the exclusive property of John Wiley & Sons Inc, the Wiley Companies, or their respective licensors, and your interest therein is only that of having possession of and the right to reproduce the Wiley Materials pursuant to Section 2 herein during the continuance of this Agreement. You agree that you own no right, title or interest in or to the Wiley Materials or any of the intellectual property rights therein. You shall have no rights hereunder other than the license as provided for above in Section 2. No right, license or interest to any trademark, trade name, service mark or other branding ("Marks") of WILEY or its licensors is granted hereunder, and you agree that you shall not assert any such right, license or interest with respect thereto

- NEITHER WILEY NOR ITS LICENSORS MAKES ANY WARRANTY OR REPRESENTATION OF ANY KIND TO YOU OR ANY THIRD PARTY, EXPRESS, IMPLIED OR STATUTORY, WITH RESPECT TO THE MATERIALS OR THE ACCURACY OF ANY INFORMATION CONTAINED IN THE MATERIALS, INCLUDING, WITHOUT LIMITATION, ANY IMPLIED WARRANTY OF MERCHANTABILITY, ACCURACY, SATISFACTORY QUALITY, FITNESS FOR A PARTICULAR PURPOSE, USABILITY, INTEGRATION OR NON-INFRINGEMENT AND ALL SUCH WARRANTIES ARE HEREBY EXCLUDED BY WILEY AND ITS LICENSORS AND WAIVED BY YOU.

- WILEY shall have the right to terminate this Agreement immediately upon breach of this Agreement by you.

- You shall indemnify, defend and hold harmless WILEY, its Licensors and their respective directors, officers, agents and employees, from and against any actual or threatened claims, demands, causes of action or proceedings arising from any breach of this Agreement by you.

- IN NO EVENT SHALL WILEY OR ITS LICENSORS BE LIABLE TO YOU OR ANY OTHER PARTY OR ANY OTHER PERSON OR ENTITY FOR ANY SPECIAL, CONSEQUENTIAL, INCIDENTAL, INDIRECT, EXEMPLARY OR PUNITIVE DAMAGES, HOWEVER CAUSED, ARISING OUT OF OR IN CONNECTION WITH THE DOWNLOADING, PROVISIONING, VIEWING OR USE OF THE MATERIALS REGARDLESS OF THE FORM OF ACTION, WHETHER FOR BREACH OF CONTRACT, BREACH OF WARRANTY, TORT, NEGLIGENCE, INFRINGEMENT OR OTHERWISE (INCLUDING, WITHOUT LIMITATION, DAMAGES BASED ON LOSS OF PROFITS, DATA, FILES, USE, BUSINESS OPPORTUNITY OR CLAIMS OF THIRD PARTIES), AND WHETHER OR NOT THE PARTY HAS BEEN ADVISED OF THE POSSIBILITY OF SUCH DAMAGES. THIS LIMITATION SHALL APPLY NOTWITHSTANDING ANY FAILURE OF ESSENTIAL PURPOSE OF ANY LIMITED REMEDY PROVIDED HEREIN.

- Should any provision of this Agreement be held by a court of competent jurisdiction to be illegal, invalid, or unenforceable, that provision shall be deemed amended to achieve as nearly as possible the same economic effect as the original provision, and the legality, validity and enforceability of the remaining provisions of this Agreement shall not be affected or impaired thereby.

- The failure of either party to enforce any term or condition of this Agreement shall not constitute a waiver of either party's right to enforce each and every term and condition of this Agreement. No breach under this agreement shall be deemed waived or excused by either party unless such waiver or consent is in writing signed by the party granting such waiver or consent. The waiver by or consent of a party to a breach of any provision of this Agreement shall not operate or be construed as a waiver of or consent to any other or subsequent breach by such other party.

- This Agreement may not be assigned (including by operation of law or otherwise) by you without WILEY's prior written consent.

- Any fee required for this permission shall be non-refundable after thirty (30) days from receipt by the CCC.

- These terms and conditions together with CCC's Billing and Payment terms and conditions (which are incorporated herein) form the entire agreement between you and WILEY concerning this licensing transaction and (in the absence of fraud) supersedes all prior agreements and representations of the parties, oral or written. This Agreement may not be amended except in writing signed by both parties. This Agreement shall be binding upon and inure to the benefit of the parties' successors, legal representatives, and authorized assigns.

- In the event of any conflict between your obligations established by these terms and conditions and those established by CCC's Billing and Payment terms and conditions, these terms and conditions shall prevail.

- WILEY expressly reserves all rights not specifically granted in the combination of (i) the license details provided by you and accepted in the course of this licensing transaction, (ii) these terms and conditions and (iii) CCC's Billing and Payment terms and conditions.

- This Agreement will be void if the Type of Use, Format, Circulation, or Requestor Type was misrepresented during the licensing process.

- This Agreement shall be governed by and construed in accordance with the laws of the State of New York, USA, without regards to such state's conflict of law rules. Any legal action, suit or proceeding arising out of or relating to these Terms and Conditions or the breach thereof shall be instituted in a court of competent jurisdiction in New York County in the State of New York in the United States of America and each party hereby consents and submits to the personal jurisdiction of such court, waives any objection to venue in such court and consents to service of process by registered or certified mail, return receipt requested, at the last known address of such party.

WILEY OPEN ACCESS TERMS AND CONDITIONS

Wiley Publishes Open Access Articles in fully Open Access Journals and in Subscription journals offering Online Open. Although most of the fully Open Access journals publish open access articles under the terms of the Creative Commons Attribution (CC BY) License only, the subscription journals and a few of the Open Access Journals offer a choice of Creative Commons Licenses. The license type is clearly identified on the article.

The Creative Commons Attribution License

The Creative Commons Attribution License (CC-BY) allows users to copy, distribute and transmit an article, adapt the article and make commercial use of the article. The CC-BY license permits commercial and non-

Creative Commons Attribution Non-Commercial License

The Creative Commons Attribution Non-Commercial (CC-BY-NC)License permits use, distribution and reproduction in any medium, provided the original work is properly cited and is not used for commercial purposes.(see below)

Creative Commons Attribution-Non-Commercial-NoDerivs License

The Creative Commons Attribution Non-Commercial-NoDerivs License (CC-BY-NC-ND) permits use, distribution and reproduction in any medium, provided the original work is properly cited, is not used for commercial purposes and no modifications or adaptations are made. (see below)

Use by commercial "for-profit" organizations

Use of Wiley Open Access articles for commercial, promotional, or marketing purposes requires further explicit permission from Wiley and will be subject to a fee.

Permission for Figure 4.2, 4.3, 4.7

JOHN WILEY AND SONS LICENSE
TERMS AND CONDITIONS

Sep 18, 2019

This Agreement between University of Alberta -- Dinara Zhalmuratova ("You") and John Wiley and Sons ("John Wiley and Sons") consists of your license details and the terms and conditions provided by John Wiley and Sons and Copyright Clearance Center.

License Number	4654590613905
License date	Aug 23, 2019
Licensed Content Publisher	John Wiley and Sons
Licensed Content Publication	Advanced Materials
Licensed Content Title	Recent Progress in Biomimetic Additive Manufacturing Technology: From Materials to Functional Structures
Licensed Content Author	Yong Chen, Qifa Zhou, Chi Zhou, et al
Licensed Content Date	Jun 19, 2018
Licensed Content Volume	30
Licensed Content Issue	36
Licensed Content Pages	34
Type of use	Dissertation/Thesis
Requestor type	University/Academic
Format	Print and electronic
Portion	Figure/table
Number of figures/tables	4
Original Wiley figure/table number(s)	Figure 1,2,3,4
Will you be translating?	No
Title of your thesis / dissertation	Reinforced Elastomer Composites and Metamaterials for Neo-aorta Applications
Expected completion date	Sep 2019
Expected size (number of pages)	1
Requestor Location	University of Alberta 10907 65 Ave Edmonton, AB T6H 1W1 Canada Attn: University of Alberta
Publisher Tax ID	EU826007151
Total	0.00 CAD
Terms and Conditions	

TERMS AND CONDITIONS

This copyrighted material is owned by or exclusively licensed to John Wiley & Sons, Inc. or one of its group companies (each a"Wiley Company") or handled on behalf of a society with which a Wiley Company has exclusive publishing rights in relation to a particular work (collectively "WILEY"). By clicking "accept" in connection with completing this licensing transaction, you agree that the following terms and conditions apply to this transaction (along with the billing and payment terms and conditions established by the Copyright Clearance Center Inc., ("CCC's Billing and Payment terms and conditions"), at the time that you opened your RightsLink account (these are available at any time at http://myaccount.copyright.com).

Terms and Conditions

- The materials you have requested permission to reproduce or reuse (the "Wiley Materials") are protected by copyright.

- You are hereby granted a personal, non-exclusive, non-sub licensable (on a stand-alone basis), non-transferable, worldwide, limited license to reproduce the Wiley Materials for the purpose specified in the licensing process. This license, **and any CONTENT (PDF or image file) purchased as part of your order,** is for a one-time use only and limited to any maximum distribution number specified in the license. The first instance of republication or reuse granted by this license must be completed within two years of the date of the grant of this license (although copies prepared before the end date may be distributed thereafter). The Wiley Materials shall not be used in any other manner or for any other purpose, beyond what is granted in the license. Permission is granted subject to an appropriate acknowledgement given to the author, title of the material/book/journal and the publisher. You shall also duplicate the copyright notice that appears in the Wiley publication in your use of the Wiley Material. Permission is also granted on the understanding that nowhere in the text is a previously published source acknowledged for all or part of this Wiley Material. Any third party content is expressly excluded from this permission.

- With respect to the Wiley Materials, all rights are reserved. Except as expressly granted by the terms of the license, no part of the Wiley Materials may be copied, modified, adapted (except for minor reformatting required by the new Publication), translated, reproduced, transferred or distributed, in any form or by any means, and no derivative works may be made based on the Wiley Materials without the prior permission of the respective copyright owner.**For STM Signatory Publishers clearing permission under the terms of the STM Permissions Guidelines only, the terms of the license are extended to include subsequent editions and for editions in other languages, provided such editions are for the work as a whole in situ and does not involve the separate exploitation of the permitted figures or extracts,** You may not alter, remove or suppress in any manner any copyright, trademark or other notices displayed by the Wiley Materials. You may not license, rent, sell, loan, lease, pledge, offer as security, transfer or assign the Wiley Materials on a stand-alone basis, or any of the rights granted to you hereunder to any other person.

- The Wiley Materials and all of the intellectual property rights therein shall at all times remain the exclusive property of John Wiley & Sons Inc, the Wiley Companies, or their respective licensors, and your interest therein is only that of having possession of and the right to reproduce the Wiley Materials pursuant to Section 2 herein during the continuance of this Agreement. You agree that you own no right, title or interest in or to the Wiley Materials or any of the intellectual property rights therein. You shall have no rights hereunder other than the license as provided for above in Section 2. No right, license or interest to any trademark, trade name, service mark or other branding ("Marks") of WILEY or its licensors is granted hereunder, and you agree that you shall not assert any such right, license or interest with respect thereto

- NEITHER WILEY NOR ITS LICENSORS MAKES ANY WARRANTY OR REPRESENTATION OF ANY KIND TO YOU OR ANY THIRD PARTY, EXPRESS, IMPLIED OR STATUTORY, WITH RESPECT TO THE MATERIALS OR THE ACCURACY OF ANY INFORMATION CONTAINED IN THE MATERIALS, INCLUDING, WITHOUT LIMITATION, ANY IMPLIED WARRANTY OF MERCHANTABILITY, ACCURACY, SATISFACTORY QUALITY, FITNESS FOR A PARTICULAR PURPOSE, USABILITY, INTEGRATION OR NON-INFRINGEMENT AND ALL SUCH WARRANTIES ARE HEREBY EXCLUDED BY WILEY AND ITS LICENSORS AND WAIVED BY YOU.

- WILEY shall have the right to terminate this Agreement immediately upon breach of this Agreement by you.

- You shall indemnify, defend and hold harmless WILEY, its Licensors and their respective directors, officers, agents and employees, from and against any actual or threatened claims, demands, causes of action or proceedings arising from any breach of this Agreement by you.

- IN NO EVENT SHALL WILEY OR ITS LICENSORS BE LIABLE TO YOU OR ANY OTHER PARTY OR ANY OTHER PERSON OR ENTITY FOR ANY SPECIAL, CONSEQUENTIAL, INCIDENTAL, INDIRECT, EXEMPLARY OR PUNITIVE DAMAGES, HOWEVER CAUSED, ARISING OUT OF OR IN CONNECTION WITH THE DOWNLOADING, PROVISIONING, VIEWING OR USE OF THE MATERIALS REGARDLESS OF THE FORM OF ACTION, WHETHER FOR BREACH OF CONTRACT, BREACH OF WARRANTY, TORT, NEGLIGENCE, INFRINGEMENT OR OTHERWISE (INCLUDING, WITHOUT LIMITATION, DAMAGES BASED ON LOSS OF PROFITS, DATA, FILES, USE, BUSINESS OPPORTUNITY OR CLAIMS OF THIRD PARTIES), AND WHETHER OR NOT THE PARTY HAS BEEN ADVISED OF THE POSSIBILITY OF SUCH DAMAGES. THIS LIMITATION SHALL APPLY NOTWITHSTANDING ANY FAILURE OF ESSENTIAL PURPOSE OF ANY LIMITED REMEDY PROVIDED HEREIN.

- Should any provision of this Agreement be held by a court of competent jurisdiction to be illegal, invalid, or unenforceable, that provision shall be deemed amended to achieve as nearly as possible the same economic effect as the original provision, and the legality, validity and enforceability of the remaining provisions of this Agreement shall not be affected or impaired thereby.

- The failure of either party to enforce any term or condition of this Agreement shall not constitute a waiver of either party's right to enforce each and every term and condition of this Agreement. No breach under this agreement shall be deemed waived or excused by either party unless such waiver or consent is in writing signed by the party granting such waiver or consent. The waiver by or consent of a party to a breach of any provision of this Agreement shall not operate or be construed as a waiver of or consent to any other or subsequent breach by such other party.

- This Agreement may not be assigned (including by operation of law or otherwise) by you without WILEY's prior written consent.

- Any fee required for this permission shall be non-refundable after thirty (30) days from receipt by the CCC.

- These terms and conditions together with CCC's Billing and Payment terms and conditions (which are incorporated herein) form the entire agreement between you and WILEY concerning this licensing transaction and (in the absence of fraud) supersedes all prior agreements and representations of the parties, oral or written. This Agreement may not be amended except in writing signed by both parties. This Agreement shall be binding upon and inure to the benefit of the parties' successors, legal representatives, and authorized assigns.

- In the event of any conflict between your obligations established by these terms and conditions and those established by CCC's Billing and Payment terms and conditions, these terms and conditions shall prevail.

- WILEY expressly reserves all rights not specifically granted in the combination of (i) the license details provided by you and accepted in the course of this licensing transaction, (ii) these terms and conditions and (iii) CCC's Billing and Payment terms and conditions.

- This Agreement will be void if the Type of Use, Format, Circulation, or Requestor Type was misrepresented during the licensing process.

- This Agreement shall be governed by and construed in accordance with the laws of the State of New York, USA, without regards to such state's conflict of law rules. Any legal action, suit or proceeding arising out of or relating to these Terms and Conditions or the breach thereof shall be instituted in a court of competent jurisdiction in New York County in the State of New York in the United States of America and each party hereby consents and submits to the personal jurisdiction of such court, waives any objection to venue in such court and consents to service of process by registered or certified mail, return receipt requested, at the last known address of such party.

WILEY OPEN ACCESS TERMS AND CONDITIONS

Wiley Publishes Open Access Articles in fully Open Access Journals and in Subscription journals offering Online Open. Although most of the fully Open Access journals publish open access articles under the terms of the Creative Commons Attribution (CC BY) License only, the subscription journals and a few of the Open Access Journals offer a choice of Creative Commons Licenses. The license type is clearly identified on the article.

The Creative Commons Attribution License

The Creative Commons Attribution License (CC-BY) allows users to copy, distribute and transmit an article, adapt the article and make commercial use of the article. The CC-BY license permits commercial and non-

Creative Commons Attribution Non-Commercial License

The Creative Commons Attribution Non-Commercial (CC-BY-NC)License permits use, distribution and reproduction in any medium, provided the original work is properly cited and is not used for commercial purposes.(see below)

Creative Commons Attribution-Non-Commercial-NoDerivs License

The Creative Commons Attribution Non-Commercial-NoDerivs License (CC-BY-NC-ND) permits use, distribution and reproduction in any medium, provided the original work is properly cited, is not used for commercial purposes and no modifications or adaptations are made. (see below)

Use by commercial "for-profit" organizations

Use of Wiley Open Access articles for commercial, promotional, or marketing purposes requires further explicit permission from Wiley and will be subject to a fee.

Further details can be found on Wiley Online Library
http://olabout.wiley.com/WileyCDA/Section/id-410895.html

Other Terms and Conditions:

v1.10 Last updated September 2015

Questions? customercare@copyright.com or +1-855-239-3415 (toll free in the US) or +1-978-646-2777.

SPRINGER NATURE LICENSE TERMS AND CONDITIONS

Permission for Figure 4.4

Sep 19, 2019

This Agreement between University of Alberta -- Dinara Zhalmuratova ("You") and Springer Nature ("Springer Nature") consists of your license details and the terms and conditions provided by Springer Nature and Copyright Clearance Center.

License Number	4672311480820
License date	Sep 19, 2019
Licensed Content Publisher	Springer Nature
Licensed Content Publication	Nature Reviews Materials
Licensed Content Title	3D printing of soft robotic systems
Licensed Content Author	T. J. Wallin et al
Licensed Content Date	May 4, 2018
Type of Use	Thesis/Dissertation
Requestor type	academic/university or research institute
Format	print and electronic
Portion	figures/tables/illustrations
Number of figures/tables/illustrations	1
High-res required	no
Will you be translating?	no
Circulation/distribution	1 - 29
Author of this Springer Nature content	no
Title	Reinforced Elastomer Composites and Metamaterials for Neo-aorta Applications
Institution name	University of Alberta
Expected presentation date	Sep 2019
Portions	Box 1
Requestor Location	University of Alberta 10907 65 Ave Edmonton, AB T6H 1W1 Canada Attn: University of Alberta
Total	0.00 CAD

Terms and Conditions

Springer Nature Customer Service Centre GmbH Terms and Conditions

This agreement sets out the terms and conditions of the licence (the **Licence**) between you and **Springer Nature Customer Service Centre GmbH** (the **Licensor**). By clicking 'accept' and completing the transaction for the material (**Licensed Material**), you also confirm your acceptance of these terms and conditions.

1. Grant of License

1. 1. The Licensor grants you a personal, non-exclusive, non-transferable, world-wide licence to reproduce the Licensed Material for the purpose specified in your order only. Licences are granted for the specific use requested in the order and for no other use, subject to the conditions below.

1. 2. The Licensor warrants that it has, to the best of its knowledge, the rights to license reuse of the Licensed Material. However, you should ensure that the material you are requesting is original to the Licensor and does not carry the copyright of another entity (as credited in the published version).

1. 3. If the credit line on any part of the material you have requested indicates that it was reprinted or adapted with permission from another source, then you should also seek permission from that source to reuse the material.

2. Scope of Licence

2. 1. You may only use the Licensed Content in the manner and to the extent permitted by these Ts&Cs and any applicable laws.

2. 2. A separate licence may be required for any additional use of the Licensed Material, e.g. where a licence has been purchased for print only use, separate permission must be obtained for electronic re-use. Similarly, a licence is only valid in the language selected and does not apply for editions in other languages unless additional translation rights have been granted separately in the licence. Any content owned by third parties are expressly excluded from the licence.

2. 3. Similarly, rights for additional components such as custom editions and derivatives require additional permission and may be subject to an additional fee. Please apply to Journalpermissions@springernature.com/bookpermissions@springernature.com for these rights.

2. 4. Where permission has been granted **free of charge** for material in print, permission may also be granted for any electronic version of that work, provided that the material is incidental to your work as a whole and that the electronic version is essentially equivalent to, or substitutes for, the print version.

2. 5. An alternative scope of licence may apply to signatories of the STM Permissions Guidelines, as amended from time to time.

3. Duration of Licence

3. 1. A licence for is valid from the date of purchase ('Licence Date') at the end of the relevant period in the below table:

Scope of Licence	Duration of Licence
Post on a website	12 months
Presentations	12 months
Books and journals	Lifetime of the edition in the language purchased

4. Acknowledgement

4. 1. The Licensor's permission must be acknowledged next to the Licenced Material in print. In electronic form, this acknowledgement must be visible at the same time as the figures/tables/illustrations or abstract, and must be hyperlinked to the journal/book's homepage. Our required acknowledgement format is in the Appendix below.

5. Restrictions on use

5. 1. Use of the Licensed Material may be permitted for incidental promotional use and minor editing privileges e.g. minor adaptations of single figures, changes of format, colour and/or style where the adaptation is credited as set out in Appendix 1 below. Any other changes including but not limited to, cropping, adapting, omitting material that affect the meaning, intention or moral rights of the author are strictly prohibited.

5. 2. You must not use any Licensed Material as part of any design or trademark.

5. 3. Licensed Material may be used in Open Access Publications (OAP) before publication by Springer Nature, but any Licensed Material must be removed from OAP sites prior to final publication.

6. Ownership of Rights

6. 1. Licensed Material remains the property of either Licensor or the relevant third party and any rights not explicitly granted herein are expressly reserved.

7. Warranty

IN NO EVENT SHALL LICENSOR BE LIABLE TO YOU OR ANY OTHER PARTY OR ANY OTHER PERSON OR FOR ANY SPECIAL, CONSEQUENTIAL, INCIDENTAL OR INDIRECT DAMAGES, HOWEVER CAUSED, ARISING OUT OF OR IN CONNECTION WITH THE DOWNLOADING, VIEWING OR USE OF THE MATERIALS REGARDLESS OF THE FORM OF ACTION, WHETHER FOR BREACH OF CONTRACT, BREACH OF WARRANTY, TORT, NEGLIGENCE, INFRINGEMENT OR OTHERWISE (INCLUDING, WITHOUT LIMITATION, DAMAGES BASED ON LOSS OF PROFITS, DATA, FILES, USE, BUSINESS OPPORTUNITY OR CLAIMS OF THIRD PARTIES), AND
WHETHER OR NOT THE PARTY HAS BEEN ADVISED OF THE POSSIBILITY OF SUCH DAMAGES. THIS LIMITATION SHALL APPLY NOTWITHSTANDING ANY FAILURE OF ESSENTIAL PURPOSE OF ANY LIMITED REMEDY PROVIDED HEREIN.

8. Limitations

8. 1. ***BOOKS ONLY:***Where **'reuse in a dissertation/thesis'** has been selected the following terms apply: Print rights of the final author's accepted manuscript (for clarity, NOT the published version) for up to 100 copies, electronic rights for use only on a personal website or institutional repository as defined by the Sherpa guideline (www.sherpa.ac.uk/romeo/).

9. Termination and Cancellation

9. 1. Licences will expire after the period shown in Clause 3 (above).

9. 2. Licensee reserves the right to terminate the Licence in the event that payment is not received in full or if there has been a breach of this agreement by you.

Appendix 1 — Acknowledgements:

For Journal Content:
Reprinted by permission from [**the Licensor**]: [**Journal Publisher** (e.g. Nature/Springer/Palgrave)] [**JOURNAL NAME**] [**REFERENCE CITATION** (Article name, Author(s) Name), [**COPYRIGHT**] (year of publication)

For **Advance Online Publication papers:**
Reprinted by permission from [**the Licensor**]: [**Journal Publisher** (e.g. Nature/Springer/Palgrave)] [**JOURNAL NAME**] [**REFERENCE CITATION** (Article name, Author(s) Name), [**COPYRIGHT**] (year of publication), advance online publication, day month year (doi: 10.1038/sj.[JOURNAL ACRONYM].)

For Adaptations/Translations:
Adapted/Translated by permission from [**the Licensor**]: [**Journal Publisher** (e.g. Nature/Springer/Palgrave)] [**JOURNAL NAME**] [**REFERENCE CITATION** (Article name, Author(s) Name), [**COPYRIGHT**] (year of publication)

Note: For any republication from the British Journal of Cancer, the following credit line style applies:

Reprinted/adapted/translated by permission from [**the Licensor**]: on behalf of Cancer Research UK: : [**Journal Publisher** (e.g. Nature/Springer/Palgrave)] [**JOURNAL NAME**] [**REFERENCE CITATION** (Article name, Author(s) Name), [**COPYRIGHT]** (year of publication)

For **Advance Online Publication** papers:
Reprinted by permission from The [**the Licensor**]: on behalf of Cancer Research UK: [**Journal Publisher** (e.g. Nature/Springer/Palgrave)] [**JOURNAL NAME**] [**REFERENCE CITATION** (Article name, Author(s) Name), [**COPYRIGHT**] (year of publication), advance online publication, day month year (doi: 10.1038/sj. [JOURNAL ACRONYM])

For Book content:
Reprinted/adapted by permission from [**the Licensor**]: [**Book Publisher** (e.g. Palgrave Macmillan, Springer etc) [**Book Title**] by [**Book author**(s)] [**COPYRIGHT**] (year of publication)

Other Conditions:

Version 1.2

Questions? customercare@copyright.com or +1-855-239-3415 (toll free in the US) or +1-978-646-2777.

Permission for Figure 4.5, 4.6, 4.8

Confirmation Number: 11844442
Order Date: 08/23/2019

Customer Information

Customer: Dinara Zhalmuratova
Account Number: 3001505643
Organization: University of Alberta
Email: zhalmura@ualberta.ca
Phone: +1 (587) 937-5657
Payment Method: Invoice

This is not an invoice

Order Details

Chemical Society reviews

Billing Status: **N/A**

Order detail ID:	71989354
ISSN:	1460-4744
Publication Type:	e-Journal
Volume:	
Issue:	
Start page:	
Publisher:	ROYAL SOCIETY OF CHEMISTRY
Author/Editor:	Royal Society of Chemistry (Great Britain)

Permission Status: Granted

Permission type: Republish or display content
Type of use: Thesis/Dissertation
Order License Id: 4654591148644

Requestor type	Academic institution
Format	Print, Electronic
Portion	chart/graph/table/figure
Number of charts/graphs/tables/figures	3
The requesting person/organization	Dinara Zhalmuratova
Title or numeric reference of the portion(s)	Figure 3 5,9
Title of the article or chapter the portion is from	Additive Manufacturing of Biologically-inspired Materials
Editor of portion(s)	N/A
Author of portion(s)	N/A
Volume of serial or monograph	N/A
Page range of portion	Page 7, 12,20
Publication date of portion	September 2019
Rights for	Main product
Duration of use	Current edition and up to 5 years
Creation of copies for the disabled	no
With minor editing privileges	no
For distribution to	Canada

In the following language(s)	Original language of publication
With incidental promotional use	no
Lifetime unit quantity of new product	Up to 499
Title	Reinforced Elastomer Composites and Metamaterials for Neo-aorta Applications
Institution name	University of Alberta
Expected presentation date	Sep 2019

Note: This item was invoiced separately through our **RightsLink service.** More info **$ 0.00**

Total order items: 1 **Order Total: $0.00**